Al-Mustansiriyah Journal of Science

ISSN 1814 - 635X

Vol. 21, No. 4, 2010

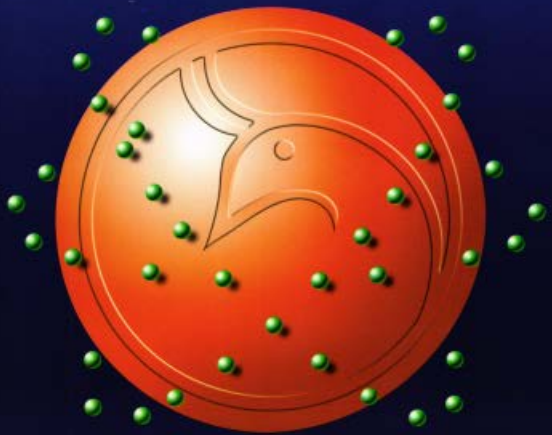

Issued by College of Science - Mustansiriyah University

Vol. 21
No. 4
2010

Al- Mustansiriyah Journal of Science

Issued by College of Science- Al- Mustansiriya University

Mobile: 07706289924
e-mail: mustjsci@yahoo.com

INSTRUCTION FOR AUTHORS

1. The journal accepts manuscripts in Arabic and English languages. Which had not been published before.
2. Author (s) has to introduce an application requesting publication of his manuscript in the journal. Four copies (one original) of the manuscript should be submitted. Should be printed by on the computer by laser printer and re produced on A4 white paper in three coppice with floppy disc should be also submitted.
3. The title of the manuscript together with the name and address of the author (s) should typed on a separate sheet in both Arabic and English. Only manuscripts title to be typed again with the manuscript.
4. For manuscripts written in English, full name (S) of author (s) and only first letters of the words (except prepositions and auxiliaries) forming title of the manuscript should be written in capital letters. Author (s) address (es) to be written in small letters.
5. Both Arabic and English abstracts are required for each manuscript. They should be typed on two separate sheets (not more then 250 words each).
6. References should be denoted by a number between two bracket on the same level of the line and directly at the end of the sentence. A list of references should be given on a separate sheet of paper, following the interactional style for names and abbreviations of journals.
7. Whenever possible, research papers should follow this pattem: INTRODUCTION, EXPERIMENTAL (MATERIALS AND METHODS), RESULTS AND DISCUSSION, and REFERENCES. All written in capital letters at the middle of the page. Without numbers or underneath lines.
8. The following pattern should be followed upon writing the references on the reference sheet: Sumame (s), intials of author (s), title of the paper, name or abbreviation of the journal, volume, number, pages and (Year). For books give the author(s) name(s), the title, edition, pages, publisher, place of publication and (Year).
9. A publication fees in the amount of ID. 25 thousand is charged upon a Receipt of the paper and 25 thousand upon the acceptance for publication for their ID. 50 thousand should be paid for the editorial board.

CONTENTS

Antimicrobial Activity of Rosemary (*Rosmarinus Officinalis* L.) Leaf Essential Oils Against Three Bacterial Species

Khaleel Ibrahim Rashid
Foundation of Technical Education

Received 27/9/2009 – Accepted 5/10/2010

الخلاصة

درست انتاجية نبات اكليل الجبل (*Rosmarinus officinalis* L.) من الزيوت الاساسية. اجري التحليل الكيميائي للزيوت الاساسية باستعمال كروماتوكرافيا الغاز (GC-MS). تميزت الزيوت الاساسية باحتواءها على المكونات الرئيسية: camphor (20.54%)، cineole (13.40%)، verbenone (12.71%)، bornyl acetate (12.22%)، carene (7.73%)، camphene (4.32%)، α-pinene (2.28%) و β-pinene (1.77%). فحصت الفعالية البايولوجية للزيوت الاساسية ضد ثلاث انواع من البكتريا (*Escheritia coli*، *Pseudomonas aeruginosa*، *B. cereus*). بينت النتائج بأن الزيوت الاساسية كانت مؤثرة ضد جميع انواع البكتريا المختبرة. كانت قيم اقل تركيز مثبط (MIC) هي: 32 مايكروغرام/ مل لـ *E. coli*، 64 مايكروغرام/ لـ *P. aeruginosa* و 16 مايكروغرام / لـ *B. cereus*. وجد ان *P. aeruginosa* هي اقل انواع البكتريا تحسساً للزيوت الاساسية.

ABSTRACT

The yield of rosemary (*Rosmarinus officinalis* L.) essential oils was investigated. The chemical analysis of essential oils was carried out using gas chromatography-Mass spectrometry (GC-MS). The major contents of rosemary leaf essential oils were; camphor (20.54%), cineole (13.40%), verbenone (12.71%), bornyl acetate (12.22%), carene (7.73%), camphene (4.32%), α-pinene (2.28%) and β-pinene (1.77%). Biological activity of essential oils was examined against three bacterial species (*Bacillus cereus, Escheritia coli, Pseudomonas aeruginosa*), essential oils were effective against all tested bacteria. The MIC values were 16 µg/ml for *B. cereus*, 32 µg/ml for *E. coli* and 64 µg/ml for *P. aeruginosa*. However, *P. aeruginosa* showed weak sensitivity to the oil.

INTRODUCTION

Rosemary (*Rosmarinus officinalis* L.) which has long been known as a spice and medicinal herb belongs to the Lamiaceae family and receiving increasing attention due to its antimicrobial, anti-inflammatory, and antioxidative constituents [1]. The leaves of rosemary contain between (1.0-2.5) % essential oil, such composition may markedly vary according to the chemo type and the development stage at which the plant has been harvested. It is an almost colorless to pale yellow liquid with a characteristics, refreshing and pleasant odor [2]. Plant material from rosemary is of commercial interest for its essential oil contents and its antioxidant compounds [3]. Chemically the essential oil are primarily composed of mono and sesquiterpenes and aromatic polypropanoids synthesized via the mevalonic acid pathway for terpenes and the shikimic acid pathway for aromatic

polypropanoids. Rosemary oils are largely used in traditional medicine, in perfumery, phytocosmetic and in liquor manufacturing. Essential oils (EOs) composition of rosemary comprise more than sixty individual components of which major substances can constitute up to 89% of the EOs [4]. Essential oils are produced using several techniques. Distillation uses water and steam to remove the oils from dried or fresh plants, and the expression method uses machines to squeeze the oil out of the plants [5]. The aim of this study is to determine the active compounds in rosemary oils using GC-MS techniques and to investigate the antimicrobial activity of against some bacterial isolates.

MATERIALS AND METHODS

Sample collection and preparation

This study was carried out in the plant tissue culture lab., Biotechnology Department, Al-Nahrain University during the period from may-september-2009. Rosemary plant was collected from College of Science- Baghdad University, gardens in May, 2009. Leaf sample was dried at 40°C for 24 hrs, ground into powder using grinding machine or a mortar, then subjected to extraction [6]. The essential oils were extracted by hydrodistillation. Samples weighting 50 g of rosemary powdered leaves were soaked in 250 ml of distilled water (20%) in a conical flask, and left for 24 hrs. Then the extract was subjected to steam distillation for 3 hrs using a Clevenger-type apparatus. Essential oils were collected after decantation [7].

Analysis conditions

Analysis of the essential oils was performed using GC-MS (Agilent 6780-USA), equipped with mass selective detector and HP-5 MS capillary column (30m x 0.25mm, film thickness 0.25 µm). Helium was the carrier gas, at flow rate of 0.8 ml/min. Samples of 1 µl were injected automatically in the split mode (split ratio 1:100). For GC-MS detection electron ionization system with an ionization energy of 70 eV was used. Quantitative data were obtained electronically from Electronic Ionized Detector (EID) area.

Antimicrobial assay

Antimicrobial assay was designed to determine the activity of essential oil of rosemary as a potential antibacterial activity against the tested microorganisms. MIC determination was conducted by well diffusion and agar dilution methods, using Mueller-Hinton (MH) agar for growth of bacteria [8]. Dimethyl sulfoxide (DMSO) was used to facilitate mixing of the oils with the broth [9]. Different concentrations of essential oils (8, 16, 32, 64, 128, 256 or 512) µl were added to sterile petri-dishes. Then melted MH agar for growth of bacterial isolates were

poured into the plates and swirled to mix the components well. They left to solidify, then 100 µl of suspension containing the tested microorganisms were spreaded using sterile glass rod and then incubated at 37 °C for 24 hrs for growth of bacterial isolates. Colonies were then counted and the count multiplied by reciprocal of sample dilutions which represented the count of the microorganisms. The MIC was taken as the lowest concentration of oil at which the tested organism did not show visible growth [10]. On other hand, wells were made in the solidified medium using cork borer. Aliquots of 100 µl of inoculums were applied to the wells, then incubated as mentioned above. Diameters of zones of inhibition were measured in mm. All the tests were performed in triplicate. Statistical analysis was performed, the data presented are an average of three replicates. Least significant difference (LSD) were calculated. Statistical Analysis System-SAS was used to analysis data [11].

RESULTS AND DISCUSSION

GC-MS analysis of essential oils

Chemical analysis of essential oils extracted from rosemary leaves revealed 22 components different in quantity as determined by percent in total oil composition. The main components were showed in table (1) and figure (1). Rosemary oil was shown to contain the highest composition of camphor (20.54%), cineole (13.40%), verbenone (12.71%), bornyl acetate (12.22%), carene (7.73%), camphene (4.32%),α-pinene (2.28%) and β-pinene (1.77%).

Table -1: Retention time (min) and peak area (%) of the different compounds found in rosemary essential oil analyzed by GC-MS

Compound	RT	Peak area %
Carene	6.19	7.73
Camphene	6.51	4.32
α-pinene	7.16	2.28
β-pinene	7.69	1.77
β-phellandrene	8.00	2.10
Cineole	9.38	13.30
3-carene	10.34	1.49
Terpinolene	11.37	1.58
Camphor	14.98	20.54
Bornyl acetate	15.89	12.22
Verbenone	17.89	12.71
Linderol	18.73	1.70
Lemonene	20.21	4.29
Thymol	20.89	0.54
Eugenol	23.89	0.78
Eucarvone	24.77	1.44
P-cymene	25.14	1.61
Humulene (α-caryophyllene)	26.64	0.65
α-amorphene	27.54	0.20
Caryophyllene oxide	31.70	0.63
Ledene	34.88	0.95
α-bisabolol	35.69	0.26
Non identified components		6.94

There is great variability in the chemical composition of EOs obtained, such variability depends on several factors including climatic, seasons, geographical location, soil structure and texture, part of the plant and the method used to obtain the EOs. Results showed that the more available constituents of the EOs of rosemary were terpenoids, monoterpenes, sesqui and diterpenes and they also contained aliphatic and aromatic esters, phenolic compounds and substituted benzene hydrocarbons.

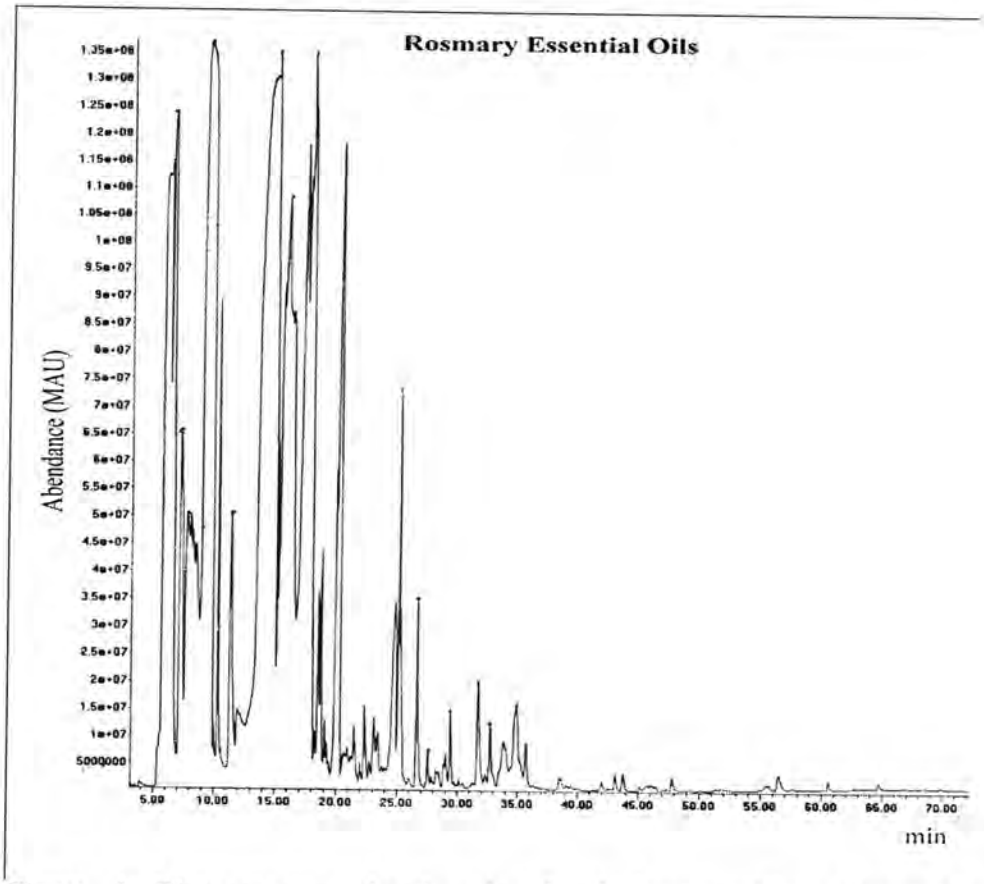

Figure -1: Chromatogram showing the chemical composition of essential oils extracted from rosemary leaves analyzed by GC

The content of EOs is depend considerably upon extrinsic and intrinsic factors, optimal harvest time to guarantee high content of EOs and high quality was reported to be at the plant development phase just before flowering [12].

[13] investigated the EOs from leaves and flowers of rosemary (collected from southern Spain), and found the main components to be camphor (32.33%) and α-pinene (11.56%). The EOs of *R. officinalis* from Spain were analyzed by [14] who found them to be rich in α-pinene (24.7%) and camphor (18.9%), they also contained some borneol (4.5%), finding that are in agreement with the results presented here.

The EOs from the fresh leaves of rosemary was by [15]. A number of 45 constituents were identified, the major constituents of the oil being camphor (26.0%) and α-pinene (11.5%). They reported that EOs had proportions of α-pinene and camphene and higher proportion of camphor, verbenone and cineole. A comparative study of the EOs was carried out, analysis of the oils by GC-MS led to the identification of 43 components, with verbenone (12.3%), camphor (11.3%) and bornyl acetate (7.6%) being the major constituents [16].

Antibacterial assay

The antibacterial activity was investigated against two G-negative bacteria (*E. coli*, *P. aeruginosa*) and one G-positive bacteria (*B. cereus*). The data in table (2) and figure (2) indicated that the essential oils of rosemary have a broad spectrum of inhibitory activity against both G-negative and G-positive bacteria used in this study with MIC regimes in the range of 16-64 µg/ml. *B. cereus* showed highest sensitivity to the oil of rosemary (MIC = 16 µg/ml). *E. coli* displayed moderate sensitivity (MIC = 32 µg/ml), while P. aeruginosa showed weak sensitivity to the oil (MIC = 64 µg/ml). However, being natural products the oils have been reported to be much safer than the commercial antibiotics. Another advantage of the essential oils was their broad spectrum activities against bacteria [17]. The oils exhibited inhibitory zones ranged of (14-26) mm in diameter. The oils showed antimicrobial activity against known food pathogens (*B. cereus*, *P. aeruginosa*) which was the cause of food spoilage and poisoning and subsequently cause human diseases. The results obtained might be different from previous reports due to the differences in oil composition which could probably be attributed to the seasonal variation, the method of extraction and environmental factors, or due to the nutrient status of the plant. The results are in agreement with [18] who reported that antimicrobial activities of rosemary essential oils are not related only to the major compounds but also the minor components of the oil. The results are similar to those documented by [5]. *E. coli* that is resistant to several antibiotics is susceptible to the essential oils of rosemary. Therefore, the essential oils of this plant can be used in pharmaceutical industry for production of new synthetic agents in the treatment of the infection disease.

Table -2: Effect of different concentrations of rosemary essential oils on bacterial growth (as inhibition zones, mm)

Concentration (µl/ml)	Inhibition zone diameter (mm)		
	Bacterial isolates		
	E. coli	P. aeruginosa	B. cereus
8	0	0	0
16	0	0	14
32	17	0	18
64	19	18	19
128	22	20	21
256	25	24	25
512	26	25	26
Control	0	0	0
@LSD ≤ 0.05	3.352*	2.596*	2.802*

@ Least Significant Differences

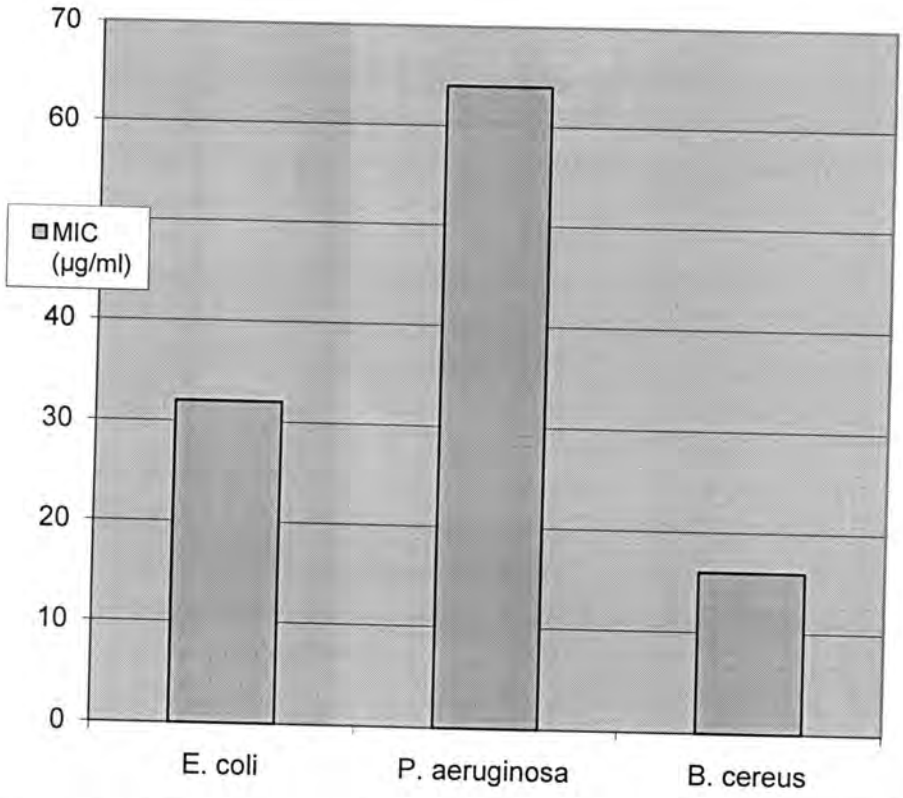

Figure -2: Minimum inhibitory concentration (MIC) of rosemary essential oils (µg/ml) against selected bacteria

REFERENCES

1. Eva, S. B.; Maria, H. T.; Attila, H.; Csilla, R.; and Szollosi, V. Antioxidant effect of various rosemary (*Rosmarinus officinalis* L.) clones. Acta Biologica szegediensis., 47(1-4): 111-113(2003).
2. Bauer, K.; Garbe, D. and Surburg, H. Common Fragrance and Flavor Materials. 3rd ed. Germany: Wiley-VCH(1997).
3. Sergi, M. and Leonor, A. Subcellular compartmentation of the diterpene carnosic acid and its derivatives in the leaves of rosemary. Plant Physiol., 125: 1094-1102(2001).
4. Burt, S. Essential oils; their antibacterial properties and potential application in foods. A review. International J. of Food Microbiol., 94: 223-253(2004).
5. Mounchid, K.; Bourjilat, F.; Dersi, N.; Aboussaauira, T.; Rachidai, A.; Tantaoul,-Elaraki, A. and Alaoui-Ismaili, M. The susceptibility of *Escheritia coli* strains to essential oils of *Rosmarinus officinalis* and *Eucalyptus globules.* African J. of Biotechnol., 4(10): 1175-1185(2005).
6. Bos, R., Analytical and phytochemical studies on valerian and valerian based preparations [Dissertation]. Groningen: Rijks

universiteit Groningen. Dept. of Pharmaceutical Biology. 184-193(1997).

7. Mounchid, K.; Bourjilat, F.; Dersi, N.; Aboussaauira, T.; Rachidai, A.; Tantaoul,-Elaraki, A. and Alaoui-Ismaili, M. Toxicity of south Morocco *Rosmarinus officinalis* essential oil: antibacterial and histopathological effects. Les Actes del'institut Agronomique et Veterinaire., (2-3): 139-144(2004).
8. Donald, R. S. and Clyde, T. Broth-dilution method for determining the antibiotic susceptibility of bacteria. Antimicrobial Agent and Chemtherapy. Amer. Soc. for Microbiol., 7: 15-21(1974).
9. Donald, C. S. and Ann, V. B. Antimicrobial susceptibility testing. Wisconsin Veterinary Diagnostic Laboratory(2006).
10. Josep, G.; Isabel, P.; Carmen, A. and Montserrat, O. *In vitro* antifungal susceptibility of nondermatophytic keratinophilic fungi. Unitat de Microbiologia, Facultat de Medicina, Universitat. Rovira; Virgili, Tarragona, Spain(2000).
11. SAS. SAS/STAT User's Guide for personal computers. Release 6.12, SAS Inst. Inc. NC. USA(2001).
12. Toth, J.; Mrlianova, M.; Tekelora, D. and Korenova, M. Rosmarinic acid – an important phenolic active compound of lemon balm (M*elissa officinalis* L.). Acta Facultatis Pharmaceuticae. Unversitatis Comenianae. Tomus(2003).
13. Tomei, P. E.; Cioni, P. L. Flamini, G. and Stefani, A. Essential oil. J of Essential oil Res., 7(3): 279-282(1995).
14. Chalchate, J. C. O.; Garry, R. P.; Michet, A.; Benjilali, B. and Chabart, J. I. Essential oils of rosemary (*Rosmarinus officinalis* L.). The chemical composition of oils of various origins (Morocco, Spain, France). J. Essential Oil *Rosmarinus*., 5: 613-618(1993).
15. Porte, A.; Godoy, R. L.; Koketsu, M.; Goncalves, S. L. and Torquilho, H. S. Essential oil. J of Essential oil Res., 12(5): 577-580(2000).
16. Martos, M. V.; Navajas, Y. R.; Fernandez-Lopez, J. and Perez Alvarez, J. A. Chemical composition of the essential oils obtained from me spices widely used in Mediterranean region. Acta Chim. Slov., 54: 921-926(2007).
17. Magenga, A. Influence of variety and organic cultural practices on yield and essential oil content of lavender and rosemary in Interior BC. Ecorational Technologies, Kamloops. 1-23(2004).
18. Marzouk, Z.; Neffati, A.; Marzouk, B.; Chraief, I.; Fathia, K.; Chekir, G. and Boukef, K. Chemical composition and antibacterial and antimutagenic activity of Tunisian *Rosmarinus officinalis* L. oil from Kasrine. J. of Food , Agric. & Environment., 4(3&4): 61-65(2006).

Comparative Activity of *Peganum harmala* Seeds Extract and Rifampicin Against *Brucella abortus* Experimentally Infection in Mice

Khalil I. A. Mohammed
College of Dentistry, University of Baghdad

Received 31/5/2010 – Accepted 5/10/2010

الخلاصة

تم تقسيم مجموعة من الفئران البيضاء بواقع 42 فأراً إلى ستة مجاميع بواقع سبعة لكل مجموعة عوملت بالمستخلص المائي لبذور نبات الحرمل لمدة ستة أيام متوالية ، والريفامبيسين لمدة ثلاثة أيام متوالية ثم حقنت بـ 5×10^5 خلية بكترية من البروسيلا المجهضة وبعد 21 يوماً قتلت الفئران وتم قياس عدد خلايا الدم البيض، معامل تضخم الكبد والطحال، فرط الحساسية الآجل اضافة إلى تعداد مستعمرات البكتريا في الطحال بعد استنباتها على الأوساط الزرعية وأظهرت النتائج زيادة أعداد خلايا الدم البيض ، فرط الحساسية الآجل ، معامل الوقاية في الفئران المعاملة بالمستخلص المائي لبذور نبات الحرمل والريفامبيسين مقارنة بالفئران المصابة فقط.

ABSTRACT

Forty two mice were divided into six groups which were treated with Rifampicin for successive three days and water extract of *Peganum harmala* for six days, then inoculated with 5 x 10^5 CFU/ML of *B. abortus* all animals sacrificed after 21 days and concern on total white blood cells count, spleen and liver indices, delayed type hypersensitivity reaction and *Brucella* enumeration in spleen.
The result showed a significant increasing of white blood cells, delayed type hypersensitivity and prophylactic index in comparison with infected alone.

INTRODUCTION

Brucella abortus is a facultative intracellular bacterium that infects humans and domestic animals. *Brucella* replicates in host mononuclear phagocytes, and survival in phagocytic cells allows the bacterium to escape the extracellular mechanism of host response such as complement and antibodies (1). *Brucella* are frequently able to survive and multiply in these cells because they inhibit the bactericidal myeloperoxidase-peroxide-halide system by releasing 5'-guanosine and adenine (2).

Brucella are transport into the lymphatic system and may replicate there locally they, also may replicate in the kidney, liver, spleen, breast tissue or joints, causing both localized and systemic infection granuloma may accompany extracellular replication of the bacteria especially in the liver and spleen (3). CD^+_4 T-cells play an important role in the protection against *Brucella* infection , either by activating CD^+_8 T-cells or secreting cytokines that mediate macrophages activation among these was interferon-γ (4). Immunopotentiation of the body immune system is obtained from mice treated with interferon pass a good immunological effect (5). Some studies demonstrated the ability

of *Peganum harmala* seed extract to induce immunostimulation against bacteria, fungi and parasites (6) in this study *P. harmala* water extract was used versus the treatment with Rifampicin the drug were assessed for their ability to eradicate bacteria from the spleen a target organ in *Brucella* infection.

MATERIALS AND METHODS

Animals:
Males of BALB/c mice, 6-8 Weeks of ages were obtained from institute for Embryos and Infertility Research, Al-Nahrain University .

Drugs:
Rifampicin (Misson viva care limited) was dissolved in sterilized water and orally administrated by gavage in a dose of (4.2 mg/kg) for three successive day's.

Bacteria:
Brucella abortus Biotype-1 was used in infection experiment .

P. harmala extract .
Water extract: of harmala seed prepared as described by Adaay *et al.*, 1989 (7) and given in a dose of 500 µg/20 gm for six successive day's according to (8).

Experimental Protocol:
The animals were divided into six groups with seven animals in each group as in the following:

1- Group of animals treated with Rifampicin.
2- Group of animals treated with Rifampicin and infected with *Brucella.*
3- Group of animals treated with *P. harmala* .
4- Group of animals treated with *P. harmala* and infected with *Brucella.*
5- Group of animals treated with 1 ml of sterilized PBS and served as a Positive control.
6- Group of animals treated with 1 ml of sterilized PBS and served as a negative control.

All groups, except treated alone and negative control were inoculated intraperitoneally with $5x10^5$ CFU/ml of *Brucella* according to method of (4).

All groups of animals were sacrificed after 21 days post infection and concern on the following parameters according to Oliveira *et al* (9)

1- Total count of white blood cells
2- Spleen and liver indices

3- Delayed type hypersensitivity.
4- *Brucella* enumeration in spleen.

Total and differential count of white blood cells:

Peritoneal fluid cellular influx, after treatment with *P. harmala* and infection with *Br. abortus* was differentially enumerate. thick smear were stained with Geimsa, than lymphocyte, neutrophil, monocytes, and Eosinophils were differentially counted according to Gravey *et al* (10).

Spleen and Liver indices :

All animals were weighed at the end of experiment time their spleen and liver were aseptically removed and weighed .The Organ Index was calculated according to the following equation (10).

$$\text{Organ Index} = \frac{\text{Organ weight}}{\text{Animal weight}} \times 1000$$

Delayed type hypersensitivity reaction:

Brucella allergens were prepared according to (9) using Rough *Br. abortus*. Then, the concentration were 60 µg/ml, then mixed with equal volume of complete Freunds adjuvant, mice were injected with 0.2 ml of *Brucella* allergen in the left leg. The right leg was injected with 0.2ml PBS as a control, the foot pad thickness was measured with a Vernier Caliper after 24 hr, the difference in the thickness between the *Brucella* allergens injected foot and control as delayed type hypersensitivity.

***Brucella* enumeration in the Spleen and Prophylactic Index:**

One mg of the spleen was individually homogenized in the sterilize PBS and each prepared volume was seeded on Trypticase Soy agar (Difco) plate *Brucella* were enumerated after six days at 37c° in 5% CO_2 according to (11). The prophylactic index was calculated according to this formula:

$$\text{Prophylactic Index} = 100 - \frac{\text{No. of colony in treated and infected group}}{\text{No. of colony in untreated infected group}} \times 100$$

Statistical analysis

ANOVA test was used to compare the results.

RESULTS AND DISCUSSION

I: Total White Blood Cell and Differential Count:

Table (1) shows the changes in white blood cells count in animals treated with Rifampicin, *P. harmala* and infected with *Brucella* .The numbers of all treated groups were significantly increased ($p<0.05$) it reached to 8280, 9500 cells /cumm in groups treated with Rifampicin and *P. harmala* seeds extract respectively. Also the number of white blood cells was increased in groups treated with Rifampicin , *P. harmala* seeds extracts and infected with *Brucella* which reached to 8100 , 8890 cells /cu mm respectively.

II: Weight of spleen and liver and their Indices.

Table (2) shows the changes in weight and indices for spleen and liver in animals post infection. The liver Index was 6.32 , 7.65 in groups treated with Rifampicin, *P. harmala* and infected, 5.37, 7.38 in groups treated with Rifampicin and *P. harmala* uninfected then untreated control (7.80) and negative control (5.42).

The splenic Index was 2.62 and 1.90 in groups treated with Rifampicin and *P. harmala* and infected, 1.05 and 1.60 in groups treated with Rifampicin and *P. harmala* uninfected with *Brucella* respectively, in infected untreated control (1.20) and negative control (1.0).

III : Estimation of delayed type hypersensitivity reaction.

Table (3) shows the changes of delayed type hypersensitivity in groups treated with Rifampicin, *P. harmala* extract and infected with *Brucella* . It which reach 0.41 mm in comparison with treated uninfected group 0.32 and 0.32 mm respectively while the positive and negative control reached 0.26 and 0.25 mm respectively

IV: Total Colony count and Prophylactic Index.

Table (4) shows the changes in number of colony count. The number was significantly decreased ($P<0.05$) in both groups treated with Rifampicin and *P. harmala* until they reached to 58.70 and 89.4 x 10^4 CFU/ml in comparison with the a positive control 290 x 10^4 CFU/ml.

Table -1: Total and differential counts of white blood cells in mice treated with Rifampicin and *P. harmala* seeds water extract and infected with *B. abortus*

Treatment	Total Count ± SD	Differential count ± SD			
		Neutrophils	Lymphocytes	Monocytes	Eosinophils
Rifampicin treatment	8280 ± 300	65 ± 0.7	24.5 ± 1.6	4.5 ± 1.5	3.1 ± 1.2
Rifampicin treated and infected with *Brucella*	8100 ± 40	61 ± 2.4	35.1 ± 1.2	4.0 ± 2.4	3.8 ± 1.0
P. harmala treatment	9.500 ± 218	89 ± 1.4	34.4 ± 10	7.6 ± 2.4	4.1 ± 1.3
P. harmala treated and infected with *Brucella*	8890 ± 301	75 ± 2.0	36 ± 0.9	6.8 ± 1.0	4.2 ± 1.4
Positive control	8720 ± 104	63 ± 0.9	17.2 ± 1.6	6.6 ± 1.2	5.0 ± 1.2
Negative control	7940 ± 212	54.4 ± 1.6	26.3 ± 1.4	5.0 ± 1.0	3.0 ± 2.0
LSD	810	7.8	6.9	6.8	2.8

Table -2: Spleen and liver indices of mice treated with *P. harmala* seeds water extract and Rifampicin then infected with *B. abortus*

Treatment	Spleen Index	Liver Index
Rifampicin treatment	1.005	5.73
Rifampicin treated and infected with *Brucella abortus*	2.62	6.32
P. harmala treatment	1.60	7.38
P. harmala treated and infected with *Brucella abortus*	1.90	7.65
Positive control	1.20	7.80
Negative control	1.00	5.42
LSD	0.45	0.79

Table -3: Effect of *P. harmala* seeds water extract and Rifampicin on delayed type hypersensitivity elicited in the foot pad swelling of mice treated and infected with *B. abortus*

Treatment	DTH Mean ± SD	DTH Index
Rifampicin treatment	0.32 ± 0.10	48
Rifampicin treated and infected with *Brucella abortus*	0.36 ± 0.07	53
P. harmala treatment	0.31 ± 0.03	38
P. harmala treated and infected with *Brucella abortus*	0.41 ± 0.19	82
Positive control	0.26 ± 0.15	4.2
Negative control	0.25 ± 0.04	0
LSD	0.07	

Table -4: Total Colony Count ($x10^4$) CFU/ml and prophylactic index in mice treatedwith *P. harmala* seeds water extract and Rifampicin then infected with *B. abortus*

Treatment	Mean ± SD CFU/ml	Prophylactic index
Rifampicin treatment	58.70 ± 7.9	79.75
P. harmala treatment	89.4 ± 7.5	69.17
Positive control	290 ± 3.0	
LSD	25.0	

The results of the experimental study with *P. harmala* showed immune enhancing activities for murine immune system which included multiple pathways. Among these was its ability to stimulate lymphocyte and other subset of white blood cells (Table 1). The activity of stimulation occurs by stimulating macrophages to secrete amonokines (8). In this study the results demonstrated that the spleen and liver weight were reduced to nearly normal weight when the infected animal treated with Rifampicin and *P. harmala* seed water extract. These results are in agreement with Oliveria (9) who treated mice with ribosomal vaccine.

Also the results are consistent with Mohammed (12) who treated mice infected with *Br. abortus* using Immunoferon daily, for six days .

Brucella colony enumeration in spleen (Table 4) indicated an increase in the prophylactic index in groups treated with Rifampicin and *P. harmala* water extract due to inhibitory effect of Rifampicin to DNA dependent RNA synthesis as it has bacteriocidal effect to brucellosis (13).

The increase in spleen and liver weight or size in untreated animals is correlated with proliferation of *Brucella* in the reticulo-endothelial system. Similar results were reported by Vitas *et al* (14) when treated *Brucella*_infection mice with outer membrane protein in mice.

The low level of bacterial specific delayed type hypersensivity reaction is correlated with disease progression in mice. This may be due to its ability to suppress the cellular coordination (2). While groups treated with Rifampicin and *P. harmala* expressed delayed type hypersensitivity.

This indicate that *P. harmala* extract has the ability to activate the macrophages and increase proliferation of the lymphocyte and induce a secretion of lymphokines (8).

REFERENCES

1. Young, E.J. Human brucellosis. Rev. Infect. Dis. 5:821, (1983).
2. Steven, M.G and Olsen, S.C. *in vitro* effect of live and killed *Brucella abortus* on bovine cytokines and prostaglandin E_2 production. Vet. Immunopathol. 40: 149. (1994).
3. Zhan, Y., Yang. T, and Cheers, C. Cytokines response of T-cells subset form *Brucella abortus* infected mice to soluble *Brucella* proteins. Infect Immmunol. 61:281 (1993).
4. Mosmann, T.R. and Coffman, R.L. Th1 and Th2 cells: different patterns of lymphokines secretion lead to different functional properities . Ann. Rev. Immunol. 7: 145 (1989).
5. Maggi, E.; Parronchi, P.; Manetti, R. Reciprocal regulatory effect of INF-γ and IL-4 on the *in vitro* development of human Th1 and Th2 clones. J. Immonol. 148: 2147 (1992).
6. Damerdagh, I.S. and Al-Banna, Y.M. *In vitro* activation of mouse peritoneal macrophages. Al-Mustansyria J. Sci. 10: 40 (1999).
7. Adaay, M.H.; Rashan, L.J.; Sulayman, K.D.; Al-Beer, M.A. and Ayoob, T.C. Anti microbial activity of different extracts from the seeds of *Peganum harmala* fitorerapia. 60: 363-368 (1992).
8. Al-Saadi, W.F.; Mohammed, K.I. and Al-Jewarii, M.M. Immunomodulation of visceral Leishmaniasis with Peganum harmala seed extract in mice. 5:184-190. (2006).
9. Oliveira, S.C. ; Zho, Y, and Splitter, G.A. Recombinant L7/L12 ribosomal protein and irradiated *Brucella abortus* induce. T-helper 1 subset response from murine $CD4^+$ T-Cells. Immunology. 83: 659-664 (1994).
10. Garvey, J. S.; Cemer, N. E. and Sussodorf D.H.C. Methods in immunology: A laboratory text for instruction and research, 3rd. ed. W. A. Benjamin INC, Canada: 425pp (1997).
11. Bosseray, N. Vaccine and Serum mediated protection against *Brucella* infection of mouse placenta. Brit. J. EXP. Pathol. 64:617 (1983).

12. Mohammed, K.I. Bacteriological, immunological and biochemical studies on human brucellosis. Ph.D. Thesis College of Science. Al-Mustansiriya University (1998).
13. Dizer, U.; Hayat, L.; Beker, C.M.; Corenek, L.; Ozguven, V. and Pahsa, A. The effect of doxycyline-rifampicin and Levamisole combination on Lymphocyte subgroup and function of phagocytic cells in patient with chronic brucellosis. Chemotherapy. 5: 27-31 (2005).
14. Vitas, A.I.; Diaz, R. and Gramozo, C. Protective effect of *Brucella* outer membrane Complex bearing liposome's against experimental marine Brucellosis FEMS Microbiol. 130: 231-236. (1995).

Taxonomical Study of *Populus euphratica* and *Populus nigra* Leaves

Khansaa Rashed Al-Joboury
Iraq Natural History Research Center & Museum University of Baghdad

Received 28/2/2010 – Accepted 5/10/2010

الخلاصة

أجريت هذه الدراسة لتصنيف اختلافات الأوراق بين *Populus euphratica* و *Populus nigra* . تم جمع 20 عينة من أوراق النوعين من منطقة الراشدية . درست الصفات المظهرية المتضمنة شكل الورقة، طول نصل الورقة ، عرض نصل الورقة، قمة الورقة، قاعدة الورقة، طول السويق، عرض السويق ، وتحليلات كيميائية من خلال نموذج الهجرة الكهربائية لبروتينات الأوراق . بينت النتائج أن هناك اختلافات كبيرة بين النوعين في الصفات المظهرية والتحليل الكيميائي من خلال الهجرة الكهربائية لبروتينات الأوراق اعتمادا على الوزن الجزيئي للبروتين. لذا فان طريقة الهجرة الكهربائية يمكن اعتمادها كطريقة تصنيفية جديدة خصوصا للنباتات المتشابهة شكليا.

ABSTRACT

This study was carried out to study the taxonomy (morphology and chemical analysis) leaves differences between *Populus euphratica* and *Populus nigra*. A total of 20 leave samples were collected from the Rashidiya area for both species. The phenotypic characters were studied included leaf shape , leaf blade length, leaf blade width, leaf apex , leaf base, petiole length, and chemical analysis through electrophorsis pattern leave protein.

The results indicated that there are major differences between *Populus euphratica* and *Populus nigra* in the phenotypic characteristics of the leaves and also in protein separation on gel electrophorsis according to the molecular weight of protein, so that electrophorsis pattern can be adopted as new technique for plant taxonomy especially for the similar morphologyical plant.

INTRODUCTION

Populus is a genus of deciduous trees in the the angiosperms [1] , which belongs to Salicaceae family [2] .The Populus (Poplar , Haur , Qauwagh) species includes between 25 and 35 species in six sections (Abaso , Aigeiros , Leucoides , Populus , Tacamahaca, Turanga) . These sections are considered to be natural depending on the taxonomic scheme. The species of the genus Populus is one of the most commercially exploited groups of forest trees [3]Trees with monopodial branching, buds with several scales, often viscid and blasmike . Leaves usually broad , commonly deltoid-ovate or rhombic-ovate , petioles long , often strongly compressed laterally, stipules generally inconspicuous and caduceus [4]

Populus euphratica: commn name euphrates poplar, firat poplar, salt poplar. Its a light-demanding species ecologically characterized as a pioneer, that grows during the summertime in shelter belts along riversides. [5]

Populus euphratica Olivier is known to exist in saline and arid environments [6]

Populus euphratica (Gharab) is a poplar species growing in arid regions of central asia [5] , where its distribution remains nevertheless restricted to river-banks or to areas with an access to deep water tables[7]

***Populus nigra* L.**: commn name black poplar is a tree of ecological and economic interest. It is a medium-sized to large deciduous tree, reaching 20-30 m (rarely 40 m) tall, with a trunk up to 1.5 m diameter leaves are diamond-shaped to triangular, 5-8 cm long and 6-8 cm broad [8] green on both surfaces.

The aim of this study is to investigate the different traits in the leaves between the two species: *Populus euphratica* and *Populus nigra* .

MATERIAL AND METHODS

Leaves samples: leaves of *Populus euphratica* and *Populus nigra* were collected for this study during September to November 2009 from the Rashidiya area taken from the top and bottom of the tree. (The plants grow in similar environmental conditions).

We studied the phenotypic and chemical analysis for the leaves of both species for the purpose of comparison between them, we studied the form of leaves and compare them with the form leaves for [9] Measurements are taken for each of the leaf blade length, leaf blade width, leaf apex, leaf base, petiole length according to [8], then the proteins were separated in a gel electrophorsis way.

Gel electrophoresis: gel containing 3 per cent (stacking gel) , 8.0 per cent or10 per cent acrylamide were prepared from a stock solution of 30 per cent by weight of acrylamide and 0.8 per cent by weight of N,N-bis-methyl acrylamide. The gels were polymerized chemically by the addition of 0.025 per cent by volume of tetramethyl ethylenediamine (TEMED) and ammonium persulphate . Ten cm gels were prepared in glass tubes of a total length of 15 cm and with an inside diameter of 6 mm . The stacking gels of 3 per cent acrylamide and a length of 1 cm containing 0.125 M Tris-HCL (PH 6.8) and 0.1 per cent SDS and were polymerized chemically in the same way as for the separating gel. The electrode buffer (PH 8.3) contained 0.025 M Tris and 0.192 M glycine and 0.1 per centSDS . The samples (0.2-0.3 ml.) contained the final concentration (final sample buffer) 0.0625 M Tris-HCL (PH 6.8) 2 per cent SDS , 10 per cent glycerol , 5 per cent 2- meracaptoethanol and 0.001 per cent bromophenol blue as the dy The proteins were completely dissociated by immersing the samples for 1.5 min in boiling water . Electrophores was carried out with a current of 3 mA per gel

until the bromophenol blue marker reached the bottom of the gel (about 7 h) . The protein were fixed in the gel with 50 per cent trichloroacetic acid (TCA) overnight, stained at 37 C with a 0.1 per cent Commassie brilliant blue solution made up freshly in 50 per cent TCA . The gels were diffution-destained by repeated washing in 7 per cent acetic acid according to [10]

RESULTS AND DISCUSSION

The leaves of the *Populus euphratica* are polymorphic [11]. That is different leaves on the same tree or even the same branch may have strikingly different shapes.The form of leaves are narrowly lanceolate or linear-lanceolate and willow-like (fig. 1 a and b) . This results were in the same description figured by [12], But in *Populus nigra* leaves are dark green, more or less uniformly rhomboid-ovate or deltoid (fig. 2) this similar to results showed by [8]. According to table-1 we see clear differences in the Leaf blade length which were from 6-14cm in *Populus euphratica* while in *Populus nigra* were from 5-10cm , leaf blade width were 0.5-1cm in *Populus euphratica* but in *Populus nigra* were 3-10cm , apex of the leaves in *Populus euphratica* were Acute or rounded while in *Populus nigra* Acute or acuminate , The base of the leaves in *Populus euphratica* were Cuneate or cordate but in *Populus nigra* were Cuneate or subtruncate , Petiole length in *Populus euphratica* were 2.5-5mm while in *Populus nigra* 5-6mm , Stipules length in *Populus euphratica* were 2.5-3mm but in *Populus nigra* were 5-7mm , Stipules width in *Populus euphratica* were 0.5-1mm while in *Populus nigra* were 3.5-5.5mm these values were in the same ranges Recorded by [4] [8].

Table -1 Phenotypic of *Populus euphratica* and *Populus nigra* analysis

description	*Populus euphratica*	*Populus nigra*
form	narrowly- lanceolate or linear- lanceolate	rhombic-ovate or deltoid
Leaf blade length(cm)	10* 3.30**	8* 2.06**
leaf blade width(cm)	1* 0.21**	7* 2.91**
Apex	Acute or rounded	Acute or acuminate
base	Cuneate or cordate	Cuneate or subtruncate
Petiole length(cm)	4* 1.04**	6* 0.47**
Stipules length(mm)	3* 0.24**	6* 0.82**
Stipules width(mm)	1* 0.20**	5* 0.85**

•each value are the average of 20 samples
*Average
**SD

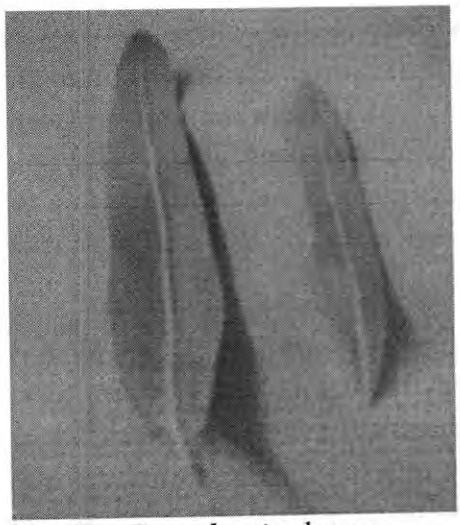

Fig -1:-a-*P. euphratica* leaves (lower leaves)

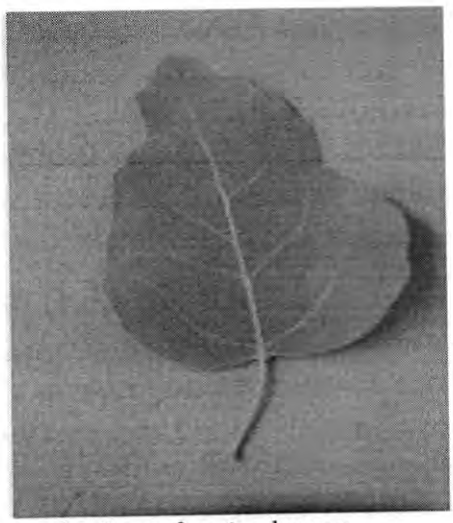

b- *P. euphratica* leaves (upper leaves)

Fig -2: *P. nigra* leaves

In the last few years botanists have shown interest in usin molecular techniques to address questions about populus biology, such as identification and relationships among populus trees. The study of genetic variation in plant species was greatly facilitated by the development of protein markers over three decades ago. [13]

There are some bands in common between all species. The phylogenetic analysis based on protein pattern, Furthermore, protien markers should be used to show the genetic structures and variations within the populations of each species .

The results showed that the separation protein by gel electrophorsis one of different Protein packages for both speciese in number and intensity according to the molecular weight of protein so this method could be used in the taxonomy of plants this similar to results of [14]

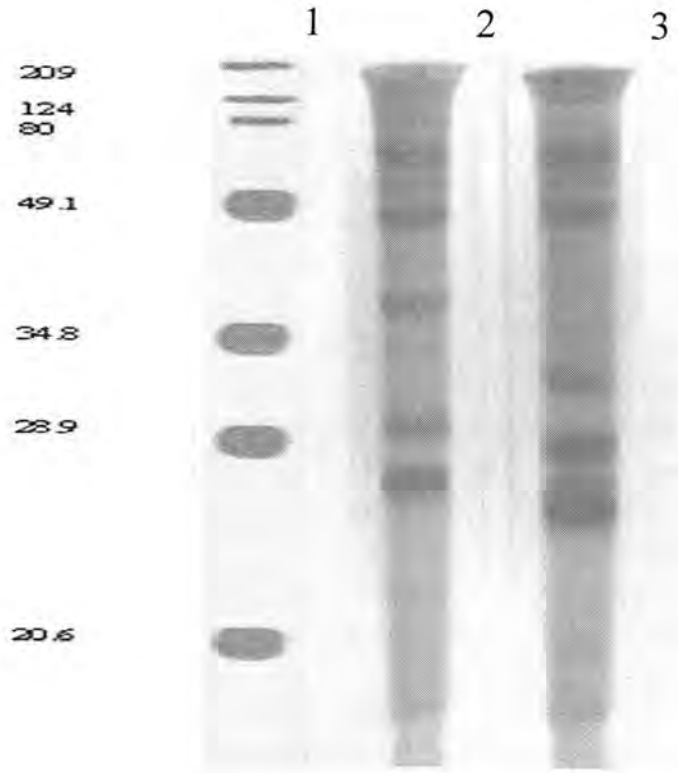

Fig.-3: Electrophoretic patterns of : 1- is a wide range molecular weight standard (from top to bottom, 209, 124, 80, 49.1, 34.8, 28.9 and 20.6 KDa) , 2- *Populus euphratica,* 3- *Populus nigra*

Based on the result of this study it can be said that gel electrophoresis is an effective way for plant taxonomy especially for the similar morphologyical plant.

REFERENCES

1. Ferreira, S. ; Batista, D. ; Serrazin, S. and Pais, M. Morphogenesis induction and organogenic nodule differentiation in *Populus euphratica* Oliv. leaf explants . Plant cell , Tissue and Organ Culture , 69(1) : 35-43 (2009) .
2. Angiosperm Phylogeny Group (APG).. An update of the Angiosperm Phylogeny Group classification for the orders and families of flowering plants: APG II. Bot. J. Lin. Soc.,141: 399-436(2003)
3. Hamzeh, M. and Dayanandan, S. of chloroplast TRNT-TRNF region and nuclear rDNA. American J. Bot., 91: 1398-1408(2004). Phylogeny of *Populus* (Salicaceae) based on nucleotide sequences
4. Townsend,C. and Guest,E. Flora of Iraq .(Vol.4,part1). Rpbert MacLehose and company Limited. Glasgow. : 244-252(1980).

5. Ferreira , S. ; Batista , D. ; Serrazina , S. and Pais , M. Proteome Profiling of *Populus euphratica* Oliv. Upon Heat Stress. Annals of Botany , 98(2): 361-377(2006).
6. Ottow, E. ; Brinker, M.; Teichmann,T.; Fritz, E.; Kaiser, W. and Brosche, M. *Populus euphratica* displays apoplastic Sodium Accumulation, Osmotic Adjustment by Decreases in Calcium and Soluble Carbohydrates, and Develops Leaf Succulence under Salt Stress . Plant Phys. , 139 : 1762-(2005).
7. Hukin,D. ; Cochard,H. ; Dreyer,E. ; Thiec, D. and Triboulot,B. Cavitation vulnerability in roots and shoots: does *Populus euphratica* Oliv., a poplar from arid areas of central asia , differ from other poplar species. J. Exp. Bot. , 56 (418) : 2003-2010(2005).
8. Ballian, D. ; Kajba , D. and Idzojtic, M. Morphological diversity of hairy european black poplar (*Populus nigra* subsp. *caudina*) in Bosnia and Herzegovina. Univ. of Banja Luka,5:13-22 (2006) .
9. الموسوي ، علي حسين عيسى . علم تصنيف النبات . مديرية دار الكتب للطباعة والنشر ، جامعة الموصل(1987).
10. Laemmli , U. Cleavage of structural proteins during the assembly of the head of bacteriophage T4 . Nature , 227: 680-685(1970) .
11. Calagari, M. ; Modirrahmati,A. and Asadi, A. Morphologic Variation in Leaf Traits of *Populus euphratica* Oliv. Natural Populations . Int. J. Agri. Biol., 8(6) : 754 – 758(2006).
12. Caixia, Z. ; Jian, Q. ; Chunning, J. ; Ning, Y.; Xiuqin, W. and Wanfu, W. Comparison of stomatal characteristics and photosynthesis of polymorphic *Populus euphratica* leaves, Frontiers of Forestry in China 2(1): 87-93(2007).
13. Loveless, M. and Hamrick,J. Ecological determinants of genetic structure in plant populations. Ann. Rev. Ecol. Syst., 15: 65–95(1984).
14. Rajora , P. Characterization of 43 *Populus nigra* L. clones representing selections, cultivars and botanical varieties based on their multilocus allozyme genotypes .Euphytica , 43(3) : 197-206 (1989) .

Local Pattern of Acute Enteric Bacterial Infection in School Students

Khalid K. Al-Bayatti[1] and Lazim H. Al-Taei[2]
[1]College of Pharmacy, University of Al-Mustansiriya
[2]Medical Laboratories,Al-Karama Teaching Hospital

Received 9/11/2009 – Accepted 20/6/2010

الخلاصة

جمعت عينات الغائط من المرضى المصابين بالإسهال الذين تتراوح أعمارهم بين 6 – 15 سنة (طلاب المرحلة الابتدائية و المرحلة المتوسطة) المراجعين للعيادة الخارجية في مستشفى الكرامة التعليمي الواقعة في منطقة الكرخ من بغداد ، خلال الأعوام 2001 و 2002 و 2003 .كان العدد الكلي للعينات التي جمعت خلال هذه الفترة 582 عينة من المصابين بالاسهال و100 عينة من غير المصابين بالاسهال (عينات سيطرة) أرسلت إلى المختبر الطبي الخاص للمستشفى لغرض التحري عن مسببات الإسهال من البكتيريا المعوية و البكتيريا الأخرى . أظهرت النتائج أن نسبة المرضى المصابين ببكتريا الإسهال خلال الاعوام2001 و 2002 و 2003 هم 9,16 % و 9,02% و 34,05% على التوالي . و كانت نسبة المرضى المصابين ببكتريا الإسهال خلال 2003 هي 4 أضعاف النسبة خلال سنوات 2001 و 2002 إن معظم أنواع البكتيريا المعزولة خلال فترة الدراسة (2001، 2003,2002) كانت E.coli و بنسبة 58,33% و 91,66% و 58,70% ، أعقبها بكتيريا Klebsiella spp. بنسبة 16,66% خلال 2001 و 20,63% خلال 2003 . أما البكتيريا المسببة للإسهال الأخرى و المعزولة فقد كانت بنسب اقل و هي Proteus spp. و Salmonella spp. و Vibrio spp. . من ناحية اخرى كانت البكتريا المعزولة من عينات السيطرة مشابهة تقريبا مع تلك المعزولة من المرضى المصابين بالاسهال ولكن بنسب اقل . ان هذه النتائج قد تسلط الضوء على زيادة نسبة التلوث في مياه الشرب أو إن إجراءات التعقيم غير كافية لماء الإسالة و التي قد تكون احدى الاسباب الرئيسية للتلوث ببكتريا الإسهال في الأطفال أو في الكبار على حد سواء في مدينة بغداد.

ABSTRACT

Stool samples were collected from out patients aged 6-15 years (primary and junior high school) attended Al-Karama hospital at Al-Karkh region of Baghdad during 3 successive years 2001, 2002, and 2003. A total of 582 samples from patients with diarrhea and 100 control samples from people of the same age were processed for Enteropathogenic bacteria. The percentage of patients with Enteropathogenic bacteria during 2001, 2002 and 2003 were 9.16%, 9.02% and 30.05% respectively. The frequency of people infected with Enteropathogenic bacteria during 2003 was four times the number in 2001 and 2002. Most of the bacterial isolates recovered were E.coli 58.33% ,91.66% and 58.70% during 2001, 2002 and 2003 respectively, followed by Klebsiella spp. 16.66% during 2001, and 20.63% during 2003, and to a less frequent other Enteropathogenic bacteria Proteus spp., Salmonlla spp. and Vibrio spp., A similar distribution but with lower rates was noted from stools of control people. These results highlights on increased contamination and/or poor purification procedure of water supply to the general public which probably was one of the main causative agent for diarrhea in Baghdad city.

INTRODUCTION

Diarrhea is responsible for high morbidity and mortality in children and adults in developing countries(1). Globally, an estimated four million children and adults die annually of infectious diarrhea (2). The

bacterial pathogen most commonly associated with endemic forms of childhood diarrhea is Escherichia coli (3) .

Reports from different parts of the world show varing frequencies of bacterial agents of diarrhea such as Salmonella, Shigella, Campylobacter, Aeromonas Escherichia coli and Yersinia spp. (4,5,6,7,8,9). In china (10) and India(11), pathogenic Escherichia coli strains were the most frequently detected pathogens in diarrhea cases, whereas in one study in Egypt(6) Campylobacter was the leading pathogen. In Nigeria, studies on bacterial etiology of diarrhea had showed a high prevalence rate for Campylobacter spp.(28%) followed by Enteropathogenic E. coli (22%), Salmonella spp.(17%), Shigella spp.(14%). Diarrheal outbreak among children in Japan suggest that a typical Enteropathogenic E. coli was significantly diarrheic pathogen. In Iraq,unfortunately no official statistics concerning cases of food-borne or water-borne diarrhea diseases in iraqi people, caused by specific strain of Enteropathogenic E.coli, or other diarrhea causing pathogenic bacteria. However, there are only some information provided by Department of instruction and public affairs, Ministry of Health, describing outbreaks of diarrhea in people under 20 years of age , especially after the year 2003, indecating that the number of diarrheal cases which was registered in Iraq was 67196 cases during 2004 while between 7th of august 2007 and 26th of september 2007, the following diarrheal cases were recorded, in Baghdad 12481 case; Kirkuk 1782 case; Sulaimaniya 906 case; Sallahddin 507 case; Messan 1000 case; Anbar 5 case; Diyalla 2 case and no data available for the rest of Iraqi cities. Most of these cases were attributed to contaminated water supply and contaminated environmental conditions. But they did not mention the bacterial etiology of diarrhea. Therefore, the purpose of this study was to determine which Gram-negative bacteria were present in stool samples obtained from primary-junior high school (6-15 years old) patients with diarrhea and control without diarrhea habitated AL-Rahmania region at AL-Karkh side of Baghdad city.

MATERIALS AND METHODS

(1). Patients and sample collection:

Stool samples were collected from outpatients, aged 6-15 years old attended Al-Karama hospital out-clinic, which is situated in Al-Karkh region of Baghdad. These patients were diagnosed by a physician as having acute diarrhea, on the bases of frequent watery stool (usually more than three times daily),lasting for less than two weeks. A large proportion of the patients also had fever, neither patients had been treated with antibiotic before sampling. Most of the patients were from low-income families probably habitated regions around Al-Karama

hospital,and were provided with tap water. And one hundred stool samples from control people of the same age were also taken from the same region. These samples were collected in clean, sterile jar and directly submitted to the medical microbiology and parasitology laboratory,at Al-Karama hospital for processing.

(2). Sample processing:

Stool samples were processed as soon as received by the laboratory, usually within few hours. For the isolation of Enteropathogens, the method described by Ogunsanya et al. (4) was employed, where faecal samples were inoculated on to the surface of MacConky agar and Eosin-Methylene blue agar (Oxoid,England), Deoxycholate citrate agar and Thiocitrate bile salt sucrose agar (Difco –Laboratories, Detroit,Michigan,USA). Specimens were also inoculated into enrichment broths such as Selenite broth, to enhance the isolation of Salmonella spp. and Shigella spp., whereas alkaline peptone water pH 8.6 was employed for the enrichment of Vibrio cholera. Selenite broth cultures were subcultured on Deoxycholate citrate agar and S.S agar, whereas pepton water broth was subcultured on to thiocitrate bile salt-sucrose agar and deoxycholate citrate agar. All inoculated media (enriched and subcultured) were incubated at 37°C for 24h. Biochemical tests (12) were employed for definitive identification of Enteropathogenic E. coli. And Klebsiella spp. were identified as described by (13). For isolation of Proteus spp.,the method described by (14) was employed, fecal samples were inoculated on MacConkey agar and blood agar and incubated at 37°C for 24h., colonies of Proteus spp. were identified according to the color and swarming features of the colonies on blood agar and inability to ferment lactose on MacConkey agar, motility test also done (15) for further confirmation.

(3). Antibiotic sensitivity test:

Antibiotic susceptibility testing were done for each bacterial species isolated from faecal samples according to the method described by (17). The following antibiotic discs were used. Ampicillin, Tobramycin, Amikacin, Co-Trimoxazol, Tetracyclin, Gentamycin, Chloramphenicol , Cefotaxim and Neomycin.

RESULTS AND DISCUSSION

Faecal samples were obtained from 131 patients with diarrhea during 2001,and 266 patients during 2002 and 185 patients during 2003. These patients which were 6-15 years old (primary and junior-high school) attended outpatient clinic and diagnosed by physician as having acute diarrhea. And most probably reside in the AL_Rahmania region around Al-Karama hospital.

The number of patients with Enteropathogenic bacteria were 12 (9.16%) in 2001 and 24 (9.02%) in 2002 and 63 (34.05%) during 2003 Table(1). The frequency of people infected with Enteropathogenic bacteria in 2003 almost 4 times the numbers in 2001 and 2002.

Table (2) shows the percentages of the pathogenic bacterial species isolated from faecal samples of patients with acute diarrhea during the years 2001,2002 and 2003. A total of 12 faecal bacterial pathogen were recovered, of which 7 isolates (58.33%) were identified as E. coli during 2001 and 24 isolates of which 22 (91.66%) were E. coli during 2002 and 63 isolates of which 37 (58.70%) were E. coli during 2003. The other bacterial pathogens recovered were Klebsiella spp.with percentages of (16.60%) and (20.60%) during 2001 and 2003 respectively, while for Salmonella Spp. were (8.30%) and (20.00%) during 2002 and 2003 respectively. Very small proportion (1.59%) was recovered for Proteus spp. during 2003 only. For Vibrio spp.only 3 isolates (25.00%) were recovered during 2001, but not for the rest of the study period. On the other hand, 100 stool samples from non-diarrheal people as control were also screened for prevalence of bacteria Table (3). The following bacterial species and their relative percentages were recorded in the control specimens, E.coli 72% , Enteropathogenic E. coli 18% , Klebsiella aeruginosa 2%, Salmonella typhimurium 1%, Salmonella paratyphi 1% Salmonella spp. 3%, Shigella spp. 1%, Pseudomonas spp. 1% and Serratia spp. 1% but no Proteus spp. or Vibrio spp.were found in control specimen. In comparing the differences between the rate of distribution of various enteric pathogens associated with diarrhea, Klebsiella spp. and Salmonella spp. comprises the most frequently encountered Enteropathogens associated with diarrhea cases during the period of the study in comparison with control rate for the same bacteria which were 2% and 5% respectively. Whereas Enteropathogenic E. coli remain the predominant enteric bacteria in both the diarrheal cases and control, while Proteus spp. and Vibrio spp.were partially detected in some diarrhea cases than in control. These results might indicate a possible association of Klebsiella spp. and Salmonella spp. with diarrhea cases in the AL-Rahmania region and probably in Baghdad city.

The results reported in this study implicate E. coli, as the most frequently encountered Enteropathogen associated with diarrhea case , this was followed in decreasing frequencies by Klebsiella spp, Salmonella spp. and least for Proteus spp. and Vibrio spp.and these results agree with Obi et al. (16),where they recorded the following percentages of diarrhea cases in urban areas of Nigeria, a high prevalence rate for Campylobacter spp. 28%, followed by Enteropathogenic E. coli 22%, Salmonella spp. 17%, Shigella spp. 14%,

Aeromonas spp. 5% and Yersinia enterocolitica 4%, whereas in rural areas E. coli was the most frequently encountered pathogen 18% and Plesiomonas shigelloides 8% and the similar rates was noted for control in both urban and rural areas of Nigeria.

The results obtained in this study did not reflect in any way statistically the actual frequency of diarrhea cases in Iraq or even in Baghdad city. We are unaware of any report on the distribution of these Enteric microorganisms among diarrhea cases in Baghdad city or in Iraq.

Our data clearly reveal the possible association of the potential pathogens E. coli, Klebsiella spp.and Salmonella spp.. with diarrhea in regions of the study.These seemingly high isolation rates observed for E. coli and Klebsiella spp. and Salmonella spp. could be related to environmentally acquired isolates from consumption of contaminated water, and there are probably a direct association between drinking of tap water and the occurance of chronic Gastroenteritis in adults and acute Gastroenteritis in children due to the Enteropathogenic bacteria specially E. coli. It is interesting to note that the isolation rates of all the pathogen encountered in this study were observed to be independent of age of the patients.

With respect to antibiotic susceptibility testing, the antibiotic sensitivity disc test was done to each positive isolate on differential media of different bacterial species .The results showed that most E. coli, Klebsiella spp., Salmonella spp., and Proteus spp. were almost 100% sensitive to Tobramycin,Gentamycin, Neumycine , Amikacin and Cifotaxim, whereas most isolates of these bacteria were shown to be resistant to Ampicillin in varing proportions, E. coli (68%), Klebsiella spp. (50%), Salmonella spp. (67%), and Proteus spp. (33%).

The study conclude that the potential pathogens which could be a causative agents of diarrhea in the study area or in Baghdad city could be a gram-negative bacteria, and that the frequency of isolation of gram-negative pathogen probably is changing with time , and possibly another group of potential pathogens were emerged, but this does not exclude involvement of other etiological agents such as parasites or viral agents. We, therefore, recommend further study to determine the extent of involvement of Enteropathogenic species as potential pathogen, and a continuing search for other possible potential bacterial agents of diarrhea that have not been previously reported in Iraq.

Table-1: Percentage of patients infected with Enteropathogenic bacteria during the years 2001,2002 and 2003 .

Year	No. of patients with Enteropathogenic bacteria	Total no. of patients with diarrhea	%of infected patients with respect to total no. of patients with diarrhea
2001	12	131	9.16
2002	24	266	9.02
2003	63	185	34.05
Total	99	582	17.01

Table -2: Percentage of the bacterial isolates from diarrhea patients During the years 2001, 2002 and 2003.

Species	No. of bacterial isolates during					
	2001		2002		2003	
	No.	%	No.	%	No.	%
E.coli	7	58.33	22	91.66	37	58.7
Klebsiella spp.	2	16.66	0	0	13	20.7
Proteus spp.	0	0	0	0	1	1.59
Salmonella spp.	0	0	2	8.33	12	19.05
Vibrio spp.	3	25	0	0	0	0
Total no. of isolates	12	100%	24	100%	63	100%

Table -3: Percentage of bacterial isolates from control stool specimens (without diarrhea).

Bacterial Species	No. of bacterial isolates	%
E. coli*	90	90
Klebsiella aeruginosa	2	2
Proteus spp.	0	0
Salmonella spp.**	5	5
Vibrio spp.	0	0
Shigella spp.	1	1
Serratia spp.	1	1
Pseudomonas spp.	1	1
Total number of isolates	100	100

Note:
* E. coli species include 72% E.coli and 18% Enteropathogenic E.coli .
** Salmonella spp. include 1% Salmonella typhimurium, 1% Salmonella paratyphi. and 3% Salmonella spp.

REFERENCES

1. Guerrant, R.L., J.M. Hughes, N.L.,Lima, and J. Crane. Diarrhea in developed and developing countries,magnitude, special setting, and etiologies. Rev. Infec. Dis. 12 (suppl. 1): S 41- S 50(1990).
2. Synder, J. D and Merson M.H. The magnitude of te problem of acute diarrheal diseases: A review on active surveillance data. Bull WHO: 60, 605-613(1980).
3. Huilan,S., L.G. Zhen, M.M. mathan, M.M. Mathew, J. Olarte ,R. Espejo, U. Khin Maung, M. A. Ghafoor , M. A. Khan, Z.Sami, and R. G, Sutton Etioloy of acute diarrhea among children in developing countries: a multicenter study in five countries. Bull.WHO. 69: 549-555 (Medline)(1991).
4. Ogunsanya, T.I.,Rotimi, V. O. and Adenuga, A.A,. A study of the etiological agent of childhood diarrhea in Lagos, Nigeria . J. Med. Microbiol. 40: 10-14(1994).
5. Blum, D. and Dosunmu- Ounbi O. In: Abstract of the 3rd- International Epidemiology Association:36(1986).
6. Pazzaglia, G., Bourgeois, A. L., Araby, I., Mikhail, I., Podgore, J. K., and Mourad A. Campylobacter associated diarrhea in Egyptian infants : Epidemiology and clinical symptoms of disease and high frequency of concomitant infection. J. Diarrheal Dis. Res : 11: 6-13(1993).
7. Moyer, N. P., Clinical significance of Aeromonas species isolated from patients with diarrhea. J Clin. Microbiol. 25: 189-193(1987).
8. Mitra, A. K., Kabir, I, and Hossain, M.A. ,Pivmecillinam resistant Shigella dysenteriae infection in Bangladesh .Lancet: 335: 1461-1462(1990).
9. Demol, P. and Bosmans E. , Campylobacter enteritis in central Africa. Lancet: 1: 604(1978).
10. Kain K. C. Berttluk, R. L. , Kelly, M. T. , Xin, H., Hua, G. D., Yuan, G., Procter, E. M.,Byrne, S.and Stinger, G. Etiology of childhood diarrhea in Beijing, China, J. Clin. Microbiol. 29: 90-95(1987).
11. Joseph, T. The isolation rates of pathogenic bacteria from stools of gastroenteritis patients. Ind. Microbiol. 25: 189-193(1987).
12. Yatsuyanagi , J., Saito,S. Sato, H., Miyajima. Y., Amano, K. I. and Enomoto, K. Characterization of enteropathogenic and enteroaggregative Escherichia coli isolated from diarrheal outbreaks. J. Clinical Microbiol. Vol. 40 no.1 :294-297(2002).

13. Alabi, S. A. and Odugbemi,T.O., Occurance of Aeromonas species and Plesiomonas shigelloides in patients with and without diarrhea in Lagos, Nigeria. . Med. Microbiol: 32: 45-48(1990).
14. Al-Izee , A. M.M. Study the relationship between Proticine production and motion of Proteus spp. isolated from patients and some biological characters. M. Sc. Thesis Department of Biology, College of Science, Al-Mustansiriya University(2008).
15. Roger,K. L., Annic, G., Harold, C. T., Rod, N. and Lue, R. B. Differential expression of nonagglutinating fimbriae and MR/P pilli swarming colonies of Proteus mirabilis, J. Bacteriol. 81: 3220-3225(1999).
16. Obi, C. L., Coker, A. O., Epoke, J and Ndip, R. N. Enteric bacterial pathogens in stools of residents of urban and rural regions in Nigeria : A comparison of patients with and without diarrhea and controls without diarrhea. J. Diarrhoeal Dis.Res. Dec; 15 (4) 241-247(1997).
17. National Committee on Clinical Laboratory Standard (NCCLS) , Method for dilution antimicrobial susceptibility tests for bacteria that grow aerobically, 8th edition NCCLS document M7-A5. Wayne, Pa. USA(2002).

Accumulation Effect of Pb and Cd on Green Alga *Cladophora crispata*

Ahmed Shaker Abdul Jabbar
Thi Qar University, College of Science Dept. of Biology

Received 12/3/2009 – Accepted 5/10/2010

الخلاصة

أستخدم الطحلب الأخضر الخيطي *Cladophera Crispata* لدراسة سمية (تراكم بعض العناصر الثقيلة، الرصاص والكادميوم) وتحت الظروف المختبرية المثالية. ثبطت تراكيز العناصر المستخدمة (5، 10، 20 و 40 ملغم/ لتر) و (0.5، 1، 2 و4 ملغم/ لتر) ، للرصاص والكادميوم على التوالي معدل نمو الطحلب وبمستويات مختلفة وأزداد التثبيط بزيادة التراكيز المضافة وفترة القياس وكان الكادميوم أكثر سمية من الرصاص. وأختلف تراكم أيونات العناصر المضافة في أنسجة الطحلب بإختلاف التراكيز المضافة وفترة القياس حيث إزداد معدل التراكم لكلا العنصرين بزيادة فترة القياس وكان أعلى معدل للتراكم 105.11 ملغم رصاص / لتر و 121.65 ملغم كادميوم / لتر.

ABSTRACT

The toxicity and accumulation of the heavy metals, Lead and Cadmium in a common filamentous green alga, *Cladophora crispata*. were studied. These algae were cultured in a modified Chu-No.10 medium, which was supplemented with 5, 10, 20 and 40 mg/l of lead and 0.5, 1, 2 and 4 mg/l of cadmium.

Growth rate of alga Sp. inhibited by metals concentration when the exposure time and concentration were increased. Cadmium was more toxic than lead. The accumulation study showed that there was significant 121.65ppm for cadmium and 105.11 ppm for lead increase of metal level in algal tissue when the exposure time and concentration were increased.

INTRODUCTION

Chlorophyta, commonly known as green algae, are responsible for most of the primary productivities in some water bodies. They subsist on inorganic nutrient and produce organic matter from Carbon dioxide by photosynthesis. In the absence of photosynthesis, the metabolic process consumes oxygen, causing oxygen depletion in the aquatic system [1].

The role of algae in waste water treatment and their affinity for heavy metal captions, based on high negative surface charge, has been recognized for several decades [2].

Algae accumulate heavy metals from their aquatic environment. Using living algae to remove toxic metals from contaminated water could be advantageous, since they are ubiquitous and have colonized almost all parts of the world. They can be grown easily have very simple growth requirements. Advantage of using living organisms over dead biomass is that they have fast growth rates and hence produce a regenerating supply of metal-removal material [3]. There is evidence

that algae accumulate heavy metals in their tissues when grow in polluted water [4, 5].

The cell wall of alga consists of chitin, lipids, polysaccharides and proteins; these macro molecules provide different functional groups such as thioether, carboxyl, imidazole, hydroxyl, carbonyl, phosphate and phenolic which can form coordination complexes with heavy metals. *Cladophora* Sp. has a branched filamentous structure and its chitin, pectose and cellulose and these constituents provide functional groups, as mentioned above, capable of binding various heavy metals [6]. This work aimed to study accumulation of Pb and Cd and their toxicities to *Cladophera crispata*.

Therefore, *Cladophera* Sp. is generally considered as the proper bioindicator of heavy metals in aquatic bodies [7, 8].

MATERIALS AND METHODS

The experiments were carried out in laboratory at the Department of biology, collage of science, University of Thi-Qar.in October 2008.

True branched green alga *Cladophora crispata* was collected from one of Abu Al-Kaseeb Rivers in Basra city, southern Iraq. Isolation and identification is according to Smith and Prescott [9, 10], while purification and mass culturing of the alga is according carried out according to Stein [11] and modified by Weideman [12]. Grown axenically in a modified Chu-No.10 medium in the laboratory under controlled conditions (27 ± 2 C°, 72 M^{-2} S^{-1} supplied cool white fluorescent tubes with photoperiod of 14: 10 light and dark cycle, PH 7.5)

The modified Chu-No.10 medium was supplemented with five nominal concentrations of Pb prepared from $Pb(NS_3)_2$ (5, 10, 20 and 40 mg/l) and Cd prepared from $CdCl_2$ (0.5, 1, 2 and 4 mg/l). Algae cultured in the nutrient medium without heavy metals served as controls. All experiments were performed in triplicate.

Total chlorophyll content was determined by the absorption spectra of algal extract in the spectrophotometer according to the methods described by Arnon [13] and McKinney [14]. Total accumulations of Pb and Cd in algae were determined using a flame atomic absorption spectrophotometer [15].

RESULTS AND DISCUSSION

The effect of Pb and Cd on growth rate of alga at different concentrations and exposure times are shown in figures (1) and (2) respectively. Low concentration of Pb (5 and 10 ppm) inhibited growth rate after 10 days of measurement, however, at concentrations higher

than 10 ppm, the species could not longer withstand exposure to Pb^{++}. On other hand, Cd^{++} had an adverse effect on growth even at very low concentration (0.5 ppm); furthermore, inhibitions caused by Cd^{++} were considerably higher than those of Pb^{++} at all concentrations. The highest inhibitions of Pb^{++} and Cd^{++} were observed after 8 days of experiments. Cd^{++} has an acute effect on growth rate and more toxic to alga than Pb^{++}.

The metals Pb and Cd accumulation by *Cladophora* Sp. at different concentrations and exposure times are shown in tables (1) and (2) respectively. There were significant increases of metals algal tissue when the exposure time and metal concentration were increased. Removal of metals from the solution by alga was high during the first days of incubation, followed by a gradual reduction. Percentage of Pb^{++} accumulation was higher than that of Cd^{++} at all concentrations. The maximum accumulations were 105.11 mg/l and 121.65 mg/l for Pb and Cd, respectively, after 10 days.

In the present study, the relative growth rate of alga exposed to Pb and Cd decreased significantly when the exposure time and metal concentration were increased. Roaa [16] studied the Pb influence on specific growth rate of *Chlorella vulgaris*. She found that high Pb concentrations (75-100 ppm) in the media significantly inhibited the growth rate of *Chlorella* Sp. under laboratory conditions. This might due to the fact that Pb induces the activity of the enzyme peroxidase that is involved in the degradation of indole acetic acid (IAA), the hormone which stimulates plant growth and multiplication.

Several studies have reported on the effect of different Cd concentrations and algal growth. Ronbanchob et al, [17] studied the heavy metals on the green alga *Caulerp lentillifera* and they found that the toxicity of all the observed parameters increased with the concentration of the heavy metals in the cultivation medium. Arunakumara et al, [18] reported that Cd had slight inhibitory effect on algal growth at low concentration (0.1 ppm).

The growth rate of *Cladophera Sp.* significantly decreased when the exposure time and Pb and Cd concentrations increased. Pb and Cd at high concentrations destroyed chloroplast of the alga, as shown in the toxicity study. It is known that Cd causes disorganization of chloroplasts leading a reduction of the photosynthetic pigments and both metals inhibit chlorophyll, leading to lower chlorophyll contents [19].

Algae have the potential to accumulate metals in their tissues. The results revealed that, under the experimental conditions, the accumulation of the metals by alga was increased when the exposure time and metal concentration is increased. Roaa [16], found that the

amount of Cd and Pb accumulated by *Chlorella Sp.* was dependent on the external metal concentration, with increasing metal concentration. Metals that penetrate into the algal cell eventually compete for protein-binding sites, active enzymes and several biological reactive groups. Interrupting the routine metabolic processes [20]. In case of Pb, membrane damage in particular thylakoids causing poor carbon assimilation seemed to be a major contributor to growth rate inhibition. However, as reported by Vymazal [21].

In the present study, *Cladophera Sp.* accumulated Cd and Pb to the highest concentration in the 12th day 105.11 mg lg and 121.65 mg lg for each metal, respectively. Several studies have founded those high levels of metal accumulation. *Scendesmus Sp.* can accumulate 11.983 mg /l Pb and 0.017 mg /l Cd, respectively [22]. *Chlorella* also accumulates 5.22 mg lg and 0.421 mg lg for Pb and Cd, respectively [16].

Table -1: Accumulation of Lead concentration (mg/l) in cell of *Cladophora* sp., mean ± SD.

Treatment, Conc. (mg/l)	Time (day)			
	5	10	15	20
control	–	–	–	–
5	15.24 ± 0.54	14.33 ± 0.31	13.91 ± 0.19	14.65 ± 0.51
10	29.16 ± 2.03	27.96 ± 0.76	26.83 ± 0.61	27.13 ± 0.79
20	58.73 ± 2.66	57.45 ± 2.86	68.12 ±0.22	76.12 ± 0.93
40	93.68 ± 4.95	93.37 ± 0.51	98.84 ± 4.48	105.11 ± 0.81

Table -2: Accumulation of Cadmium concentration (mg/l) in cell of *Cladophora* sp., mean ± SD.

Treatment, Conc. (mg/l)	Time (day)			
	5	10	15	20
control	–	–	–	–
0.5	22.12 ± 0.17	21.19 ± 0.14	20.75 ± 0.92	21.19 ± 0.61
1	27.78 ± 0.02	29.31 ± 0.71	31.24 ± 0.70	36.23 ± 0.73
2	46.42 ± 3.09	57.82 ± 3.23	67.18 ±1.75	87.46 ± 1.68
4	75.28 ± 1.123	91.62 ± 1.06	102.15 ± 1.89	121.65 ± 4.53

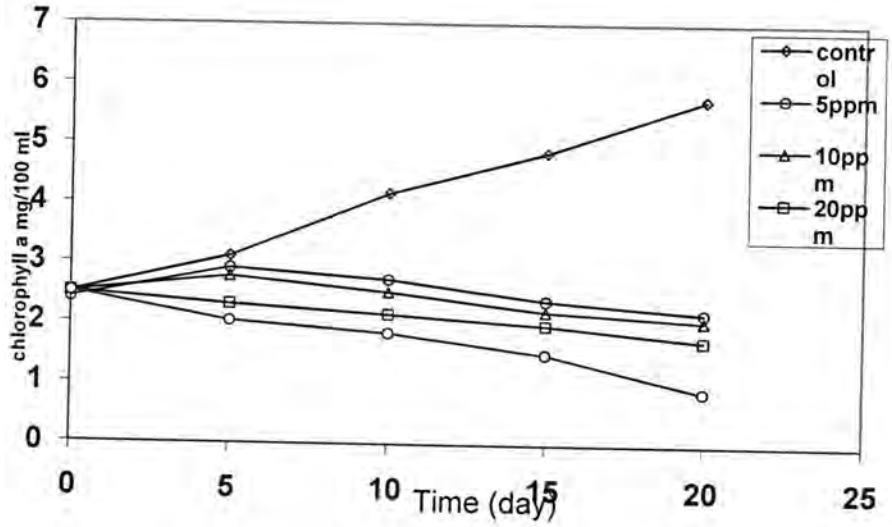

Figure -1: Effect of different concentrations of Lead in nutrient media on growth of *Cladophora* sp.

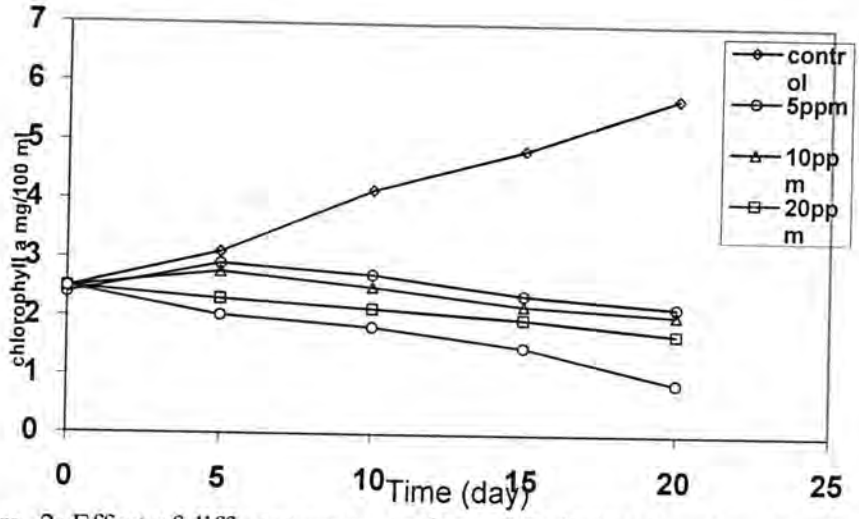

Figure -2: Effect of different concentrations of Cadmium in nutrient media on growth of *Cladophora* sp.

REFERENCES

1. Forstner U. and Prosi F. "Heavy metals pollution in freshwater ecosystems". In: O. Ravera (Ed). Biological aspects of freshwater pollution, Pergamon press, Oxford, New York, pp: 129-161(1979).
2. Rao S. Adaptation of algae to heavy metals toxicity.Int.J. Environ. Studies 27, 210-223 (1986).
3. Sobhan R. and Sternberg S. P. "Heavy metals removal by using *Cladophora*". Sp. Environ sci health part A 34, 53-72(1999).
4. Kim Y., Park J. Yoo J. and Kwak J. "Removal of Lead using ranthated marine brown alga, *Undaria Pinnatifia*". Process Biochem 34, 647-52(1999).

Serum samples collected in the study were taken from each patient and stored at (-20° C) until testing for detection specific antibody against *C.pneumonia*, the *C.pneumonia* IgM antibody was detected by (ELISA), LAB SYSTEM, FINLAND.

RESULTS AND DISCUTION

According to serological test, a total of (18) of the (96) COPD patients were infected by *C.pneumonia* .
Table (1) show the high percent in age group (70-79) year and reach peak in age group (80-89) year.

Table -1: Distribution of patients with *C .pneumonia* infection according to the age groups

Age group	Patients No.	Patients %
40-49	2	11
50-59	3	17
60-69	2	11
70-79	5	28
80-89	6	33
Total	18	100

Current cigarette smokers were more likely to have sub many infection due to *C.pneumonia* .These associations are showed in table (2).

Table – 2: Impact of cigarette smoking and co- morbidity condition.

Co morbid Condition	Proportion of patients with morbid condition%
Cigarette Smoker	16
Pulmonary Infection	2
Asthma	4
Diabetes Mellitus	2

By comparing the mean titers of IgM anti *C.pneumonia* antibodies with the control group, this study proved that there is a related difference in the distribution of there antibodies were noted in fig (1).

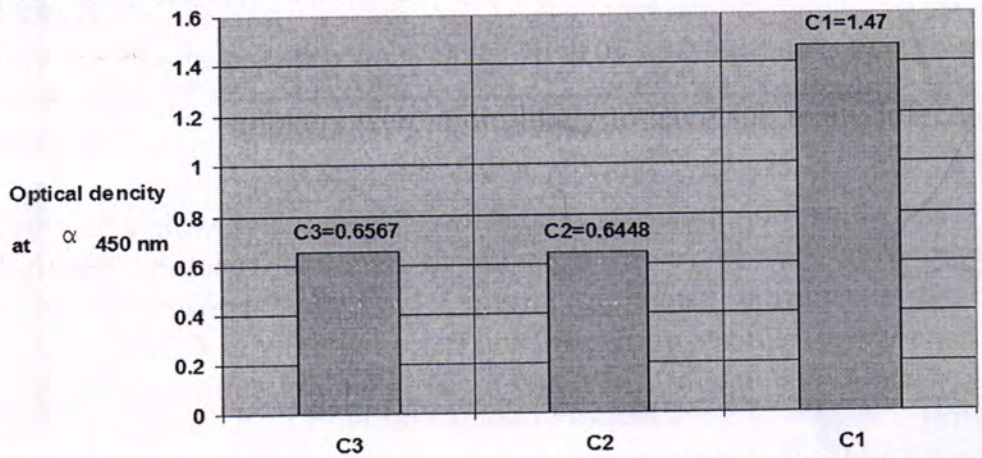

Figure -1:Percentage distribution of samples obtained in patient in COPD Disease

Fig. -1: Titer of IgM anti *C.Pneumonia* in the patients and control groups
C1- Positive patients with *C.pneumonia* infection.
C2- Control group.
C3- Negative patients.

The Fig. (1) Shows the high mean titer (at pressed as O.D.) of IgM anti *C.pneumonia* antibodies in C1 group (1.4700). As compared with C2 group & C3 group Frequency (0.6448) and (0.6567).

Among patients with COPD disease, *C.pneumonia* was detected in (20%), this study in agreement with other study, who reported that *C.pneumonia* was identified in (24%) among COPD patient (4).

Results of the present study slightly lower than study done by Principi *et al* 2001,

who found a high prevalence (40%) among COPD (5), also another study found a

low percent (12.5%), complied with diagnostic of acute *C.pneumoniae* infection in COPD patients (6).

The seroprevalence mean titer of *C.pneumoniae* IgM antibodies were higher in (COPD) patients than control. Lieberman *et al*.2001 showed an association between

C.pneumoniae serology, determined by a commercial immuno -assay and (COPD) exacerbation (7). The present study revealed that *C.pneumoniae* infection was increased with increase age and higher percent of infection detected at age (80-89) years, the results also in agreement with Gorden, 2000 (8), but disagreement with american thoracic society, suggested that *C.pneumoniae* was not common in the elderly patient (9).

Current cigarette smoking had the higher rate of infection with *C.pneumoniae*. Smoking is well known important risk factor for COPD patients through alteration in mechanisms of the host defense system (10). In the present study, there was association found between smoking and *C.pneumoniae* infection, the results are in contract to Ruiz *et al* study 1999 which reported that there was no association between the current cigarette smoking and infection due to atypical bacterial pathogens especially *C.pneumonia* (11).

In conclusion *C.pneumoniae* infection is reported in high percent in COPD patients, Co-morbid pulmonary diseases and current cigarette smoking were also associated with *C.pneumoniae* infection.

REFERENCES

1- Barnes PJ;"Chronic obstructive pulmonary disease"N. Engl J med, 343(4):269-280(2000).
2- Murray CJ, Lopez AD.' Alternative Projections of mortality and disability by cause 1990-2020: Global Burden of disease study". Lancet, 349(9064): 1498-1504 (1997).
3- Seth: JM, Rochester CL"Somking and chronic obstructive pulmonary disease". Clin Chest MED, 21(1):67-86, (2000).
4- Marek S.,Richard L, Astrid P, Syivia C,Dennis K."Smoking, season, and detection of *Chlamydia pneumoniae* DNA in clinically stable COPD Patients". BMC Infectious Disease, 2:12:10.1186/1471-2334-2-12(2002).
5- Principi, N.; Esposito, S.; Blasi, F.; Allegea, L.Role of Mycoplasma Pneumonia and *Chlamydia Pneumonia* in children with community-acquired lower respiratory tract infection. Clinic. Infect .Dis.32:1281-9(2001).
6- Charles H, Max C. and James B."*Chlamydia Pneumania* in Community- acquired Pneumonia".Journal of infection:45,3,135-138(2009).
7- Lieberman D,Ben-Yaakov M,Lazarovich Z,Ohana B,Boldur I."Chlamydia pulmonary Disease: Analysis of 250 Hospitaliztion"Eur.J.Clin.Microbiol.Infect.Dis. 20:698-704 (2001).
8- Gordon, RC.2.Community-acquired pneumonia adolescents. Adolescent Medicine: State of the Art Reviews.11,3:681-692,(2000).
9- American Thoracic society. Guidelines for the management of adults with community-acquired pneumonia. Am.J.Respir. Crit. Care. Med.163:1730-1754(2001).
10- Straus, W.L.J.F. Plouffe,T.M.J. Hackman,S.J. Salstrom,R.F. Benson, R.F. and the Ohio Legionnaires Disease Group. Risk Factors for domestic acquision of Legionnaires disease. Arch. Intern.Med.156: 1685-1692(1996).
11- Ruiz,M.;Ewig,S.; Marcos,MA.;Martinez,JA.;Arancibia,F.: Mensa, J.;Torres,A.Etiology of community-acquired pneumonia impact of age,comorbidity and severity.Am.J.Respir .Crit .Care .Med. 160:397-405(1999).

Sustained Release of Fluoride from Fluoridated Muco-adhesive Oral Tablets in Saliva

Omar J. Abdul Hassan Alsareff
Dept. of Basic Science, College of Dentistry University of Al Mustansiryia

Received 22/3/2010 – Accepted 20/6/2010

الخلاصة

تم تحضير حبوب تحتوي 2 ملغم صوديوم فلورايد مع هيدروكسي كاربوكسي مثيل سليلوز وكاربوبول 934 ومغنيسيوم ستياريت ومانيتول بنسب مختلفة لجعلها لاصقة في الاغشية المخاطية وتمديد الفترة الزمنية لتحرر الفلورايد منها داخل الفم لاطول فترة زمنية ممكنة. انجزت الحبوب اللاصقة في الاغشية المخاطية بالخلط المباشر للصوديوم فلورايد مع هيدروكسي كاربوكسي مثيل سليلوز وكاربوبول 934 ومغنيسيوم ستياريت ومانيتول. وبعد ذلك تم ضغطها بماكنة احادية القالب. تم اعطاء الحبوب الحاوية على 2 ملغم فلوريد الصوديوم الى (22) متطوعا بالغا من الذكور والاناث تتراوح اعمارهم بين 35-55 سنة ومعدل اوزانهم بين (65- 90) كغم حيث لم يتناولوا اي طعام لمدة ساعتين والاكتفاء بالماء فقط. وبعد ذالك تم وضع الحبة على الاغشية المخاطية (في الدهليز الشفوي الفكي) تحت الشفة السفلى ولمدة (8) ساعة. وقد تم تحديد تركيز الفلورايد في اللعاب بأوقات مختلفة بالطريقة المباشرة. لوحظ المظهر الطبيعي للاغشية المخاطية للفم قبل وبعد تماس الحبة وتبين أنها مقبولة من قبل المتطوعين، وان النسبة المئوية للفلورايد في اللعاب هي من التركيز الكلي للحبة الحاوية على 2 ملغم من الفلورايد. ولا توجد فروقات احصائية بين تراكيز الفلورايد المتحرر في اللعاب ($P > 0.05$). في هذا البحث وجد تحرر واسع للفلورايد في اللعاب من الحبة اللاصقة في الاغشية المخاطية حيث بلغ 40 % من الفلورايد في الساعتين 1 ، 2 ولوحظ ايضا التحرر البطيء للفلورايد بلغ حوالي 60 % من الفلورايد في 6 ساعات المتبقية وهذا يعني وجود الفلورايد في اللعاب لمدة (8) ساعات.

ABSTRACT

To prepare Muco-adhesive tablets containing sodium fluoride (2 mg), hydroxypropyl methylcellulose HPMC, Carbopol - 934, and manitol, by different ratio to obtain controlled and sustained release of fluoride in saliva from the tablet and to be evaluated *in vivo*. Muco-adhesive tablets have achieved by direct mixing of sodium fluoride, hydroxypropyl methylcellulose HPMC, Carbapol - 934, magnesium stearate, and manitol, then the mixture was compressed in a single-punch machine. The assays were carried out on 22 healthy adult males and females volunteers aged 35-55 years and their mean weight 65-90 kg the subject were instructed not to eat 2 hours before the administration of tablet except water. The tablet was placed on the mucous membrane of the mouth (Maxillary or mandibular labial vestibule) inside the lower lip for 8 hour. The concentration of fluoride in saliva was determined after different periods. Fluoride was estimated by the direct method. The result show that typical appearance of intact human oral mucosa was seen before and after contact with the tablet. The tablet taste was accepted by the volunteers. The percent concentration of fluoride in saliva calculated from the total amount of fluoride in the muco-adhesive tablet which containing 2 mg. There was no statistical differences between fluoride concentration in saliva individuals ($P > 0.05$). In conclusion, the Immediate release of fluoride from muco-adhesive fluoride tablets was over 40% of the drug in first (2) hours, There was fluoride in saliva during the 8 hours.

INTRODUCTION

The muco-adhesive drug delivery systems have been developed basically to increase the retention of drug in the oral cavity and or to keep a sustained release of drug towards the medium from where it is

constantly removed (1, 2). Different muco-adhesive pharmaceutical dosage forms containing nystatin, (3) miconazole (4), and fungicidal agents (5) has been reported. Similar systems have also been proposed to treat other buccal affections such as periodontitis (6, 7) or to supply the buccal environment with flour supplement. (8)This kind of drug delivery system very useful for the treatment of buccal diseases among which oral candidiosis is one of the most important (9). The clinical treatment of this pathology using conventional pharmaceutical dosage forms such as solutions, gels, suspensions, and mouthwashes is usually not very effective, mainly because drugs are quickly removed from the oral cavity. The dental caries which is a multifactorial disease and one of the main public health problems is usually prevented by fluoride. The strategy for designing muco-adhesives is based principally on the utilization of polymers with suitable physicochemical properties, such as polyacrylic acid (carbomer [CB]) and cellulose derivatives (hydroxypropyl methylcellulose [HPMC]) the formulations showed no evidence of interaction between the drug and polymers (1, 10, 11,). study revealed that the drug is in crystalline form in the polymer matrix. The results indicate that suitable bio-adhesive buccal tablets with desired permeability could be prepared. (12) HPMC and Carbopol 934 in a muco-adhesive delivery has been reported to improve the muco-adhesiveness of the combined system(13). Perez Marcos et al., studied the potential of combining Carbopol 974 P and HPMC K4M using propranolol hydrochloride as a model drug and found that the amount of water imbibed in Carbopol was lower than that by HPMC alone or 1:1 mixture of two polymers. HPMC and CP934 were added extra granularly without exposing the polymers to granulation fluid for compaction purpose so the HPMC permit the diffusion of drug from the matrix (14). Carbopol 934 is readily absorb water, get hydrated and swell. In addition to its hydrophilic nature, its cross-linked structure and its essentially insolubility in water makes Carbopol a potential candidate for use in controlled release drug delivery system (15). The Carbopol polymers produce tablets of excellent hardness and low friability.

These polymers can be successfully formulated into a variety of different tablet forms, including the traditional swallowable tablets, chewable tablets, buccal tablets, sublingual tablets, effervescent tablets, and suppositories providing controlled-release properties as well as good binding characteristics (16). Tablet formulations using Carbopol polymers have demonstrated zero-order and near zero-order release kinetics (17).

The aim of this work was to design of a muco-adhesive tablet containing 2 mg sodium fluoride and hydroxypropyl methylcellulose

(HPMC) and Carbopol 934 for sustained release controlled amounts of fluoride in oral cavity for a long time to treat a dental caries.

MATERIALS AND METHOD

This work achieved by cooperation between college of Pharmacy, University of Baghdad and college of Dentistry, University of Al-mustansiriya.

Preparation of Sodium fluoride muco-adhesive oral tablets:

Tablets formulation:

The preparation of the tablets have achieved by direct mixing of sodium fluoride, carbopol 934, hydroxypropyl methylcellulose, magnesium stearate and mannitol. A physical blend of polymers was mixed with mortar and pestle for 15 minutes. Then the mixture was compressed in a single-punch (8 mm) eccentric press (single punch tablet machine manesty type 3 - England, Industry pharmacy laboratory, College of pharmacy - university of Baghdad) by direct compression under 1500 kg/ cm^2 for 5 seconds, resulting in a circular biconvex (4 mm) thick tablet. (18) Yamasani et al. (12) used HPMC and Carbopol 934 as mucoa-dhesive polymers, tablets of carvedilol were prepared. One-hundred tablets were weighed individually and the average weight was determined. Percentage deviation was calculated and checked for weight variation. Thickness was measured using vernier calipers. Samples were prepared. The ingredients of the prepared tablets were listed as follows:

Chemical compounds	Weight (mg)
Sodium fluoride	2.00
Carbopol 934	150.00
Hydroxylpropyl methylcellulose	50.00
Magnesium stearate	4.00
manitol	14.00
Total weight/tablet	220.00

Materials used in this study:

HPMC: Trade Name: Hypromellose Shin - Etsu chemicals, co Ltd., Japan

(HPMC 100,000 CP Hypromellose). Carbopol 943: Equivalent weight (76 ± 4), BF Goodrich, (Cleveland, OH).

Sodium fluoride Powder: NaF (molecular weight 42) Riedel- de Haen-Germany. White odorless hygroscopic powder, Widely used in water fluoridation, mainly in small installations.

Fluoride measurement:

Fluoride was estimated by the direct method, using a fluoride specific electrode and an ion analyzer (201 E. HANNA instrument ,China) (19). Prior to the samples analysis, a set of standards (ranging between 0.025-3.2 ppm F) was prepared in triplicate, using serial dilution from a 100 ppm NaF stock solution (E.Merck, Darmstadt, Germany). The millivoltage potentials were converted to µg fluoride using a standard curve

Statistical analysis

Statistical analysis was conducted to describe different variables and parameters in current study and to describe relationships with each other as well. Independent t-test of significant was used for two group comparison. All satirical evaluation have been achieved by using SPSS-10.

RESULTS AND DISCUSSION

Table (1) showed the complete releasing of fluoride spread over a period of (8) hours in saliva, The immediate release of fluoride from adhesive tablets was over 40% of the drug (fluoride) in (2) hours, also slower release of drug is observed, about 60% of the drug is delivered in (6) hours. Table (2). Represent the statistical evolution of tablet releases concentration. Table(3). Represent the one sample statistical evaluation of the fluoride release tablet.

This study showed that a single layer tablet of NaF released 40% of fluoride in the first two hours and 60% released in the remaining six hours. Polymer mixtures containing high percentages of carbopol showed the best in vivo muco-adhesion, statistical analysis showed the high significance concentration of fluoride released tablet ($P < 0.01$) table (3). While Liabot *et al* (20) found in their work who used 2-layered muco-adhesive oral tablets containing nystatin, the immediate release of nystatin from lactose layer of tablet was over 50% in one hour, and the slower rate of drug released is observed about 80% of drug is delivered in (6) hours. Vishnu et al, (21) used sodium carboxymethylcellulose (SCMC) and Carbopol-934 (CP) as bio-adhesive polymers to impart muco-adhesion and ethyl cellulose (EC) to act as an impermeable backing layer, to establish muco-adhesive buccal devices of propranolol hydrochloride in the forms of bilayered and multilayered tablets. Maximum in vitro drug release of bilayered tablets was 97% over a period of 6 hours. All bilayered tablets remained intact during the 6-hour. Also Bottemberg *et al.*, showed that several muco-adhesive polymers were tested in vitro and in vivo from the polymers (polyacrylic acid, polyethylene glycol and modified corn starch), one polyethylene glycol and a mixture of modified starch with 5% polyacrylic acid showed a high adhesion together with a good

biocompatibility. Tablets made from these substances, containing 0.1 mg of fluoride, were shown to sustain significantly elevated fluoride levels in saliva during seven hours (22). Bottenberg *et al.*, concluded that the application of a bio-adhesive fluoride tablet can sustain elevated fluoride concentrations at several sites in the oral cavity for at least 4 hrs. The highest bioavailability of fluoride, and other drugs, can be obtained from a tablet placed in the labial sulcus. Further clinical studies are required to ascertain whether the released substances do clinical effect and if a population of untrained patients can indeed have a use the tablets efficiently without supervision. (23) Chowdary & Kamalakara (24) found in their research that the Muco-adhesive tablets formulated with nifedipine alone or with beta-cyclodextrin and the mucoa-dhesive polymers sodium carboxy methylcellulose and carbopol were investigated as oral controlled release tablets of nifedipine. Muco-adhesive tablets containing nifedipine alone gave very low dissolution, whereas those with its beta-cyclodextrin gave slow, controlled and complete release spread over a period of 12 h. Drug release from these tablets followed zero order kinetics up to 85-90% release and the release was diffusion controlled. Also in this work we found that the percent CB:HPMC 3:1 mixtures with sodium fluoride for the formulation of the tablet differed from other formulation containing drugs with single or doubled or multiple layers because sodium fluoride is a salt and it's an ionic compound, dissolving to give separated Na+ and F− ions, easily dissolved in water and diffused inside the channels of these polymers to the saliva. Also the position of the tablet inside the lower lips provide an excellent release and sustained fluoride for 8 hours. While Liabot *et al* (20) found in their work that the percent CB:HPMC 9:1 mixtures for the formulation of the polymeric layer the incorporation of nystatin in the polymer blend had an unexpected outcome: a considerable increase in muco-adhesion was observed. It is possible that the presence of nystatin may be responsible for the increase in the osmotic pressure and a rise in the water uptake of the mixture, facilitating the interaction between the polymers and the mucus. Machida and Nagai (25) showed that the polymer swelling is a property related to the muco-adhesion of the system. Polymers and hydrophilic macromolecules containing groups able to form hydrogen bonds have showed good adhesion properties that seem to be enhanced by the incorporation of amine and carboxylic groups.

The muco-adhesive tablets containing sodium fluoride (2 mg) and hydroxypropyl methylcellulose HPMC- carbopol - 934 was formulated in this work can release over (40%) of fluoride in first two hours also slower release of fluoride is observed about (60%) of fluoride is

delivered as a sustained release in (6) hours. These tablets have been developed specifically for use as a safe, highly effective in dental caries, carefully control and sustain the release of specified concentrations of fluoride a practically constant rate.

Table -1: The percent amount of fluoride released in saliva is declining with time

Time (hours)	Percent amount of fluoride released in saliva	Concentration of fluoride released in saliva (mg)
1st	20 %	0.40
2nd	20 %	0.40
3rd	15 %	0.30
4th	10 %	0.20
5th	10 %	0.20
6th	9 %	0.18
7th	8 %	0.16
8th	8 %	0.16

Table -2: The statistical evaluation of fluoride relaease from mucoadhesive tablet containing (2 mg) sodium fluoride.

Statistical functions	Concentration of NaF released in saliva from tablet/ mg	
N	8	
Mean	0.2500	
Std. error of mean	3.625×10^{-02}	
Std. deviation	0.1025	
Variance	1.051×10^{-02}	
Range .	0.24	
Minimum	0.16	
Maximum	0.40	
Sum	2.00	
Percentage	25 %	0.1650
	50 %	0.2000
	75 %	0.3750

Table -3: Represent the one sample statistical evaluation of the fluoride release tablet.

t	df.	Sig. (2-tailed)	Mean difference	95 % confidence interval of difference	
6.896	7	0.0001	0.2500	Lower	Upper
				0.1643	0.3357

REFERENCES

1. Machida Y., Nagai T. Bio-adhesive preparation as topical dosage Forms. In: Mathiowitz E, Chickering III D E, Lehr C M, eds. Bio-adhesive drug delivery systems. New York, NY: Marcel Dekker Inc. 98:646-647. (1999).
2. Weatherell J. A., Robinson C., Rathbone MJ. The flow of saliva and its influence on the movement, deposition and removal of drugs administered to the oral cavity. In: Rathbone MJ ed. Oral mucosal drug delivery. New York, Marcel Dekker Inc. 74:157. (1996)
3. Millns, B., Martin MV. Nystatin pastilles and suspension in the treatment of oral candidosis. Brit Dent J. 181(6):209-211. (1996).
4. Bouckaert S, Schautteet H, Lefebvre RA, Remon JP, Van Clooster R. Comparison of salivary miconazole concentrations after administration of a bioadhesive slow-release buccal tablet and oral gel. Eur J Clin Pharmacol. 43:137-140. (1992).
5. Codd JE, Deasy PB. Synergistic antifungal interaction between miconazole nitrate and chlorhexidine acetate. Int J Pharm. 173:3-11. (1998).
6. Bromberg LE, Buxton DK, Friden PM. Novel periodontal drug delivery system for treatment of periodontitis. J Control Release. 71:251-259. (2001).
7. Bromberg LE, Braman VM, Rothstein DM, et al. Sustained release of silver from periodontal wafers for treatment of periodontitis. J Control Release. 68:63-72. (2000).
8. Bottemberg P, Cleymaet R, DeMuynck C, et al. Development and testing of bioadhesive, fluoride-containing slow-release tablets for oral use. J.Pharm.Pharmacol. 43:457-464. (1991).
9. Carr D, Corbett CE, Koo PJS.. Mycotic and Parasitic Infections. In: Herfindal ET, Gourley DR eds. Textbook of therapeutic: drug and disease management, 6th ed. Baltimore MD: Williams & Wilkins: 1432. (1996)
10. Bottemberg P, Herman J, and Coomans D,. Bioadhesion of fluoride-containing slow-release tablets on porcine oral mucosa in vitro. STP Pharma.5(12):863-866.(1989).
11. Nagai T. Topical mucosal adhesive dosage forms. Med Res Rev. 6(2):227- (1986).
12. Yamsani, V. V., Gannu, R. Kolli, C. Banoji, M. E., and Yamsani, M.R. Development and in vitro evaluation of buccoadhesive carvedilol tablets. Acta Pharma. 57: 185-197. (2007)
13. Khanna, R., Agarwal, S.P., Ahuja, A.,. Muco-adhesive buccal tablets of clotrimazole for oral candidiasis. Drug Dev. Ind.Pharm. 23, 831–837. (1997)

14. Perez Marcos, B., Ford, J.L., Armstrong, D.J., Elliott, P.N., Hogan, J.E., Release of propranolol hydrochloride from matrix tablets containing hydroxypropyl methylcellulose K4M and Carbopol 974. Int. J. Pharm. 111, 251–259. (1994)
15. Garcia-Gonzalez N, Kellaway, I W, Blanco, Fuente H, Anguiano, Igea S, Delgado, Charro B,Otero, Espinar F J, Mendez J: "Influence of Glycerol Concentration and Carbopol Molecular Weight on Swelling and Drug Release Characteristics of Metoclopramide Hydrogels" Int. J. Pharm., 104,107-113. (1994)
16. Durrani, Manzer J, Whitaker, Roy, Benner, Samuel C: "A Comparative Concentration," Amer. Assoc Pharm. Sci., (Nov.). (1992)
17. Durrani M J, Manji P A, Whitaker R F, Huvard G S:. "Controlled-Release Studies on Carbopol 971P Polymer," Proc. Int. Symp. Controlled Release. Bioact. Mater, 21ST, 738- 739. (1994).
18. Alderborn, G. Tablet and Compaction in Aulton M. The science of dosage form design by mechael. 2 nd. ed. Churchill Livengstone: 398, 410, 411, 415, 416. (2004).
19. Orth MR, Assaf AV, Zanin L, Mialhe FL, Klein AL, and Medina MRJ. Concentração de flúor nos principais dentifrícios comercializados no Brazil e impacto da nova portaria de regulamentação. Revista Odonto Ciência; 16:27-33. (2001).
20. Liabot J M , Manzo R H and Alemand D A. Double-layered mucoadhesive tablets containing Nystatin, College of pharmacy , University of Nacional de Cordoba, Argentina. (2002).
21. Vishnu M. Patel, Bhupendra G. Prajapati, and Madhabhai M. Patel Formulation, Evaluation, and Comparison of Bilayered and Multilayered Mucoadhesive Buccal Devices of Propranolol Hydrochloride *AAPS Pharm.Sci.Tech.* 8: (1). (2007).
22. Bottemberg, P . , Zahnerhaltung K. f. und Aachen, P. Efficient fluoride enrichment using mucous membrane adhesives with slow release tablets. Oralprophylaxe 13(4):148-52. (1991).
23. Bottenberg , P., Bultmann C. and Gräber, H. G. Distribution of fluoride in the oral cavity after application of a bio-adhesive fluoride-releasing tablet J Dent Res. 77 (1): 68-72. (1998).
24. Chowdary K P , Kamalakara R G, Controlled release of nifidipine from mucoadhesive tablets of its inclusion comp. PDA Pharmazie Oct; 58 (10) :721-4. (2003).
25. Machida Y, Nagai T. Bioadhesive preparation as topical dosage Forms. In: Mathiowitz E, Chickering III D E, Lehr C M, eds. Bioadhesive drug delivery system. New Yourk, NY Marceel Dekker Inc. 98: 646-647. (1999).

Isolation of Salmonella from Some Species of Wild Birds In Sulaimania

Zaid K. Khidhir[1] and Eman. D. Aref[2]
[1]Animal production dep., College of Agriculture, Sulaimania University
[2]Microbiology dep, College of vet . Medicine, Sulaimania University

Received 22/3/2010 – Accepted 5/10/2010

الخلاصة

تلعب الطيور البرية دور ميكاينكيا وبايولوجيا في نقل الخمج الى حقول الدواجن . تم اصطياد136 طير من 3 انواع من الطيور البرية(*Passer domestics, Streptopelia decaoto* and *Columba livia*) خلال الفترة من كانون الثاني الى كانون الاول 2006 من مناطق مختلفة حول حقول الدواجن في مدينة السليمانية . تم عزل عزلة واحدة من *Salmonella typhimurium* (%0.73) من الطير نوع *Streptopelia decaoto* عند استعمال الطريقة التقليدية في العزل وبعد استعمال طريقة الاغناء الثانوي المتاخر تم عزل عزلة اضافية من الطير نوع *Columba livia* لتصل نسبة العزل الى (1.4 %) .

ABSTRACT

Free living birds play a mechanical and biological role in transmission of infection to poultry farm. One hundred thirty six birds were captured from 3 species of wild birds (*Passer domestics, Streptopelia decaoto* and *Columba livia*) during the periods from January 2006 to December 2006 from many Location around poultry farm in Sulaimania City. One Isolated was *Salmonella typhimurium* (%0.73) from *Streptopelia decaoto* when make a classic method for isolation and after used method of delay secondary Enrichment addition Isolated from *Columba livia* are detected (% 1.4).

INTRODUCTION

Salmonella and Campylobacter spp. are one of the most common foods – borne zoon tic pathogens in developed countries(1).

In many countries Salmonellosis continues to be one of the major causes of gastroenteritis. (2). Largely through consumption of infected poultry and beef. Wild birds have been implicated as a source of live stock contamination or direct transmission to humans. (3)., and wild birds may functions as effective spreader's of salmonella bacteria to humans and to different animal species through contamination of the Environment (4).

In Norway, sporadic indigenous cases and national outbreak of human Salmonellosis, caused by serovar typhimurium, have been related to infections in small passerines (5,6). Investigation in England had found almost 10% of herring gulls carrying Salmonella apparently without affecting their health (7).

Also wild bird may contaminate the feed of animals, and free flying birds play a mechanical and biological role in transmission of salmonella to poultry farms (8). The aim of this study was to investigate

the contamination of some wild bird species with salmonella spp. in Sulaimania City and vicinity around the poultry farm.

MATERIAL AND METHODS

One hundred thirty six wilds birds. Including three species were collected during period from January 2006 to December 2006 from different locations of Sulaimania City and vicinity around the poultry farms.

Cloacae swabs were taken from dead and live bird, swab was inserted directly into test tubes of peptone waters and pre enrichment in peptone at 37°c for 18h., then transferred 1ml to test tubes of 10 tetrathionate broth (Selective Enrichment) and then Incubated at 42 °c for 24h.

The broth cultures were streaked on salmonella shigella agar. Brilliants green agar (Selective media) following 24h incubation on 37 °c after purified on blood Agar. The Suspected colonies were confirmed by biochemical tests as recommended by (9).

The slide agglutination test was performed for the tubes showing reactions typical of *Salmonella.* Serotyping of the isolated *Salmonella* isolate was performed

In case of negative sample the selective Enrichment tube are kept in room temperature for 7 day after (delay secondary enrichment) and transferred 1 ml to new tubes of tetrathionate broth and make the steps of culturing as in above. (These method for stimulate the *Salmonella* which may inhibited)

RESULTS AND DISCUSSION

Salmonella bacteria especially Salmonella enteric a serotype typhimurium, are a commonly found in the intestine of wild birds, these organisms are maintained within birds population by several mechanisms (10).

It's appear to be relatively resistant to disease but may serve as effective carriers of salmonella and thus area consider as a source of infection for other animal or directly transmitted to humans (11).

Between January 2006 to December 2006, one hundred thirty six birds' capital and species are shown in table (1).

One Isolated was *Salmonella typhimurim* from *Streptopelia decaoto* and additional Isolated or *S. typhimurium* from *Columba livia* after makes of delay secondary enrichment and this methods (DSE) effected in increase of percent of Isolative (12).

No Cases of salmonella were noticed in the *passer domestics*.

Since wild birds feed at sewage in disposal areas, water sources and grain storage, therefore they possess a meant potential in disseminating any pathogen that they might carry (13).

S. typhimurium is the most common seravors found in people in Norway (14). And also are the most serotype Isolated from feed of poultry in the Nineveh province (15).
These infected birds may transmit infection to humans, either directly as results of handling, or more commonly, as results of exposure to domestic Cats infected by preying on sick and moribund birds. (10).

Table -1: type of wild birds and number of *Salmonella* Isolated from wild bird in Sulaimania region.

Bird species	Numbers of birds	Positive	Percent% of the salmonella Isolated
Passer domestic's	53	—	
Streptopelia decaoto	51	1	%1.96
Columba livia.	32	1	%3.1
Total	136	2	%1.4

REFERENCES

1. Thorns C.J. Bacterial food borne zoonoses .Revue Scientifique et Technique del International des Epizooties 19:226-239. (2004).
2. Hall, G., Kirk, M.D, Becker, N., Gregory, J.E, Unicomb, L., Millard, G. Estimating Food borne gastroenteritis, Australia. Emerging Infectious Diseases 11:1257-1264. (2005).
3. Refsum, T., K.Handeland, D.L. Baggesen, G.holstad, and G.Kapperud. .Salmonellae in avian wildlife in Norway from 1969 to 2000. Appl.Environ. Microbiol.68:5595-5599.(2002)
4. Handeland, k. G., Kapperud, T.,Refsum, B.,Strom , G., Holstad, G., Knutsen, I.Soiberg, and J.Schultze.prevalence of Salmonella Typhimurium in Norwegian hedgehog populations associated with two human disease outbreaks .Epidemiol.infect.128:523- 527.(2002).
5. Kapperud, G., H.Stenwig, and J.Lassen. Epidemiology of Salmonella Typhimurium O: 4-12 infection in Norway .Evidence of transmission from an avian wildlife reservoir .Am.J.Epidemiol.47:774-792. (1998).
6. Kapperud, G., J.Lassen, K.Dommarsnes, B.E.Kristiansen, D.A. Caugant, E.Ask, and M.Jahkola. Comparison of epidemiological marker methods for identification of Salmonella typhimurium isolates from an outbreak caused by contaminated chocolate.J.Clin.Microbial.27:2019-2024. .(1989).
7. Monaghan, P., C. B. Shedden, K. Ensor, C. R. Fricker, and R. W. A.Girdwood. Salmonella carriage by herring gulls in the Clyde area of Scotland in relation to their feeding ecology. J. Appl. Ecol. 22:669–680. (1985).

8. Soliman, A., Mousa, S., Bayonmi, A.H., Nahed, G. and Atta, M. The role of played by free flying birds in the transmission of avian pathogens 11. *Mycoplasma* and enterobacteriacae.Assiut.Vet.Med. J 20(40).185-190. (1988).
9. Douglas Waltman, R.K.Gast and E.T. Mallinson, Salmnellosis. In: Swayne, D.E., Glisson, J.R., Jackwood, M.W., Pearson,j.E., and Reed, W.m (Eds.), A laboratory Manual for the Isolation and Identification of Avian Pathologens .The American Association of Avian Patholgists,Pennsylvania,pp:4-13. (1998).
10. Tizard I . Salmonellosis in wild birds.Seminares in Avian and Exotic Pet Medicine 13:50-66. (2004).
11. Craven, S.E, Stern, N.J, Line E., Bailey J.S, Cox N.A,and Fedorka, C. P .Determination of the incidence of *Salmonella* spp., *Compylobacter jejuni* ,and *Clostridium Perfringens* in wild birds near broiler chicken houses by sampling intestinal droppings.Avian Diseases 44:715 – 720. (2000).
12. Waltman, W.D.,Horne ,A.M., pirkle,C.,and Johnson, A. Prevalence of Salmonella enteritidis in spent hens ,Avian Diseases 36:251-255. (1992).
13. Wilson,J.E.and Macdonald,J.W. Salmonella infection in wild birds .British vet. J.123:212-219.(1976).
14. Kapperud, G., S. Gustavsen, I. Hellesnes, A. H. Hansen, J. Lassen, J. Hirn, M. Jahkola, M. A. Montenegro, and R. Helmuth. Outbreak of Salmonella typhimurium infection traced to contaminated chocolate and caused by a strain lacking the 60-megadalton virulence plasmid. J. Clin. Microbiol. 28:2597-2601. (1990).
15. Alhakim, Z.k. Contamination of the parent stock environment with *Salmonella* in Nineveh province .Thesis. Collage of Vet.Medicine, Univ.Mosual, Iraq. (2003).

Comparative Study of Biochemical and Bacteriological Analysis of Wound Fluid and Serum from Non Healing and Healing Skin Ulcers

Emane N. Najee[1], Zahid J. Mohammed[2], and Mohanad A. Kassim[3]
[1,3]Biology department \College of Science, AL-Mustansyria University
[2]Basic of Clinical Science\ College of Nursing \Baghdad University.

Received 4/1/2010 – Accepted 5/10/2010

الخلاصة

الهدف من هذه الدراسة هو التحري ومقارنة المكونات البايوكيمائيه والمحتوى الميكروبي للسوائل الراشحه من الجروح المزمنة و مصول إحدى وعشرون مريضا خلال فترتي الإصابة والشفاء، فحصت نماذج السوائل الراشحة و المصول من خلال إجراء التحاليل البايوكيمياوية العامة إضافة لاختبار مصلي واحد وهو C-reactive protein . أظهرت النتائج أن مستوى العناصر الأيونية كان متقاربا في كلا السوائل الراشحة ومصول المرضى وان مستوى الكلوكوز كان منخفضا في السوائل الراشحة مقارنة بمستواه في المصل وان مستويات الألبومين و البروتين الكلي في السوائل الراشحة نصف مستواها في المصل وذلك خلال فترة الإصابة، فيما في مرحلة الشفاء أظهرت مستويات الكلوكوز نقصان في السوائل الراشحة فيما لم تتغير مستويات C-reactive protein. تم الحصول على عشرون عزلة تعود لأنواع مختلفة من البكتريا الموجبة و السالبة لصبغة كرام ويعود البعض منها لأنواع *Staphylococcus aureus* و *Pseudomonas aeruginosa* ، اظهر(13) نموذجا انخفاضا في أعداد البكتريا خلال فترة الشفاء، وأظهرت هذه الدراسة بأن السوائل الراشحة من القرح الجلدية المزمنة تعد سوائل راشحة (exudate) و أن محتواها البايوكيميائي يعطي تصورا عن المحتوى البايوكيميائي للسوائل الخارج خلوية (extracellular) وان نقصان المحتوى الميكروبي خلال فترة الشفاء يدل على أن القرح تتجاوب للعلاجات.

ABSTRACT

The purpose of this study was to investigate and compare the biochemical and bacteriological composition of fluid taken from chronic wounds and serum of (21) patients during both healing and non healing phase. Wound fluid and serum samples were examined of general biochemical analysis and one serological test which was C-reactive protein. The results showed that Electrolyte levels were essentially identical in both wound fluid and serum samples, the Glucose levels were lower in wound fluids compared to its levels in serum , Albumin and total protein levels in wound fluid were on average half those of serum levels during non healing phase while during healing phase the glucose levels decreased in wound fluids and C-reactive protein levels remained unchanged. Twenty isolates of different Gram positive and Gram Negative bacteria were detected in the study, some of those isolates belongs to *Staphylococcus aureus* and *Pseudomonas aeruginosa*,13 samples showed decrease in the numbers of bacteria during healing phase. The study showed that Wound fluids collected from chronic skin ulcer is an exudates with the biochemical composition expected in extracellular fluid, and the decrease in the microbial content during healing phase indicates that the ulcers are responding to the treatment.

INTRODUCTION

There are considerable clinical research in treatment of chronic skin ulcer, (1) the analysis of wound fluid has been used to get more information fact about wound environment. This research is based on the role that fluid collected from the wound surface represents

extracellular fluid from the wound itself so that analysis of wound fluid may give real information value about the conditions inside the wound .(2)

There has been no detailed biochemical analysis of wound fluid to characterize its composition and to make a comparison with serum. Wound fluid remains undefined, in addition there has been no demonstration of biochemical and bacteriological changes might occur in skin ulcer during chronic infection and after healing. Such information would help to give a better understanding of the healing process in chronic skin ulcer. (3)

The purpose of this study is to compare wound fluid collected in a standardized way, with serum to understand whether wound fluid truly represents extracellular fluid, to identify changes in the biochemical composition of wound fluid collected from chronic skin ulcers at non healing and healing phases also the last aim of this study which is the qualitative and quantitative bacteriological analysis which aims to diagnose the most important kind of bacteria infected skin ulcers and the changes in bacterial number during the transformation from non healing to healing phase.

MATERIALS AND METHODS

All patients (21) examined in this study had chronic skin ulcers especially in leg. The cause of each ulcer was assessed by careful history, examination and a series of investigation. By measuring ulcer size during two months and arterial Doppler pressures (4) on the other hand a standard biochemical tests urea, creatinin, electrolytes two of liver function test, glucose and C. reactive protein.

ULCERS SIZE AND MEASUREMENT

The surface area of all ulcers was measured during two weeks of hospitalization beginning from the first day of admission. these measurements were used as a good marker for healing occurring.

COLLECTION OF WOUND FLUID AND SERUM SAMPLES

Wound fluid and blood samples were collected from 21 patients within 24 hours of admission to the (AL-Kindy hospital) with chronic skin ulcers in both non heating and healing phase, There were 16 male and 5 female patients, with a medium age of 49 years range (45-71). after three weeks of bed rest and regular medication (healing phase) wound fluid was collected from each patient was fasted for 12 hours and the fluid was aspirated from deep area. Under the ulcer and surround it and transferred in to the serum collection tubes. (2)

BIOCHEMICAL ANALYSIS

Wound fluid and serum samples were analyzed for general biochemical test and measured with Automated Biochemical Analyzer type Optima 600

These biochemical tests includes sodium, potassium, urea, creatinin, uric acid, calcium, phosphate, glucose, alkaline phosphates, total bilirubin, total protein, albumin , cholesterol, triglycerides, and serological test C- reactive protein. The serum normal value ranges of each examined test (4) are included in table (1).

BACTERIOLOGICAL ANALYSIS

Qualitative bacteriologic characteristics were determined by taking swabs of the ulcer which were then cultured in selective media.

Quantitative bacteriologic study was also carried out on the wound fluid samples. Wound fluid is mixed and 10 ml from the supernatant was serially diluted. Dilution was plated on blood agar and the number of colonies on each plate were counted and the number of bacteria per milliter of wound fluid were calculated.

STATISTICAL ANALYSIS

Medium values were calculated and paired samples were compared statistically by using sign-rank test.

RESULTS AND DISCUSSION

The medium initial size of the ulcers was 45 cm^2 with range of 35cm^2-68cm^2. All ulcers showed sings of granulation tissue formation and new skin formation after the three weeks of a hospitalization.

When comparing wound fluid with serum it was noted that there was no significant difference in sodium phosphate, urea, creatinine ,and calcium levels between fluid and serum samples ($P>0.05$) (table1).The concentrations of potassium were higher significant in serum compared with wound fluid ($P < 0.01$).and glucose levels were significantly lower in wound fluid (2-1 mmol /L) when compared with paired serum samples (6-5 mmol /L) ($P < 0.001$).

Both albumin and total protein levels in wound fluid (18and33 gm /L respectively) were approximately half the levels present in serum (38and71 gm/L respectively)is significant ($p < 0.001$, $p < 0.001$) ,this may be belong to alpha, beta and gamma globulin concentration. The levels of C-reactive protein look significant ($P > 0.05$) it was in wound fluid (6 gm /L) and serum (12 gm /L).Cholesterol and triglyceride significant ($p< 0.001$,$p< 0.01$) concentration were also reduced in wound fluid relative to serum, which is nearest to the lower protein levels.

Other important result we found a higher total bilirubin content and lower uric acid level in wound fluid($p< 0.01, p< 0.05$). When we analyzed changes in the wound fluid from non healing to the healing phase (table 2), it was noted that there was a significant increase in the levels of glucose, albumin, total protein, cholesterol, and triglyceride.

On other hand there was no significant change in the level of C-reactive protein, as well as all other parameters. When we compare the results of the analysis for non healing and healing serum (table 3), one can notice that there was real increase (significant increase) in the serum level of total protein and albumin during the healing process whereas other biochemical tests like glucose, cholesterol, triglyceride, C-reactive protein and all other parameters remained unaltered .

Table- 1: Comparison between serum normal value of biochemical analysis for all serum and wound fluid samples.(non healing phase)

Biochemical test	Wound fluid		Serum		Normal value ranges	P Value
	Ranges	median	ranges	median		
Sodium	136-145	142	139-146	141	136-145 mmol /L	NS
Potassium	3.3-5.5	4.2	3.6-6.8	5.1	3.6-5 mmol /L	< 0.01
Urea	15-42	33	22-45	39	15-50 mg /dL	NS
Creatinine	0.2-0.5	0.26	0.25-0.56	0.3	0.2-0.9 mg /dL	NS
Uric acid	220-610	415	245-780	478	140-480 mmol /L	< 0.05
Calcium	1.9-2.5	2.2	2.0-2.3	2.1	2.15-2.5 mmol /L	NS
Phosphate	0.95-1.38	1.18	0.9-1.55	1.1	0.8-1.48 mmol /L	NS
Glucose	0.533-6	2.1	4.0-9.3	6.5	3.5-5.5 mmol /L	< 0.001
Alkaline	20-138	95	49-235	148	35-120 U /L	< 0.01
phosphate	8.3-56	28	8-31	17	3-20 mmol /L	< 0.01
Total bilirubin	20-49	33	63-85	71	55-80 gm /L	< 0.001
Total protein	16-48	18	36-51	38	35-50 gm /L	< 0.001
Albumin	6-24	6	6-72	12	≤ 6 mg /dL	> 0.05
C-Reactive	1.9-4.1	2.3	2.3-7.8	4.9	5.5 mmol /L	< 0.001
protein	0.6-5	0.9	1.1-4.2	2.2	0.3-1.8 mmol /L	< 0.01
Cholesterol						
Triglycerides						

NS: Not Significant

- Significant level for comparison of wound fluid value to paired serum value

The results of the qualitative bacteriological analysis (table 4), showed that all ulcers were contaminated with bacteria at both phases, that bacteria detected in the ulcers were *Pseudomonas aeruginosa* (5 isolation), *Escherichia coli* (3 isolation), as G-ve bacteria. The median number of bacterial cells /ml were (2×10^5, 2×10^7) respectively and *Staphylococcus aureus* (6 isolates), the normal flora of the skin *Staphylococcus epidermids* (2 isolate),α- hemolytic Streptococcus (3 isolates) and β- hemolytic Streptococcus (1 isolate) as G +ve bacteria.

The median number of the bacterial cells /ml were (2×10^4, 2×10^3, 1×10^4, 1×10^5) respectively. The G-ve bacteria *E coli* showed the higher range (1×10^4- 2×10^7) cell / ml.

Samples from 13 patients showed decrease in the number of bacteria during healing, and 7 samples showed increase in the number of bacteria in the wound fluid during healing phase.

The analysis of fluid collected from acute and chronic human wounds and skin ulcer is being used as an investigative tool more than before. (5,6) the study of wound fluid is best on the assumption that it is exudates representing the extracellular fluid of the tissue so it gives real information about the changes happened during the healing phase of the wound. (7)

It is very important to know that the wound fluid has biochemical composition equivalent to the extracellular fluid, so in this study it has the electrolyte composition, urea, creatinin and calcium levels equivalent to serum so it represent the extracellular environment of the wound.(8,9)

On the basis of comparative studies, biologic fluids such as pleural effusion and ascites may be categorized as exudates or transudates. Exudates can be defined as a fluid deposit in tissues (as a result of inflammation or infection) that has high viscosity and high protein (> 30 gm/L). Transudates are fluid that has high fluidity and low protein (< 30 gm/L). (8,10). The results of the protein analysis in this study (median total protein 33 gm/L) indicate that wound fluid collected from chronic skin ulcers is exudates. The albumin and cholesterol levels spurted this result. The increase in protein and albumin during healing phase of the chronic wound may represent the nutritional conditions during hospitalization because this changes is present both in serum and wound fluid (11). The low level of glucose in wound fluid when compared with serum suggests altered state of metabolism within the wound and the utilization of bacteria of the carbon source for their cell development and growth.(12)

The changes observed in C-reactive protein was very little, there is no difference in the level of C-reactive protein in the total wound fluid compared with serum (anon reason).(13)

The changes observed in wound fluid during healing of the skin ulcers could be due to factors other than changes in the healing processes.(6) A reduced bacterial contamination of the ulcers as result of hospitalization could be a good factor to inhibition inflammation progress. However, only few samples did not show an alteration in the type of bacteria and reduction of there counts, due to the highly resistant of antibiotic.

Table -2: Comparison selected significant biochemical results from non healing and healing wound fluid.

Biochemical tests	Non healing		healing		P Value
	range	median	range		
Glucose	0.9-9.8	3	0.53-6	2.1	< 0.05
Total protein	32-54	42	20-49	33	< 0.01
albumin	21-52	27	16-48	18	< 0.01
Cholesterol	1.7-4.2	2.7	1.9-4.1	2.3	< 0.05
Triglyceride	0.5-4.9	1.4	0.6-5	0.9	< 0.05

Table -3: Comparison selected significant biochemical results fro non healing and healing serum.

Biochemical tests	Non healing		healing		P Value
	range	median	range	median	
Glucose	4.2-9.7	6.3	4-9.3	6.5	NS
Total protein	56-90	78	63-85	71	< 0.05
albumin	36-53	44	36-51	38	< 0.05
Cholesterol	2.4-9.1	5.3	2.3-7.8	4.9	NS
Triglyceride	0.9-3.6	2.25	1.1-3.2	2.2	NS

Table -4: Quantitative and qualitative bacteriological results from non healing wound ulcer.

Name of species	Range No. of bacterial cell /ml	NO. of isolate	Median
Pseudomonas aeruginosa	1×10^3 - 2×10^6	5	2×10^5
Escherichia coli	1×10^4- 2×10^7	3	2×10^7
Staphylococcus aureus	1×10^4- 2×10^4	6	2×10^4
Staphylococcus epidermid	1×10^3- 2×10^3	2	2×10^3
α hemolytic Streptococcus	1×10^2- 1×10^4	3	1×10^4
β- hemolytic Streptococcus	1×10^5	1	1×10^5

REFRENCES

1. Finetti G. and Farina M., Recombinant human basic fibroblast growth factor: different clinical dressings for clinical application in wound healing. Farmaco,; 47:967-78.(1992)
2. Drinkwater S. L. , Smith A. and Burnand K. G., What Can Wound Fluids Tell Us About the Venous Ulcer Microenvironment? INT J LOW EXTREME WOUNDS.1: 184-190 (2002)
3. Caldwell M., Mastrofrancesco B., Shearer J., Bereiter D., The temporal change in amino acid concentration within wound fluid a putative rationale. In: Barbul A., Caldwell M., Eglestein Wh, Clinical and experimental approaches to dermal and epidermal repair: normal and chronic wounds. Wiley-Liss New York, 205-22.(1991)
4. Fischbach F., and Bunning M., A Manual of Laboratory and Diagnostic Test,8th ED., Lippinccot Williams &Wilkins ,Philadelphia. P.265-711(2009)
5. Moseley R. Hilton JR. Waddington RJ. Harding KG. Stephens P. Thomas DW.., Comparison of oxidative stress biomarker profiles between acute and chronic wound environments. Wound Repair and Regeneration. 12 (4). 419-429.(2004)
6. Naomi J. Trengove, Michael C. Stacey, Shawn Macauley, Neil Bennett, Jane Gibson, Frank Burslem, Gillian Murphy, Gregory Schultz, Analysis of the acute and chronic wound environments: the role of proteases and their inhibitors. Wound Repair and Regeneration. 7 (6).442- 452. (1999)
7. Romero S. Candela A. Martin C. Hernandez L. Trigo C., Evaluation of different criteria for the separation of plural transudates from exudates. Chest; 104:399- 404(1993)
8. Widmaiex, P.E.,Strang, T.K. and Raff, H.Human Physiology,5th ED., Mc Graw-Hill Companies, P.322-341(2006)
9. Hunt T.,Wound fluid : the growth environment.Clinical and experimental apporoaches to dermal and epidermal repair:normal and chronic wounds;112:18-23. (1994)

10. Young B. Lowe J. Stevens A. Heacth J. Deakins P., Functional Histology : A text and color Atlas,7th ED., Churchill Livingstone, London. p512-544(2002)
11. Celhann B.and Celikel T.,Serum-effution albumin gradient in separation of transudative and exudative pleural effusions.Chest,105:974-5. (1994)
12. Ryrn J., and Ray G.,(editors).Sherris Medical Microbiology,4th ED., Mc Graw-Hill Companies, London. P.417-438(2003)
13. Gronroos J and Irjala K.Phospholipase A2.C-reactive protein ,and white blood cell count in the diagnosis of acute appendicitis.Clin Chem,40:1757-60.(1994)

Synthesis and Antimicrobial Activity of Some New Acetylenic Amine of Isatin Derivatives

Suaad M. H. Al- Majidi and Khitam T. A. Al- Sultani
Department of Chemistry College of Science University of Baghdad

Received 17/2/2010 – Accepted 10/5/2010

الخلاصة

تم في هذا البحث تحضير بعض امينات الاستيلين للايساتين [أندول- 3,2- دايون]، وذلك من خلال تحضير3-(3,2- داي مثيل فنيل امينو)-1H- أندول- 2-اون [1] والذي حصلنا عليه بتكاثف الايساتين مع 3,2- داي مثيل فنيل امين وبوجود حامض الخليك الثلجي والايثانول المطلق كمذيب.وعند معاملته مع الصوديوم هيدريد في داي مثيل فورمامايد في درجة(صفر م°) ليعطي ملح الصوديوم للايساتين العالق وتواصل التفاعل مع البروبرجيل برومايد وتم الحصول على المركب الرئيسي3- (3,2- داي مثيل فنيل امينو)-2-اوكسو-1- اندول(1-برو-2-يان)[2].

أجراء تفاعل مانخ Mannich reaction للمركب [2] مع البارافورمالديهايد ، ومختلف الامينات الثانوية بوجود كلوريد النحاسوز كعامل مساعد، وقد تم الحصول على المركبات الجديدة [3-17] . شخصت المركبات المحضرة بالطرق الطيفية [FTIR، ^{1}H-NMR، ^{13}C-NMR] وتعين بعض خواصها الفيزياوية واجراء بعض الكشوفات النوعية. كما تم دراسة تأثير هذه المركبات على اربعة انواع من البكتريا وخميرة واحدة.

ABSTRACT

In the present work, a series of some new acetylenic amines of Isatin(Indole-2,3-dione), were prepared 3-(2,3-dimethy phenyl- imino)-1H-indole-2-one [1] which was prepared by condensation Isatin with 2,3- dimethy phenyl amine in the presence of glacial acetic acid and absolute ethanol as solvent.The product was treated with sodium hydrite in DMF at 0 °C to give asuspension of the sodium salt of Isatin derivative and subsequent reaction with propargy bromide to obtain, 3-(2,3-dimethy phenyl- imino)-2- oxo-1-indol-(1-prop-2-ynyl) [2].

Mannich reaction was carried out on compound [2] using paraformaldehyde and different amine, cuprous chloride as catalyst, and the compounds were obtained [3-17]. The prepared compounds were identified by spectral methods [FTIR,^{1}H-NMR, ^{13}C-NMR] and some of its physical properties were measured, furthermore the effects of the new compounds on four types strains of bacteria and one yeast were studied.

INTRODUCTION

Isatin (Indole-2,3-dione) was first obtained by Erdman and Lauren in 1841. three reviews have been published regard in the chemistry of this compound: the first by sumpter, 1954[1], a second by popp in 1973[2], and the third on the utility of isatin as a precursor for the synthesis of other heterocyclic compounds[3]. The synthetic versatility of isatin has stemmed from the interest in the biological and pharmacological properties of its derivatives[4]. Isatin derivatives have show a wide scale of biological activities such as (antimicrobial and antitubercular)[5], fungal[6], (anticancer and antiangiogenic agents)[7], and anti-inflammatory[8]. As far as many isatin derivatives have been used as dyes for wool and silk [9], hair and plastic materials[10].

Isatin will mainly react at three different site, namely aromatic substitution, N-reactions at position I, and carbonyl reaction at C-3.

If the system carries electron- with drawing groups in the benzene ring or at the nitrogen atom, attact at C-2 can also occur[10,11].

Use of acetylenic compounds as drugs is potentially important because acetylenic drugs are frequently more active, less toxic, and more easily absorbed into the body than their olefinic and saturated analogs[12]. Acetylenic compounds possess divers pharmaceutical [13]. Therefore we aimed to prepare anovel series of N-substituted isatin-3-hydrazones by following Schiff bases and Mannich reaction and establish their antimicrobial potency against both bacteria and yeast.

MATERIALS AND METHODS

Instruments

Melting point were determined on a Gllenkamp FB.600-olof melting point apparatus. FTIR Spectra were recorded using solid KBr dises by tests scan shimadzu FTIR 800 series.The ^{1}H-NMR and ^{13}C-NMR Spectra were recorded on a make bruker model ultrashied 300MHz, NMR at Al-Albyt university , Jordan .DMSO-d^{6} was used as solvent and TMS as internal reference.

Chemical

All starting chemical compounds were obtained from Fluka or Aldrich.

Synthesis of 3-(2,3-dimethylphenyl-imino)-1H-indole-2-one.[1][14]

Amixture of Isatin (Indole-2,3-dione) (5 gm., 0.03 mol.) and 2,3-dimethy aniline (o.36 ml., 0.03 mol.) in absolute ethanol(50 ml.) was refluxed for 4 hrs. at (50-60)°C in the presence of 9-10 drops of glacial acetic acid.After cooling, was filtered and recrystallised from ether to give compound [1]. Physical properties are listed in Table (1).

Synthesis of 3-(2,3-dimethy phenyl- imino)-2-oxo-1-indol-(1-prop-2-ynyl)[2][15]

A solution of compound [1] (4gm., 0.016 mol.) in DMF (8 ml.) was cooled to 0°C, and sodium hydride (0.38gm., 0.016 mol., 60% in mineral oil) was periodically added to the solution in small portions. propargyl bromide (1.41ml., 0.016 mol., 80% in toluene) was added to the slurry via syringe, and the reaction mixture was slowly warmed to room temperature. The reaction was quenched with water after 12 hrs., and the resulting solid was removed via filtration. The filtrate was concentrated under reduced pressure and crude product was purified via

recrystallization toluene: EtOAC, 1:1 v\v). Physical properties are listed in Table (1-4).

Table-1: Physical properties of the prepared compounds

Comp. No.	Molecular formula (M.wt.)	Comp. Structure	m.p. °C	Yield %	Colour	Recryst. solvent
1	$C_{16}H_{14}N_2O$ 250	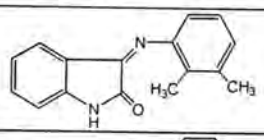	218-220	90	Yellow orange	Ether
2	$C_{19}H_{16}N_2O$ 288	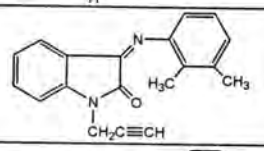	128	85	Brick-red	Toluene-ethyl acetate
		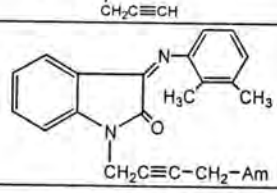				
3	$C_{22}H_{23}N_3O$ 345	Am-N-$(CH_3)_2$	120-122	65	Yellow	Ethanol-water
4	$C_{24}H_{27}N_3O$ 373	Am-N-$(CH_2CH_3)_2$	152-154	70	Yellow	Methanol
5	$C_{26}H_{31}N_3O$ 401	Am-N-$(CH_2CH_2CH_3)_2$	55-60	72	Deep yellow	Ethanol
6	$C_{26}H_{31}N_3O$ 401	Am-N-$[CH(CH_3)_2]_2$	110-112	68	Yellow	Ethyl acetate
7	$C_{28}H_{35}N_3O$ 429	Am-N-$(CH_2CH_2CH_2CH_3)_2$	138-139	55	Pale yellow	Chloroform-petroleum ether
8	$C_{28}H_{35}N_3O$ 429	Am-N-$[CH_2CH(CH_3)_2]_2$	107-108	65	Pale brown	Chloroform
9	$C_{27}H_{25}N_3O$ 407	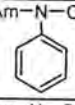	119-121	68	Deep yellow	Ether-petroleum
10	$C_{28}H_{35}N_3O$ 421	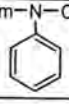	160 decom.	55	Deep yellow	Ethanol-water
Comp. No.	Molecular formula (M.wt.)	Comp. Structure	m.p. °C	Yield %	Colour	Recryst. solvent
11	$C_{34}H_{31}N_3O$ 479	Am-N-$(CH_2C_6H_5)_2$	77-80	45	Dark brown	Methanol
12	$C_{24}H_{21}N_3O$ 367	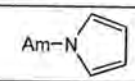	140-142	72	Brown	Ethanol-water
13	$C_{25}H_{27}N_3O$ 385	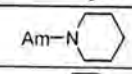	178	77	Dark yellow	Acetone
14	$C_{26}H_{29}N_3O$ 399	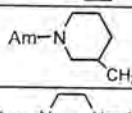	144	80	Brown	Ethanol
15	$C_{44}H_{42}N_6O$ 686	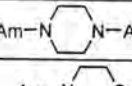	88-90	73	Dark brown	Ethanol
16	$C_{24}H_{25}N_3O$ 387	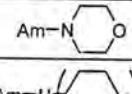	110	58	Light brown	Cyclohexane
17	$C_{32}H_{39}N_3O$ 481	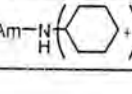	131-133	67	Oval-yellow	Ether-petroleum

General synthesis of 3-(2,3-dimethyl phenyl-imino)-2-oxo-1-indol-(1-buto-2-ynyl-4-amino) [3-17][16]

Compound [2] (0.5 gm., 0.001 mol.) was allowed to the Mannich reaction with different (aliphatic, aromatic, cyclic, and hetro cyclic) secondary amine respectively (0.001 mol.) in the presence of absolute ethanol(10 ml.) and using paraformaldehyde, (0.03 gm., 0.001 mol.), cupr-ous chloride as a catalyst, the reaction mixture was stirred at room temperature for over night. The mixture was cooled, the solid product was filtered and washed with petroleum ether and then crystallized from the appropriate solvent and vacuum dried. Physical properties are listed in Table (1-4).

RESULTS AND DISCUSSION

The present work aimed to synthesize of some new acetylenic amine of Isatin, the synthetic route used is shown in scheme (1).

3-(2,3-dimethyphenyl imino)-1H-indole-2-one [1] was prepared by condensing Isatin with 2,3-dimethy amine in absolute ethanol according to the following equation

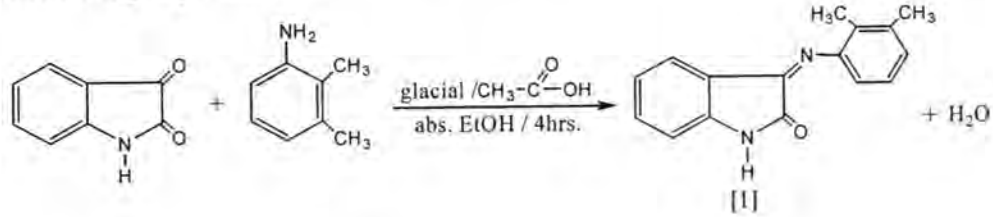

Nucleophilic addition at position C-3, the structure of [1] was confirmed by physical properties which are listed in table (1). FTIR spectra showing the absorption at 3190 cm^{-1} for (νN-H indol), 3100 cm^{-1} for (νC-H arom.), (2985, 2931) cm^{-1} for (νCH_3) aliph., 1675 cm^{-1} for (νC=N), 1612 cm^{-1} for (ν^2C=O) and disappearance the absorption of (ν^3C=O) group. The compound [1] through reaction with sodium hydrite in Dimethylformamad at 0°C to have sodium salt of Isatin derivative and subsequent reaction addition of the propargy bromide to obtained 3-(2,3-dimethy phenyl- imino)-2- oxo-1-indol-(1-prop-2-ynyl) [2] according to the following equation

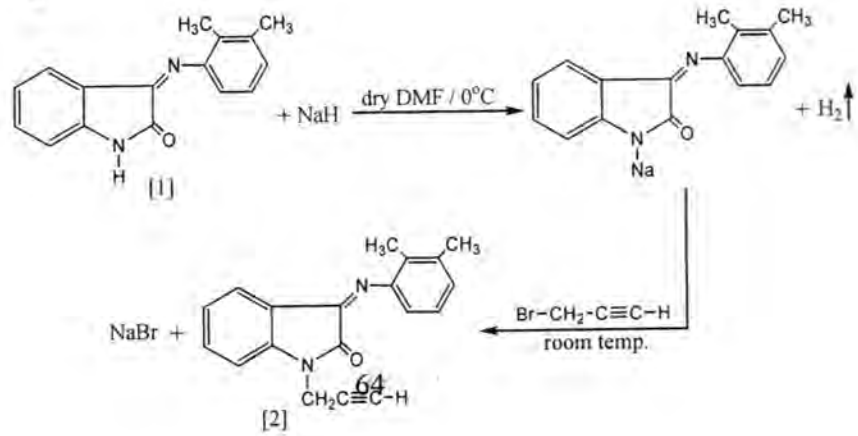

The reaction should be carried in dry condition due to that the existence of water, caused to water to react with sodium hydride according to the following equation:

$$NaH + H_2O \longrightarrow NaOH + H_2\uparrow$$

The mechanism of the prepared compound [2] is as follow:

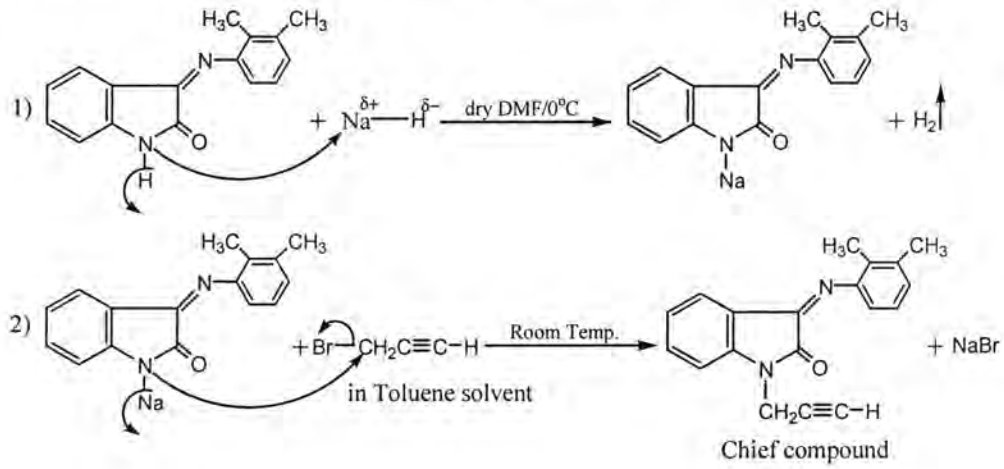

FTIR spectra of compound [2] showing the absorption at 3294 cm^{-1} for (ν≡C-H), 3070 cm^{-1} for (νC-H arom.), (2916; 2862; 2738) cm^{-1} for (νCH_3 and νCH_2), 2160 cm^{-1} for (νC≡C), 1658 cm^{-1} for (νC=N), 1604 cm^{-1} for (νC=O) and disappearance the absorption of (νN=H) group.

While ^{1}H-NMR spectra data of compound [2][17] δ ppm in DMSO-d^6 solvent. 1.9 (s, 3H,-CH_3); 2.2 (s, 3H, -CH_3); 2. 5 (S, 1H, (≡C-H); 4.6(s, 2H , >N-CH_2; 6.4-7.8(m, 7H, Ar-H). Figure (1).

^{3}C-NMR spectrum shows result were listed in table(4). Figure (2) other chemical test was carried out to characterize the prepared[2] such as Tollen reaction[18], and KI\$HgCl_2$ reaction[19].

The Mannich bases (3-17) were obtained in good yield through the reaction of compound [2] with different (aliphatic, aromatic, cyclic, and hetrocyclic) secondary amine (sheme1).The FTIR spectrum of compound [3-17] are listed in table(2). All the spectrum data show disappearance the absorption of ν≡C-H group. While the ^{1}H-NMR and ^{13}C-NMR spectrum shows result were listed in table (3 and 4) respectively.

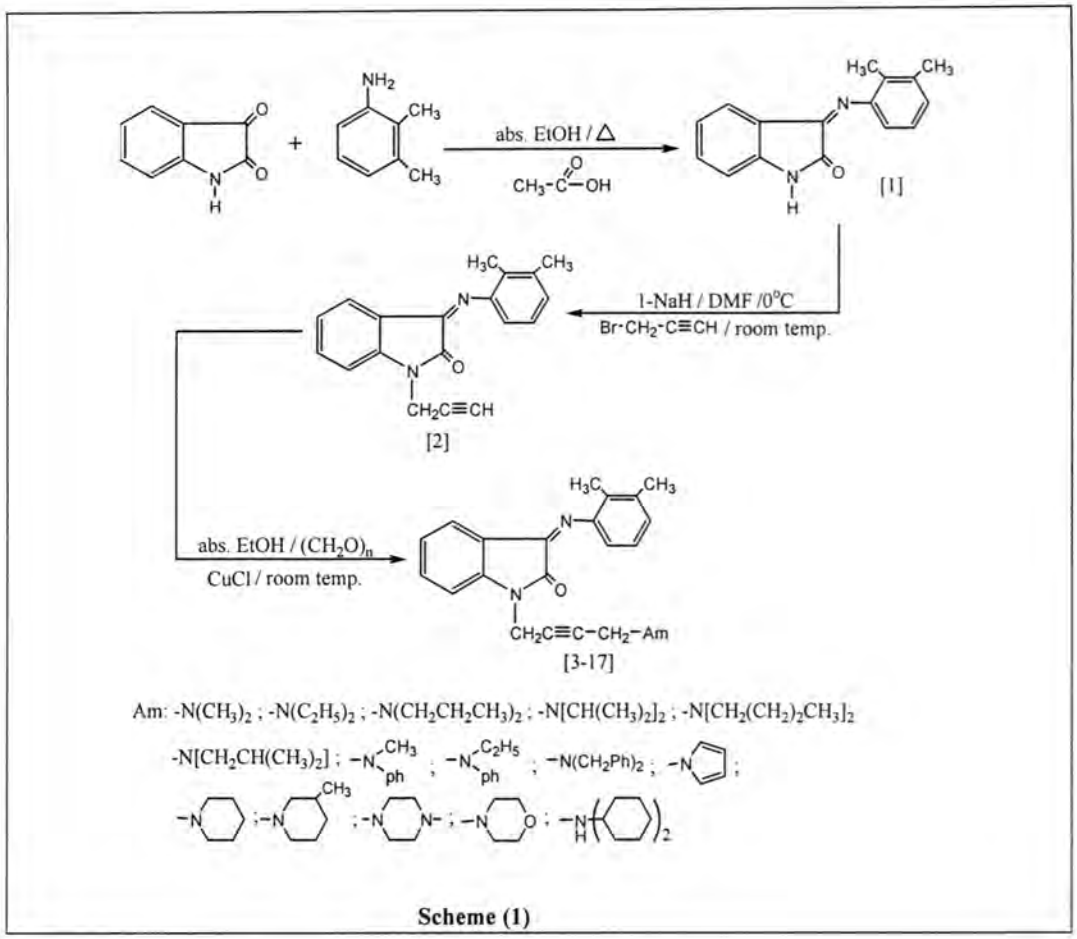
abs. EtOH / Δ
CH3-C(=O)-OH
[1]
1-NaH / DMF /0°C
Br-CH2-C≡CH / room temp.
[2]
abs. EtOH / (CH2O)n
CuCl / room temp.
[3-17]
Am: -N(CH3)2 ; -N(C2H5)2 ; -N(CH2CH2CH3)2 ; -N[CH(CH3)2]2 ; -N[CH2(CH2)2CH3]2
-N[CH2CH(CH3)2] ; -N(CH3)ph ; -N(C2H5)ph ; -N(CH2Ph)2 ;

Scheme (1)

Table -2: FTIR absorption spectra data $(cm)^{-1}$ of the prepared compounds

Comp. No.	Comp. Structure	νN-H aromatic	νCH_2 and CH_3 alph.	νC=O	νC=N	Other band
1	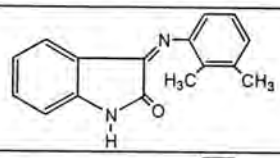	3100	2985; 2931; 2869	1612	1675	νC-N 3190 δN-H 435
2	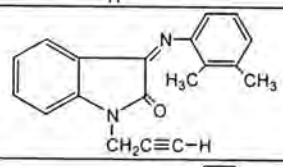	3070	2916; 2862; 2738	1604	1658	ν≡C-H 3294 νC≡C 2160
	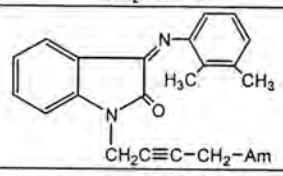					
3	$Am\text{-}N\text{-}(CH_3)_2$	3037	2981; 2916	1605	1659	νC≡C 2155
4	$Am\text{-}N\text{-}(CH_2CH_3)_2$	3032	2980; 2912	1608	1655	νC≡C 2162
5	$Am\text{-}N\text{-}(CH_2CH_2CH_3)_2$	3050	2981; 2916; 2882	1605	1650	νC≡C 2162
6	$Am\text{-}N\text{-}[CH(CH_3)_2]_2$	3030	2988; 2916; 2860	1610	1658	νC≡C 2135
7	$Am\text{-}N\text{-}(CH_2CH_2CH_2CH_3)_2$	3050	2916; 2862, 2730	1605	1657	νC≡C 2145
8	$Am\text{-}N\text{-}[CH_2CH(CH_3)_2]_2$	3056	2960; 2917; 2835	1612	1645	νC≡C 2110
9	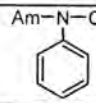	3095	2965; 2935	1615	1655	νC≡C 2160
10	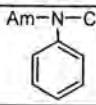	3055	2910; 2860; 2735	1604	1685	νC≡C 2148
11	$Am\text{-}N\text{-}(CH_2C_6H_5)_2$	3051	2930; 2842; 2733	1604	1658	νC≡C 2121 ν out of plane 758
12	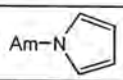	3055	2932; 2901	1658	1604	νC≡C 2112
13	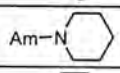	3055	2939; 2869	1612	1680	νC≡C 2121
14	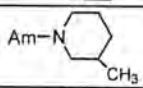	3062	2923; 2882	1612	1675	νC≡C 2121
15	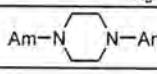	3053	2931; 2923	1604	1650	νC≡C 2119
16	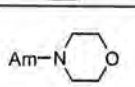	3045	2916; 2854	1604	1658	νC-O-C 1010 cyclic ether νC≡C 2090
17	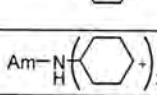	3100	2918; 2854	1624	1660	νC≡C 2133

Table -3: ^{1}H-NMR spectra for selected compounds

Comp. No.	H-NMR parameters (ppm) δ-H
2	1.9(s,3H, CH_3); 2.2(s,3H, CH_3); 2.5(s,1H, ≡C-H); 4.6(s,2H, $>N-CH_2$); 6.4-7.8(m,7H, Ar-H).
11	1.9(s,3H, CH_3); 2.2(s,3H, -CH_3); 3.5(s,4H, $N(CH_2-)_2$); 4.3-48(t,4H, CH_2); 6.3-7.7(m,7H, Ar-H).
14	0.8(s,4H, -CH_2-N cyclic); 3.9(s,4H, -CH_2- cyclic); 1.4(brod, 1H, CH cyclic); 2.5(s, 4H, -CH_2-N cyclic); 3.9(s,2H, ≡C-CH_2); 4.9(s,2H, $>N-CH_2-$); 6.3-7.8(m,7H, Ar-H).

Table -4: ^{13}C-NMR spectra for selected compound

Comp. No.	Structure	^{1}C	^{2}C	^{3}C	^{4}C	^{5}C	^{6}C	^{7}C	C all aromatic	^{8}C	^{9}C, $^{9'}$C	^{10}C	C Cyclic amine
2	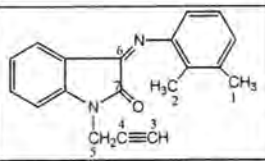	21.39	29.48	29.13	40.82	78.04	156.40	163.96	(114.51-155.26)				
11	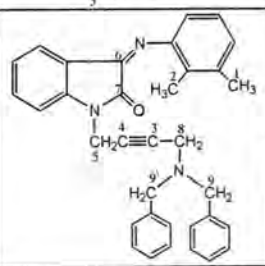	20.23	29.47	39.97	41.19	78.06	154.11	161.82	(114.15-149.29)	49.71	57.22		
14	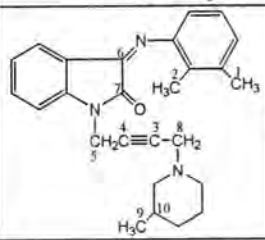	20.24	29.47	39.98	40.81	78.09	154.11	163.97	(114.53-149.30)	75.25	14.00	19.95	20.2-40.8

Antimicrobial Activity test

The test was performed according to the disk diffusion method[20]. The some of the prepared compounds were tested against two strain of Gram +ve (*Staphyloccus aureus*, *Bacillus Cerus*), and two strain of Gram –ve bacteria (*Escherichia Coil* and pseudomonas aeraginosa). Also tested against one strain of yeast (*Candidau*). Whatman No.1 Filter paper disk of 5mm diameter were sterilized by autoclaving for 15 min. at 121 C° the sterile disk were impregnated with different compounds (800 µg / disk). Agar plates were surface inoculated uniformly with 100µ from the broth culture of the tested microorganisms. The impregnated disk were place on the medium suitably spaced apart and the plates incubated at 5°C for 1hr. to premit good diffattion and then transferred to an incubator at 37 C° for 24 hrs. the inhibition zones

caused by the various compounds on the microorganisms were examined. The results are listed in table (5). From the data it is clear that all compound possess between very high and moderat activity against of yeast (*Candidau),* while compounds [2,15] possess high activity against two types of bacteria. As far as compound [16] possess high activity against three types of bacteria, while compounds [1,2, 7, and 15] showed inactive against two types of bacteria.

Table -5: Results of antimicrobial activity of the tested prepared compounds

Comp. No.	*Staph. aure*	*Staph. epide*	*Pseu. aur*	*E. Coli*	*Candidau*
1	+	-	++	-	++++
2	+++	-	+++	-	++++
7	-	-	++	+	++++
10	+++	+++	-	-	++
12	+++	++	-	++	++
15	+++	-	+++	-	++
16	+++	+++	-	+++	++

* Solvent: DMSO, [C] = 800 µg/ml , Key to symbols:
Very Highly active = ++++ (inhibition zone 21-27 mm)
Highly active = +++ (inhibition zone 15-20 mm)
Moderately active = ++(inhibition zone 10-14 mm)
Slightly active = + (inhibition zone 6-9 mm)
Inactive = - (inhibition zone < 6 mm)

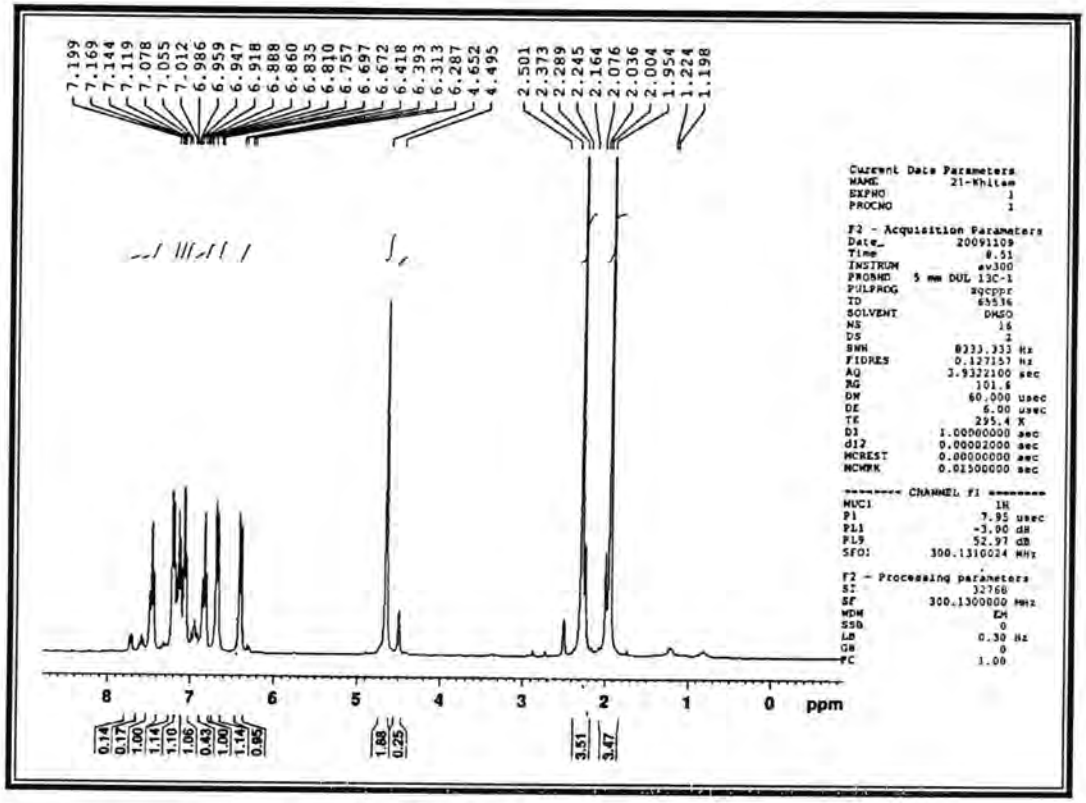

Figure -1: ^{1}H-NMR for compound No.[2]

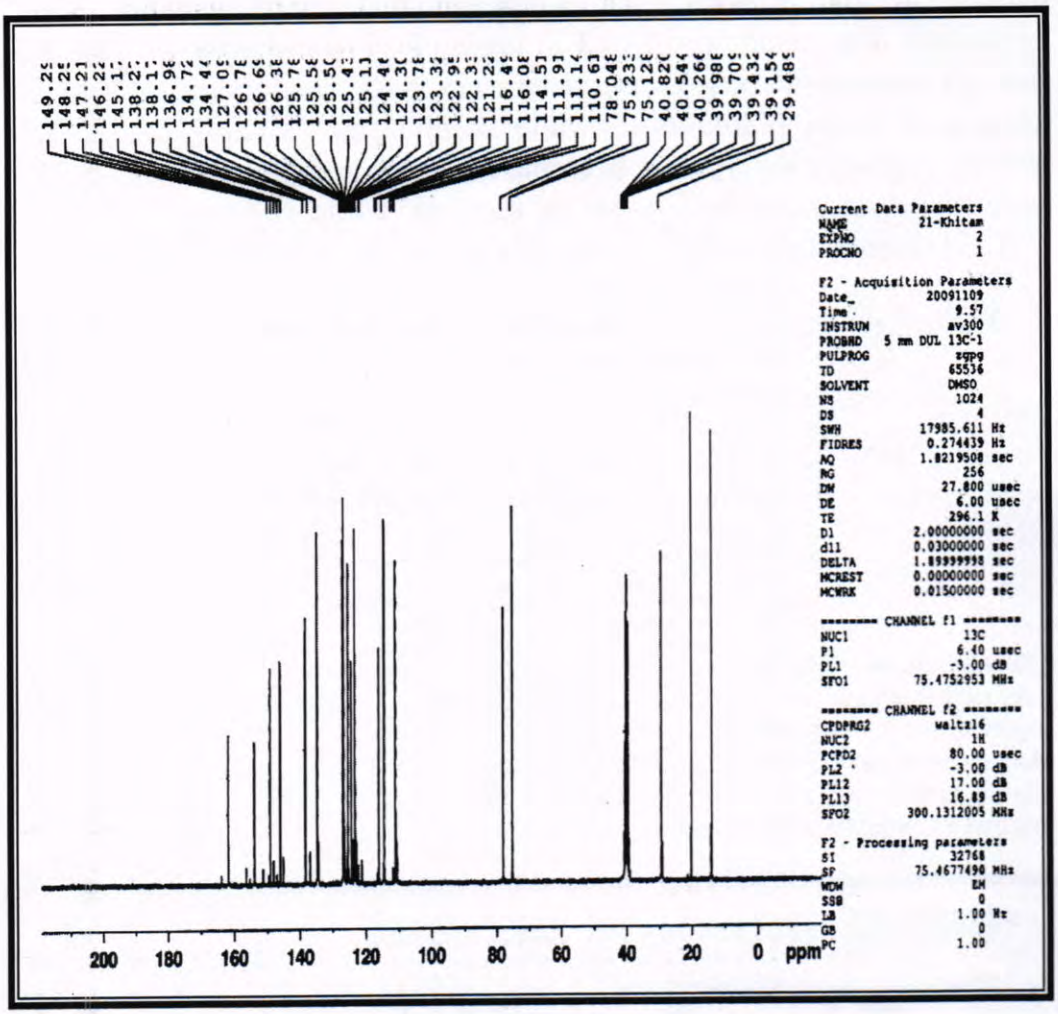

Figure -2: ^{13}C-NMR for compound No.[2]

REFERNCES

1. Sumpter , W.C., chemistry of Isatins , preparation and characterization, Chem. Rev., 34, 407. (1954).
2. Popp, F. D., General Method for chemical synthesis of Isatin , Adv. Heterocyclic. Chem.,18, 1. (1973)
3. Hvekhgeimer, M. G. A. Chem., General synthesis and Application of Isatin derivatives, Heterocycl. Compd. (Engl. Transl.)., 32, 249, (1996).
4. Dinesh, B., Chirag., Shweta, S.,Vijay, K.S., and Talesara, G.L., synthesis and pharmacological studies of some phthalimidoxy substituted spirothiazolidinone derivatives of isatin. Indian, J. Chem., Vol.48B, p: 1006-1012, (2009).

5. Surendra, N.P., Sivakumar, S., Mayank, J., and Seshaiah, K.S., Biological activities of isatin and its derivatives, Actapharm., Vol.55, P: 27-46, (2005).
6. Ankur, P., Sanjay, B., Gokul, T., Jitendra, P., and Manda, S., synthesis and antimicrobial activity of some new isatin derivatives., Iranian, J, Pharm . Res., Vol.4, p: 249-254, (2006).
7. Ashraf, H.A., Sahar, M. Ab-Seri, Doaa, E.Ab-RA., Christian, K., Olivier, L., and aurent, M. Synthesis of 3-substituted-2-oxoindole analogues and their evaluation as kinase inhibitors, anticancerant antiangio-genic agents, European, J. Med., Chem., Vol.41, p: 296-305, (2006).
8. Alagarsamy, V. and Ramseshu, K.V., Synthesis and pharmacological investigation of some novel 2,3-disubstituted quinazolin-4(3H)-on as analgesis and anti-inflammatory agents. phar., Vol.58, p: 233-336, (2003).
9. Robert, G., Jon, B., Application of Isatin in organic synthesis., J. Inds. and Ing. Chem., p: 805,(1922).
10. Silva, J. F. M., Garden, S. J., and pinto, A. C., synthesis and pharmacological investigation of some novel 2,3-disubstituted quinazolin-4(3H)-ons as analgesic and anti-inflammatory agents pharmazie, J. Braz. Chem. Soc., 12(3), p: 273-324, (2001).
11. Cerhiaro, Gand Ferreira, A. M. D.,Trityl isothiocyanate support for solid-phase synthesis, J. braz. chem. Soc., 17(8), p: 1473-1485, (2006).
12. Rutledge, T.F, In "Acetylenic Compounds, Preperation and substitution reaction" Reinhold Book corporation, Newyork, A msterdam, London, (1968).
13. Suaad, M.H. Al-Majidi, synthesis and antibacterial activity of some new acetylenic 2-mercaptobenzimidzol deriva-tives. Iraqi, J, Sci., Vol. 40A, P: 34-47, (1999).
14. Bari, S.B., Agrawal, A.O., and patil, U.K., Synthesis and pharmacological Evalution of some novel Isatin derivative for antimicrobial ctivity, J. Sci. Islamic Republic of Iran, , Vol.19(3), p: 217-221, (2008).
15. Radul, O.M., Zhungietu, g.l., Rekhter, M. A., and Bukhuyuk, S.M., Simple method for the preparation of 1-substituted isatin, Chem. Hetrocycl. comp., Vol.19, p: 286- 288, (1983).

16. Suaad, M.H. Al-Majidi, M.SC., Thesis, synthesis of actylenic 2-mercpto Benzimidazol derivatives with have Biological activity, university of Baghdad, , Baghdad, Iraq, (1995).
17. Sliverstien, R.M., and Websters, X., Spectrometric identification of organic compound, 6thEd., (1998), John wiely and sone, New york, P: 181-212, (1998).
18. Shriner, R.L.; Fuson, R.C., Cartin, D.Y., and Morril, T.C., "The systematic Identification of organic compounds" 8th ed., , John wiley and Sone, New york, p: 170, (1980).
19. Mannion, J. J., and Wany, T.S., spectrachim Acta, , Vol.17, 990, (1961).
20. Vignolo, G.M., Surian, F., Hogado, A.P. and Oliver, G., Antibacterial activity of lactobacillus strains isolated from by fermented sausage, J. APP. Bac., , Vol.75, P: 344-349, (1993).

Synthesis of Some New 3-β-D-Ribofuranosyl-2-iminothiazoline and 2-iminobenzothiazoline N-nucleosides.

Hussein I. Khalaf
Polymer Research Unit, Science College, AL-Mustansiryia University

Received 7/2/2010 – Accepted 20/6/2010

الخلاصه

تم تحضير عدد من مشتقات 2- امينوثايزول a(1-7) و2 - ا مينوبنزوثايزول a(8-12) باستخدام كاشف الهلجنه ثنائي مثيل بروموسلفونيوم بروماید (BDMS)حولت هذه المشتقات المحضره الى مركبات سلايل المناظره لها باستخدام هكسامثلين ثنائي السيليزن (HMDS) اجريت بعدها عملية ربط هذه المركبات بمشتق سكر الرايبوز باعتماد العامل المساعد سلفونات ثلاثي مثيل سلايل ثلاثي فلورو ميثان والحصول على نيوكليوسيدات مناظره جديده c (12-1). اعتمدت قيم ترددات طيف الاشعه تحت الحمراء ودرجة الانصهاروالتحليل الدقيق للعناصر(C.H.N.) لاثبات المركبات المحضره.

ABSTRACT

Various derivatives of 2-Aminothiazole (1-7)a and 2-Aminobenzothiazole (8-12) a were synthesized by using a halogenating agent dimethylbromosulfonium bromide (BDMS). These derivatives were converted to the corresponding silane compounds by hexamethyldisilizane (HMDS) reagent. Finally, the glycosidation was done by using trimethyl silyl triflouromethane sulfonate as catalyst to synthesis some new 3-β-D-ribofuranosyl-2-iminothiazoline and 2-iminobenzothiazoline N-nucleosides (1-12) c. The Infrared, Melting Points and Elemental Analysis (C.H.N.) of these compounds were used to confirm the formation of these compounds.

INTRODUCTION

Nucleoside analogous generally posses outstanding activity mainly as antitumor and antiviral agents. This nucleoside analogous may be made by a modification of the base or sugar units, thereby producing a biological activity [1-7].

After ribofuranosyl nucleosides(in which the base moiety is a five-membered heterocyclic ring) have been found to display chemotherapeutic activity [8]. More significant among these are Pyrazomycin, Showdomycin, Virazole (Ribavirin) and Tiazofurin [9, 10].

Tiazofurin is (2-β-D-ribofuranosyl thiazole carboxamide) has been used as a drug for treatment of human lymphoid tumors, which is represented as typical example of five-membered thiazole base. Traditionally the synthesis of these nucleosides analogous has been accomplished by Silyl-Hilbert Johnson method [11-14].

In these methods, the nucleosides were obtained from the Friedel-Crafts catalyzed reaction of polyacylated sugar and silylated heterocyclic compound in a protic solvent.

The production of five-membered base N-nucleoside, 5-Amino-2-(β-ribofuranosyl)-1, 2, 4-thiadiazole-3-one, which represents a new class of cytidine analogous[15], and several 2-Iminothiazolines were synthesized by treated of an alkyl halide with 2-Aminothiazoles through

the nitrogen of the ring[16] encouraged us to continue our previous work [17]to synthesize some of new 2-Iminothiazoline N-nucleosides analogous promising have a biological activity.

MATERIALS AND METHODS

Instruments:

Melting points were obtained on a Gallenkamp melting point apparatus are uncorrected. Infrared spectra (KBr) recorded on a Shimadzu 8261 PC Spectrophotometer. Elemental analysis (C. H. N) was performed on a Perkin 240C Elemental Analyzer.

Thin layer chromatography was performed on Fluka T.L.C-cards silica gel (0.2 mm) with fluorescent indicator. The compounds were detected with a UV light (254nm), or by spraying the plates with 30% H_2SO_4 in ethanol and heating at 110°C.Evaporation was carried out with a Buchire RE120 rotary evaporator under reduced pressure. Most of the chemicals used in this work were purchased from either Fluaka AG or BDH ltd with high degree of purity and they were used without purification. All the solvents were dried by the methods explained in Vogel practical organic chemistry textbook. The starting material, 1-O-Acetyl-2, 3, 5-tri-O-benzoyl-β-ribofuranose was prepared according to Recondo method [18].

Synthesis of Bromodimethyl Sulfonium Bromide (BDMS):

To a solution of dimethylsulfide (10ml, 130mmol) in methylene chloride (100ml) cooled to -40°Cunder liquid nitrogen, a bromine (15.01g,94mmol) solution in methylene chloride (30ml) was added within 30 minutes. A yellow precipitate was formed immediately. The mixture was stirred for 20 minutes, and then 100ml of ether was added. The precipitate was filtered and washed twice with ether and pentane to afford bromodimethylsulfonium bromide as a crystalline compound (18.5g, 88%).

Synthesis of α-Bromodicarbonyl Compounds (1-7):

A 1, 3- dicarbonyl compound (2-2.5mmol) was dissolved in 50ml of cooled (0°C) methylene chloride and added with stirring continuously for 40-60 minutes to a solution of BDMS, (2.5mmol) in cooled (0°C) solvent (methylene chloride: acetonitrile, 25ml: 25ml) .The mixture was keept at zero temperature. A yellowish white precipitate was obtained; the precipitate was filtered and washed with ether and pentane. A 50ml of water containing sodium bicarbonate (7.0g) was added to the precipitate and warming up to 35°Cfor 15 minutes. The mixture was extracted with methylene chloride(3×25ml).The methylene chloride layer was washed with water and dried on sodium sulfate. The

methylene chloride was evaporated under vacuum to give α-bromodicarbonyl solid product. The melting point and infrared spectrum bands values of each compound are reported in table 1.

Synthesis of Substituted 2-Aminothiazole Compounds (1-7) a:

The prepared compound α-bromodicarbonyl (8.3mmol) was dissolved in a mixture of $CHCl_3$: EtOH $_{(abs)}$ (25ml: 25ml) along with thiourea (17mmol). The mixture was refluxed with stirring under Nitrogen for 12h, then cooled and the solvent evaporated to get a solid product. Dissolution of the solid was affected (5ml, 95%EtOH: H_2O, 1:20). Adjustment the pH of the solution to be 10 by conc.NH_4OH. The solution was cooled to (5°C) overnight. The obtained yellow solid precipitate was filtered out, dried and purified by recrystalization from 96%EtOH. The melting point and infrared spectrum bands values of each compound are shown in table 2.

Synthesis of Fused 2-Aminobenzothiazole Compounds (8-12) a:

To a cooled mixture of para-substituted aniline or 3-aminopyridine (3.2mmol) and ammonium thiocyanate (6.0mmol) in Acetonitrile(30ml), a bromodimethyl sulfonium bromide (3.0mmol) dissolved in acetonitrile (30ml) was added slowly with stirring for 60 minutes at room temperature. The solvent of the mixture was evaporated under vacuum. The solid product that was obtained washed with chloroform. The result product was dissolve in rectified spirit (100ml) and basified with ammonia solution. The precipitate was filtered, washed with water and dried over sodium sulfate. Recrystalization by aqueous ethanol (80%) was done. A white crystalline solid were obtained. The melting point and characteristic infrared spectrum bands values of each compound are shown in table 3.

General Method for Silylation of 2-Aminothiazoles and 2-Amino-benzothiazoles:

A stirred mixture of the dry 2-aminothiazoles or 2-aminobenzothiazoles (10mmol),
hexamethyldisilinzane (HMDS) (50ml) and ammonium sulphate (50mg) was heated in 100ml round bottom flask fitted with a reflux condenser provided with $CaCl_2$-tube. The solution was kept for 2 hrs. under refluxing. After cooling, the excess of HMDS was removed completely under diminished pressure at 60°C on rotary evaporator. Finally the residue was coevaporated with dry toluene (2×25ml); the drying was continued 6hrs to give 2-trimethylsilylaminothiazoles as viscous oil, which was used without purification for the nucleosidation reaction.

Synthesis of 3-(2, 3, 5-tri-O-benzoyl-β-D-2-iminothiazoline ribofuranosyl)-N-nucleosides (1-12) b:

A crude prepared silylated 2-aminothiazole was dissolved in 30 ml of dry acetonitrile and added to a solution of 1-O-Acetyl-2, 3, 5-tri-o-benzoyl-β-D-ribofuranose (4.025g, 8.0 mmol), dissolved in 20ml of dry acetonitrile in 100ml round bottom flask. The mixture was ice cooled and a trimethylsilyl triflouromethane sulfonate catalyst (1.8ml, 10mmol) was added slowly with exclusion of moisture. The yellow homogeneous solution was kept for 8 hrs. at room temperature until t.l.c (solvent system, toluene:acetic acid:H_2O, 5:5:1) indicated completion of the reaction. The solution was evaporated and the residue was partitioned between an aqueous solution of $NaHCO_3$ (40 ml) and chloroform (2×40ml) . The combined extracts were dried on Na_2SO_4, filtered and evaporated to dryness to give a crude product, which purified on a silica gel chromatographic column (40g) and eluted with $CHCl_3$ MeOH (95:5) to give on subsequent evaporation an amorphous product.Recrystallization from ethanol gave 2-Iminothiazoline nucleoside as a solid product. The melting point and characteristic infrared bands values are shown in table 4.

Synthesis of 3-(β-D-ribofuranosyl) 2-imino-thiazoline N-nucleosides (1-12) c:

A solution of the prepared blocked 2-Iminothiazoline N-nucleosides (0.54g, 1mmol) in methanol (10 ml) was stirred with methanolic ammonia (saturated at 0c°, 20ml) in a stoppard pressure flask at room temperature for two days. The solvent was evaporated under vacuum on a rotary evaporator, and the product was crystallized from ethanol to give the 3-(β-D-ribofuranosyl) 2-iminothiazoline N-nucleoside.The melting point, characteristic infrared spectrum bands values and C. H. N analysis are shown in table 5.

RESULTS AND DISCUSSION

The derivative 1-O-Acetyl-2, 3, 5-tri-O-benzoyl-β-D-ribofuranose (as sugar unit of the nucleosides) was synthesized freshly, starting from ribose sugar by a slightly modified of Recondo and Rinderkecht method [18]. The derivative was characterized by its melting point (130-132°C) and infrared spectrum (Lit.).

The brominating agent (BDMS) was synthesized according to Yuan [19] procedure with very good yield as a light orange solid has a sharp melting point (83°C).

This reagent was used to prepare the α-_bromodiketones with efficient yield, fast and easy procedure [20] .These products were characterized by

υ^{C-Br} (770-788) $\upsilon^{C=O}$ (1725-1740) cm^{-1} and υ^{CONH}(1660-1690) cm^{-1}, that are shown in table 1.

The 2-aminothiazole derivatives were prepared with very good yield according to Beriln procedure [21]. It is an application of Hantzsch reaction [9]. The infrared absorption spectra of these compounds showed two medium intensity bands at 3455-3205 cm^{-1} region and strong band at 1450-1590 cm^{-1} region related to stretching vibration and deformation vibration respectively, for NH_2 group attached to carbon position two in the thiazole ring. In addition a weak band at 640-665 cm^{-1} region was appeared due to the υ^{C-S-C}. All these compounds showed strong band at 1600-1690 cm^{-1} region and other one or two medium bands at 1440-1560cm^{-1} region which are characterized of thiazole structure.

The fused 2-aminobenzothiazoles were prepared by depending Bhalerao method [22], in which (BDMS) reagent have been used directly. The infrared spectra of these compounds indicated the presence of NH_2 group in addition to stretching vibrations at 1450-1470cm^{-1} region, 1230-1270cm^{-1} and 1020-1050cm^{-1}region as benzothiazoles characteristic bands[23].

In this investigation, the 2-amino group of the prepared 2-aminothiazole was silylated by reacted with (HMDS) using ammonium sulfate as efficient catalyst according to a standard procedure [16].The silylated products were viscose, oily or semisolid; they were used in nucleosidation directly without purification.

Trimethyl silytrifluoromethane sulfate ($Me_3SiDSD_2CF_3$) was used as catalyst in the glycosylation of silylated 2-aminothiazoles with the ribofuranosyl derivative.This catalyst was prepared freshly by simple method [12] from heating trimethylsilyl chloride (TMS) and trifluorosulfonic acid (CF_3SO_3H). Good yields of blocked 3-(2-Aminothiazoline) ribofuanose were obtained from the glycosidation. Table 4. showed typical infrared spectra bands values of this products. They were indicated the absence of the acetate group at anomeric carbon number one in the ribofuranosyl derivative, due to the absence of the characteristic bands at 1370-1390cm^{-1} and 935-945cm^{-1}. In addition, a broad beak at 3420-3310cm^{-1} and weak intensity band at 650-670cm^{-1} were appeared due to N-H imino group and υ^{C-S-C} respectively.

To obtain a good yield from glycosidation process we must remove any excess of (HMDS) from the silylated 2-aminothiazoles by heating under efficient vacuum and the prepared 1-O-Acetyl-2, 3, 5-tri-O-benzoyl ribofuranose should be always powered and dried at 70°C under reduced pressure. This was done to keep the glycosidation catalyst ($Me_3SiDSO_2CF_3$) from decay.

The mechanism of the glycosidation reaction can be summarized as follows [12]:

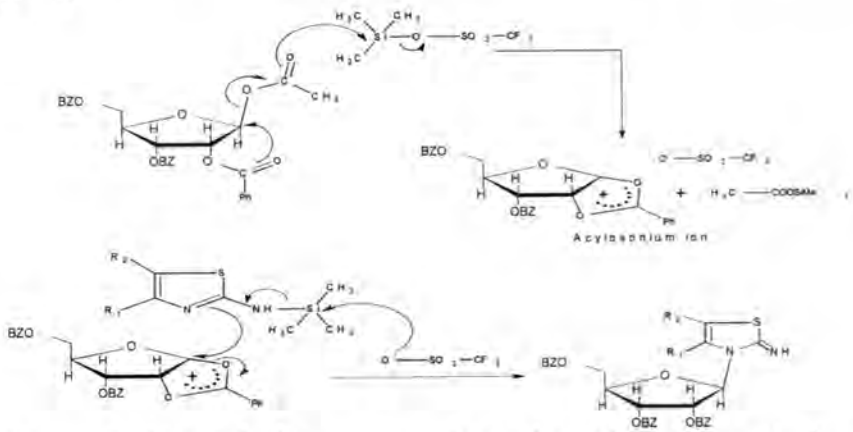

Debenzoylation of the prepared nucleosides proceeded well in methanol saturated with ammonia gas at room temperature to give in almost yield of corresponding nucleosides.Table 5. showed the melting point, infrared spectra bands values and C. H.N. analysis of the final 3-β-D-ribofuranosyl-2-iminothiazoline compounds. The infrared values indicated the removing of benzoyl groups of the ribofuranose sugar due to the absence of $\upsilon^{C=O}$ at 1725-1740 cm^{-1}, moreover a broad band was appeared at 3380-3245 cm^{-1} due to hydroxyl groups of sugar unit.

A total of new 12 Iminothiazole N-nucleoside analogues were synthesized, starting from 1- O –Acetyl-2,3,5-tri-O-benzoyl-β-D-ribofuranos , which was prepared from D-ribose sugar. BDMS reagent was efficient chemoselective brominating agent to prepare α-bromodiketones, which were used to prepare some new 2-aminothiazole and 2-aminobenzothiazole derivatives. The amino group of 2-aminothiazoles can be silylated with HMDS successfully and it was easily converted to imino group in the glycosidation process.

Table -1: The Synthesized α-Bromodiketons Compounds (1-7).

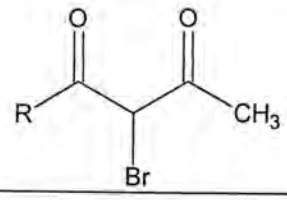

Comp. No.*	R	Infrared vibrations(cm^{-1})	m.p °C	Yield %
1	NH_2	3300,3250(υ, NH_2), 2980(υ,CH_3), 1735(υ,C=O), 1660(υ,$CONH_2$),1440(υ,N-H deformation),1230(υ,C-N) 779 (υ,C-Br)	77-81	95
2	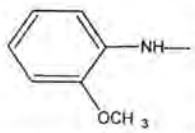	3170(υ,NH),3020(υ,C-H romatic),2985(υ,CH_3), 1730(υ,C=O), 1662(υ,$CONH_2$),1575,1540(υ, C=C aromatic),1245(υ ,C-N),770(υ,C-Br)and (ortho-disub. benzene)	114-117	89
3	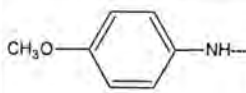	3180(υ,NH), 3040(υ,C-H aromatic), 2980(υ,CH_3) ,1733(υ,C=O),1665(υ,CONH2),1565, 1520(υ C=C aromatic),1260(υ, C-N), 758(υ,C-Br),820(para-disub. benzene)	135-140	88
4	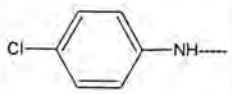	3150(υ,NH),,3030(υ,C-H aromatic) ,2987(υ,CH_3) , 1725(υ,C=O),1690 (υ,$CONH_2$), 1550,1520(υ C=C aromatic), 1285(υ , C-N),780(υ ,C-Cl),745(υ,C-Br) ,835(para-disub. benzene)	155-160	85
5	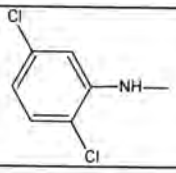	3110(υ,NH),3020(υ,C-H aromatic),2990(υ,CH_3), 1733(υ,C=O),1690(υ,$CONH_2$),1590,1530(υ C=C aromatic), 1295(υ ,C-N),779(υ,C-Cl), 750(υ,C-Br), 860(multi-sub. benzene)	122-126	89
6	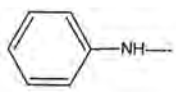	3200(υ,NH), 3030(υ,C-H aromatic),2983(υ,CH_3), 1740(υ,C=O),1670(υ,$CONH_2$),1570,1520(υ C=C aromatic), 1225(υ ,C-N),780(υ,C-Br), 759,695(monosub.benzene)	104-109	90
7	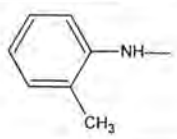	3150(υ,NH),3030(υ,C-H aromatic),2900(υ,CH_3), 1733(υ,C=O),1692(υ, $CONH_2$), 1580, 1510(υ, C=C aromatic) 1245(υ , C-N),788(υ, C-Br), 748(ortho-disub. benzene)	125-129	90

*

1.α-Bromoacetoacetamide, 2. α-Bromoaceto-2-methoxyacetanilide, 3. α-Bromoaceto-4-ethoxyacetanilide, 4. α-Bromoaceto-4-chloroacetanilide, 5. α-Bromoaceto-2,5-dichloroacetanilide,6.α-Bromoacetoacetanilide, 7. α-Bromoaceto-2-methylacetanilide.

Table -2:The Synthesized 2-Aminothiazole Derivative Compounds (1-7) a.

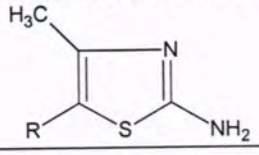

Comp. No.*	R	Infrared vibrations(cm^{-1})	m.p°C	Yield %
1-a	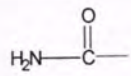	3410,3290(υ, NH_2), 2985(υ,CH_3), 1680 (υ,$CONH_2$) , 1610(υ,C=N),1580 (υ,C=C),1205,1050,660(υ,thiazole ring)	160-165	80
2-a	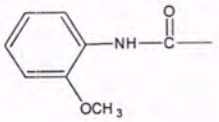	3405,3285(υ, NH_2), 3020 (υ, C-H aromatic) , 2980 (υ,CH_3) ,1670 (υ,$CONH_2$) , 1620 (υ,C=N) , 1560 , 1450 (υ, C=C aromatic) and (C=C,thiazol), 1200 , 1070,640 (υ,C-S-C,thiazole ring),760 (ortho-disub. benzene)	180-185	80
3-a	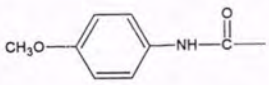	3420,3290,3130, (υ, NH_2),3035(υ, C-H romatic) , 2987 (υ,CH_3) , 1684(υ,$CONH_2$) , 1613(υ,C=N),1562,1477 (υ C=C aromatic) and (C=C,thiazol),1200,1057,660 (υ,C-S-C,thiazole ring), 810(para-disub. benzene)	200-205	88
4-a	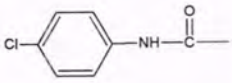	3400,3288,3120 (υ, NH_2),3033(υ, C-H aromatic), 2982 (υ,CH_3), 1690(υ,$CONH_2$),1610(υ,C=N),1550,1438(υ, C=C aromatic) and (C=C,thiazol),1190, 1055,647,783 (υ,C-S-C thiazole ring), 765 (υ ,C-Cl)	220-224	84
5-a	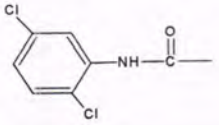	3440,3250,3170(υ, NH_2), 3035(υ, C-H romatic), 2990(υ,CH_3),1693(υ,$CONH_2$),1630(υ,C=N),1556,1440(υ C=C aromatic) and (C=C,thiazol) , 1205,1060,650, (υ,C-S-C,thiazole ring), 770(υ,C-Cl),840 (multi-sub. benzene)	215-218	87
6-a	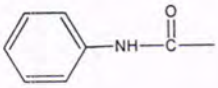	3455,3280,3120(υ, NH_2),3030(υ, C-H romatic), 2985(υ,CH_3), 1680(υ,$CONH_2$), 1600 (υ,C=N), 1566 , 1480(υ C=C aromatic) and (C=C,thiazol), 1179, 1050, 665(υ,C-S-C,thiazole ring), 750,675(monosub.benzene)	198-200	86
7-a	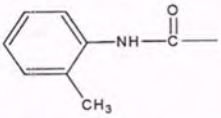	3440,3205,3170(υ, NH_2),), 3035(υ, C-H romatic), 2987(υ,CH_3), 1687(υ,$CONH_2$), 1599(υ,C=N), 1590,1450, (υ, C=C aromatic) and (C=C,thiazol),1200,1030,647(υ,C-S-C,thiazole ring), 770 (ortho-disub. benzene)	210-214	89

*(1-a) 2-Amino-4-methyl-5-thiazole carboxamide,(2-a) 2-Amino-4-methyl-5-thiazole 2-methoxyacetanilide,(3-a) 2-Amino-4-methyl-5-thiazole 4-methoxyacetanilide,(4-a) 2-Amino-4-methyl-5-thiazole 4-chloroacetanilide,(5-a) 2-Amino-4-methyl-5-thiazole 2,5-dichloroacetanilide,(6-a) 2-Amino-4-methyl-5-thiazolo acetanilide,(7-a) 2-Amino-4-methyl-5-thiazole 2-methylacetanilide

Table -3: The Synthesized 2-Aminobenzothiazole Derivative Compounds (8-12) a.

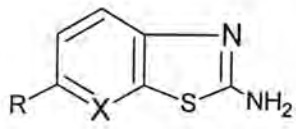

Comp. No.*	R	X	Infrared vibrations(cm^{-1})	m.p. °C	Yield %
8-a	OEt	C	3440,3295,3100(υ, NH_2),3020(υ, C-H aromatic), 2989,2880(υ,CH_3CH_2), 1610 (υ,C=N) , 1590, 1450,1250,1020, 660 (υ,benzothiazole ring)	161-166	87
9-a	Cl	C	3430,3280,3097(υ, NH_2),3027(υ, C-H aromatic), 1600(υ,C=N),1587, 1438,1270,1030 , 677(υ,benzothiazole ring) ,767((υ,C-Cl)	199-202	82
10-a	F	C	3400,3250,3120(υ, NH_2),3033(υ, C-H aromatic), 1600(υ,C=N),1615,1460,1270,1050 , 670(υ,benzothiazole ring) ,783(υ,C-F),	182-185	84
11-a	Br	N	3410,3280,3130(υ, NH_2),3040(υ, C-H aromatic), 1610(υ,C=N),1598,,1465,1250,1045 , 644(υ,benzothiazole ring),770(υ,C-Br),	245dec.	86
12-a	Cl	N	3430,3280,3133(υ, NH_2),3020(υ, C-H aromatic), 1605 (υ,C=N),1599,1470,1230, 1044 , 640(υ,benzothiazole ring),779(υ,C-Cl)	260dec.	85

*
(8-a) 2-Amino-6-ethoxybenzothiazole,(9-a) 2-Amino-6-chlorobenzothiazole,(10-a) 2-Amino-6-flourobenzothiazole,(11-a) 2-Amino-6-bromopyridothiazole,(12-a) 2-Amino-6-chloropyridothiazole

Table-4: The Synthesized 3-(2, 3, 5-Tri-O-benzoyl β-furanosyl) - 2-iminothiazoline and -2-iminobenzothiazoline compounds (1-12) b.

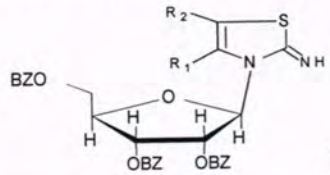

BZ= $-C^{//}_{O}$-Ph

Comp. No.	R_1	R_2	Infrared vibrations(cm^{-1})	m.p. °C	Yield %
1-b	CH_3	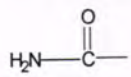	3340,3150 (υ,N-H amine& imino), 3030(υ,C-H aromatic) ,2970(υ,CH_3) ,1725(υ,C=O) ,1660(υ, $CONH_2$), 1600 (υ,C=N) ,1550 ,1500 (υ ,C=C aromatic), 1320 ,1270 , 1220 , 650 (υ,thiazoline ring),	165-170	72
2-b	CH_3	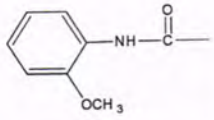	3334,3130,(υ,N-H amide& imino), 3025(υ,C- H aromatic) ,2983(υ,CH_3) ,1730 (υ,C=O) ,1657 (υ,C ONH_2) ,1599 (υ,C=N) , 1545 1505(υ ,C=C aromatic), 1290,1268 , 1200 , ,665(υ,thiazoline ring) , 750 (ortho-disub. Benzene)	155-158	70
3-b	CH_3	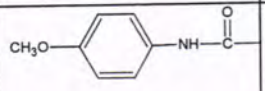	3348,3160 (υ,N-H amide& imino), 3040(υ,C- H aromatic) ,2988(υ,CH_3) ,1733 (υ,C=O) , 1660(υ, $CONH_2$) ,1600(υ,C=N),1550, 1500 (υ , C=C aromatic), 1295,1260, 1200 , 670 , (υ,thiazoline ring) ,800 (para-disub. benzene)	166-170	74
4-b	CH_3	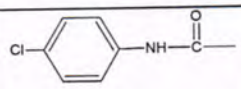	3310,3110, (υ,N-H amide& imino), 3020(υ,C-H aromatic) , 2970(υ,CH_3) ,1734 (υ,C=O) ,1665(υ, ONH_2) ,1605 (υ,C=N) ,1560, 1498(υ , C=C aromatic),1260, 1310, 1200, 665 (υ,thiazoline ring) , 800 (para-disub. benzene)780(υ,C-Cl)	176-180	69
5-b	CH_3	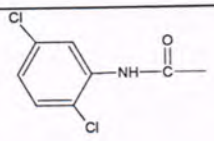	3330,3170 (υ,N-H amide& imino), ,3040(υ,C- H aromatic), 2975(υ,CH_3) 1740 (υ,C=O) , 1660(υ, $CONH_2$) , 1610 (υ,C=N) , 15501490(υ , C=C aromatic) ,1250, 1320 1205, ,667, (υ,thiazoline ring) ,785 (υ,C-Cl)	174-177	77
6-b	CH_3	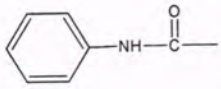	3420,3150 (υ,N-H amide& imino) , 3020 (υ,C- H aromatic), 2970(υ,CH_3) 1732(υ,C=O) ,1680(υ, $CONH_2$) ,1600 (υ,C=N) ,1540 , 1490(υ , C=C aromatic),1304, 1230 660(υ,thiazoline ring), 780,675 (monosub.benzene)	145-150	74
7-b	CH_3	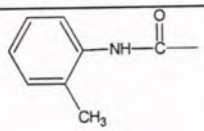	3355,3120 (υ,N-H amide& imino), 3040(υ,C- H aromatic) ,2988(υ,CH_3) ,1740 (υ,C=O) , 1660(υ , $CONH_2$) ,1598 (υ,C=N), 1520 , 1480(υ , C=C aromatic),, 1300, 1270, 1200, ,670(υ,thiazoline ring)	175-178	66

8-b	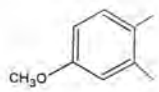	3345(υ,N-H imino) , 3030 (υ,C- H aromatic) , 2990(υ,CH_3) ,1730 (υ,C=O) , 1610 (υ,C=N) ,1560 1500(υ , C=C aromatic),1300,1290, 1250, ,670, (υ,benzothiazoline ring),745(sub.ring)	144-150	70
9-b	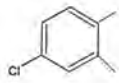	3320(υ,N-H imino) , 3015 (υ,C- H aromatic), 1728(υ,C=O) , 1597(υ,C=N) 1505, 1470(υ , C=C aromatic), 1298, 1287, 1260, ,665(υ,benzothiazoline ring), 760 , 805(sub.ring)	166-170	71
10-b	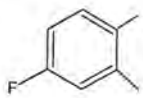	3335(υ,N-H imino),3020(υ,C- H aromatic), 1730(υ,C=O), , 1610 (υ,C=N), 1570, 1520(υ , C=C aromatic), 1260,1230, ,670(υ,benzothiazoline ring), 750 , 790(sub.ring)	156-158	69
11-b	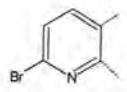	3330(υ,N-H imino), 3010(υ,C- H aromatic),1725(υ,C=O), 1580(υ,C=N) 1520 , 1480(υ , C=C aromatic) ,1270, 1250, ,670 (υ,benzothiazoline ring),745,800(sub.ring)	180-185	65
12-b	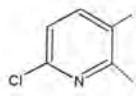	3318(υ,N-H imino), 3020(υ,C- H aromatic), 1728(υ,C=O) 1600(υ,C=N), 1530 , 1495(υ , C=C aromatic) ,1300, 1260, ,660(υ,benzothiazoline ring), 745,800(sub.ring)	200-204	65

Table-5: The Synthesized 3-β-D-Ribofuranosyl-2-iminothiazoline and -2-iminobenzo- thiazoline Compounds (1-12) c.

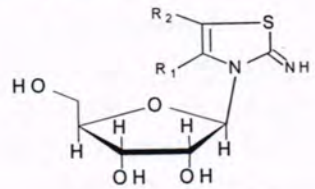

Comp. No.*	R_1	R_2	Infrared vibrations(cm^{-1})	m.p. °C	Yield %
1-c	CH_3	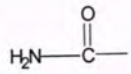	3380,3190(υ,NH & OH), 2985(υ,CH3) , 1690(υ,$CONH_2$) , 1585(υ,C=N), 1555 (NH_2,)bending,1300, 1210, 650 (υ,thiazoline ring),1040(υ,C-O-C)	190-194	85
2c	CH_3	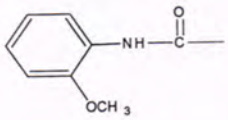	3310,3180(υ,N-H & OH) ,3040 (υ,C-H aromatic),2995(υ,CH_3),1670(υ,$CONH_2$), 1600(υ,C=N),1550,1475(υ,C=C aromatic),1320,1210,680(υ,thiazoline ring),1030(υ,C-O-C),735(ortho-disub. benzene)	175-179	87
3-c	CH_3	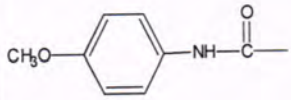	3315,3120(υ,N-H & OH), 3030(υ,C-H aromatic)2980(υ,CH_3),1650(υ,$CONH_2$) , 1605(υ,C=N) ,1560, 1440(υ ,C=C aromatic), 1290, 1220, 730(υ,thiazoline ring) 1038(υ,C-O-C), 805(para-disub. benzene)	185-188	89
4-c	CH_3	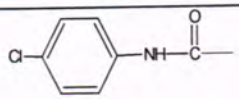	3370,3089(υ,N-H&OH), 3040(υ,C-H aromatic)2960(υ,CH_3),1670(υ,$CONH_2$ 1615(υ,C=N) 1520,1430 (υ ,C=C aromatic), 1295, 1190, 660(υ,thiazoline ring) 1035(υ,C-O-C), 800(para-disub. benzene)	196-200	84
5-c	CH_3	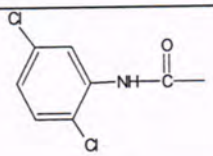	3340,3100 (υ,NH & OH), 3020 (υ,C-H aromatic)2965(υ,CH3),1680(υ,$CONH_2$) ,1580,1540(υ ,C=C aromatic) ,1300, 1205 ,687(υ,thiazoline ring) 1030(υ,C-O-C), 820(sub.ring)	204-207	88
6-c	CH_3	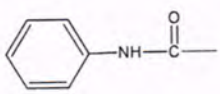	3300,3100(υ,NH&OH)3010(υ,C-H aromatic),2990(υ,CH_3)1660(υ,$CONH_2$) , 1580 (υ,C=N) ,1550 1485 (υ , C=C aromatic),1295, 1200, ,650(υ,thiazoline ring), 1045 (υ,C-O-C),730, (monosub. benzene)	165-169	86

7-c	CH_3	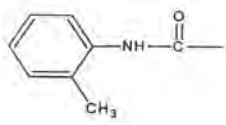	3330,3100(υ,NH&OH),2986(υ,CH_3),1675 (υ,$CONH_2$) ,1580 (υ,C=N),1560,1490 (υ , C=C aromatic),1286,1200,670 , (υ,thiazoline ring), 1035 (υ,C-O-C), 725 (ortho-disub. benzene)	190-193	86
8-c		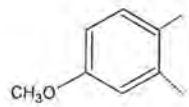	3265,3120(υ,NH&OH),2985(υ,CH_3), 1608(υ,C=N),1540, 1500(υ , C=C aromatic) , 1289 ,1220 ,680 (υ, benzo thiazoline ring) 1038(υ,C-O-C) , 740(sub.ring)	170-172	83
9-c		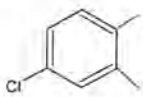	3290,3105(υ,NH&OH), ,1607 (υ,C=N) ,1560,1510(υ ,C=C aromatic),1300,1230, 666, (υ, benzo thiazoline ring)1048(υ,C-O-C) , 754(υ,C-Cl), 788(sub.ring)	187-190	80
10-c		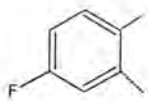	3300,3120(υ,NH&OH), ,1608 (υ,C=N) ,1540,1505(υ ,C=C aromatic), 1295,1210 ,660(υ, benzothiazoline ring),1028(υ,C-O-C) 790(υ,C-F),730(sub.ring)	174-179	85
11-c		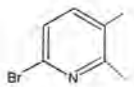	3245,3130(υ,NH&OH), ,1607(υ,C=N) ,1530,1500(υ ,C=C aromatic) 1290, 1190 680, (pyridothiazoline ring)1050(υ,C-O-C) , , 655 (υ,C-Br) ,740(sub.ring)	205-208	88
12-c		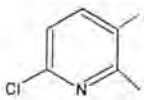	3300,3150(υ,NH&OH), ,1608(υ,C=N), 1560,1500(υ ,C=C aromatic) 1289 ,1205, 670(pyridothiazoline ring) 1045(υ,C-O-C) , 710 (υ,C-Cl) ,780(sub.ring)	215-217	86

* **1-c**. 3-(β-D-ribofuranosyl),4-methyl,5-caboxyamide-2-iminothiazoline,**2-c**. 3-(β-D-ribofuranosyl),4-methyl,5-(2-methoxycarboxyanilide-2-iminothiazoline,**3-c.**3-(β-D-ribofuranosyl),4-methyl,5-(4-methoxycarboxyanilide-2-iminothiazoline,**4-c.** 3-(β-D-ribofuranosyl),4-methyl,5-(4-chlorocarboxyanilide-2-iminothiazoline,**5-c.** 3-(β-D-ribofuranosyl),4-methyl,5-(2,5-dichlorocarboxyanilide-2-iminothiazoline,**6-c.** 3-(β-D-ribofuranosyl),4-methyl,5-(carboxyanilide-2-iminothiazoline,**7-c.** 3-(β-D-ribofuranosyl),4-methyl,5-(2-methylcarboxyanilide-2-iminothiazoline,**8-c.** 3-(β-D-ribofuranosyl),5-methoxy-2-iminobenzothiazoline,**9-c.** 3-(β-D-ribofuranosyl),5-chloro-2-iminobenzothiazoline,**10-c.** 3-(β-D-ribofuranosyl),5-flouro-2-iminobenzothiazoline,**11-c.** 3-(β-D-ribofuranosyl),5-bromo-2-iminopyridothiazoline,**12-c.** 3-(β-D-ribofuranosyl),5-chloro-2-iminopyridothiazoline,

Table -6: Chemical Formula and C, H, N Analysis of the Synthesized 2-Iminothiazoline and 2-Iminobenzothiazoline N-nucleosides (1-12) c.

Compound*	Formula	Mol.wt	Found (required) (%)		
			C	H	N
1-c	$C_{16}H_{19}N_3O_5S$	365	52.60(53.05)	5.20(5.42)	11.5(11.23)
2-c	$C_{17}H_{21}N_3O_6S$	395	51.64(52.00)	5.31(5.50)	10.63(10.80)
3-c	$C_{17}H_{21}N_3O_6S$	395	51.64(51.75)	5.31(5.00)	10.63(11.04)
4-c	$C_{16}H_{18}N_3O_5SCl$	399	48.12(47.90)	4.51(4.93)	10.52(10.33)
5-c	$C_{16}H_{17}N_3O_5SCl_2$	433	44.34(44.45)	3.92(4.01)	9.69(10.00)
6-c	$C_{10}H_{15}N_3O_5S$	289	41.52(41.83)	5.19(5.42)	14.53(14.11)
7-c	$C_{17}H_{21}N_3O_5S$	379	53.82(54.05)	5.54(5.55)	11.08(11.35)
8-c	$C_{14}H_{18}N_2S$	246	68.29(69.00)	7.31(7.75)	11.38(11.14)
9-c	$C_{12}H_{13}N_2SCl$	252	57.14(57.90)	5.15(6.00)	11.11(12.05)
10-c	$C_{12}H_{13}N_2SF$	236	61.01(61.40)	5.50(5.33)	11.86(12.25)
11-c	$C_{11}H_{12}N_3SBr$	298	44.29(44.55)	4.02(4.15)	14.09(14.44)
12-c	$C_{11}H_{12}N_3SCl$	253	52.17(51.90)	4.74(5.00)	16.61(17.11)

* **1-c**. 3-(β-D-ribofuranosyl),4-methyl,5-caboxyamide-2-iminothiazoline,**2-c**. 3-(β-D-ribofuranosyl),4-methyl,5-(2-methoxycarboxyanilide-2-iminothiazoline,**3-c.**3-(β-D-ribofuranosyl),4-methyl,5-(4-methoxycarboxyanilide-2-iminothiazoline,**4-c.** 3-(β-D-ribofuranosyl),4-methyl,5-(4-chlorocarboxyanilide-2-iminothiazoline,**5-c.** 3-(β-D-ribofuranosyl),4-methyl,5-(2,5-dichlorocarboxyanilide-2-iminothiazoline,**6-c.** 3-(β-D-ribofuranosyl),4-methyl,5-(carboxyanilide-2-iminothiazoline,**7-c.** 3-(β-D-ribofuranosyl),4-methyl,5-(2-methylcarboxyanilide-2-iminothiazoline,**8-c.** 3-(β-D-ribofuranosyl),5-methoxy-2-iminobenzothiazoline,**9-c.** 3-(β-D-ribofuranosyl),5-chloro-2-iminobenzothiazoline,**10-c.** 3-(β-D-ribofuranosyl),5-flouro-2-iminobenzothiazoline,**11-c.** 3-(β-D-ribofuranosyl),5-bromo-2-iminopyridothiazoline,**12-c.** 3-(β-D-ribofuranosyl),5-chloro-2-iminopyridothiazoline,

REFERENCES

1. Agroglio L.A., Gillaizeau I., and Saito Y., Palladium-Assisted routes to nucleosides Chem.Rev. 103, 1875-1880 (2003).
2. Abarbri M., Thibonnet J., Berillon L., etal.,Synthesis and antiviral of certain 9-β-D- ribofuranosyl purine -6-carboxamide, J.Org.Chem. 65, 4618-4622 (2000).
3. Kappe C.O., Microwave-Assisted green and efficient synthesis of N^6 – (2-Hydroxyethyl) adenosine and its analogues, Angew.Chem. , 116, 6408-6414 (2004).
4. Field H.J., Field E.Declereg, Effect of 1-β-D-ribofuranosyl 1, 2, 4-triazole 3-carboxamide on influenza virus application, Microbiology today, 31, 5861-5866 (2004).
5. Kijoa A., Sawangwong P., Nucleoside analogous and nuleobases in cancer treatment, Drugs, 2, 73-82 (2004).
6. Michael P.B.,Anders R.,Stephen L., Frank M.,Brgitte M. and Jure P.,Nucleoside analogues are activated by bacterial deoxyribonucleoside kinases in a species-specific manner,J.of Antimicrobial Chemotherapy,60,3,510-520(2007).

7. Lanver A., Schmalz H.G., Microwave –Assisted amination of chloropurine derative in the synthesis of acyclic nucleoside analogues, Molecules, 10,510-520 (2005).
8. Belshe R.B., Human Virology, Chap.8, Antiviral Chemotherapy, 5th.ed., 193-230 (1984) PSG publishing company.
9. Lowe P.A. "Heterocyclic Chemistry", vol.1, 4th.ed. 119-138 (1980) H.Suschitzky and O.Meth Cohn, Eds, Chemical Society, London.
10. Sirvastava P.C., Pickering M.V., Allen i.B. and Streeter D.C. Synthesis and antiviral activity of certain thiazole c.nucleosides ,Med.Chem.,20,2, 256-262 (1977).
11. Nedballa V. and Vorbruggen H., A general synthesis of N-glycosides on the mechanism of the stannic chloride catalyzed Silyl Hilbert-Johnson reaction. Org.Chem.41, 2084(1976).
12. Vorbruggen H., Krolikewicz K. and Bennua B., Direct glycosylation of 1, 3, 5-triazinones, Chem. Ber. 114,1256 (1981)
13. Pvemishetti P., beiby R.W., Abushanab E. and Panzica R.P., A practical synthesis of ethyl 1,2,4-triazole-caroxylate and its use in the formation of chiral 1,2,-seco-nucleosides of ribavirin, J.Heterocyclic Chem.25, 651-654(1988).
14. AL-Masodi N.A.L.and Pfleiderer W., Synthesis and reactions of 1-(5-thio-β-D-xylo pyraonsyl) Lumazine and pyrimidine nucleosides, Tetrahedron, 49, 7579-7592(1993).
15. Revankar G.R. and Robins R.K., Synthesis of 5-amino-2-(2-deoxy-α-D-ribofuranosyl)-1, 2, 4-thiadiazole -3-one J.Heterocyclic Chem.13, 169(1976).
16. Werbel L.M., Degnan M.B., Harger G.F., Capps D.B., Islip P.J., 1-Alkyl-3-(3-alkyl- 5- nitro -4 –thiazol in-2 -ylidene) urea's and related compounds as schistosomicides, J.Med. Chem. , 15, 9,955-963(1972).
17. Khalaf H.I., Synthesis, and antimicrobial activity of some new N-ribofuranosyl Nucleosides, PhD Thesis submitted to the college of science,AL- Mustansiriy University, 1996.
18. Recondo E. and Rinderkecht H.,The synthesis of 3-(β-D-ribofuranosyl) derivative from ribose sugar,Helv.Chem.Acta, 42, 1171-1175(1959).
19. Yuan L.C., and Bert H.B., The electrophilic addition of Dimethylbromosulfonium bromide to conjugated enones:efficient synthesis of α-bromo enones,CAN.J.CHEM., 60, 2268-2274(1982).
20. Khan A.T., Khan M.A.Ali, Goswami P.,and Choudhury L.H.,A mild and Regioselective method for α-bromination of β-keto esters and 1,3-diketones using bromodimethylsulfonium bromide, J.Org.Chem., 71,8961-8969(2006).

21. Berlin K.D. and Herd D.M.,Novel 2-amino-4-Aryl-Substituted-and 2-amino-4,5-disubstituted-thiazoles, Proc.Okla.Acad.Sci, 71, 29-33(1991).
22. Bhalerao D.S.,and Agaanchi K.G.,Efficient and novel method for thiocyanation of aromatic and htero-aromatic compounds using bromodimethylsulfonium bromide, Synlett 2952-2960 (2007).
23. 23. Bhsari KP., Amerkar ND.,Khedekar PB.,Kale MK.,and Bhole RP.,Synthesis and invtro antimicrobial activity of some new 4-amino-N-(1,3-Benzothiazol-2-yl)benzenesulfonamide derivative, Asian J.Research Chem.,1, 2, 53-58(2008).

Study of Dissociations Constants and Association Thermodynamic Functions of Alanine Acid In Dimethyl Formamide Mixtures By Conductance Measurements

Ahmed Najem Abd[1], Haeder A. J. AL-Meisslmawy[2], Muna S. S. AL-Jeelo[3], and Ahlam M. Farhan[4]
[1]College of Veterinary medicine , University of Diyala
[2]Kufa University - Dentistry College
[3]College of Science for Women, Baghdad University
[4]Department of Chemistry, College of Science for Women, Baghdad University

Received 14/12/2009– Accepted 5/10/2010

الخلاصة

تم دراسة تأثير درجة الحرارة على ثوابت التأين الثرموديناميكي للحامض الألنين في مزيج داي مثيل فورم أمايد بنسبة وزنيه 40,% w/w في درجات الحرارة التي تراوحت بين 293.15 K -308.15 وذلك من القياسات المباشرة للتوصيل الكهربائي للمحاليل واستكملت الدراسة في كل درجة حرارية على كسر مولي وهو 0.141 .

واستخدمت النتائج المستحصلة في ايجاد ثابت تفكك والدوال الثرموديناميكية للحامض في مزيج المذيب وفي كل الدرجات الحرارية من 293.15 K - 308.15 كانت قيم pk_1 و pk_2 تزداد مع ازدياد درجة الحرارة.

ABSTRACT

The dissociation of alanine in Dimethyl formamide mixtures over the temperature range 293.15-308.15K, has been studied by direct conductance measurements. The acid dissociation at each temperature was investigated at solvent composition (X_2) involving 0.141.

The conductance measurements enabled the estimation of the degree of the acid dissociation, the molar conductivity of the acid at infinite dilution and the activation energy for the movement of cation and anion ions the in solvent mixture at infinite dilution.

The resulting data have been used to determine the dissociation constant and the associated thermodynamic functions for the acid dissociation in the solvent mixture. At temperature in the range 293.15 - 308.15 K . The pKa1 and pKa2 increased with increasing temperature.

INTRODUCTION

There is a lack of knowledge regarding the dissociation of alanine in dimethyl fromamide mixtures despite numerous studies on the dissociation and thermodynamic properties of the acid in a number of other mixtures (1)

Amino acids are comprised of basic amino and acidic carboxyl functional groups as well as a characteristic side chain acid from participating in condensation reactions that lead to peptide formation , the amino and carboxyl groups give the amino acid unusual electrolytic properties(2) . The amine group is protonded to form $-NH_3^+$ at low pH . The carboxylic acid group is deprotonded to form $-CO_2^-$ at high pH. The sequence of these amino acids in the protein polypeptides

determines the shape, properties, and hence biological role of the protein that function as chemical messengers and as intermediates in metabolism . The study of the behavior of the amino acids in aqueous solutions is useful models for understanding the thermodynamics behavior of proteins(3,4). The physical and chemical properties of proteins are determined by its constituent amino acids(5). The study of the dissociation constant and the associated thermodynamic properties of acid mean of investigating the change in the solute-solvent interaction patterns that are attributed to the variation of the solvent composition . Such investigations include studies of glycine in 50 mass% water . glycine in pure water and in 50 mass% methanol-water , and glycine in 0.05,0.1 mole fraction of 1.2-propanol-water from 5 to 45 oC . The change in pka as a function of the properties of mixed solvent which allow a wide range in the dielectric constant can provide useful information concerning the nature of solute–solvent interaction patterns in binary solvent systems(6).Various measurements of thermodynamic properties of aqueous solutions of amino acid have also been reported as a function of temperature in the geochemical literature , including molar volumes, densities, and molar heat capacities(7-9) . Amino acid dissociation constants have also been reported as a function of temperature(10) .The effect of temperature on the thermodynamic ionization constants of compound with dipole moments greater than those of the α-amino acids has not here to for been studied. In this paper results are given for dissociation of alanine in dimethyl formamide mixture at various temperatures from direct conductance measurements.

MATERIALS AND METHODS

Alanine 99% pure (BDH), was used after re-crystallization from doubly distilled water . They were dried and stored in a glass desiccators over P_2O_5. Dimethyl formamide (DMF) of purity > 99% obtained from fluke was passed through a freshly prepared activated molecular sieve without any further purification. The solvent containing 40% W/W DMF water was prepared by mass ratio using doubly distilled water and then used for preparation of amino acid in the concentration of study.

Viscosities were determined using a suspended level ubbelohde viscometer. The flow times were recorded electronically with an electronic timer of precision ± 0.015 and the temperature of the bath was controlled to be better than ± 0.018 C°. The instrument was calibrated with distilled water. Flow times were reproducible to 0.015[11] . Tacussel electronique conductometer, type CD810, was used to measure the conductivity of the deionized water and of the prepared solutions with an accuracy of 1 ± 10^{-9} $S.cm^{-1}$[12].

The dielectric constants were measured using Radelkis precision dielectrometer type OH -302 of maximum error on the dielectric constant scale of (2%)[13]. Densities of the mixed solvents were measured with the help of digital precision system DMA 60/602(Anton paer) the reproducibility of density measurements was $\pm 3x10^{-5}$ g.cm^{-3}. Details of the system and the calibration procedure were adequately covered in previous work[12]. The density and the dielectric constant data of (DMF) at various temperatures have been used to estimate the appropriate values of the Debye-Huckel-Onsagar constants A and B using the relation ships :

$$A = \frac{82.4}{\eta (DT)^{1/2}} \quad and \quad B = \frac{8.2x10^5}{(DT)^{3/2}}$$

Where D , η and T represent respectively the dielectric constant , the viscosity and the temperature ; the resulting values of the constants A and B are presented in table 1 .

The solvent composition was expressed in terms of the mole fraction (x) of Dimethyl formamide in the DMF + water mixture. The investigation covered one solvent compositions (x) which was 0.141 corresponding to 40% weight percentages of DMF in the mixtures.

RESULT AND DISCUSSION

1. Degree of dissociation

The acid dissociation of amino acids offer interesting examples of the relations between the function Ka and the true or 'thermodynamic' constant Ka of alanine . In the dissociation of alanine[14].

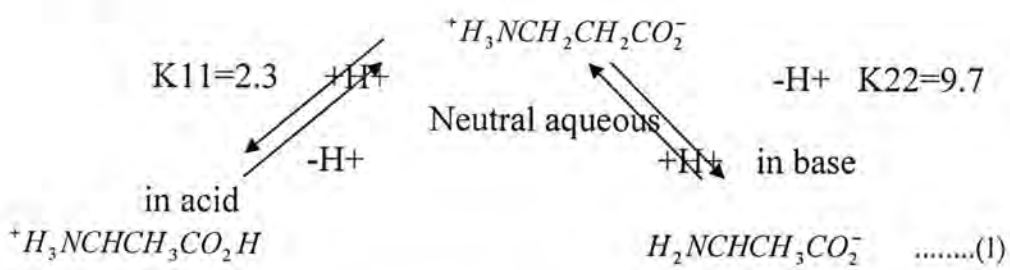

The microscopic constants are defined in terms of particular ionic species K11, K12, K21, K22 and so we define the first acid dissociation constant K1, a macroscopic dissociation constant by

$$K_1 = \frac{(H^+)[(^{+}H_3NCH_2CH_2CO_2^-)+(H_2NCH_2CH_2CO_2H)]}{(^{+}H_3NCH_2CH_2CO_2H)} \qquad ...(2)$$

And second acid-dissociation constant is given by

$$K_2 = \frac{(H^+)(^+H_2NCH_2CH_2CO_2^-)}{[(^+H_3NCH_2CH_2CO_2^-)+(H_2NCH_2CH_2CO_2H)]} \quad ...(3)$$

An amino acid is said to be isoelectric at the pH at which there are equal concentrations of the positively and negatively charged forms setting $(H_3N^+CH_2COO^-)$

And substituting from equations (2) and (3) yields

$$(H^+)^2_{isoelectric} = K_1K_2$$

Which may be written

$$pH_I = \frac{1}{2}(pK_1 + pK_2) \quad ...(4)$$

The onsager equation for incompletely dissociated electrolytes , can be written as [14,15]

$$\Lambda = \alpha[\Lambda_0 - (A + B\Lambda_0)(\alpha C)^{1/2}] \quad ...(5)$$

Where A and B are onsager constants and Λ_o is the molar conductivity of the weak electrolyte at infinite dilution, Eqn.(5) may be written as:

$$\Lambda = \alpha\Lambda^- \quad ...(6)$$

Where

$$\Lambda^- = \Lambda_0 - (A + B\Lambda_0)(\alpha C)^{1/2} \quad ...(7)$$

$$\Lambda^- = \Lambda_0 - K(\Lambda C/\Lambda^-)^{1/2} \quad ...(8)$$

Λ^- is the molar conductivity of 1 mole of free ions, at the concentration C mole per liter, at the actual ionic concentration in the solution, where K , representing $A + B\Lambda_o$, is constant for a given solute in a particular solvent at a definite temperature.

In order to estimate the value of α in Eqn.(6), an approximate value of Λ_o for amino acid, for a given solvent composition and temperature, was first made by extrapolating the experimental data of Λ^- against $(C)^{1/2}$.

As a first approximation, Λ^- in the term. $(\Lambda C/\Lambda^-)^{1/2}$ of Eqn.(8) was then taken as equal to Λ_o and hence apreliminary value of Λ could be derived from Eqn.(8), by utilizing the experimental value of Λ at the concentration (C). The result for Λ^- , thereafter, inserted under the square root sign in Eqn.(8), thus obtaining a better value of Λ^- an here of α. Using such values of Λ^- and α in Eqn.(7), it was possible to derive the correct values of Λ_o from the plots of Λ^- values against the corresponding values of $(\alpha C)^{1/2}$.

Table 3 gives the resulting value of x2 at a given temperature. The exact values of Λ_o could be derived, as mentioned earlier, from Λ^-,

$(\alpha C)^{1/2}$ for solvent mixtures and temperatures and data obtained are presented in table 3.

The values of Λ_o (table 3) are then plotted against the experimental temperature (T) as indicated in Fig. (1).

Fig. (1) shows that Λ_o at $X_2 = 0.141$ followed the sequence 308>303>298>293, implying an increase in Λ_o with increasing temperature.

The change in Λ_o with change of temperature in the range 293.15–308.15 K is seen in Fig. (1) to be almost linear suggesting a constant dependence of Λ_o values on temperature over the range referred to above . Thus, the increase of temperature invariably results in an increase of ion conductance. Since the conductance of an ion depends on its rate of movement, it seems reasonable to treat the conductance in a manner analogous to that employed for other processes taking at a definite rate which increases with temperature, thus:

$\Lambda o = A\, e^{-E/RT}$ .....(9)

Where A is constant, which may be taken as being independent of temperature over relatively small range; E is the activation energy of the processes which determines the rate of movement of ions, R is the gas constant and T is the temperature in Kelvin , Eqn.(9) may be written as :

$d \ln\Lambda_O / dt = (1/\Lambda_O)(d\Lambda_O / dt) = E / RT^2$

and

$E = \alpha RT^2$ ..... (10)

Where $\alpha = (1/\Lambda_o)(d\Lambda_o / dt)$ is the temperature dependence of Λ_o. From the slopes of the lines in Fig. (1) it was possible to evaluate the corresponding values of E, from Eqn.(10) , that cover the temperature range 293.15-308.15K, the such values of Λ_o have then been combined with the appropriate values of $d\Lambda_o/dt$ to calculate the values of α *and* E . Table 4 gives the values α *and* E alanine acid in Dimethyl form- amide at infinite dilutions.

2. The Dissociation constant for the acid

The relation between the function K_a and the true or "thermodynamic" constant K of alanine may be written as :

$K = Ka\, f+ f-$ .....(11)

Where $Ka = \alpha 2C / (1 - \alpha)$.

If the solution is sufficiently dilute for the Debye-Hukel law to applicable, it follows, for alanine type electrolyte, that

$Log f^{+} = Log f^{-} = -A(\alpha C)^{1/2}$ ..... (12)

The ionic strength, $1/2\sum C_i Z_i^2$, being equal to

$1/2[(\alpha C X_1^2)+(\alpha C X_1^2)]$, i.e.; to αC .

Eqn.(12) may be expressed as :

$$Log\,K = Log\,Ka - 2A(\alpha C)^{1/2} \quad \text{..... (13)}$$

The plot Log Ka , obtained at various concentrations C, against (αC)1/2 should be thus give a straight line of intercept Log K .

Combining equations (6) and (13) , one may written :

$$Log\,K = \log\left[\frac{\Lambda_2 c}{\Lambda-(\Lambda--\Lambda)}\right]-2A(\Lambda c/\Lambda-)-2 \quad \text{..... (14)}$$

Since Λ^- for various concentration can be obtained from conductance data (Table 2) and On sager Eqn.(7), by method already described in the previous section, it would be possible to derive the values of the dissociation function ka for various acid concentration , and the Ka_2 is obtained from the Eq.(13) :

$$Ka_2 = 4\alpha_2 C_2 / 1-\alpha \quad \text{..... (15)}$$

and , thereafter, calculate pH_1 from Eqn.(4) . Such results for the dissociation of alanine in Dimethylformamide mixture at different temperature are given in (Table 5) .

The manner in which the pK values change with temperature as described in Fig. (3) , suggests a relatively large dependence of pk on temperature; The dissociation constants (K_1 and K_2) of alanine derived in the present work (Table 5) are substantially less than those reported[16,17] for the acid in water and in a number of other solvents. This is likely to be due to greater basicity and lower dielectric constant of DMF mixture than water.

The dependence of pk values for alanine dissociation in DMF mixture an temperature could be expressed as:

$$PK = \frac{A_1}{T} - A_2 + A_3 T \quad \text{..... (16)}$$

Where A1,A2 and A3 are values a given solvent composition (x=0.141) over the temperature range 293-308k Inserting the appropriate values of pk and temperature from table (5) in Eqn.(16), the values of the constant (A1,A2,A3) could be calculated and the results are given in table (6).

3. Thermodynamic of the acid dissociation :

The standard thermodynamic function for alanine dissociation in DMF mixture may be calculated from equations [18] as following :

$$\Delta G^{o} = (R\ln 10)(A_1 - A_2 T + A_3 T^2) \quad \text{..... (17)}$$

$$\Delta H^{o} = (R\ln 10)(A_1 - A_3 T^2) \quad \text{..... (18)}$$

$$\Delta S^{o} = (R\ln 10)(A_2 - 2A_3 T) \quad \text{..... (19)}$$

$$\Delta C^{o}_{Po} = (R\ln 10)(-2A_3 T) \quad \text{..... (20)}$$

Table (7) summarizes the values of the standard thermodynamic functions which have been derived by Eq.(17) to (20) for the dissociation of the alanine in DMF mixture at four temperature .

From the Table (7) could be obtained the information as following:

1. The value of ΔG^{o} is negative values for pk is refer to spontaneous reaction at all temperature reflect the non spontaneous reaction .
2. The values of ΔH is high negative values at all temperature is refer the large exothermic step .
3. The values of ΔS^{o} were generally negative which did not change significantly with the variation of temperature .
4. ΔCop values were negative for solvents with x2=0.141, $\Delta C^{o}p$ reflects , the effect of temperature on H^{o} so that one can write

$$C^{o}_{P} = dH^{o}/dT \quad \text{..... (21)}$$

It is shown in Table(7) that the negative sign of ΔCop, is due to decreasing tendency of ΔH^{o} with the increase temperature .Thus the relatively more endothermic behavior and the greater increase in ΔS^{o} .

The two sorts of interactions have to be considered ; the first the maximum interaction between the two components of the solvent mixture and the second is the expected strong solute – solvent interaction due to the polarity and possibility of hydrogen bounds formation .

The values of ΔS^{o} were generally negative which did not change significantly with the all temperature . The values of ΔS for pka decrease refer to decomposition of alanine is order the reactant at second stape pka2 .

Moreover, the high negative ΔH values at this stage indicates that the undissociated acid molecules are highly stable so that the release of these molecules and subsequent dissociation stage should highly be endothermic.

Table -1: Dielectric constants (D) , Viscosity , and the onsager constants (A and B) for dimethyl form amide at four temperature .

X_2	T / K	Dialectic (D)	Viscosity	Values (A)	Values (B)
0.141	293	63.01	2.338248	1.418005	0.3268874
	298	62.22	2.039288	1.264859	0.3497220
	303	60.32	1.810804	1.103171	0.3318375
	308	54.39	1.561893	0.994360	0.3781892

Table -2: Values of Λ (S mol^{-1} cm^2) , $\overline{\Lambda}$ (S mol^{-1} cm^2) , α and Ka (mol L^{-1}) for versus concentrations C (mol L^{-1}) of alanine in dimethyl formamide + water mixture at different temperature (293.15-308.15)K at $X_2 = 0.141$

T/K	Conc.	Values Λ	$\overline{\Lambda}$	α	Ka1	Ka2	pH_I
293.15	0.0181662	1.953	2.829126	0.690319201	0.207954371	0.001412245	0.014678308
	0.0338056	1.187	2.813263	0.42192998	0.010410917	0.000593988	0.010707911
	0.0564004	0.608	2.833633	0.214565542	0.003305919	0.000160027	0.003385933
	0.0883981	0.477	2.802611	0.170198433	0.003085885	0.000185711	0.003178741
	0.192991	0.2351	2.791036	0.084233955	0.001495295	9.72324E-05	0.001543911
	0.33067	0.1775	2.745536	0.0646504	0.001477622	0.000126354	0.001540799
298.15	0.0181662	1.981	2.937793	0.674315719	0.025362605	0.001242743	0.013302674
	0.0338056	1.215	2.921167	0.415929661	0.010012978	0.00056316	0.010294558
	0.0564004	0.6609	2.932632	0.2253607	0.003697763	0.000188001	0.003791763
	0.0883981	0.4852	2.911797	0.166632495	0.002945274	0.000173536	0.003032042
	0.192991	0.2416	2.89837	0.083340894	0.00146233	9.40807E-05	0.001509371
	0.33067	0.1804	2.856409	0.063156222	0.001407861	0.000117606	0.001466665
303.15	0.0181662	2.358	3.541645	0.665792308	0.024094904	0.001165703	0.012630304
	0.0338056	1.281	3.542185	0.36164119	0.006925954	0.000338693	0.0070953
	0.0564004	0.6808	3.555624	0.191471314	0.002557374	0.000110469	0.00261608
	0.0883981	0.5008	3.536552	0.141606853	0.00206525	0.000103398	0.002116724
	0.192991	0.2544	3.522079	0.072230066	0.001085257	6.05129E-05	0.001115514
	0.33067	0.1833	3.489271	0.52532463	0.000963132	6.6921 E-05	0.000996593
308.15	0.0181662	2.599	3.918082	0.663334764	0.023742767	0.001144427	0.012443597
	0.0338056	1.423	3.917529	0.363239174	0.007004831	0.000344064	0.007176863
	0.0564004	0.7728	3.929234	0.196679556	0.002715888	0.000120507	0.002776141
	0.0883981	0.5307	3.918334	0.135440215	0.001875613	8.98243E-05	0.001920525
	0.192991	0.2949	3.888681	0.075835483	0.001200971	7.03076E-05	0.001236125
	0.33067	0.2398	3.829103	0.062625633	0.001383522	0.000114602	0.001440823

Table -3: Values of the molar conductivity dimethyl formamide at infinite dilution (Λo/S mol^{-1} cm^2) at X_2 =0.141 and different temperature (293.15-308.15)K .

X_2	temperature			
0.141	293.15	298.15	303.15	308.15
	Values of Λo			
	3.414	3.511	4.08	4.53

Table -4: The temperature coefficients (α) and the energies of activation (E) at infinite dilution as a function of the X_2=0.141

X_2	dΛo/dt	Λo	slope	E(KJ/mole)	α
0.141	1.852	0.0140	0.008109	0.15224	2x10-7

Table-5: Values of pK for the dissociation of alanine in diethyl form amide + water mixtures at four temperature at X_2=0.141

X_2	T/K	pK1	pK2	pH_I
0.141	293.15	1.937	1.0089	1.407
	298.15	2.408	1.860	2.178
	303.15	2.668	1.875	2.254
	308.15	2.801	1.948	2.3403

Table -6: Values of the temperature dependence constant A1, A2 and A3 at X_2=0.141 of DMF + water

Values of P	A1	A2	A2
PKa1	$1.52x10^3$	19.42	0.068
PKa2	$3.4x10^3$	4.543	0.0496
PpH_I	$2.64x10^3$	19.51	0.0346

Table-7: Values of pK for the dissociation of alanine in dimethyl formamide + water mixtures at four temperature at X_2=0.141

Values of P	T / K	ΔG^o J / mol	ΔH^o J / mol	ΔS^o J / mol	Δcp^o J/ K * mol
PKa1	293.15	-25.8	-141	-393.661	-765.445
	298.15	-23.8	-145	-406.732	-778.507
	303.15	-21.7	-149	-419.786	-791.57
	308.15	-19.6	-153	-432.848	-804.632
PKa2	293.15	-9.14	-147	-471.188	-558.764
	298.15	-6.76	-150	-480.714	-567.769
	303.15	-4.33	-153	-490.24	-577.29
	308.15	-1.86	-156	-499.767	-586.81
PpH_I	293.15	-19.2	-64.8	-155.544	-3890.61
	298.15	-18.2	-84.4	-221.937	-3957.
	303.15	-17	-104	-288.329	-4023.39
	308.15	-15.4	-125	-354.722	-4089.79

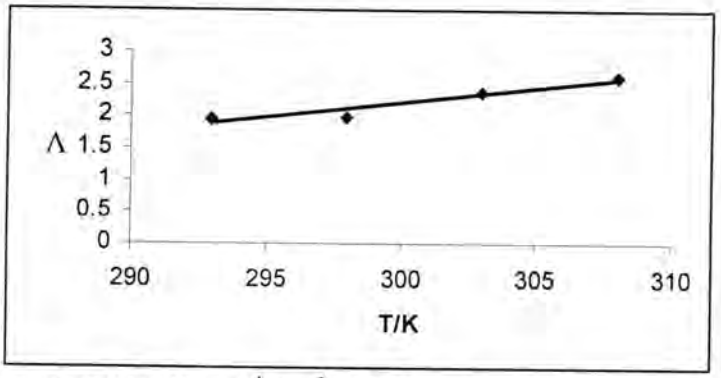

Fig.-1:Molar conductivity (S mol^{-1} cm^{-2}) of alanine in DMF + water mixture as a function of the temperature T

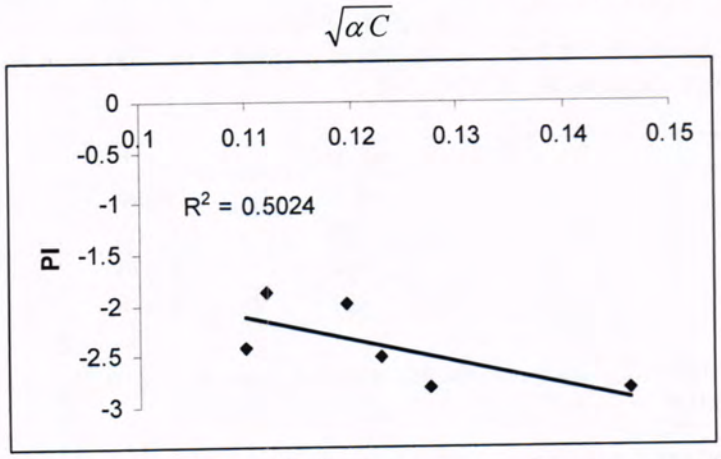

Fig -2: Log PI Versus $\sqrt{\alpha C}$, (C) expressed in moles per Liter

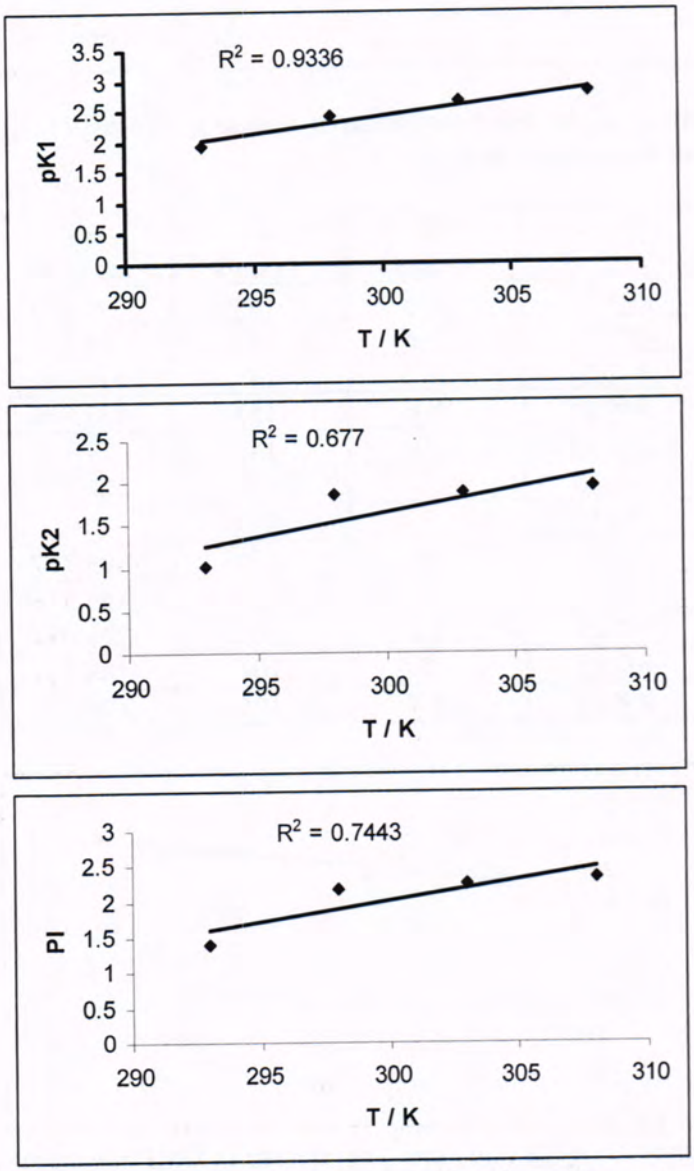

Fig -3: pK1 , pK2 , and pH_I value of alanine as a function of temperature

REFERENCES

1. Philip , S. B. and Christina A. B., Organic Chemistry ; A brief Survey of concepts and application Prentice Hall Inc. London 6th ed (2000).
2. John, E. K and Michael T. , L. 21,8743-8750 , Amino Acid Adsorption on Zeolite β (2005).
3. Peter, A. M. , Harpers Biochemistry, Drwael California, 26th ed(1993).
4. Zena, M. S., A study of some physical properties for amino acid solutions in aqueous and acidic media over temperature range (293.15-308.15) k M. Sc, thesis, Naharin University(2005).
5. Wade, L. G., Organic chemistry. Prentice Hall, Inc. New Jersey, 4th ed(1999).
6. Jia-Zhen Y., Jie W. and Han L.,Journal of Solution Chemistry ,Vol.21,No.11, , Thermodynamics of Amino Acid Dissociation in Mixed Solvents , 3:Glycine in Aqueous Glucose Solutions from 5 to 45(1992).
7. Clarke, R. G.and Tremaine, P. R., B. Amino Acid Under Hydrothermal Conditions : Apparent Molar Volumes of Aqueous α-Alanine, β-Alanine, and Proline at temperature from 298 to 523 K and Pressures up to 20.0 MPa. J. Phys. Chem., 103,5131-5144(1999).
8. Hakin, A. W.; Duke, M. M.; Groft, L. L.; Marty, J. L.and Rushfeldt, M. L., Calorimetric Investigations of Aqueous Amino Acid and Dipeptide Systems from 288.15 to 328.15 K Can. J. Chem..73,725-737(1995).
9. Clarke, R. G.; Hnedkovsky, L.; Tremaine, P. R.and Majer, V., Amino Acids under Hydrothermal Conditions: Apparent Molar Heat Capacities of Aqueous α-Alanine, β-Alanine, Glycine, and Proline at temperature from 298 to 500 K and Pressures up to 30.0 MPa. J. Phys. Chem. B. 104,11781-11793(2000).
10. Hidetada N. Kuwabara K. , and Giorgio, C., J. Chem. Eng. Data, 53, 679-627, Temperature Dependence of the Dissociation Constants of Several Amino Acids(2008).
11. Isa, S. A. and Farhan, A. M., Partial molal Volume and viscosity study of glycine, DL-Alanine and DL-Valine in aqueous dimethyl formamide solutions at 298k. Iraqi, J. Sci, 41A, (3):64-77(2000).
12. Al-Namer, J. S., The Electrochemical behavior of hydrochloric acid glycine and DL-Alanine in glycerol – water and ethylene glycol-water mixtures – ph. D. thesis, Naharin University (1994).
13. Al-Noori, M. K. , Al-Namer, J. S. and Isa, A. S., Partial molal Volume and viscosity study of glycine and DL-Alanine in ethylene

glycol-water mixture at different temperatures, Iraqi, T. Sci, 42A, (2): 12(2001).

14. Robinson, R. A. and Stockes, R. H.,Electrolytic solution. Butter Worths, 2nd ed, P.94(1970).
15. Hrned, H. S. and Owen, B. B., The physical chemistry of Electrolytic solution, Reinhold, New York (1950).
16. Azzouz, A. S.P and Othman, S. S.,The dissociation constants of benzo aldoximex, J. Edu. Sci. 26, 86(1997).
17. Salah, R. A., Electrochemical studies of the thermodynamics of dissociation and transfer of glycine. M. Sc. thesis, Baghdad University(1985).
18. Jalal, M. S., Nasrin, M. and Naema, A. H., Dissociation constants and Association thermodynamic functions of acetic in urea water mixtures from conductance measurement, Iraqi, J. Sci, 31,1,1(1990).

Study of Some *Cucurbita moschata* Duchesne expoiret Leaves Components and Effect of Its Extracts on Different Microorganisms and Identification of Some Flavonoids by HPLC

Abdul Kadir M. N. Jassim
Department of Chemistry, College of Science, Al-Mustansiriyah University

Received 18/2/2009 – Accepted 20/6/2010

الخلاصة

شملت الدراسة معرفة المكونات الكيميائية الفعالة الموجودة في أوراق نبات القرع *Cucurbita moschata* Duchesne ex poiret ، إذ أظهرت الدراسة أن محلولي المستخلصين المائي والكحولي ذا طبيعة حامضية وتحتوي على مجموعة من المركبات الكلايكوسيدية والعفصية والفينولية والفلافونويدات والبروتينات في حين لا تحتوي على القلويدات والصابونيات والراتنجات .

كما تم دراسة تأثير المستخلصات المائية والكحولية على أنواع مختلفة من الأحياء الدقيقة (البكتريا والفطريات) حيث لوحظ أن للتركيز 50 ملغم /مل تأثيرا فعالا تجاه تثبيط نمو بكتريا *Proteus mirabilis*، و *Staphylocoous aureus* خاصة تجاه المستخلص الكحولي بينما كان للتركيز 10ملغم/مل فعالية لتثبيط نمو فطريات *Aspergillus niger* و *Aspergillus flavus* .كما اثبت التحليل الدقيق للعناصر المعدنية لأوراق النبات احتواءها على تراكيز عالية من Mg , K, Na وهي 14.9 و 13.6و 12.4ppm ،على التوالي وكميات اقل من Fe,Zn وهي 3.1و 2 ppm على التوالي.

كما تم استخدام كروماتوغرافيا السائل عالي الأداء HPLC لتشخيص المركبات الفلافونويدية ومقارنتها مع المركبات القياسية إذ اثبت التحليل وجود مركب الكمبفيرول في أوراق النبات وعدم احتواءها على المورين .

ABSTRACT

In this study, the chemical components of the *Cucurbita moschata* Duchesne ex poiret leaves in the watery and alcoholic extracts were identified .The results showed that the extract had acidic nature and contain : glycosides ,tannins ,phenolic compounds ,flavonoids and proteins ,while the alkaloids , saponins and resins were not found.

The effect of these extracts on different microorganisms were studied .It has been found that 50 mg/ml concentration was effective inhibitor of the growth of the *Staphylocoous aureus* and *Proteus mirabilis* ,specially when alcoholic extracts was used , while the 10 mg/ml concentration was efficient to inhibit fungal growth such like *Aspergillus niger* and *Aspergillus flavus* .The result also showed that there were high concentrations of the following trace elements in the leaves Na, K , Mg with 14.9, 13.6, 12.4 ppm , respectively and low concentrations of Zn, Fe with 3.1, 2 ppm , respectively. The flavonoids were identified using high performance liquid chromatography (HPLC), as compared with standard .The results showed present of kaempferol ,while morin was not found .

INTRODUCTION

The Cucurbitaceae family consists of 90 genera and approximately 700 species .The Cucurbitaceae are characterised by long flexible stems ,a crawling or climbing growth habit and fruit that differ widely in colour and shape ,having a thick and impermeable skin protecting a juicy fibrous pulp(1).

The majority of the Cucurbitaceae used as food such like *Cucurbita*

It considered (an ancient classical Latin name, also called ,Pumpkin ,squash ,Marrow ,Gourd ,etc...) ,as the most important genus economically and is represented by three species cultivated in Iraq : *Cucurbita moschata* Duchesne ex poiret , *Cucurbita maxima* Duchesne ex poiret, *Cucurbita pepo* L..

The leaves of this herb ,broadly ovate-cordate ,less deeply lobed less scabrid ,often marked with white a long the vein ,the lobes triangular ,petiole with rather slender scabrid hairs ,8-19 cm. long , fruit-stalk often long ,markedly expanded at attachment to the fruit ,seeds 11-12mm. long ,with a some what ragged margin (2).

The Cucurbitaceae have long been cultivated not only for food but also for their medicinal properties .Particular medical properties have been attributed to part of the fruit and the plant .

Cucurbita or Pumpkin has received considerable attention in recent years because of the nutritional and health protective value of the seeds as well as the polysaccharides from the fruits (3,4).A slice of gourd pulp (*lagenaria*) mixed in one liter of water was used as laxative to treat intestinal diseases and to satisfy thirst .The seeds were noted as an effective remedy against taenia ,a parasitic worm that is paralyzed by the action of Cucurbitine (3-amino-3-carboxypyrrolidine) contained in the skin of the seeds (1). Preliminary Investigation showed that Pumpkin-rich diet could reduce blood glucose(3,5,6),and the active polysaccharides from the Pumpkin fruits could obviously increase the level of serum insulin ,reduce the blood glucose levels ,improve tolerance of glucose ,and hence could be developed as new anti-diabetic agent(7,8).Many other researcher mentioned the chemical composition ,anti-complementary activity and extraction of different component of *Cucurbita moschata* (9-13).

Flavonoids , a large group of compounds that ubiquitously exist in natural products ,and have been considered as active ingredients of many medicinal plants .Generally ,they have the structure of a 15-Carbon skeleton ,consisting of two phenyl rings and a hetrocyclic ring (14).High performance liquid chromatography HPLC has been employed to characterize and identify the falvonoid (kaempferol) in this plant .

Accordingly ,the leaves of *Cucurbita moschata* has drawn the attention for researches and consumers and an understanding of the chemical and pharmacological properties should be of importance from scientific points of view ,therefore, this study is aimed at evaluating the leaves components ,trace elements ,ash contents ,pH , and effect of its extracts on different microorganisms and identify the flavonoid (Kaempferol) .

MATERIALS AND METHODS

Collection and treatment of samples:

The leaves of *Cucurbita moschata* were collected from Baghdad ,Iraq ,in November which classified and applied to the Flora of Iraq (2) .The leaves were transported to the laboratory ,washed with water,cleaned with filter paper or soft clothes to remove all traces of dust and insects , then dried in shad 25-30°C for one week, with continuous overturn to prevent mould .weighed ,ground in a mortar and pestle ,placed in airtight bottles and stored in the dissicator for extraction .

Preparation of extracts:

a) Watery extract:

Air dried leaves (50 g) were suspended in one liter of distilled water and left for 24 hrs at 35°C with continuous stirring in shaking incubator .Then the mixture was filtered by filter paper ,the filtrate was centrifuged for 10 min. at 2500 rpm ,and the extract evaporated to dryness at 40°C in the incubator. pH of the extract was determined using pH-meter (orion,SA720) .

b) Alcoholic extract:

Prepared as in watery extract described above ,but with using 70% ethanol instead of water to give alcoholic extract powder (15-18).pH of this extract was also determined .

Determination of Ash content:

Dried leaves (2 g) were taken and heated at 900°C for 20 min. in muffle furnace until the material converted to white powder ,cooling ,and the percentage of ash content was determined (19).

Chemical detection of the plant components:

The chemical components of the prepared watery and alcoholic extract were detected (15-17, 20).They included: glycosides, proteins, saponins, phenolic compounds, tannins, resins, flavonoids and alkaloids.

Determination of trace elements:

Dried leaves (3 g) were taken and mixed with 8 ml of concentrated nitric acid and 2 ml of 60% prechloric acid in conical flask, the mixture kept for 24 hrs which covered with watch glass .After that it was left for another 6 hrs at the sand bath at 80°C ,until the

digestive material converted to white powder .Deionized water 8 ml was added to this powder, and the trace elements were determined (19) by (Shimadzu AA-670, Flame Atomic Absorption Spectrophotometer).

The biological activity:

The biological activity against various bacterial species was determined by using wells-diffusion method. From gram negative bacteria ,*Proteus mirabilis* was chosen while *Staphylococcus aureus* was used as gram positive bacteria .From fungi ,*Aspergillus niger* , *Aspergillus flavus* were chose . These isolates were obtained from department of Biology/College of Science /Al-mustansiryih University .The concentrations for both extracts were 1,10,50,100 mg/ml (17,18) .

HPLC Analysis:

Analysis of flavonoids ,Kaempferol and Morin, were carried out in chemical research center, ministry of science and technology ,by using (Shimadzu ,LC2010A ,Japan) HPLC .Standard solution (25 ppm in methanol) were prepared (standard Kaempferol and Morin were kindly gift from Dr.Mohammed Mustafa Radi).

A luna 5U C18Column(250mm x 4.6 x 5µm)Was used and coupled with 20µl at 40°C with a linear gradient mobile phase containing solvent A (water) ,solvent B (acetonitrile) and solvent C (5% formic acid in water ,v/v) with flow rate set at 0.2ml/min. .

The linear gradient program started with 88% A:10% B:2% C (v/v) and finished at 73% A:25% B:2% C (v/v) with in 10min..The chromatograms were recorded at 280nm. Standard and leaves extracts samples were made at (25ppm) then analyzed directly by HPLC (21).

RESULTS AND DISCUSSION

Our results show that pH value for watery and alcoholic extracts are pH =6.49, 6.87, respectively (This also means there is no alkaloid in the extracts) .The Ash content for the *Cucurbita moschata* leaves is (15.5%).The qualitative chemical analysis of the watery and alcoholic extracts are represented in Table 1.Which shown, that leaves contents are (glycosides,proteins,tannins,flavonoids and various phenolic compounds) similar results are also obtained by other studies (8,22), while the alkaloids ,saponins and resins are not found.

Table-1: Chemical components analysis for watery and alcoholic extracts of *Cucurbita moschata* leaves.

components	Reagents	Note	Result Watery extract	Result Alcoholic extract
Glycosides	Iodine test Molish test Benedict test	Blue ppt. Violet ring Orange ppt.	Ve- Ve+ Ve-	Ve- Ve+ +Ve
Proteins	Folin-Ciocalteau reagent	Blue color	Ve+	Ve+
Saponins	Fast stirring Mercuric Chloride	Dense foam for long time White ppt.	Ve + Ve -	Ve- Ve-
Phenolic compounds	Aqueous%1 Ferric chloride	Green ppt.	Ve+	Ve-
Tannins	Aqueous%1 Ferric chloride Lead acetate%1	Green ppt. Preface yellow ppt.	Ve+ Ve+	Ve- Ve-
Resins	Ethanol + Boiling + D.w.	No turbidity	Ve-	Ve-
Flavonoids	aqueous%1 Ferric chloride Ethanol hydroxide alcohol	Green ppt. Yellow ppt.	Ve+ Ve+	Ve- Ve-
Alkaloids	Mayer's reagent Wagner reagent Picric acid	No white ppt. No Brown ppt. No Yellow ppt.	Ve- Ve- Ve-	Ve- -Ve -Ve

The trace elements in *Cucurbita moschata* leaves are represented in Table .2 .which shows ,high concentrations of (Na ,K , Mg) with (14.9, 13.6, 12.4) ppm, respectively and low concentrations of (Zn, Fe) with (3.1, 2) ppm, respectively ,and (Mn ,Cu ,Ni ,Cd) were not founds .

Table-2: The trace elements contents of *Cucurbita moschata* leaves.

Trace elements		Concentration (ppm)
Sodium	Na	14.9
Potassium	K	13.6
Magnesium	Mg	12.4
Zinc	Zn	3.1
Iron	Fe	2.0
Chrome	Cr	Nil
Manganese	Mn	Nil
Cadmium	Cd	Nil
Nickel	Ni	Nil

The effect of these extracts on different microorganisms were studied and compared between them .However ,the results can seen in Table .3 ,which they show that the concentrations 50,100 mg/ml exhibit very effective inhibition towards the two types of bacteria , *P. mirabilis* ,gram negative bacteria and *S. aureus* ,gram positive bacteria specially for the alcoholic extract ,while less inhibition effects were seen for the same concentrations when the watery extract was used .In general , when the both extracts were tested against the intended bacteria they were found to possess no activity at concentration of 1 mg/ml .

Table -3: The effect of watery and alcoholic extracts of *Cucurbita moschata* represented by inhibition zone (mm) against different bacteria species.

Bacterial species	*mg/ml(Alcoholic extract)*				*mg/ml(Watery extract)*			
	1	10	50	100	1	10	50	100
S. aureus *gram + ve)*	-	+	+++	+++	-	-	+	+
P.mirabilis *(gram - ve)*	-	-	+++	+++	-	-	+	+

(-) No inhibition zone
(+) Inhibition zone between (7-10) mm.
(++) Inhibition zone between (10-15) mm .
(+++) Inhibition zone between (15-20) mm .

The watery and alcoholic extracts showed variable activity against fungal species (Table .4). Concentration 10 mg/ml was effective on the inhibition of the growth of intended fungal (*A. niger* , *A. flavus*) ,while these fungal were not inhibited at 1 mg/ml with alcoholic extracts .In watery extract 50 and 100 mg/ml were not effected to inhibit any of these fungal species as compared with the alcoholic extract ,this result may be due to the instability of the effective compounds in this extracted solution .these finding needs more study to be confirmed.

Table -4 : The effect of watery and alcoholic extracts of *Cucurbita moschata* represented by inhibition zone (mm) against different fungal species .

Fungal species	*mg/ml(Alcoholic extract)*				*mg/ml(Watery extract)*			
	1	10	50	100	1	10	50	100
A. niger	-	+	+	+	+	+	-	-
A. flavus	-	+	+	+	-	+	+	+

(-) No inhibition zone
(+) Inhibition zone between (8-16) mm .

However, antibacterial and antifungal activity may be due to (glycosides and/or tannins and/or flavonoids like kaempferol and/or proteins and/o various phenolic compounds) present in the plant extracts ,and these compounds have an activation effect on the bacterial or fungal cells membrane which may be caused destroy of these microorganisms by inhibit its activity (8,17) .

The HPLC chromatogram in Figure 1, shows the standard Morin (A), standard Kaempferol (B) and leaves extract sample (C).

Identification of Kaempferol in leaves extract sample was determined according to retention time obtained from standard run at identical conditions but Morin retention time in leaves extract sample was not identical with standard one.

The two major peaks were separated and detected with identical value between Kaempferol (fig.1, B) with retention time 3.3 and 3.56min. and leaves extract sample (fig.1,C) with retention time 3.3 and 3.55min., while the major peak for Morin at 2.35min. .This confirmed the presence of Kaempferol in the leaves of *Cucurbita moschata* and the Morin not found.

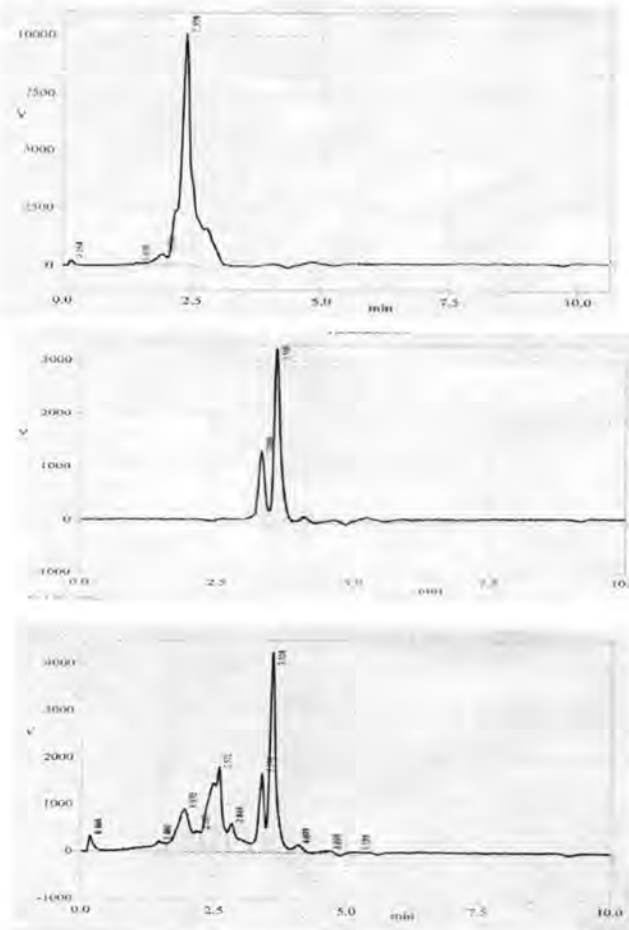

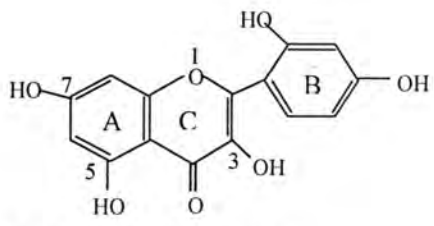

(A)Standard Morin

(B) standard Kaempferol

(C)leaves extract
Cucurbita moshata

Fig -1: HPLC chromatogram of (A) standard Morin ,(B) standard Kaempferol ,(C)leaves extract ,for *Cucurbita moschata* leaves.

In Conclusion ,the present study confirm that the watery and alcoholic extracts for *Cucurbita moschata* leaves posses *in vitro* antibacterial and antifungal activity because of its content ,(glycosides ,tannins ,flavonoids like kaempferol ,proteins ,various phenolic compounds , trace elements) ,however if plant leaves extracts are to be used for food preservation or medical purposes ,issues of safety and toxicity will need to be addressed ,and this results will serve as a precursor for further research and improvement strategies of this important plant .

REFERENCES

1- Francois,G.,Nathalie,B.,Jean-pierre,V.,Daniel,P. and Didier,M.,Effect of Roasting on Tocopherols of Gourd Seed (*Cucurbita Pepo*),GRASAS Y ACETES,57(4):409-414,(2006) .

2- Towensend,C.C.,Guest,E. and Omer,S.A.,Flora of Iraq, Ministry of Agriculture and Agrarian Reform,Repobic of Iraq ,Vol.4,Part 1,206-208,(1980) .

3- Fu,C.L.,Shi,H. and Li,Q.H.,A review on Pharmacological Activities and Utilization Technologies of Pumpikin, Plant Foods Hum. Nutr.,61:70-77,(2006) .

4- Fu,C.L.,Tian,H.J.,Cai,T.Y.,Liu,Y. and Li,Q.H., Some Properties of an Acidic Protein-Bound Polysaccharide From The Fruit of Pumpkin, Food Chem.,100:944-947,(2007) .

5- Li,Q.H.,Tian,Z. and Cai,T.Y.,Study on The Hypoglycemic Action of Pumpkin Extract In Diabetic Rat, Acta Nutr. Sin.,25:34-36,(2001) .

6- Zhang,Y. and Yao,H., Study on Effect of Hypoglycemic of Different Type Pumpkin,J.Chin. Food Sci.,23:118-120,(2002) .

7- Jun,H.I.,Lee,C.H.,Song,G.S. and Kim,Y.S.,Characterization of The Pectic Polysaccharide From Pumpkin Peel, LWT-Food Sci.Technol.,39:554-561,(2006).

8- Yang,X.,Zhao,Y. and Lv,Y.,Chemical Composition and Antioxidant Activity of an Acidic Polysaccharide Extracted From *Cucurbita moschata* Duchesen Ex Poiret,J.Agric.Food Chem.,55:4684-4690,(2007) .

9- Yang,J.O.,Oh,S.R.,LeeH.K.,Kim,C.J. and Song,K.B.,Isolation of Anticomplementary Substances From *Cucurbita moschata* Duch,Journal of Food Science,67(4):1348-1351,(2002) .

10- Sae-Lim,S.,Jiryasin,J.,Narapan,J. and Vanduangden,S., Determination of Fatty Acid From Seeds of *Cucurbita moschata* Duche.,34th Congress on Science and Technology,1-2,(2005) .

11- Choi,H.,Eo,H.,Park,K.,Jin,M.,Park,E.,Kim,S.,Park,J.E. and Kim,S., A Water-Soluble Extract from *Cucurbita moschata* Shows Anti-Obesity Effects by Controling Lipid Metabolism in a High Fat Diet-Induced Obesity Mouse Model, Biochemical and Biophysical Research Communications,359:419-425,(2007) .

12- Evangelina,G.,Mariana,M.,Monica,N., and Beatriz,L.D.M., Carotenoid Composition and Vitamin A Value of Argentinian Squash (*Cucurbita moschata*),Archivos Latinomericanos De Nutricion,51(4),(2001) .

13- Achu,M.B.,Fokou,E.,Tchiegang,C.,Fotso,M. and Tchouanguep,F.M.,Nutritive Value of Some Cucucrbitaceae Oil Seeds From Different Regions in Cameroon, African Journal of Biotechnology,4(11):1329-1334,(2005) .

14- Zhang,J.,Yang,J.,Duan,J.,Liang,Z.,Zhang,L.,Huo,Y.and Zhang,y., Quantitative and Qualitative Analysis of Flavonoids in Leaves of *Adinandra Nitida* by High Performance Liquid Chromatography with UV and Electrospray Ionization Tandem Mass Spectrometry Detection, Analytical Chimica Acta,532:97-104,(2005).

15- Al-Bayati,R.I.H.,Naji,N.A. and Al-Sedah,M.M.M.,Study on The Effect of *Capparis Spinosa* Fruits Extracts on Acetylcholinesterase Activity in Human Blood, Al-Mustansiriya J.Sci.,13(1):146-131,(2002) .

16- 16)Al-Bayati,R.I.H.,Al-Janabi,S.A. and Al-Mudarees,M.F., Hypoglycemic Activity of *Mentha Longifolia* Leaves Composites, Iraqi Journal of Chemistry,27(1):(2001) .

17- Jassim,A.M.N.,Study of Some *Eucalptus Rostrata* Leaves Components and Effect of Its Extract on Different Microorganisms,Al-Mustansirya J.Sci.,16(2):62-71,(2005) .

18- Mohammed,M.T., Study of Some *Vinca Rosea l.* (Apocynaceae) Leaves Components and Effect of Its Extract on Different Microorganisms,Al-Mustansirya J.Sci.,18(1): 28-36,(2007) .

19- الدليمي،نصر حامد،دراسة مظهريه وفسلجيه وخلوية كمؤشر على آلية تحمل نبات الحنطة للجفاف،اطروحة ماجستير،الجامعة المستنصرية ،(1997).

20- Plummer,D.T.,An Introduction of Practical Biochemistry,2ed,145-146,McGRAw-HILL Book Co.,England ,(1978) .

21- Hu,C. and Kitts,D.D.,Dandelion(*Taraxacum Officinale*) Flower Extract Suppresses Both Reactive Oxygen Species and Nitric Oxide and Prevents Lipid Oxidation *In Vitro*,Phytomedicine,12:588-597,(2005).

22- المياح ،عبد الرضا علوان ،النباتات الطبية والتداوي بالاعشاب ،جامعة البصرة –جامعة تعز ،مركز عبادي للدراسات والنشر ،صنعاء ،الجمهورية اليمنية ،ص 113،(2001) .

Gas Chromatography-Mass Spectrometry (GC-MS) Analysis of Active Compounds Produced from Rosemary (*Rosmarinus Officinalis* L.) Callus and Leaf Extracts

Salah K. Mahmoud
Foundation of Technical Education

Received 28/9/2009 – Accepted 5/10/2010

الخلاصة

درست انتاجية نبات اكليل الجبل (*Rosmarinus officinalis* L.) من المركبات الفعالة ، كانت انتاجية الكالس متميزة مقارنة مع انتاجية النبات الكامل. حفز نسيج الكالس على النشوء من اجزاء الورقة واديم على وسط MS مجهز بتوليفة من 2,4-D و BA بفترة اضاءة 16 / 8 ساعة. تم الحصول على اعلى وزن طري للكالس من التوليفة 2 ملغم/ لتر 2,4-D و 0.5 ملغم /لتر BA حيث بلغت 1780 ملغم. اجري التحليل باستعمال كروماتوغرافيا الغاز GC-MS للمستخلص الكحولي للورقة وظهر بأن اكثر المكونات هي:isocarnosol (%5.85)، camphor (%3.88)، ferruginol (%4.53)، cineole (%2.66)، verbenone (%2.50) و borneol (%1.50).

اظهر التحليل الكيمياني للمستخلصات الكحولية لنسيج الكالس اكثر المركبات ولكن بنسب اعلى مقارنة بمستخلصات الاوراق. ظهورالقلويدات quinoline لأول مرة في نسيج الكالس والتي تمتلك قيمة علاجية كبيرة في الصناعات الدوائية.

ABSTRACT

The yield of rosemary (*Rosmarinus officinalis* L.) from active compounds was investigated. Yield of callus tissue was compared with the intact plant production. Callus was induced in leaf explants and maintained on Murashige and Skoog medium (MS) supplemented with 2,4-D and BA. Maximum callus fresh weight was obtained in the combination of 2 mg/l 2,4-D and 0.5 mg/l BA under 16/8 hrs photoperiod, which reached 1780 mg. The GC-MS analysis of leaf ethanolic extracts revealed the most abundant components; isocarnosol (5.85%), camphor (3.88%), ferruginol (4.53%), cineole (2.66%), verbenone (2.50%) and borneol (1.50%). The chemical analysis of callus ethanolic extracts showed the most compounds but at higher percentages than in leaf extracts. Quinoline alkaloids, were found for the first time in callus have been of great therapeutic value in pharmaceutical industries.

INTRODUCTION

Rosemary (*Rosmarinus officinalis*) is a very important medicinal plant which belongs to the family Lamiaceae, has been cultivated for a long time [1]. Rosemary is widely used as a culinary spice, and is also used for its fragrance in soaps and cosmetics. Traditionally, rosemary has been used medicinally to improve memory, relieve muscle pain and spasm, stimulate hair growth, and support the circulatory and nervous systems [2]. The family Lamiaceae contains an extremely wide variety of aromatic plants, among this rich array of plants yielding essential oils [3].

Labiates are known for their essential oils common to many members of the family. Many of the active essential oils have been isolated from various members of this family. Plant cells and callus cultures have been extensively used to explore the possibility of producing useful secondary metabolites through biotechnology methods. The induction of callus growth and subsequent differentiation is accomplished by the differential application of growth regulators and the control of conditions in the culture medium. With the stimulus of endogenous growth substances or by addition of exogenous growth regulators to the nutrient medium, cell division, cell growth and tissue differentiation are induced [4].

Plants are the traditional source for many chemicals used as pharmaceuticals. Medicinal plants are used in crude or purified form in the preparation of drugs in different systems [5].

The leaves of rosemary contain between (1.0-2.5)% essential oil, such composition may markedly vary according to the chemo type and the development stage at which the plant has been harvested. It is an almost colorless to pale yellow liquid with a characteristics, refreshing and pleasant odor [6].

Some of the more commonly lavender, sage, rosemary, eucalyptus, jasmine, lemon, orange, rose and tea tree oil [7]. Rosemary oils are largely used in traditional medicine, in perfumery, phytocosmetic and in liquor manufacturing. EOs composition of rosemary comprise more than sixty individual components of which major substances can constitute up to 89% of the EOs [8].

Essential oils are produced using several techniques. Distillation uses water and steam to remove the oils from dried or fresh plants, and the expression method uses machines to squeeze the oil out of the plants. Other techniques may use alcohol or solvents to remove essential oils from plant materials [9].

MATERIALS AND METHODS

This study was carried out in the plant tissue culture lab., Biotech. Dept., Al-Nahrain University during the period 1/3/2009-1/9/2009. Rosemary plant was collected from the gardens belongs to College of Science-Baghdad University.

Callus induction and maintenance

After surface sterilization, leaf explants were cut at the ends into sections of approximately 1cm in length. Explants were placed on the medium in Petri-dishes (100 x 15 mm). For callus induction the basal medium was supplemented with various concentrations 0.0, 0.5, 1.0 or 2.0 mg/l of 2,4-D, BA at the concentrations 0.0, 0.2, 0.5 or 1.0 mg/l. For maintenance of callus cultures, the friable callus obtained from leaf

explants of rosemary were subcultured in 16 hrs photoperiod at 25±2°C on agar solidified MS medium containing 2.0 mg/l 2,4-D and 0.5 mg/l BA and 3% sucrose was added.

Preparation of leaf ethanol extracts

Powdered rosemary leaves (50 g) were soaked into 250 ml of 70% ethanol. The mixture was kept for 24 hrs in tightly sealed vessels at room temperature, protected from sunlight and mixed several times with a sterile glass rod, the mixture was then filtered through Wattman no.1 filter paper. The extracted liquid was subjected to rotary evaporation in order to remove the ethanol [10].

Preparation of callus ethanol extracts

Callus was dried at 40°C for 24 hrs, ground into powder using grinding machine or a mortar, then subjected to extraction. A quantity of 10 g of callus powder was extracted with 50 ml of 70% ethanol by soxhlet apparatus for 6 hrs at 60°C. The solution then evaporated to dryness as mentioned above, then the extract was stored at 4°C in refrigerator for future use [11].

Gas Chromatography/ Mass Spectrometry Analysis (GC-MS)

Analysis of the essential oils was performed using GC-MS (Agilent 6780-USA), equipped with mass selective detector and HP-5 MS capillary column (30m x 0.25mm, film thickness 0.25 μm). For GC-MS detection electron ionization system with an ionization energy of 70 eV was used. Samples were injected automatically in the split mode at split ratio of 1:100. All the tests were performed in triplicate.

RESULTS AND DISCUSSION

Maintenance of callus cultures

Table (1) revealed that the addition of 2,4-D exhibited a positive effect on rosemary callus growth at the concentration of 2.0 mg/l in combination with 0.5 mg/l of BA. Inclusion of 2,4-D at the concentration of 2.0 mg/l gave significantly higher callus fresh weight (1099.2) mg than other concentrations, while the lowest fresh weight (75.5) mg obtained in 2,4-D free medium. Addition of 0.5 or 1.0 mg/l of 2,4-D gave 450.7, 814.2 mg of callus fresh weight.

Table-1: Effect of different concentrations of 2,4-D and BA and their interactions on rosemary callus fresh weight (mg) grown on MS maintenance medium at 16 hrs photoperiod (initial callus weight was 50 mg)

2,4-D (mg/l)	BA (mg/l)				
	0.0	0.2	0.5	1.0	Mean
0.0	52.8	56.4	112.0	81.0	75.5
0.5	406.4	492.1	776.4	127.	450.7
1.0	559.2	878.5	1228.9	590.2	814.2
2.0	667.1	1103.5	1780.0	846.4	1099.2
Mean	421.4	632.6	974.3	411.3	
LSD ≤ 0.05	BA: 21.205*		2,4-D: 21.205*	BA x 2,4-D: 42.41*	

The highest callus fresh weight obtained from BA treatment (974.3) mg was at the concentration 0.5 mg/l. Treatment with 1.0 or 2.0 mg/l of BA gave 411.3 or 632.6 mg of callus fresh weight as compared to the control which recorded 421.4 mg. The interaction between 2,4-D and BA at the treatments 2.0 mg/l or 1.0 mg/l of 2,4-D with 0.5 mg/l of BA, resulted in maximum callus fresh weight (1780.0) mg or (1228.9) mg respectively. The interaction between 2,4-D at the concentration of 2.0 or 1.0 mg/l and BA at the concentration of 1.0 mg/l gave 846.4 or 590.2 mg of callus fresh weight. The interaction between 0.5 mg/l of 2,4-D and 1.0 mg/l of BA gave 127.0 mg of callus fresh weight, which was less than the control treatment, whereas the interaction between 0.5 mg/l of 2,4-D and 0.2 mg/l of BA gave higher callus fresh weight which reached 492.1 mg. All the treatments were significantly higher than the control (52.9) mg. The results are in agreement with [12] who proved that rosemary callus grown on solid MS medium containing 2.0 mg/l 2,4-D increases in size. [13] found that induction and maintenance of callus was obtained in MS basal medium supplemented with 2.0 mg/l 2,4-D and 0.5 mg/l BAP, and the leaf segment showed the best response for callus Induction of *Flacourtia jangomas* Lour. [14] also studied the effect of different concentrations of 2,4-D in the presence and absence of calcium silicate on callus formation of three rice genotypes. Among the combinations (1-2) mg/l of 2,4-D were found the best for callus induction (100%) and maintenance. Cultures grown on MS medium under a photoperiod of 16 hrs were mostly, friable, grew fast and large in size. Light has been shown to be an important regulator in various plant species, light has significantly enhanced callus initiation, callus fresh weight was light dependent, this may be due to the influence of both irradiation and light quality on callus cultures which is in agreement with [15]. The daylight fluorescent tubes give important emission bands at red and blue spectral wavelength. These conditions have been found to give the best culture growth rates [16].

GC-MS analysis of rosemary leaf extracts

Rosemary leaf ethanol extracts were tested by GC-MS, their chemical composition showed about 12 components. Table (2) and figure (1) showed that the most abundant component was isocarnosol (5.85%). The extract also contain camphor (3.88%), ferruginol (4.53%), cineole (2.66%), verbenone (2.50%) and borneol (1.56%) as a major components. The composition of rosemary leaf extracts was qualitatively similar to those obtained by other authors [17, 18] but with different quantitative composition.

Table -2: Retention time and peak area (%) of the different compounds found in rosemary leaf extracts analyzed by GC-MS

Compound	RT (min)	Peak area%
Cineole	8.80	2.66
α-caryophyllene	11.71	0.40
Camphor	13.36	3.88
Borneol	14.44	1.56
Terpinen-4-ol	14.88	0.25
Non-identified	15.59	0.59
Verbenone	16.26	2.50
2-methyl-4-vinylphenol	21.09	0.15
Eugenol	22.85	0.09
Pyrazolobis (bbn) thiolium	57.58	9.65
Ferruginol	58.70	4.53
Isocarnosol	61.69	5.85
Non identified components		67.89

These differences in the chemical composition could be attributed to climatic effects on the plants, besides the following factors should be considered when observing differences between studies; genotypic and environmental differences within species, sample extraction time and extraction technique used to obtain the rosemary extract [19].

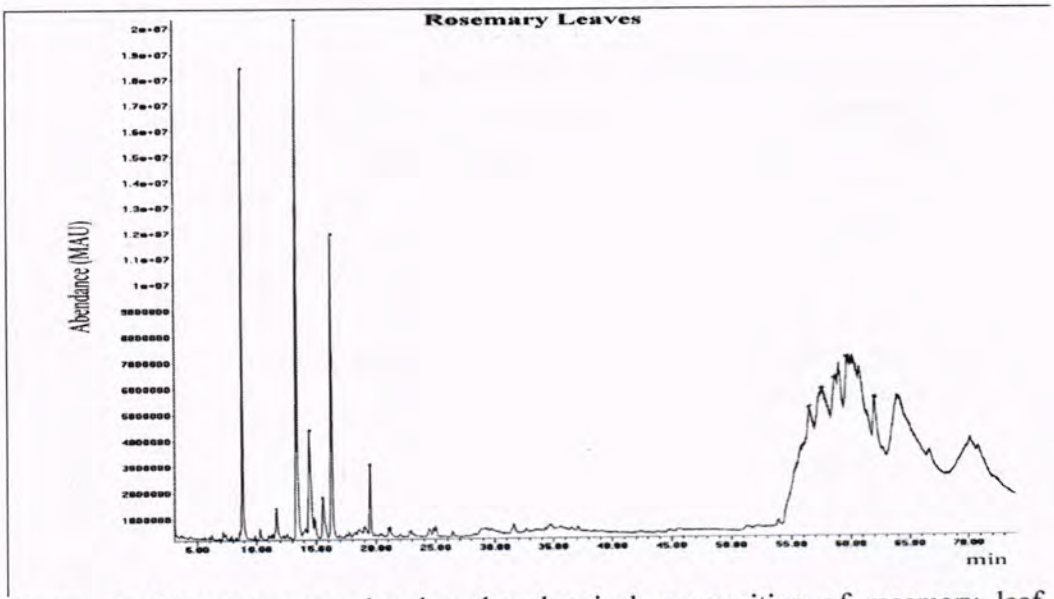

Figure -1: Chromatogram showing the chemical composition of rosemary leaf ethanolic extract analyzed by GC

GC-MS analysis of rosemary callus extracts

The GC-MS analysis of untreated callus of rosemary plant was revealed the main constituents, their relative percentage of the total peak area and retention times as shown in Table (3) and figure (2). The data indicate that 18-21 components were identified in callus ethanol extract. The major constituents being, cineole (4.44%), camphor (2.51%), verbenone (2.30%), borneol (1.91%) and caryophyllene (0.64%). Callus extract also contained Ferruginol (1.59%), isocarnosol (1.27%), Stearic acid (0.71%), phytol (9.12%),qiunoline (16.78%) and many other non-identified components.

Table -3: Retention time and peak area (%) of the different compounds found in rosemary callus extracts analyzed by GC-MS

Compound	RT (min)	Peak area%
Cineole	9.36	4.44
Camphor	15.10	2.51
Borneol	16.58	1.91
Verbenone	19.04	2.30
5-oxymethylfurfurol	22.29	0.72
Eugenol	23.66	1.66
Caryophyllene	31.59	0.64
Ferruginol	58.07	1.59
Isocarnosol	61.89	1.27
Stearic acid	62.35	0.71
Bornyl acetate	64.41	1.66
Phytol	64.82	9.12
Quinoline	67.11	16.78
Dihydronomorphinone	67.47	3.73
Sclareol	67.78	0.71
Non identified components		53.98

The data showed that callus extract produced high percent for some constituents as compared with the same constituents in leaf extract. Cineole percentage was reached 4.44% in callus extract of rosemary, while it was found 2.66% in leaf extract. Borneol and caryophyllene percentage was 1.91%, 0.64% in callus extract, while it was recorded 1.56%, 0.40% in leaf extract respectively. Eugenol percentage was 1.66% in callus, while it was trace in leaf (0.09%). Other constituents such as, isocarnosol, bornyl acetate, phytol, sclareol and quinoline were found only in callus extract at the percentages of 1.27, 1.66, 9.12, 0.71 and 16.68% respectively, while they were absence in rosemary leaf extract. It was clear that callus extract of rosemary plant contain more constituents than that found in leaf extract and at higher percentages. Quinoline alkaloids (which was found in callus) have been of great therapeutic value, the antimalarial activity of these alkaloids has been documented, besides their pharmaceutical uses, they are used frequently in the food and soft drink industry [20].

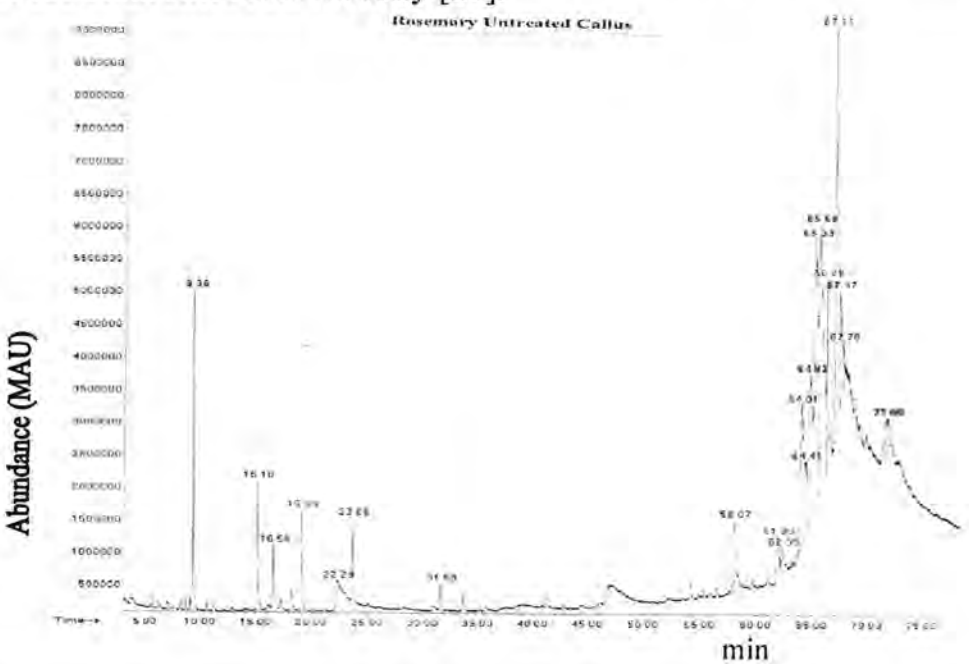

Figure -2: Chromatogram showing the chemical composition of rosemary callus ethanol extract analyzed by GC

REFERENCES

1- Eva, S. B.; Maria, H. T.; Attila, H.; Csilla, R.; and Szollosi, V. Antioxidant effect of various rosemary (*Rosmarinus officinalis* L.) clones. Acta Biologica szegediensis., 47(1-4): 111-113(2003).
2- Foster, S. and Tyler, V. The honest herbal; A sensible guide the use of herbs and related remedies. 4th ed. Haworth Herbal Press., 321-322(1999).
3- Chalchate, J. C. O.; Garry, R. P.; Michet, A.; Benjilali, B. and Chabart, J. I. Essential oils of rosemary (*Rosmarinus officinalis* L.). The chemical

composition of oils of various origins (Morocco, Spain, France). J. Essential Oil *Rosmarinus*., 5: 613-618(1993).

4- Leena, T. and Jaindra, N. T. Role of biotechnology in medicinal plants. Tropical Journal of Pharma. Res., 2(2): 243-253(2003).

5- Robins, R. L. Secondary products from cultured cells and organs: Molecular and cellular approaches. In: Dixon, R. A., Gonzates, R. A. (eds). Plant Cell Culture. Oxford; IRL, Press(1999).

6- Bauer, K.; Garbe, D. and Surburg, H. Common Fragrance and Flavor Materials. 3rd ed. Germany: Wiley-VCH(1997).

7- Hayashi, K.; Kamiya, M. and Hayashi, T. Virucidal effects of the steam distillate from *Houttuynia cardata* and its components on HSV-1, influenza virus and HIV. Planta. Med., 61: 237-241(1995).

8- Burt, S. Essential oils; their antibacterial properties and potential application in foods. A review. International J. of Food Microbiol., 94: 223-253(2004).

9- Mounchid, K.; Bourjilat, F.; Dersi, N.; Aboussaauira, T.; Rachidai, A.; Tantaoul,-Elaraki, A. and Alaoui-Ismaili, M. Toxicity of south Morocco *Rosmarinus officinalis* essential oil: antibacterial and histopathological effects. Les Actes del'institut Agronomique et Veterinaire., (2-3): 139-144(2004).

10- Akueshi, C. O.; Kadiri, C. O.; Akueshi, E. U.;Agina, S. E. and gurukwem, B. Antimicrobial potential of *Hyptis sauvedens* Poit (Lamiaceae), Nigeria. J. Bot., 15: 37-41(2002).

11- Harborne, J. B. Phytochemical Methods. A guide to modern technique of plant analysis, Chapman Hall, London(1984).

12- Caruso, J. L.; Callahan, J.; DeChant, C.; Jayasimhulu, K. and Winget, G. D. (2000). Carnosic acid in green callus and regenerated shoots of *Rosmarinus officinalis*. Plant Cell Rep. Vol., 19: 500-503.

13- Chandra, I. and Bhanja, P. Study of organogenesis i*n vitro* from callus tissue of *Flacourtia jangomas* (Lour.). Current Science, 83. Burdwan University, India(2002).

14- Islam, M. M.; Ahmed, M. and Mahaldar, D. *In vitro* callus induction and plant regeneration in seed explants of rice (*oryza sativa* L.). Research J. of Agric. and Biol. Sci., 1: 72-75(2005).

15- Senger, H. The effect of blue light on plants and microorganisms. Phytochem., 35: 911-920(1982).

16- Roland, R.; Davin, C. and Zryd, J. Betalain production cell cultures of *Beta vulgaris* L. Var. Bikores monogerm (Red beet). *In vitro* Cell. Dev. Biol., 28: 39-45(1992).

17- Panizzi, L. Composition and antimicrobial properties of essential oils of four Mediterranean Lamiaceae. J. of Ethnopharm. Livorno / Pisa., 39: 167-170(1993).

18- Aziza, K. G.; Haiko, H.; Artur, S. J. and Simone, M. S. Rosemary (*Rosmarinus officinalis*) a study of composition, antioxidant and antimicrobial activities of extracts obtained with supercritical carbon-dioxide. Cienc. Technol. Ailment., Campinas., 28(2): 463-469(2008).

19- Gachkar, L. Chemical and biological characteristics of *Cuminum cyminum* and *Rosmarinus officinalis* essential oils. Food Chem., 102: 898-902(2007).

20- Ramawat, K. G. Plant Biotechnology. S. Chand and company LTD, Ram Nagar, New Delhi(2008).

Study the Effects of Specific Absorption Rate in Electromagnetic Energy Radiated From Mobile Phones on Human Body

Hanan A. Naif
Al-Mustansiriyah University, College of Science, Department of Physics

Received 24/1/2010 – Accepted 20/6/2010

الخلاصة

في السنوات الاخيرة، انتشر استعمال جهاز الهاتف المحمول الشخصي بشكل واسع وذلك لانه سمح للأشخاص بالحفاظ على الاتصال المستمر بدون اعاقة وبحرية تامة في التنقل.
ان استعمال هذا الجهاز وتطبيقاته تزايد تدريجياً في العقود الاخيرة تقابله زيادة في مجال الاشعة الكهرومغناطيسية في المحيط. وان احد التاثيرات السلبية لتطور الاتصال بالجهاز المحمول على الاشخاص هو التعرض لمجال الاشعة الكهرومغناطيسية الناتجة من حمل هذا الجهاز.
ولقد اصبح من المعروف منذ سنوات ان التعرض للاشعة الكهرومغناطيسية يمكن ان يكون مؤذي وذلك لإن جسم الانسان يقوم بامتصاص هذه الاشعة، وان المصطلح الذي يستخدم للتعبير عن هذا الامتصاص هو (نسبة الامتصاص النوعية).
في هذا البحث سوف نقوم بدراسة العوامل المؤثرة على نسبة الامتصاص النوعية مثل بعد مصدر الاشعة الكهرومغناطيسية عن جسم الانسان، التردد، مقدار المجال الكهربائي، وبعض المؤثرات الاخرى.

ABSTRACT

In recent years, personal mobile phones have become popular in worldwide, because they allow people to maintain continuous communication without hampering and freedom of movement.
The use and application of this device steadily increased over the past decades resulting in a corresponding increase in electromagnetic (EM) fields in the environment, and one of the undesired effects of growth of mobile communication on population is exposure to electromagnetic field produced by handheld mobile telephone.
It has been known for many years that the exposure to radiofrequency (RF) radiation can be harmful, because the body is absorbed this radiation and the quantity used to characterize this absorption is called the Specific Absorption Rate or (SAR).
This paper is present the parameters are effect of the (SAR), such as position of the (RF) source near the human body, frequency, electric field and some other factors.

INTRODUCTION

Electromagnetic radiation consists of waves of electric and magnetic energy moving together through space. Radio waves and microwaves released by transmitting antennas are one form of electromagnetic energy. They are called Radiofrequency (RF) or energy radiation[1].

Electromagnetic waves can be characterized by a wavelength and a frequency, the wavelength is the distance covered by one complete cycle of the electromagnetic wave, while the frequency is the number of

electromagnetic waves passing a given point in one second [2], and this parameters are related through in this equation[3]:

$$E = h\upsilon \quad ...(1)$$

Where:

h: is Plank's constant

υ: is the frequency of radiation

Since the speed of light does not change, high frequency electromagnetic waves have short wavelength and low frequency waves have long wavelength[4].

The electromagnetic spectrum includes all the various forms of wavelengths, to x-rays and gamma rays, which have very high frequencies and corresponding to short wavelength[4]. The RF portion of the electromagnetic waves have frequencies in the range from about 3KHz to 300GHz.[5]

The photon energies of (RF) electromagnetic waves are not great enough to cause the ionization of atoms and molecules, therefore, (RF) energy characterized as non-ionizing radiation, along with visible light, infrared radiation and other forms of electromagnetic radiation with relatively low frequencies[6].

THEORETICAL PART

(SAR) is a measure of the rate at which radiofrequency (RF) energy is absorbed by the human body when exposed to radiofrequency electromagnetic field[6,7] and it is usually expressed in units of watts per kilogram (W/Kg) or milliwatts per gram (mW/g)[4,8,9].

The mathematical conditions on the external boundary are low reflecting, which means that the result will be influenced by the limitation of the computational domain with sphere[10].

A center-fed half-wave length dipole antenna that emits electromagnetic waves at the frequency of ($1.8x10^9$Hz) is considered as the electromagnetic field source[10].

In order to get closer to the parameters of a mobile phone, the antenna is calibrated so that the power emitted is (0.125W) (the intensity of the magnetic field is specified on the antenna). The lateral surface of the antenna is considered to be a magnetic field emitter[10].

The electrical conductivity (σ=0.48S/M) and the relative permittivity (ε_r=17.84), a value of 1100Kg/m^3 is assigned to the equivalent mass density [10,11].

The strength of the induced electric field (E) and the specific energy absorption rate (SAR) were calculated and displayed in two planes.

Limiting exposure guidelines[12] state, as a reference level, the (rms) value of (58V/m) as the maximum allowed electric field strength at 1.8GHz. It is generally accepted that (SAR) is the most appropriate metric for determining electromagnetic energy exposure in the very near field of a (RF) source[13,14].

The (SAR) can be determined at any point from the E-field by [11,15,16,17,23]:

$$SAR = \frac{\sigma |E|^2}{2\rho} \quad ...(2)$$

Where:

$|E|^2$: is the maximal strength of the time harmonic electric field[17]

σ: is the conductivity ($\Omega^{-1}m^{-1}$) of the tissue.

ρ: is the mass density (Kg/m^3)

In other hand, (SAR) is defined as that has been widely adapted, as the time derivative of the incremental energy (dW) absorbed by, or dissipated in an incremental mass (dm) contained in a volume element (dV) of a given density (ρ), which described by[18,19]:

$$SAR = \frac{d}{dt}\left(\frac{dW}{dm}\right) \Rightarrow \frac{d}{dt}\left(\frac{dW}{\rho(dV)}\right) \quad ...(3)$$

$$SAR = \frac{1}{\rho}\left(\frac{dW}{dt}\right) \quad ...(4)$$

Where:

dw: energy absorbed

dm: the mass

dv: volume element

The Federal Communications Commission (FCC's) exposure guidelines, the Institute of Electrical and Electronics Engineers and American National Standards Institute (ANSI/IEEE), and the National Council on Radiation Protection (NCRP) guidelines conducted by the World Health Organization (WHO) in (1999), the Canadian Royal Society (1999), and a review on mobile phones and health by an expert Committee in the United Kingdom, this fact has been updated in light of recent reviews of the effects on human beings of exposure to radiofrequency (RF) fields and limited the safe exposure to (RF) energy produced by mobile devices (1.6W/Kg)[4,20,21,19,17].

The first two parameters of (SAR) effects are the electric and magnetic fields, because the (RF) electromagnetic field has both an electric and magnetic components, it is often convenient to express the intensity of the (RF) field in terms of units specified for each

component[4]. The standards and guidelines for personal safety in radiofrequency (RF) and microwave electromagnetic fields dictate that the electric and magnetic field strength to which a person is exposed must exceed certain frequency dependent limits[3].

At frequencies above 300MHz is usually sufficient to measure only the electric field to characterize the (RF) environment if the measurement is not made too close to the (RF) emitter[22].

The total energy stored in the electric and magnetic fields[23], the electrical part is produced by a voltage gradient and is measured in (Volt/meter)[V/m], and the magnetic part is generated by any flow of current and is measured in (Amperes/meter)[A/m] that's is called (Tesla)[24,25].

The interaction of external radiowaves with biological bodies produces internal electric and magnetic fields that leads to give biological effects, but the magnetic field is more dangerous since it penetrates and damages the living tissue more easily[24,18].

In addition to electric and magnetic fields, the frequency of an (RF) electromagnetic wave can be important in determining how much energy is absorbed[4]. The frequency of maxima absorption is called the resonance frequency (for humans it is between 70 and 100MHz), and depends on orientation with respect to the incident field[26,18].

The distance is effected in the (SAR) too, and the maximum electric field values were measured from the front side very close to the mobile phones for different phones[6].

The conductivity and permittivity of a tissue that determine how electromagnetic radiation is absorbed. The permittivity of a tissue is a strong function of frequency, the whole body averaged value permitvity is approximately 2/3 that of muscle tissue[18].

Another commonly used at for characterizing and (RF) electromagnetic field is "power density"[22], it is defined as power per unit area, usually expressed in terms of milliwatts per square centimeter (mW/cm^2)[20,22,23].

The power density is given by[26]:

$$S = \frac{E^2}{\eta} = H^2\eta \qquad ...(5)$$

Where:

H: the amount magnetic field

η: constant

In the far field region, the field has a predominantly plane wave character (i.e the electric field vector is perpendicular to the magnetic field vector is perpendicular to the magnetic field vector, and they are both transverse to the direction of propagation). The ratio of the electric

field strength to the magnetic field strength is constant at any location and in free space it is equal to[26,18]:

$$\frac{E}{H} = \eta = 377\Omega \quad ...(6)$$

The time-averaged rate of energy absorption for steady state sinusoidal fields per unit volume (W/m^3) at a point inside an absorber is[18]:

$$P = \sigma E^2 \quad ...(7)$$

Where: E: is the root-mean square magnitude of the electric field vector at that point inside the materials.

σ: is the conductivity

COMPUTATION METHOD

To measure the parameters that effects of the (SAR), we must determine the distance between the mobile phones and human body.

The values of (SAR) calculated in different distance starting from (0.01mm) to (0.30mm) in the same time measuring the amount of electric field by using the equation (2).

Also, we calculated the energy radiation by using the equation (1), and changes the frequency in range (100-300)MHz because the mobile phone system operate at frequencies between (800)MHz and (1800) MHz.

The power density can measure by using the equation (4), we can changes the electric field in range (1-300)V/m and measure the (SAR) in this point, and we can calculation the (SAR) as a function of times ranged from (1-60)min.

RESULTS AND DISCUSSION

(SAR) results depend on various parameters, such as position of the (RF) source near the human body, power density, frequency, electrical properties and duration of exposure.

Figure (1) shows the relation between the variation of (SAR) with distance, which decrease as the distance increases.

The (SAR) at (0.01mm) from the mobile phone was found to be (1.57W/Kg). For this estimate, we can confident that no hazard exists for a person standing along side as this is the minimum distance. The results are in good agreement with study Bangay et al., 1999[11].

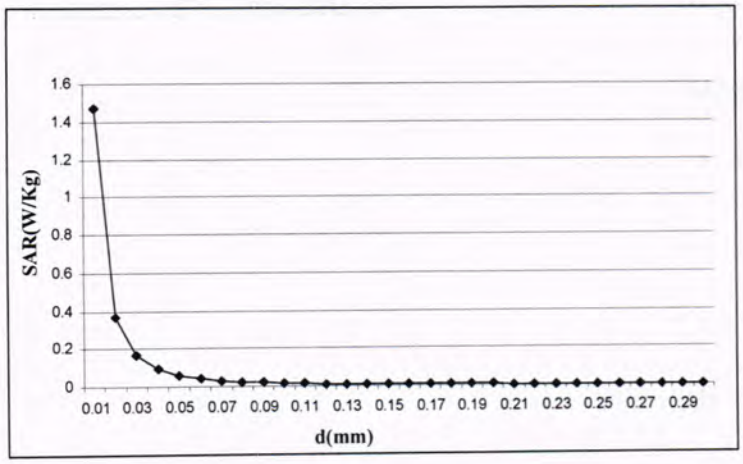

Figure -1: The relation between the values of (SAR) with the distance between the mobile phone and the human body

Also, the distance is effected to the amount of the electric fields, as it is clearly indicated from Figure (2), the electric field intensity is gradually decreased as a function of distance and the results are in good agreement with Seker S., 2000 and Kassar A., et al.,(2000) [6,27].

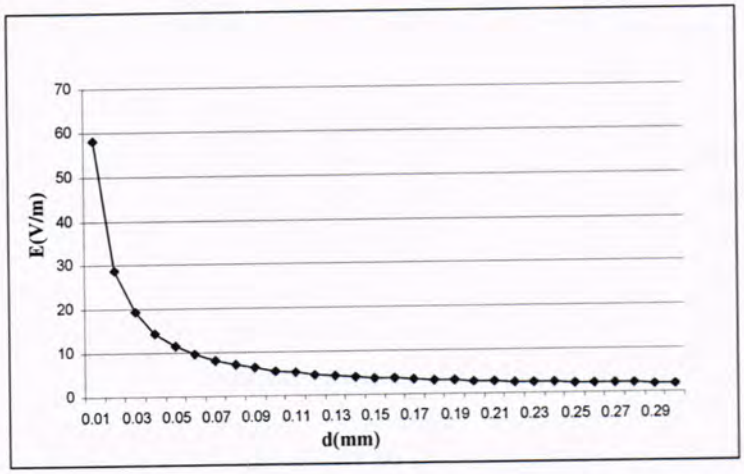

Figure-2: The relation between the distances with the values of the electric field

The electric field from mobile phones has been evaluated. It was observed that electric fields from mobile phones were two times higher during speaking than listening[6].

Like electric fields, magnetic fields are strongest close to their origin and rapidly decrease at greater distances from the sources.

Depending on the above results, we can prove the relation between the values of (SAR) with the electric field intensity as shown in figure (3), that's mean if the electric field reaches (290V/m), the (SAR) reaches it maximum value.

The (SAR) varies from point to point in the human body, because the electric field changes with position, and the conductivity is different for different types of tissues.

At points (0.01mm) from mobile phone, the maximum values of the electric field are calculated to be about (58V/m).

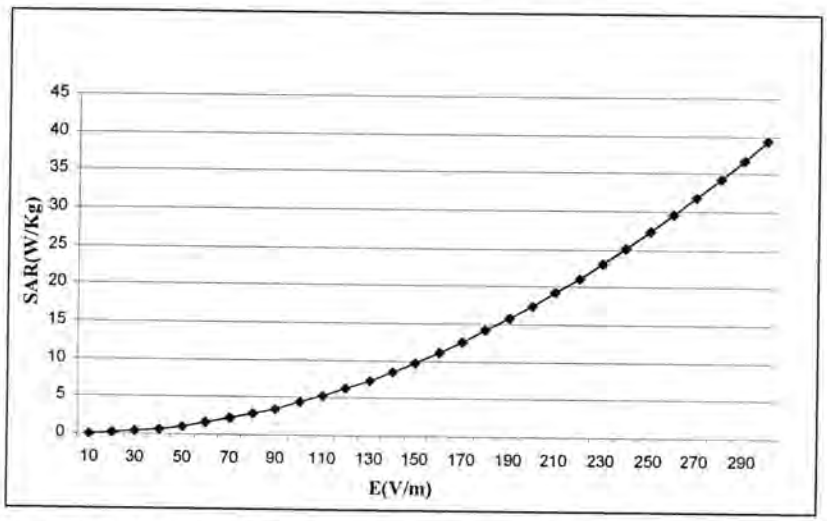

Figure -3: The relation between the values of SAR with the electric field

The frequency is one of the main characteristic which define an electromagnetic field (EMF). It could be important in determining how much energy is absorbed. The mobile phone system operate at frequencies between 800 and 1800MHz.

Figure (4) shown the relation between the energy and frequency, the electromagnetic radiation can only be absorbed in quanta of energy ($h\upsilon$).

Now, the energy needed to remove an electron from an atom or molecule is a few electron volt (eV), so if the quantum of energy is less than about (1eV) it is essentially impossible for ionization to occur.

The amount of energy of (RF) radiation is in fact many thousand times less than (1eV), so (RF) radiation cannot ionize atoms or molecules and is described as non-ionizing radiation.

Radiofrequency fields penetrate the human body that decreases with increasing frequency, and we can see from Figure (5) the changes of absorption energy with the amount of electric field.

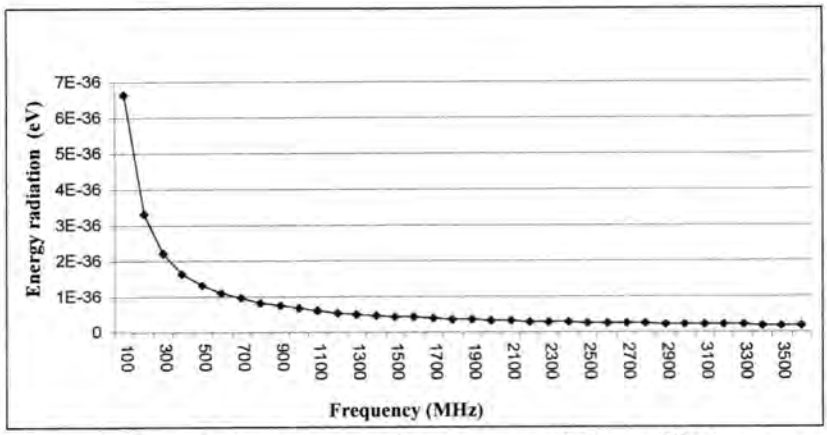

Figure -4: The relation between the energy radiation with frequency

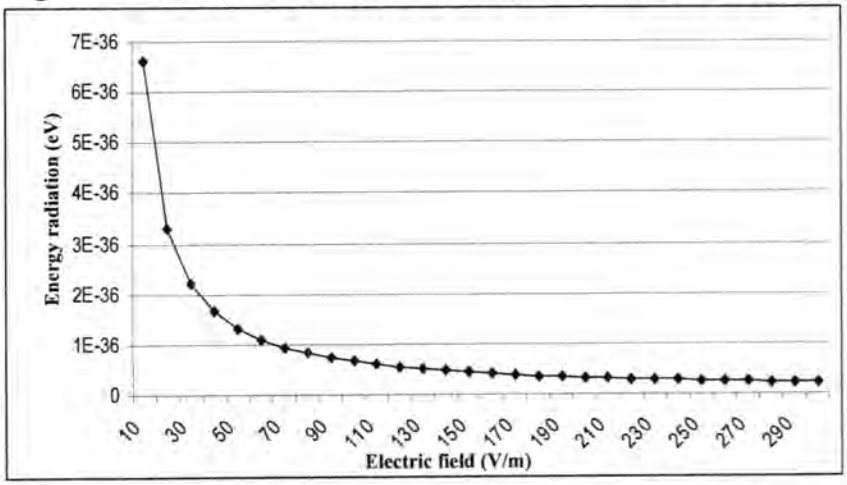

Figure -5: The relation between the energy radiation with the electric field

The effects of electromagnetic fields on the human body depend not only on electric field level but also on their frequency and energy.

From these results, we can determine the relation between the electric field with frequency and it noted by figure (6).

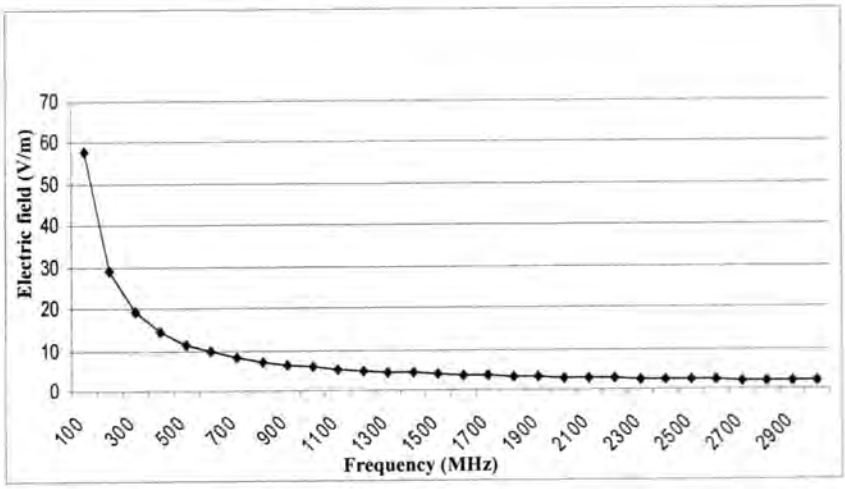

Figure -6: The relation between the frequencies with the electric field

With respect to frequencies in the mobile phones, power density is usually used to express the intensity since the exposures that might occur would likely to be in the far-field. The power density of the electromagnetic waves incident on a specific surface area in free space the mean values of the exposure field as obtained by spatially a verging the squares of the field strengths or a verging the power densities over an area equivalent to the vertical cross section of the human body, or a smaller area depending on the frequency.

Figure (7) shows the relation between the values of (SAR) with power density, it is previous the values of the SAR reduced with increasing the power density, and figure (8) shows the power density is increasing if electric field increased, so the power density decreases with increasing frequency as shown in Figure (9), these results are in good agreement with E.S.H. manual [23].

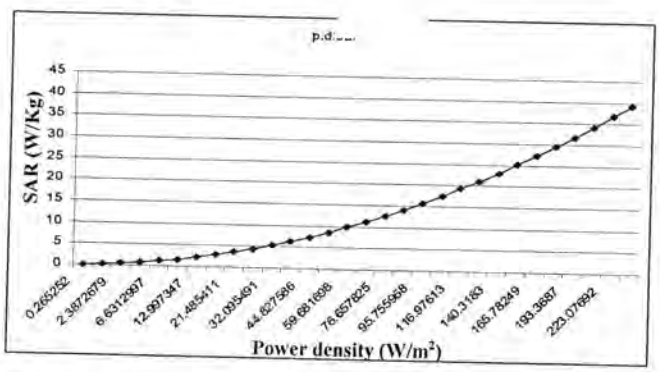

Figure -7: The relation between the values of (SAR) with power density

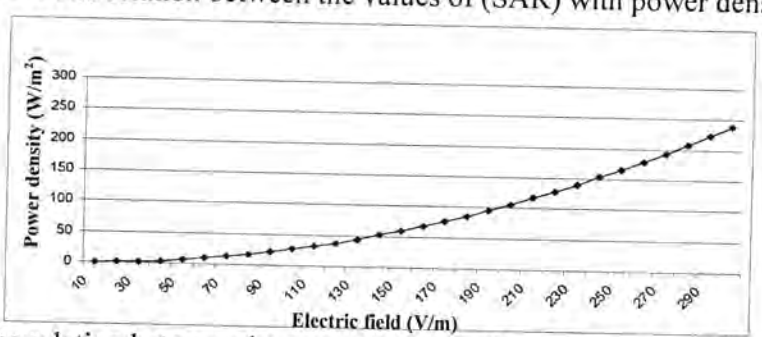

Figure -8: The relation between the power density with the strength of electric field

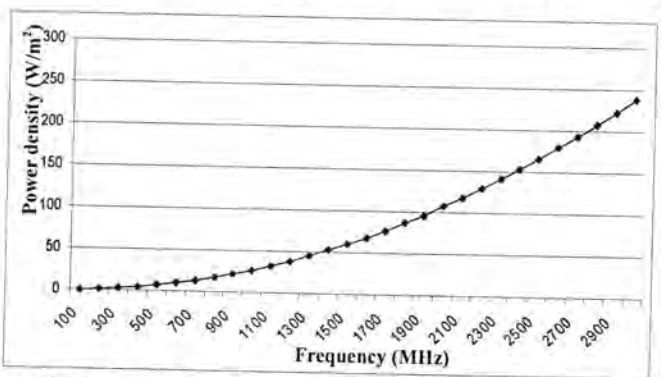

Figure -9: The relation between the power density with the frequency

From the definition of the (SAR) (eq.4) we can notice that the relation between the (SAR) with time, figure (10) shows these relation and it is clearly that the (SAR) increases with increasing the time exposure. This study is shown in ref. [28] experimentally when it performed to high light the variation of the radiation levels during the call progress that is represented by during conversation (silence, speaking) and termination and its greater in the set up.

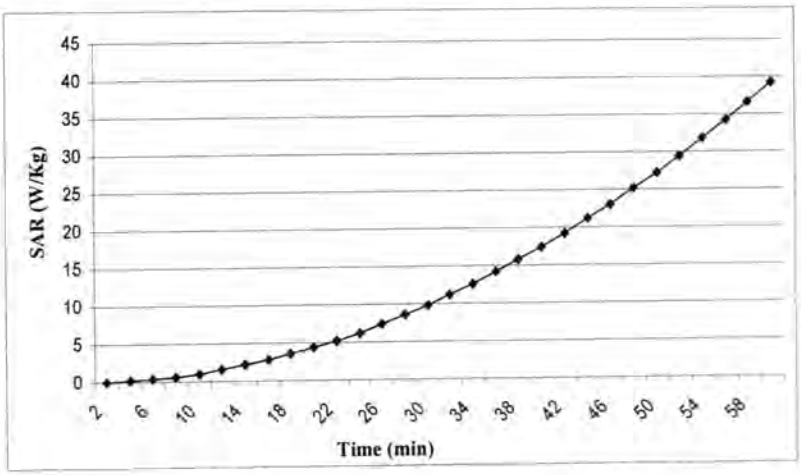

Figure -10: The relation between the values of (SAR) with time exposure

We can conclude that:

1. The main parameters which effected by the value of (SAR) is "distance", it is decreases with increasing the distance that's lead to say the distance between the mobile phone and the human body reduced the strength of the electric and magnetic fields when the electromagnetic energy absorbed.
2. The increasing power density is affected with the value of (SAR), it is lead to increase the value of (SAR) because it affected by the amount of the electric and magnetic fields.
3. If the value of (SAR) is less than or equal to (1.6W/Kg), the use of the mobile phone is not dangerous in human body.

REFERENCES

1. Federal Communications Commission. "Frequently asked questions about cell phones and your health", CDC, Fact sheet, Department of health and human services centers for disease control and prevention safer, Healther.People. March (2005).
2. Federal Communications Commission. "Information guide for telecommunication facilities" City of Laguna Beach, Community Development Department, section 704, (1996).

3. Schallner M., Waldmann J., Hubner S., Lanstorfer F. "The influence of the human body on electric and magnetic fields components in the immediate vicinity of the body". Institut für Hochfrequnztechnik, universität Stuttgart Helmat Keller, Rainer Bitzer, Wandel and Goltormann, Frequenz 52, P.9-10, (1998).
4. Robert F., Cleveland J., Jerry L. "OET Bulletin 56" Office of Engineering and Technology Federal Communications Commission, Washington, D.C.20554, 4th edition, August (1999).
5. Insurance group "Non-ionizing radiation" Loss Control Data Guide, Great American Insurance Company, F.13784 (1960).
6. Seker S., Apaydin G. "Effects of electromagnetic fields on human beings and electronic devices", Bogazici University, Electric-Electronic Engineering Department, Bebek, Istanbul, Turkey, No.:BAP03A207(2000).
7. Specific Absorption Rate, Wikipedia, the free encyclopedia.
8. Polk C., Postow E. "Handbook of Biological effects of electromagnetic fields, CRC press, LLC, ISBNO. 8493-0641-8, (1996).
9. ICNFRP "Specific Absorption Rate", RSAC paper 2/2002, Guidelines for limiting exposure to time varying electric, magnetic, and electromagnetic fields (up to 300GHz), (1998).
10. ICNFRP "Specific Absorption Rate", Guidelines for limiting exposure to time varying electric, magnetic, and electromagnetic fields (up to 300GHz), (2002).
11. Bangay M., Zombolas C.: "Advanced measurements of microwave oven leakage", Australian Government, Australian Radiation Protection and Nuclear Safety Agency, Conference paper, EMC technologies, Pty. Ltd(1999).
12. Nikitin P., Rao K.V.S "Theory and measurement of Backscattering from RFID Tugs", IEEE Antennas and propagation, Vol.48, No.6, PP.212-218, (2006).
13. Allen S.G "Radiofrequency field measurement and hazard assessment", Journal of Radiological Protection, Vol.11-1, (1996).
14. Chou C.K., Bassen H., Osepchuk J, Balzano Q., Peterson R., Meltz M., Cleveland R., Lin J.C. and Heynick L. "Radiofrequency electromagnetic exposure: Tutorial Review on Experimental Dosimetry, Bioelectromag., Vol.17, No.3, (1996).
15. Robert L. "The numerical evaluation of a SAR measurement phantom at the Telstra research laboratories", McIntosh, Ray McKenzie, Amico Carratelli, Electromagnetic energy safety research Telstra research laboratories, 770 Blackburn Rd, Clayton, Victoria, Australia, 3168(2006).

16. Gabriel C. "Compilation of the dielectric properties of body tissues at RF and microwave frequencies", Brooks Air force Base, report No.AL/OE-TR-0037, (1996).
17. Samfirescu S., Moregu M. "3D reconstruction of the human head for FEMLAB analysis of the exposure of mobile phone users to microwaves", Politehnica University of Bucharest, ATEE, (2004).
18. NCRP "Absorption of RF radiation", NCRP report, No.119 (2000).
19. Darmindra D.A., Daniel W.E. "Specific Absorption Rates in muscle tissues for UHF RFID reader systems", university of texasat Arlington, 416 yates street, Arlington, TX 76010 (1998).
20. IEGMP: "Independent expert group on mobile phones and health", National Radiological Protection Board (UK), (2000).
21. ICNIRP: "Draft guidelines for complying with limits for human exposure to electromagnetic fields (Base station Antennas and mobile telephones/ Radio Terminals)" (c) TEC, Telecommunication engineering centre, New Delhi-110001, India, (1997-1998).
22. Poljak D.: "Human exposure to electromagnetic fields", WIT press, LLC, ISBN, 1-85312-997-6, (2004).
23. Department chemical and general safety non-ionizing radiation: "Non-ionizing radiation:selected radiofrequency exposure limits", E.S.H Manual, Chapter 50, SLAC Environment, Safety, and health manual (SLAC-1-720-OA298-001), 27 Mar., (2008).
24. Jokela K., Puranen L., Sihvonen A.: "Assessment of the magnetic field exposure dye to the battery current of digital mobile phones", Health Physics, 86:56-66, (2004).
25. Racuciu M., Creanga D.E., Miclaus S.: "The absorption of electromagnetic energy in the mammal tissues", University L.Blaga, Sibiu, Faculty of Sciences, Tomul II, S. Biofzica, Fizica medicala si fizica mediului (2006).
26. Official Publications Guidelines: "Guidelines for the measurement of radiofrequency fields at frequencies from 3KHz to 300GHz", Industry Canada, spectrum management and telecommunications (2001).
27. Kassar A., Mustafa Y.: "The harmful impact of the electromagnetic fields on seafarers", Arab Academy for Science and Technology and Maritime Transport, P.O.1029 Miami, Alexandria, Egypt (2000).
28. Abdelati M.: "Electromagnetic radiation from mobile phone base stations at Gaza", The Islamic University of Gaza, Journal of the Islamic University of Gaza (Natural Sciences Series), Gaza, Palestine, Vol.13, No.2, P129-146, (2005).

Effect of the Thickness on the Optical Properties of (TiO_2) Thin Films.

Arwaa F. Saleh, Batool D. Balawa and Areej A. Hateef
Department of Physics, College of science, Al-Mustansiriyah University
Received 5/4/2010 – Accepted 5/10/2010

الخلاصة

حضرت الأغشية الرقيقة لثاني أوكسيد تيتانيوم TiO_2 بإستعمال تقنية التحلل الكيميائي الحراري على قواعد زجاجية سُخنت لدرجة حرارة (210 °C) و بإسماك مختلفة (100, 200, 300, 400 , 500 nm) ، أشارت فحوصات XRD لأغشية TiO_2 بأن الأغشية كانتْ من نوع anatase ، كان لسمك تأثير على الخصائص البصرية للأغشية الرقيقة (كمعامل إمتصاص، و معامل الخمود، و معامل الامتصاص، و فجوة طاقة للإنتقالات المباشرة)، دُرست الخصائص البصرية للاغشية و وجد ان قيمها كالتالي : معامل الامتصاص يتراوح بين ($1.5x10^5$- $4.7x10^5$ cm^{-1})، ومعامل الخمود (0.353-1.097)، ومعامل الانكسار - (2.8 3.1)، وفجوة الطاقة المباشرة المسموحة (3.6-3.605 eV)، أما فجوة الطاقة الممنوعة فكانت - (3.2857 3.1857 eV) لجميع الاسماك المحضرة.

ABSTRACT

Thin films of titanium dioxide TiO_2 were prepared using chemical spray pyrolysis technique on glass substrate preheated at (210 °C) with different thickness (100, 200, 300, 400 and 500 nm). XRD study indicated these films were anatase. The thickness dependence on optical properties (absorption coefficient, extinction coefficient, refractive index and energy gap for direct transitions) of transparent (TiO_2) thin films were studied. Their values: for absorption coefficient is about ($1.5x10^5$-$4.7x10^5$ cm^{-1}), and for extinction coefficient is about (0.353-1.097), and for refractive index is varied from (2.8 - 3.1), and direct energy gap for allowed is about (3.69 - 3.605 eV), while that for forbidden is (3.2857 - 3.1857 eV) for all films prepared.

INTRODUCTION

Over the last few decades, titanium dioxide (TiO_2) has been widely investigated recently for its interesting optical properties, electronic properties and stability in the adverse environmental for its high refractive index, wide band gap and chemical stability, poly crystalline TiO_2 films are used for a variety of applications such as optics industry **[1]**, dye sensitized solar cells **[2]**, dielectric applications **[3]**, self cleaning purposes **[4]**, and photo catalytic layers **[5]**. The highly transparent TiO_2 films have been widely used as antireflection coatings for increasing the visible transmittance in heat mirrors **[6]**. TiO_2 can exist as an amorphous layer and also in three crystalline phases: anatase (tetragonal), rutile (tetragonal), brookite (orthorhombic). The refractive index at (500 nm) for anatase and rutile bulk titanium is about 2.5 and 2.7 respectively **[7]**. There are many deposition methods used to prepare TiO_2 films **[8]** such as thermal evaporation in vacuum deposition (TEVD), sputtering method, chemical vapor deposition (CVD), pulse laser deposition.(PLD), chemical spray pyrolysis deposition (CSPD)

[9]. In this study TiO_2 films are prepared using low cost techniques which is chemical spray pyrolysis method.

Chemical spray pyrolysis technique is basically a chemical deposition technique in which the fine droplets of the solution containing the desired species are sprayed on a preheated substrate. Thermal decomposition take place on the heat substrate giving continuous rise to the film thickness, the permanent features of this method of deposition are large and deposition with uniformity, low fabrication cost, simplicity, fast, vacuumless, low deposition temperature.

The optical and electrical properties of deposition of thin films are markedly different from these of bulk specimens and are dependent on many parameters such as thickness, film structure, and substrate temperature.

The aim of this research project is Preparing and studying (TiO_2) thin films, for different thickness by chemical spray pyrolysis technique, substrate temperature at (210 °C), and studying the effect of thickness on the optical and properties of (TiO_2) films.

MATERIALS AND METHODS

TiO_2 were prepared by spraying an aqueous solution of titanium chloride $TiCl_3$, which prepared with (0.05 ml/ mol) by dissolving in distilled water (50 ml) of (H_2O) , then the resulting solution was sprayed on clean preheated glass substrate at (210 °C). TiO_2 thin films were formed according to equation:

$$2TiCl_3 + H_2O \longrightarrow Ti(OH)_2Cl_2 + TiCl_4$$

$$Ti(OH)_2Cl_2 \xrightarrow{\phi} \downarrow TiO_2 + \uparrow 2HCl \quad \text{..... (1)}$$

The resulting films were transparent, white yellowish color, stable free from pen holes and have good adhesive properties. They were prepared with different thickness, measured by weight and laser methods. The selected thickness were (100, 200,300,400 and 500 nm). The spectra of x- ray diffraction have been obtained for these films which show that the TiO_2 films were polycrystalline as shown in fig. (1). The results of x- ray diffraction are a good agreement with the ASTM card. The absorptance and transmittance of the prepared films were measured using (UV-1650PC Shimadzu software 1700 1650, UV-Visible recording Spectrophotometer), (Phillips), Japanese company in the wavelength range (300-900 nm).

RESULTS AND DISCUSSION

1)) Absorption coefficient (α):

The absorption coefficient (α) of the prepared thin films was calculated in the fundamental absorption region from the relation **[10]**:

$$\alpha = 2.303 \frac{A}{d} \quad \text{..... (2)}$$

Where A : absorptance of the thin film.
d : thickness of thin film.

Fig. (2) shows the relation of absorption coefficient as a function of incident photon energy for TiO_2 thin films. The figure shows the high variation. Also we can evidently see that TiO_2 thin films have high value of absorption coefficient ($\alpha > 10^5$ cm^{-1}) which leads to increasing the probability of occurrence direct transitions. From the same figure we can notice an increasing in absorption coefficient with increasing of film thickness. This can be linked with the formation stage of anatase and with increase in grain size and density of layers and it may be attributed to the light scattering effect for its high surface roughness.

2)) Refractive index (n):

The refractive index (n) of the prepared thin films was calculated according to the eqn. **[11]**

$$n = \frac{1 + \sqrt{R}}{1 - \sqrt{R}} \quad \text{..... (3)}$$

Where R : reflectance of thin film.

Fig. (3) shows the variation of refractive index (n) with photon energy of the prepared thin films which have values in the range (2.8-3.1) and it increases by increasing the thickness of thin films. The increase may be attributed to higher packing density and the change in crystalline structure, this increase due to the enhancement of growth crystalline **[8].**

3)) Extinction coefficient (K):

Extinction coefficient (K) of the prepared thin films was calculated according to the eqn. **[12]**

$$K = \frac{\alpha \lambda}{4 \pi} \quad \text{..... (4)}$$

Where λ : wavelength of the incident photon.

Fig. (4) shows the variation of extinction coefficient with photon energy, extinction coefficient of prepared films have values in the range (0.353-1.097) and its increases by increasing the thickness of the film, i.e. its behavior was similar to that of absorption coefficient.

4)) Energy gap (E_g):

All electronic transitions for the prepared thin films were studied, the direct allowed energy gap in the fundamental absorption region of TiO_2 thin films was calculated from relation: **[13]**

$$\alpha h\upsilon = B\left(h\upsilon - E_g\right)^r \quad \text{..... (5)}$$

Where $h\upsilon$: photon energy.

E_g : direct allowed energy photon.
B : constant depends on the type of transition.
r: exponential constant, its value depended on type of transition,
r =1/2 for the allowed direct transition.
r =3/2 for the forbidden direct transition.

Fig. (5) shows the relation of $(\alpha h\nu)^2$ against photon energy, from straight line obtained at high photon energy the direct allowed energy gap could be determined which was equal (3.690, 3.675, 3.645, 3.620, 3.605 eV) for the thickness (100,200,300,400 and 500 nm) respectively, and Fig. (6) shows direct forbidden energy gap equal (3.2857, 3.2714, 3.250, 3.2142, 3.1857 eV) for the same thickness. The increase may be attributed to the improvement of crystallinity of anatase phase **[8].** In this research, the direct band gap results are in good agreement with research **[14].**

The following major conclusions be drawn from this work on the thickness dependence of optical properties of prepared TiO_2 thin films:

1. Prepared thin films have high values of absorption coefficient for the wavelength range (300-900 nm). Especially at the high value of photon energy.
2. Absorption and refractive index of TiO_2 thin films increase as film thickness increase.
3. The direct allowed energy gap of TiO_2 thin films was about (3.69-3.605 eV), and for forbidden energy gap was about (3.2857-3.1857 eV).
4. The direct allowed energy gap of TiO_2 thin films was independent on film thickness of the prepared thin films.

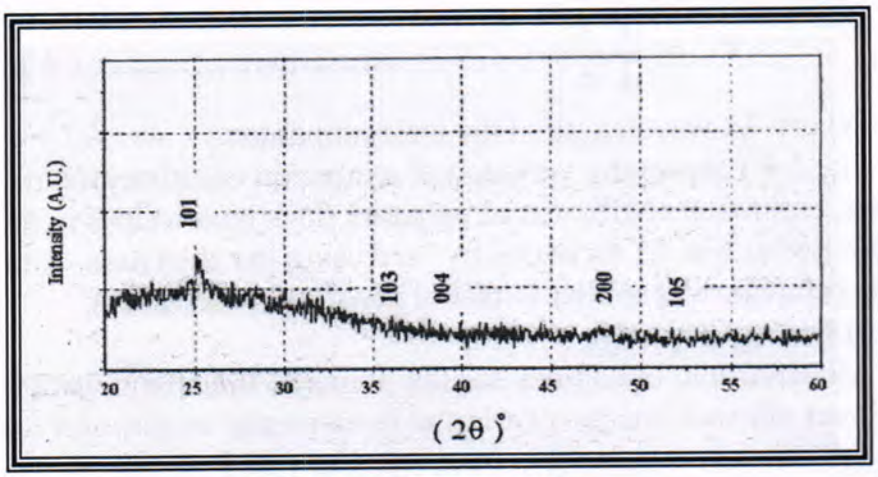

Fig. -1: (XRD) of TiO_2

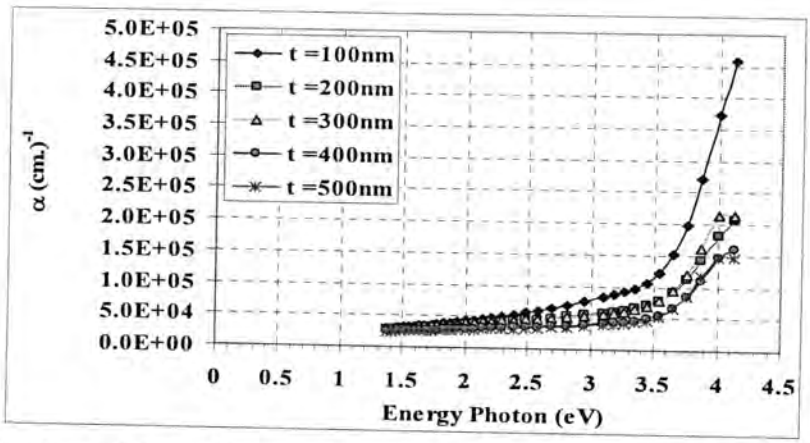

Fig. -2: Absorption coefficient as function of energy photon for different thickness.

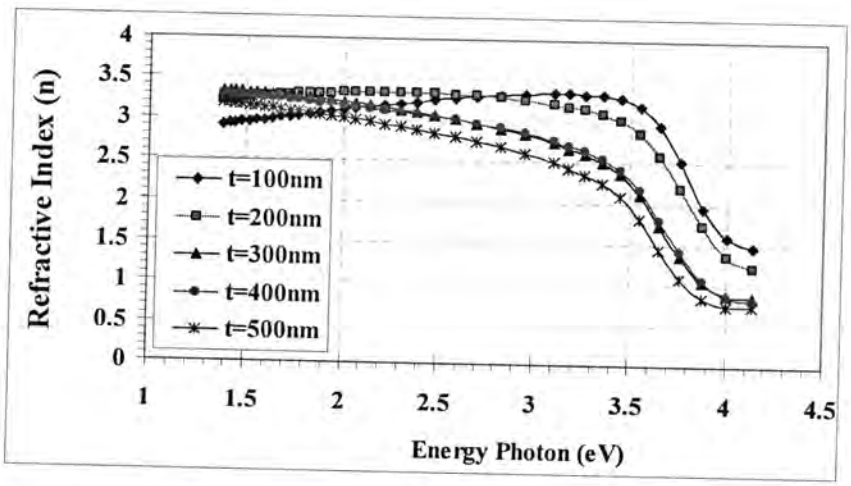

Fig.-3: refractive index as function of energy photon for different thickness.

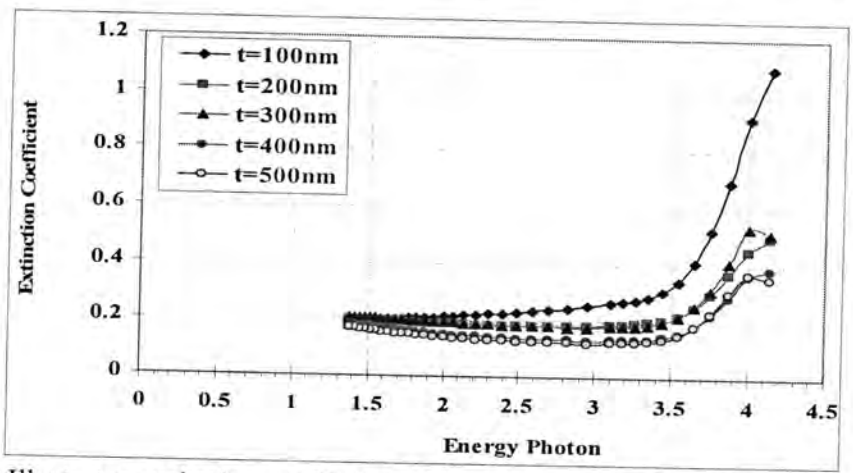

Fig.-4: Illustrates excitation coefficient with energy photon for different thickness.

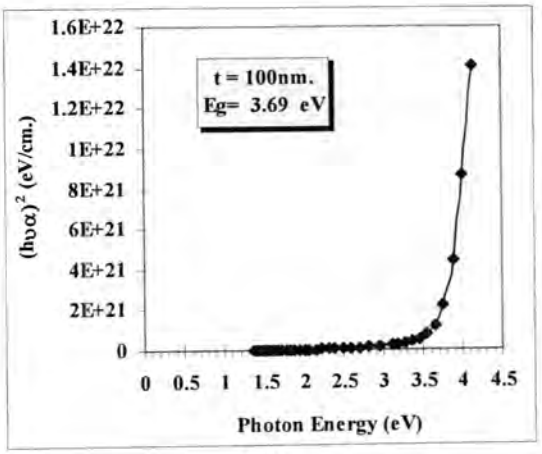

(a)

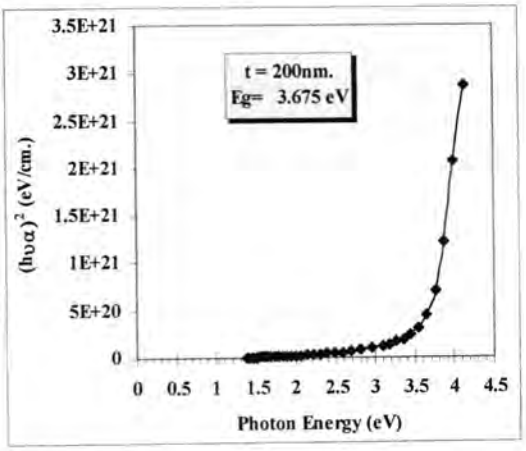

(b)

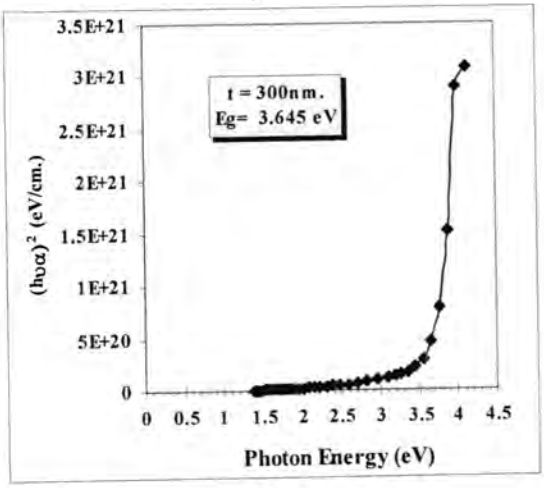

(c)

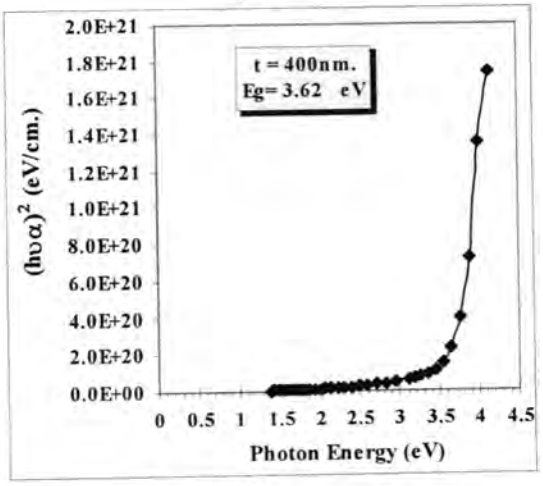

(d)

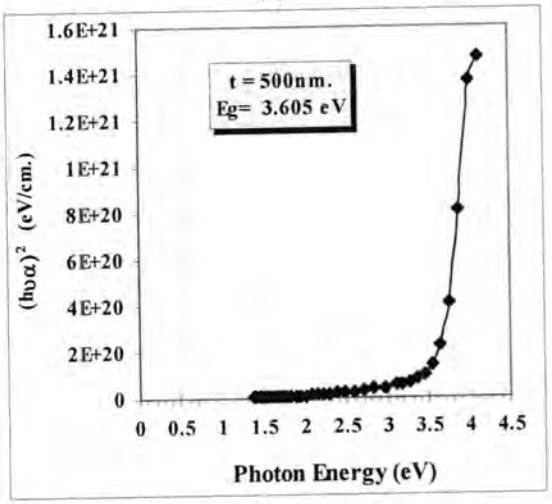

(e)

Fig. -5: Illustrates allowed direct electronic transitions
(a) t=100nm. (b) t=200nm. (c) t=300nm. (d) t=400nm. (e) t=500nm.

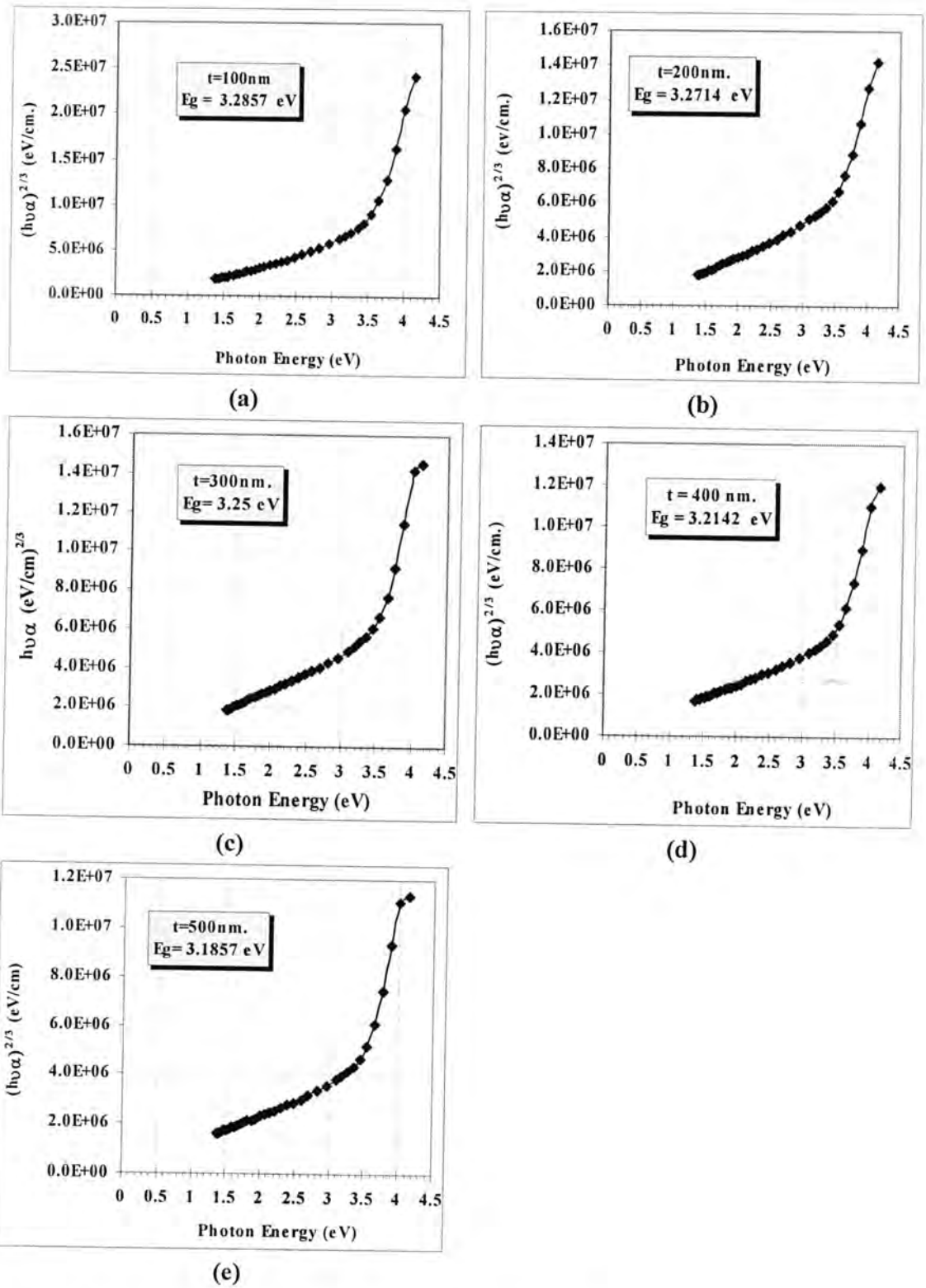

Fig. -6: Illustrates forbidden direct electronic transitions
(a) t=100nm. (b) t=200nm. (c) t=300nm. (d) t=400nm. (e) t=500nm.

REFERENCES

1. Pulker H.K., "coating on glass ", Elsevier, Amsterdam(1990).
2. Sung Y.M., Kim H.J., "sputter deposition and surface treatment of TiO_2 films for dye – sensitized solar cell using reactive RF plasma", "Thin solid films", Vol.515, pp.4996-4999(2007)
3. Yang W., Wolden C.A., "plasma – enhanced chemical vapor deposition of TiO_2 thin films for dielectric applications", "Thin solid films", Vol.515, pp.1708-1713(2006)
4. Euvananont C., Junin C., Inpor K., Limthongkul P., Thanuchayanont C., "TiO_2 optical coating layers for self – cleaning application", " Ceramic International" , Vol.34, pp. 1067-1071(2008)
5. Tavares C.J., Vieria J., Rebouta L., Hungetord G., Countinho P., Teixetriaj V., Carneiro O., Fermandes A.J., "Reactive sputtering deposition of photocatolytic TiO_2 thin films on glass substrate", "Mat. Sci. Eng." B, Vol.138, pp.139-143(2007)
6. Okada M., Tazawa M., Jin P., Yamada Y., Yoshimura K., "Fabrication of photocatolytic heat mirror with TiO_2/TiN/ TiO_2 stacked layers", "Vacuum" , Vol.80, pp.732-735(2006)
7. Ye Q., Liu P.Y., Tang Z.F., Zhai L., " Hydrophilic properties of nano TiO_2 thin films deposited by RF magnetron sputtering", "Vacuum", Vol.81, pp.677-631(2007)
8. Hasan M.M., Hasseeb A.S.M.A., Saidur R., Masjuki H.H., "Effect of annealing treatment on optical properties of anatase TiO_2 thin films" , "International Journal of Chemical and Bimolecular Engineering" , Vol.1, pp.93-97(2008)
9. Chopra K.L., "Thin films phenomena", Mc.Graw-Hill, NewYork (1969).
10. Donald A. N., "Semiconductor Physics and Devices", Irwin, USA(1992).
11. Chopra K.L., "Thin Film Devices Application", Plenum Press,New York (1983).
12. Eckortova L., "Physics of Thin Films ", (plenum press) (1977).
13. Nilens A. G., "deep imparity in semiconductors", Wiley -Interscience publication (1973).
14. R.Mechiakh, R.Bensaha, "Analysis of optical and structural properties of soi-gel TiO2 thin films", M.J.Condensed Mat.",V.7, N.1, pp.54-57(2006).

Enhancement of Rate Deposition and Structural Properties of Cadmium Iodide Deposited in External Magnetic Field

Randa K. Hussain, Ruba T.Salim, and Sahar Abd Alaziz
Physics Dept., College of Sciences, Almustansiriyah University.

Received 22/3/2010 – Accepted 5/10/2010

الخـلاصـة

تم ترسيب أغشية سميكة($1.05x10^{-4}$ to $6.17x10^{-3}$ cm) من يوديد الكادميوم بطريقة الترسيب من المحلول عند درجة حرارة الغرفة. أجريت الدراسة تحت ظروف مختلفة: تركيز المحلول و زمن الترسيب تتراوح بين (0.0085 ، 0.017 ، 0.034 و 0.043 مولاري) و(4.5، 9.25، 18.5 و 23.5 ساعة) على التوالي ومجال مغناطيسي شدتة (1.52، 2.94 و 4.5 ملي تسلا) واتجاهه (عمودي وموازٍ للقاعدة). لقد تمت معاينة معدل الترسيب (السمك) و الخصائص التركيبية بوجود وبغياب المجال المغناطيسي الخارجي ، واظهر معدل الترسيب تحسنا عند تسليط مجال مغناطيسي عمودي. وقد أظهرت طبقات CdI_2 السميكة تراصف جيد باتجاه c-axis عموديا على مستوي القاعدة؛ وتتحسن الخصائص التركيبية عند تسليط مجال مغناطيسي، كما كانت قراءات XRD متفقة مع ASTM . كما اظهرت طبقات CdI_2 سلوك (B-H) لها خصائص بارامغناطيسية ، نفاذيتها المغناطيسية النسبية (1.45233). كذلك وجد ان تسليط مجال مغناطيسي لمدة 3 ساعات لة تاثير افضل من زيادة التركيز الى 6 مرات.

ABSTRACT

Cadmium iodide thick films ($1.05x10^{-4}$ to $6.17x10^{-3}$ cm) were deposited by solution deposition method at room temperature. The investigation were taken at different conditions: CdI_2 concentration (0.0085, 0.017, 0.034, and 0.043 mole/liter), deposition time (4.5, 9.25, 18.5, and 23.5 hours), magnetic field intensity (1.52, 2.94, and 4.5 mT), and its direction (normal and parallel to substrate). The thickness and structural properties were investigated with and without external magnetic field, rate deposition shows enhancement by using normal magnetic field. The CdI_2 thick films show good c-axis alignment normal to substrate plane, and their structural properties were improved by deposition in magnetic field, and XRD data was in agreement with ASTM. Thick layer of CdI_2 shows (B-H) behavior, has paramagnetic properties, and its relative permeability (μ_r =1.45233). It is found that applying magnetic field for 3 hours has better effect than increasing the concentration to 6 times.

INTRODUCTION

Many materials that candidates to be active materials for deposition from solution need to be good solubility, then they need to deposited fast as possible with high rate of deposition. High yielding required that the most or all of materials are soluble, and then the soluble materials separated from solvent and re-building towards substrate. Three choices may be valid to improve yield: increasing concentration, long time of deposition, and use assistant factors like heat and chemical agents. Recently, modified and enhanced to improve the deposition rate of thin solid film was studied, that technique was based on using the external magnetic field of a permanent magnet or electromagnetic coil [1]. The magnetic field profiles, which were produced magnetic field gradient gives different rate of deposition

dependents on these magnetic field profiles. A coil current with 137.7A if a SmCo permanent magnet is the largest, and the highest deposition rate of the hydrogenated amorphous silicon (a-Si:H) film was observed [2].

The influence of an in-situ magnetic field during pulsed laser deposition to prepare epitaxial nickel zinc ferrite thin films was investigated. An air core coil (solenoid coil) was installed between a target and a substrate [3].

In this paper magnetic field play that role to increase rate of deposition (thickness per time) and to accomplish the deposition process faster and little amount of material, by exposing the material during deposition process to external magnetic field. The thickness as a function of time deposition and material concentration will be discussed. As well as the magnetic field effect on structural properties of CdI_2.

MATERIALS AND METHODS

1. Materials: CdI_2 solution was prepared by dissolved of (0.0625-0.3125)gm of CdI_2 in 20 mL water to acquire solution of (0.0085-0.043) molar concentration. Polyvinyl alcohol (PVA) small amount (about 0.5% of the started material weight) was added to the initial solution as binding material; to increase the inter layers adhesion, as well as adhesion to the substrate.

2. Deposition: layer of CdI_2 was deposited from solution at room temperature. Optical glass slid was carefully cleaning, and then putting in piker to be the substrate. The prepared solution is pilled into the piker which is immersed in magnetic field. After material deposition on substrate, the extra solvent is pulled out, then the drying is complete.

3. Thickness measurement: because the layers deposited with high thicknesses, weight method was adopted to measure the layer thickness. Sensitive electrical balance Metler AE-160 was used, with precision reaching 10^{-4} gm. The following mathematical relationship was adopted:

$$thickness = \frac{\Delta m}{\rho_f * A_f} \quad \ldots\ldots\ldots\ldots (1)$$

Δm: represents the deposited thin film weight, which is equal to the difference between weight of the glass slide before and after the deposition process.

ρ_f: the layer density (PVA has no effect on the density of the deposited layer).

A_f : the area of substrate.

4. Magnetic field: external magnetic field of solenoid coil with air gap was used at different intensity (1.52-4.49 mT) in normal and parallel according to substrate as in figure (1-a, and 1-b) . The experimental setup is consisting of the digitally solenoid coil, supplied with ammeter, voltmeter. The uniformity of magnetic field is measured by scaled sensor. The substrate is horizontally sits in the piker that put in middle of the glass cylinder figure (1-c), where the magnetic field is uniform. The piker containing the solution is immersed in magnetic field for the first 3 hours of deposition process where the concentration is higher.

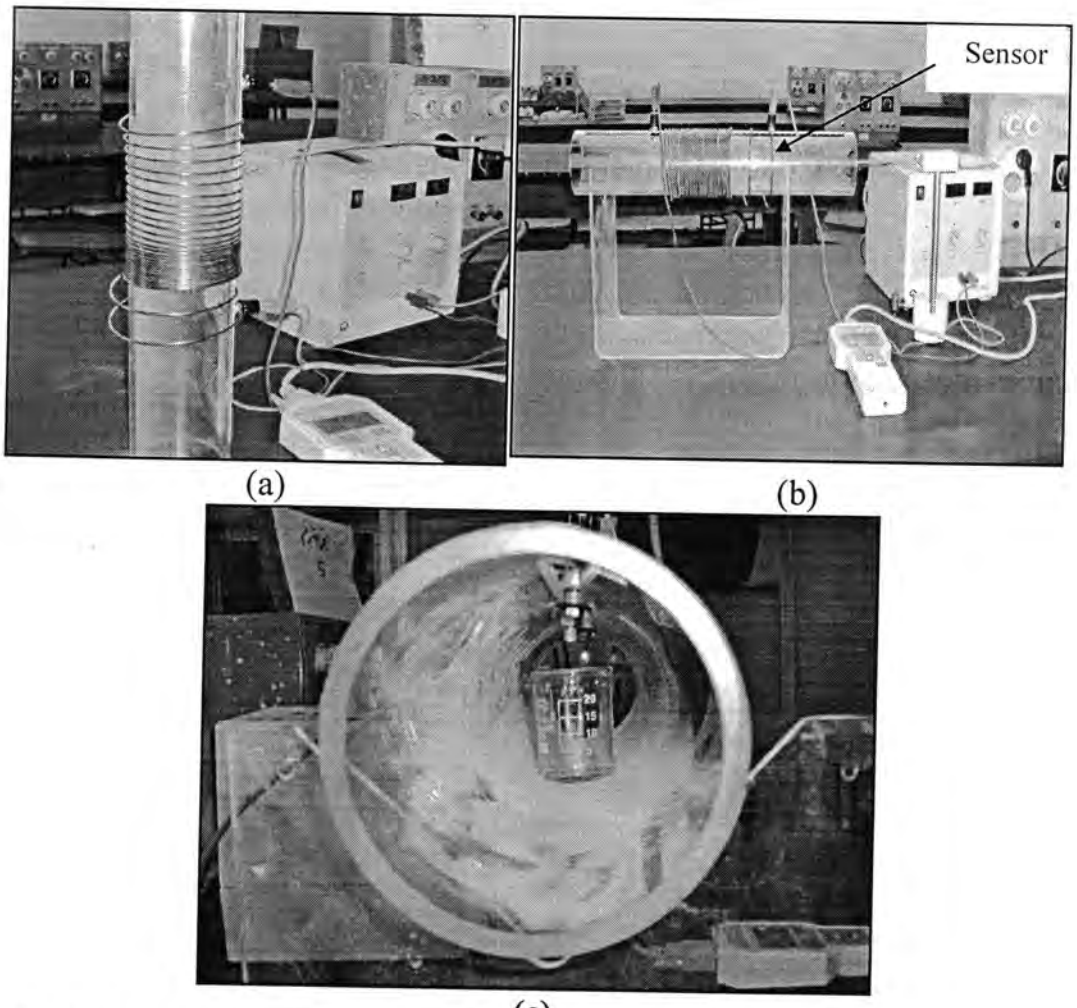

Fig-1: Experimental setup: (a) normal mod, (b) parallel mod, and (c) piker position in cylinder .

5. Characterization and analysis: Layers structural properties were characterized by x-ray diffraction technique, The richly polytypic cadmium iodide exhibits polytypism in almost all forms of crystal growth and habits. Among the polytypes 2H, 4H, 18H & 12R (

hexagonal and rhombohedral structures) the pure CdI_2 crystals have four layered hexagonal structure i.e. 4H-polytype which is the most stable structure of CdI_2, both at room temperature and at higher temperatures [4].

RESULTS AND DISCUSSIONS

1. Concentration Effect:

The material molecules undergo damages in their bonds as a result of polar solvent effect which is water in this case. The broken bonds molecules (ions) were directed down word covered by the gravitation and begin to accumulate on substrate surface to re-building their bonds; where the ions tend to be in the stable state that could be occur if the ions re-building themselves to form molecules. The new forming molecules will accumulate on the substrate surface, and it is strongly dependent on the started material solution (its concentration and its temperature). The accumulated material amount on substrate surface may be expressed as layer thickness, which is become thicker as the solution is more concentrated; figure (2) shows increasing in the thickness with increasing the concentration for samples deposited for 18.5 hours.

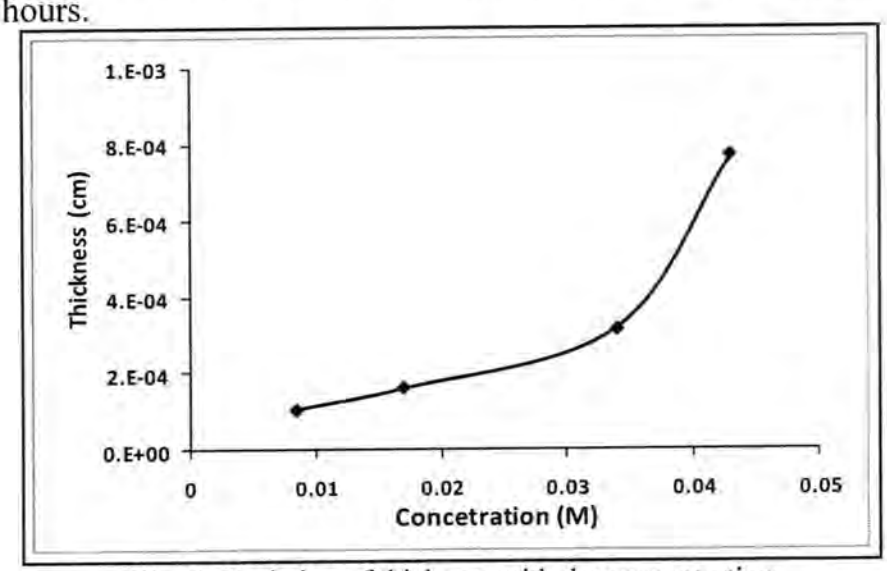

Fig.-2: Variation of thickness with the concentration

2. Time Effect:

More deposition time gives chance to bonds to re-building themselves forming molecules, and hence, the layer will be thicker by give them more time. But this increasing become slowly after 18.5 hours of deposition; the layer is continuous in growth after 18.5 h but in rate much less than before 18.5 h (i.e. there is a deposition process and does not stopped). That variation of increasing in thickness may be attributed to deposit most of material and the little amount is still

suspending in solvents. This behavior makes the longer deposition time is usefulness. Figure (3) illustrates time effect on layer thickness for samples of 0.017 M concentration.

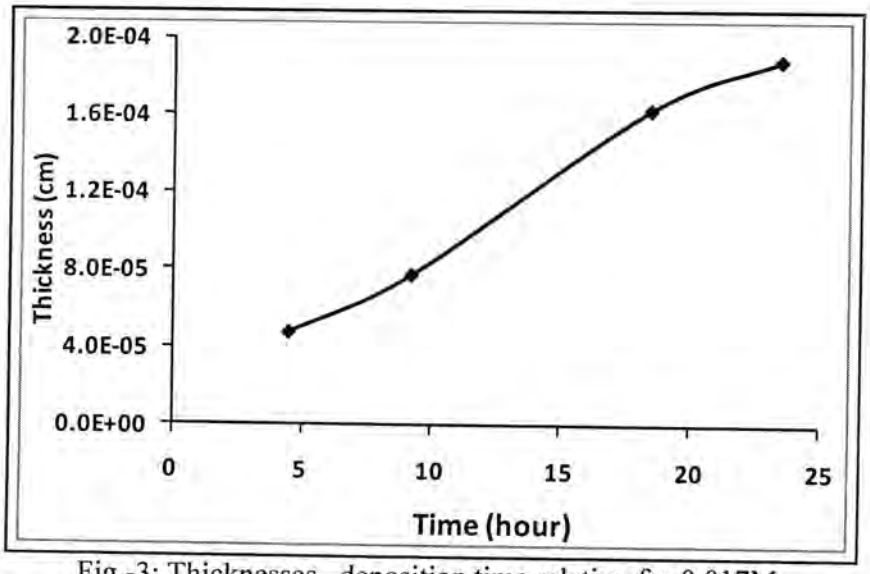

Fig.-3: Thicknesses –deposition time relation for 0.017M.

3. Magnetic Field Effect:

The magnetic field is other parameter that effect on the broken molecules towards its direction (toward substrate). The field makes the molecules flow faster and it is also helps or excites the suspended molecules to direct toward the substrate and then re-building their bond to make thick layer. Figure (4) shows the increasing of layer thickness with magnetic field; parallel and normal to the substrate for (0.017 M) at 3 hours deposition in magnetic field. The normal field seems to be more effective to increase the layer thickness than parallel field, where the increasing in thickness were two orders (from 1.18×10^{-5} cm to 5×10^{-3} cm at 4.49mT) and one order (from 1.18×10^{-5} cm to 7.16×10^{-4} cm at 4.49 mT) for normal and parallel respectively. Figure (5) exhibits increasing in thickness came from exceeding in concentration (0.034 M) comparing with figure (4-(b)) for same time of deposition.

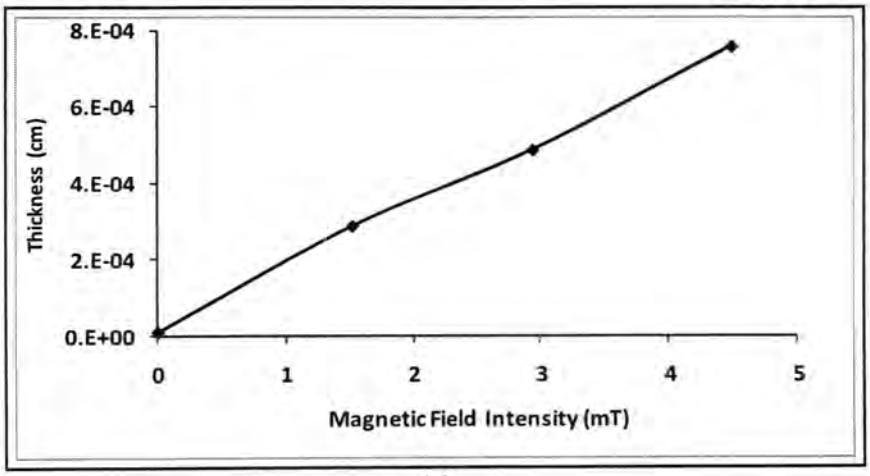

(a)

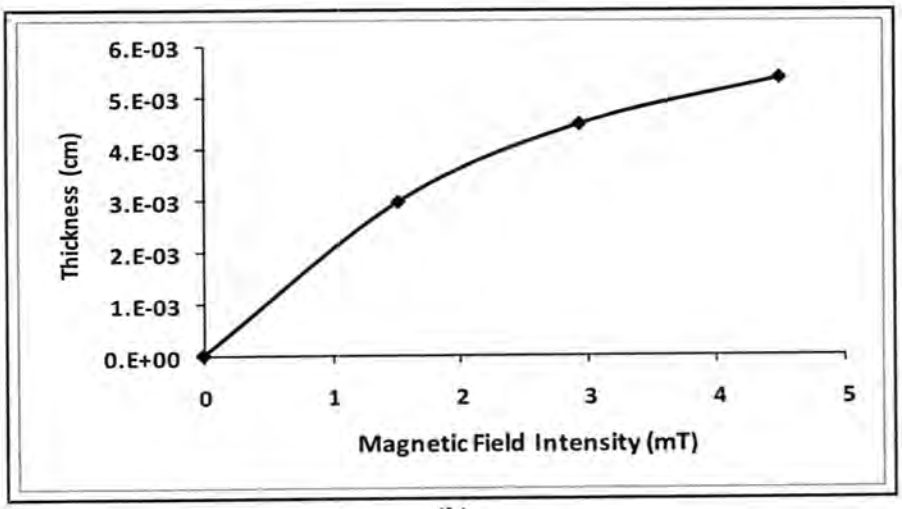

(b)

Fig.-4: Thickness variation with magnetic intensity for, (a): parallel magnetic field, and (b) normal magnetic field for 0.017 M and t=3h.

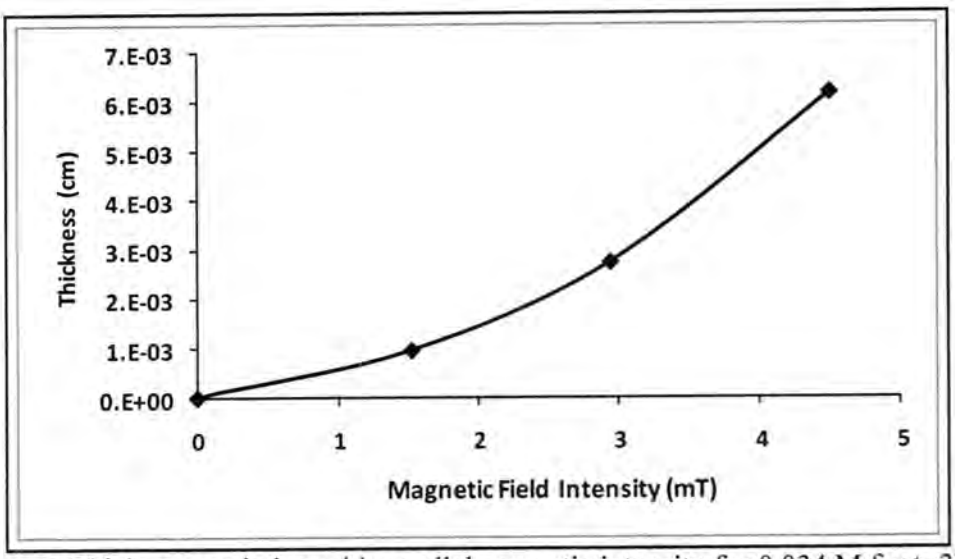

Fig.-5: Thickness variation with parallel magnetic intensity for 0.034 M for t=3h.

4. Rate Deposition: Normal magnetic field for 3hours increased the deposition better than deposition without magnetic field for 18.5 hours. The behaviors of rate deposition (rate of deposition is the thickness produced in a time [5]), were close to be the same, which means that the magnetic field is accelerated the process and keeps its mechanism without serious changing. It may say that figure (6) represent the factor's study; concentration, magnetic field acted in rate deposition as a function of concentration. The rate deposition is generally increased with concentration for all cases, but the magnetic field applied just for 3 hours exhibits high increasing in rate deposition. To compare values for as example: sample of (0.017M) the rate deposition increased from ($8.75x10^{-6}$ cm/h) at B=0 to reach ($1.2x10^{-3}$cm/h) at B=4.49mT in 137 time increasing in 1/6 of time. Influence of a parallel magnetic field on crystal growth was examined in terms of the magnetic susceptibility force, which is caused by the magnetic susceptibility gradient in the vicinity of the crystal surface. crystal grows via two processes, i.e. deposition of solute and attachment of micro-crystals. Magnetic field effects on the crystal growth rate may be explained by the mechanical forces, which influence CdI_2 transportation from the bulk solution to the seed crystal surface. This convection of the solution is caused by the density gradient due to deposition of CdI_2 on the seed crystal surface. In addition, in situ observation of the CdI_2 solution during crystallization reveals that micro-crystals with a few micrometers in length grown in the bulk solution move around and occasionally attach on the seed crystal surface. crystals were oriented in a magnetic field, with their crystallographic c-axis by angle with the field direction. This magnetic orientation of crystals may be explained by their anisotropy of magnetic susceptibility. The growth of crystals along the c-axis was suppressed by the magnetic field. Thus magnetic is suppressed of crystal growth [6].

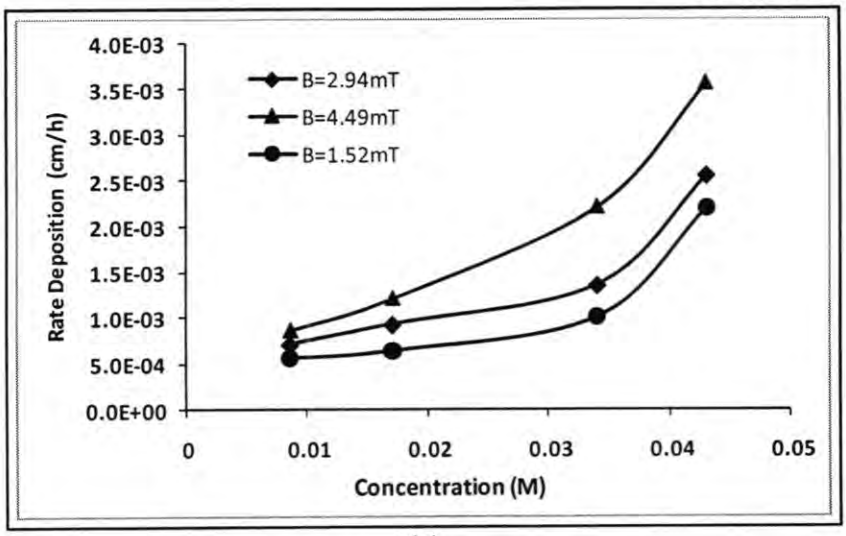

(a)

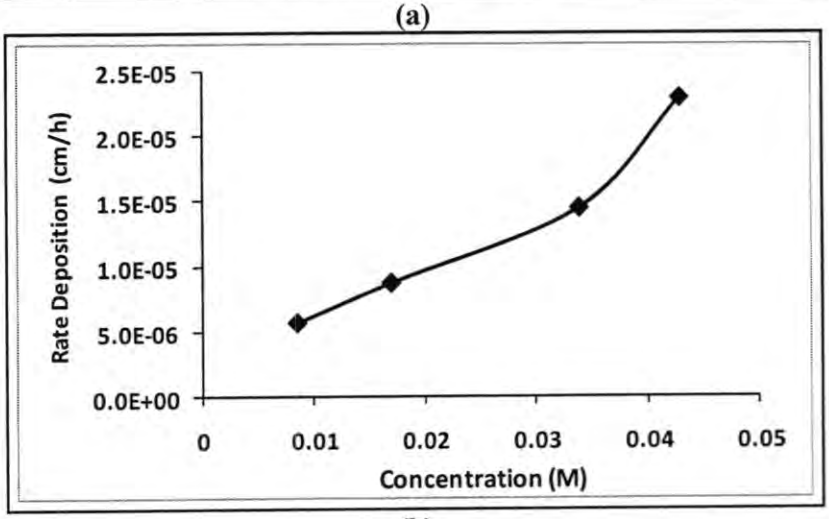

(b)

Fig.-6:Rate deposition as function to concentration in:(a)exist and,(b) absence of B.

5. Structural Properties (X-Ray Diffraction):

Crystals of the common CdI_2 polytype is 4H (hexagonal 4-layered unit cell). According to the known standard crystallographic data for the polytype 4H, the unit cell parameters are $a = b = 0\square428$ nm, $c = 1\square3728$ nm; $a = b = 90°$, $g = 120°$, which confirmed in the STM observations. XRD pattern confirms the polycrystalline hexagonal structure of cadmium iodide, as shown in figure (7), and the data is in agreement with ASTM.

The crystals have three preferred orientations: the main reflection is in the plane (111), (311) (220), as well as the major reflections as (200) and (220). The plans (001) and (101) have small amount of reflections. However, a small amount of non zero reflections were observed, this indicates a slight misalignment among the grains. The intensity in (111) plane is 4 times that in (220) and much higher than (311) plans, this implies that the deposited occur in c-plane more than a-b plane. This

result is in a good agreement with [7]. Table (1) shows the peaks data occurred from XRD analysis for a sample of (0.017M) deposited for 23.5 hours to get ($0.11787x10^{-4}$cm) thickness.

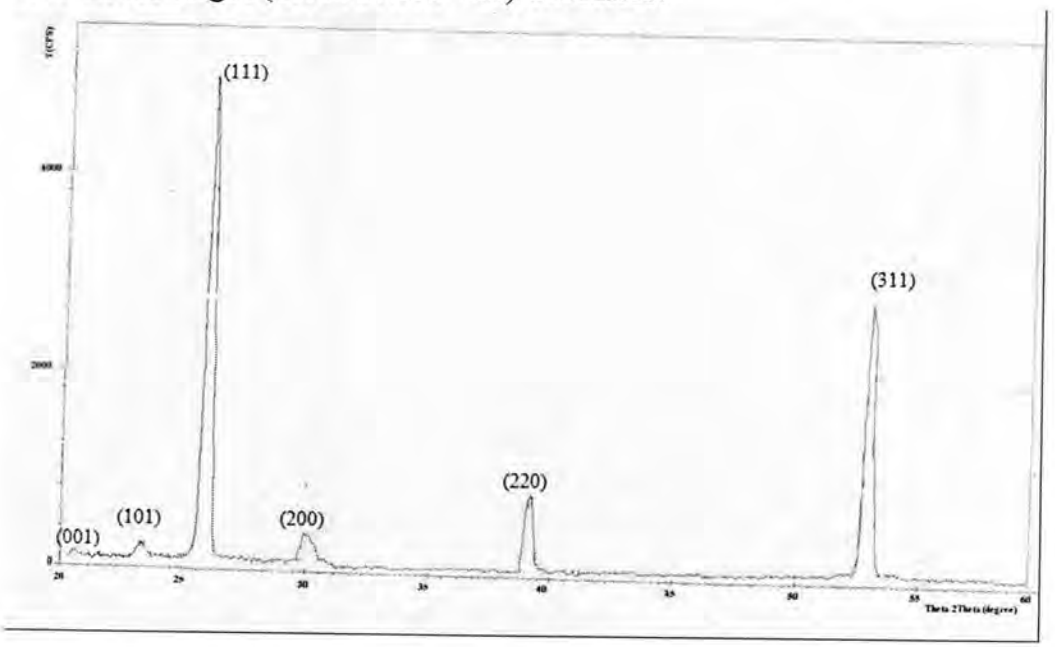

Fig.-7: XRD for (0.017M) at 23.5 hours of deposition sample.

Table-1:: Peaks data for (0.017M) at 23.5 hours of deposition.

Peak No.	2Theat (degree)	d (A)	I/I_0 (%)	FWHM (degree)
1	23.2822	3.81751	3	0.40170
2	25.9058	3.43654	100	0.36100
3	30.1166	2.96495	4	0.39690
4	39.3050	2.29041	17	0.35630
5	53.2990	1.71738	60	0.37530

The FWHM of sample (0.017M) was 0.36100°, while the FWHM of the same concentration sample deposited in magnetic field was 0.1459°. This indicates that application of magnetic field has strong effect on the crystal structure of CdI_2, companied with increasing in the grain size.

The deposition in exist of magnetic field make the material more ordered and alignment, the pattern peaks higher intensities with about 2.5 times, and missing more of small peaks as it indicate to high orientation, as shown in figure (8). Table (2) summarized the data list of the sample deposited in (4.49 mT). The XRD analysis shows a high degree of orientation with the plane parallel to substrate and *c*-axis normal to substrate plane as indicated by the total absence of (001), and (101) reflections and transform (200) to very small peak.

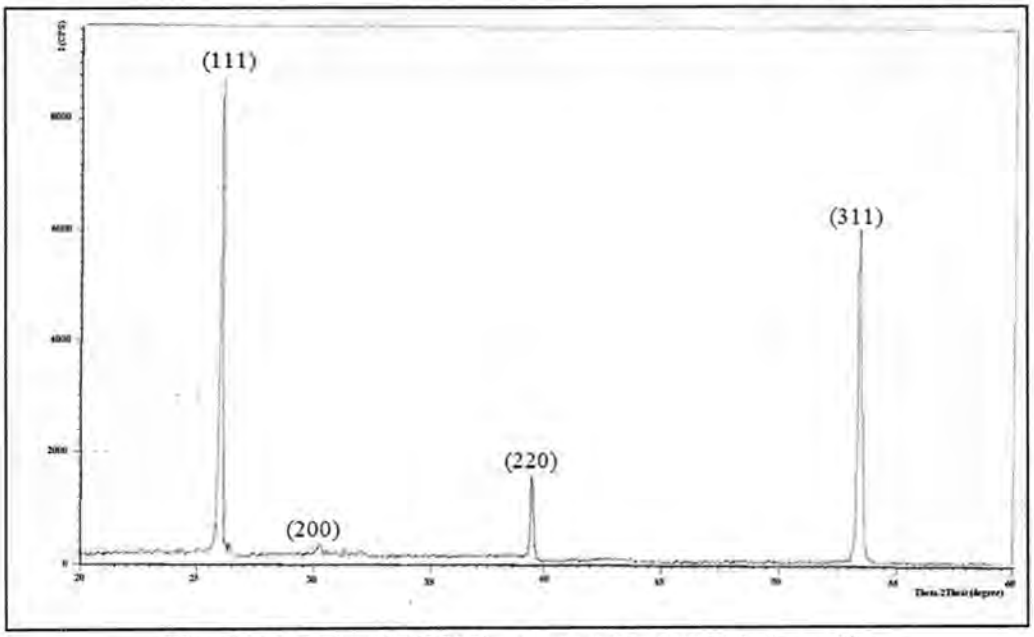

Fig.-8: XRD for (0.017M), parallel B=4.49mT, time=3hours

Table -2: Peak data list of (0.017M), parallel B=4.49mT, time=3hours.

Peak No.	2Theat (degree)	d (A)	I/I_0 (%)	FWHM (degree)
1	25.9948	3.42497	100	0.1459
2	39.4034	2.28492	20	0.1488
3	53.4175	1.71385	89	0.1516
4	53.6857	1.70592	4	0.1075

6. Magnetically

Magnetic field has a function of the magnetic susceptibility in hexagonal crystal material, which own anisotropy for the susceptibility. anisotropic susceptibility make the susceptibility along c-axis is differs from that towards a- and b-axis, that means it is in direction of c-plane (z-axis in Cartesian coordinate) is much more than in a-, and b-plane (x-y plane). The magnetization of material excites the crystal to growth vertically, where the preferred orientation direction.

CdI_2 has hexagonal structure and anisotropy of magnetic susceptibility, and the deposited grains can be oriented.

In hexagonal crystals, generally, crystallization process under magnetic field, crystals can align toward the specific direction where the magnetization energy becomes minimum (Magnetization energy is proportional to square of magnetic field, and the coefficient includes the magnetic susceptibility).

Relative magnetic permeability (μ_r) of CdI_2 is evaluated from the slope of magnetic field – magnetic flux (B-H) curve, taken into account the space permeability ($\mu_o = 4\pi \times 10^{-7} H/m$), figure (9) shows

(B-H) behavior of CdI_2 layer. Thick layer of CdI_2 has relative permeability larger than unity in small a mount (μ_r=1.45233), that means the material acquired paramagnetic properties [8] via deposition in magnetic field.

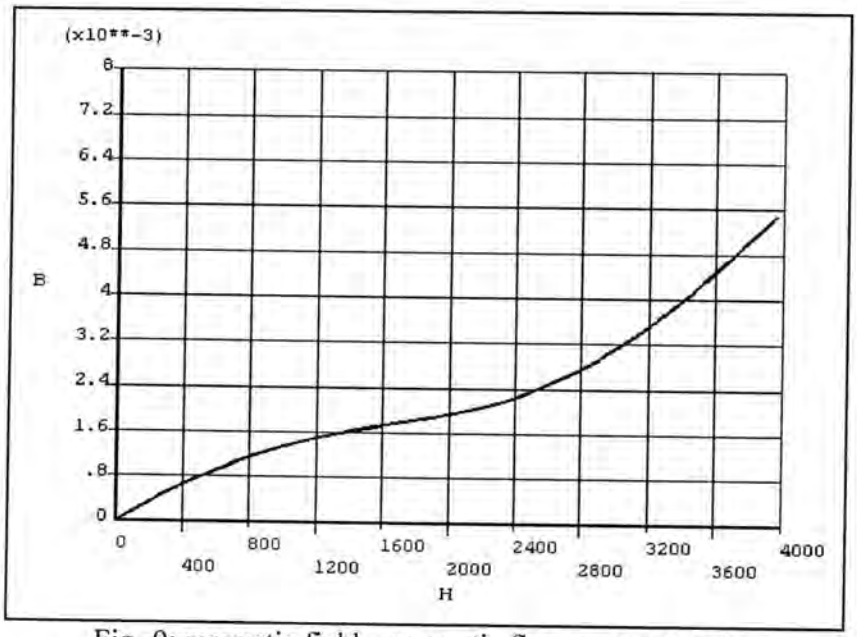

Fig.-9: magnetic field – magnetic flux curve property.

Conclusions

The cadmium iodide concentration has good effect on thickness, in other hand, the long time deposition was not high effect on thickness. Applying external magnetic field excited to build the thick layer, especially in the normal mod. The rate deposition was highly increasing because of magnetic field.

The cadmium iodide thick films show good *c*-axis alignment normal to substrate plane and a slight misalignment sets in is overcome by applying magnetic field as observed by XRD analysis. Thick layer of CdI_2 shows paramagnetic properties.

REFERENCES

1. H. Takikawa, M.Nagayama, R. Miyano, and T. Sakakibara,"Enhancement of shielded cathodic arc deposition', Surface and Coatings Technology, 169 –170, 49–52, (2003).
2. H. Yuehui, C. Guanghua, Z. Xiuhong, R. Yandong, G. Zhuo, L. Ying, and Z. Huaien, ", Growth rate of a-Si:H film influenced by magnetic field gradient in MWECR CVD plasma system", Vacuum Electron Sources Conference, 2004. Proceedings. IVESC 2004. The 5th International Volume , Issue 6-10 268 – 270, (2004).

3. N. Wakiya, T. Nagamune, K. Shinozaki and N. Mizutani ,"In-Situ Magnetic Field Induced Structure and Properties of Epitaxial Spinel Ferrite Thin Films Prepared by Pulsed Laser Deposition (PLD) (Dynamic Aurora PLD Method)" Mater. Res. Soc. Symp. Proc. Vol. 853E, (2005).
4. T. Kozuka, K. Shimomai, T. Kenjo, and M. Kawahara, "Effect of Intense Magnetic Field on Electro-deposited Thin Film of CdTe", International Scientific Colloquium Modelling for Electromagnetic Processing Hannover, October 27-29, (2008).
5. A. Walthera, K. Khlopkovc, O. Gutfleischc, D. Givorda and N. Dempseya," Structural, magnetic and mechanical properties of 5 μm thick SmCo films for use in Micro-Electro-Mechanical-Systems", Journal of Applied Physics 103, 043911, (2008).
6. M. Sueda, A. Katsuki, Y. Fujiwara, Y. Tanimoto, " Influences of high magnetic field on glycine crystal growth", Science and Technology of Advanced Materials, 7, 380–384, (2006).
7. H. Khallaf, I. Oladeji, G. Chai, and L. Chow," Characterization of CdS thin films grown by chemical bath deposition using four different cadmium sources", Thin Solid Films, 516, 7306–7312, (2008).
8. B. Culty, "Introduction To Magnetic Materials", Addison-Weley, USA, (1978).

Calculation the Heating Parameters for Entry Space Vehicle in Multiple Entry Angles

Waleed I. yaseen
Department of Astronomy, College of Science, University of Baghdad
Baghdad-Iraq

Received 31/5/2009 – Accepted 20/6/2010

الخلاصة

عند دخول المركبات الفضائية(المكوك الفضائي والصواريخ البالستية والاقمار الاصطناعية) الى الغلاف الغازي الارضي ستتعرض الى عدة قوى نتيجة اصطدامها بهذا الغلاف تسمى القوى الايروديناميكية، ومن اهم هذه القوى هي قوة الاعاقة التي تعتمد بصورة كبيرة على السرعة وكثافة الهواء، وتقوم هذه القوة بتقليل سرعة المركبة بشكل كبير وكنتيجة لهذا ستتحول الطاقة الحركية للمركبة الى طاقة حرارية. تم في هذا البحث بحساب عناصر الطاقة الحرارية عند تغيير زاوية الدخول ودراسة تاثير هذه الزاوية على تلك العناصر. وتم ايضا حساب هذه العناصر مع تغيرات سرعة المركبة وارتفاعها. ان حساب هذه العناصر مهمة جدا خلال عملية الرجوع للمركبات ومنها يمكن تحديد ارتفاع المنطقة التي يحدث فيها اعظم قيمة لمعدل الحرارة، وكذلك معرفة تاثير زاوية الدخول على ارتفاع هذه المنطقة ومن خلالها معرفة الزاوية المناسبة للدخول. ومن تلك الدراسة نلاحظ عندما تكون زوايا الدخول صغيرة بحدود 5 deg فان حمل الحرارة الكلية على المركبة ينخفض كثيرا وكذلك فان سرعة الدخول تقل الى 37km/sec اما معدل الحرارة عند هذه الزاوية فيبقى نفسه عند الزوايا الاخرى بحدود 1. اذن زوايا الدخول الواطئه تكون جيده عند الدخول ولكنها تزيد من زمن الطيران وهذا غير مفيد لمركبات الدخول لذلك يجب تقليل الزمن بزيادة قليلة لزاوية الدخول حوالي 20 deg لتكون مناسبة للحرارة وسرعة الدخول وكذلك لزمن الطيران. اما عند الزوايا العالية 90 deg فان سرعة الدخول والحرارة تكون عالية جدا وخطرة بالرغم من ان زمن الطيران يكون قليل.

ABSTRACT

When the space vehicles (space shuttle, missile, and satellite) are entered into the earth's atmosphere, there are many forces acting on it, called aerodynamic forces. The drag force is important and which so much depended upon the velocity and air density. This force rabidly reduces vehicle velocity. As result for this, the kinetic energy of the vehicle is converted into heating energy. In this paper the heating parameters by various entry angles are calculate, and the effects this angle upon these parameters are studying. The heating parameters with various velocity and altitude are calculated. The calculations of these parameters is very important through entry and reentry operation for the vehicles, and from this we can select the region altitude which the maximum heating rate is occur in it. All one knowing the entry angle affects on altitude this region and from through it we can know the suitable angle for entry. From this study we noted, on smaller entry angle 5 deg the total heat load is more decrease, also the entry velocity decrease into 37 km/sec, while the heat rate in this angle is remain on this value 1 for other angle. Therefore lower entry angle is good through entry, but these lower angles are cause increase in flight time. This feature is not useful for entry vehicle, therefore must reduce of flight time by increase for entry angle into 20 deg for it be suitable for heating, entry velocity and flight time. While on high entry angle 90 deg the entry velocity and heating may reach to very high values and become very danger on vehicle although the flight time is very few.

INTRODUCTION

Before the vehicle approach the atmosphere of the earth it's coming from the space with a large amount of kinetic energy due to high speed as well as maximum potential energy due to its position above the earth. When the vehicle is impact in atmosphere the shock wave will generated ahead of the nose of the vehicle due to aerodynamic force and heating atmosphere to have very high temperature. As the vehicle plunges into a deeper and denser atmosphere it will increasingly be heated by this enveloping layer of incandescent atmosphere, while the speed of vehicle will continuously be reduced by the braking force of the atmosphere. By this manner, that the vehicle's kinetic energy is converted into heat. If the entire vehicle's energy were converted into heat energy within the vehicle itself it would be more than enough to vaporize the vehicle and any cooling system it could carry [1]. The survival of meteorites is physical evidence that not all of the energy appears within the body itself. Reality a large part of the total energy is diverted away from the vehicle. This energy conversion fraction depends on vehicle's shape, mass, velocity and altitude. At very high altitudes in the free-molecule flow region where the heat energy is developed directly at the vehicle's surface as much as one-half the vehicle's lost energy can appear as heat in the body. At lower altitudes in the continuum-flow region thermal energy appears in the gas between the shock wave and the body, heat is transferred from this hot gas to the body by conduction and convection. Radiation from the hot gas may also contribute appreciably to the surface heating for very blunt bodies and for velocities some what greater than satellite velocity [2]. As well as the heat generation also depends on entry type and entry angle. The heating experienced by a vehicle during entry is composed of both radiation and convection. Radiative heating is due to thermal excitation of the air particles passing through the shock wave in front of the vehicle, while convective heating is caused by friction as the gas in the shock layer passes over the vehicle [3].

The aerodynamic heating parameters studied excellently by Allen and Eggers [1]. By using Allen and Egger's analysis we may summarize their generalized treatment as follows:

Three aspects of the aerodynamic heating are important namely:

1- The total heat input.
2- The time rate and maximum time rate of average heat input per unit area.
3- The time rate and time rate of local stagnation region heat input per unit area.

In the present work we will study the heating effect for atmospheric of the earth upon the entry vehicles, and calculate heating parameters for

this vehicles at various entry angle and calculate the variation for this parameters with velocity and altitude.

Aerodynamic forces

The aerodynamic force is as the force on a vehicle caused by that part of the pressure distribution which is due to motion. Thus gravity does not enter into the specification of this force. The aerodynamic force can be resolved into two component forces; one at right angle to V and other opposite to V. the lift force L and drag force D can be define as:

$$L = \frac{1}{2} C_L \rho V^2 A \qquad D = \frac{1}{2} C_D \rho V^2 A$$

Where C_L and C_D are called respectively the coefficient lift and coefficient drag. V velocity of the vehicle and A is the vehicle cross section area [4].

Types of entry

The heat transfer and heat conversion depend on the entry types of the vehicle. Considering a vehicle, coming from low earth orbit, which encounters the upper layer of the Earth atmosphere, three types of entry paths are possible:

Ballistic entry

The vehicle has little or no aerodynamic lift and has high entry angle (45^o-90^o). It falls through the atmosphere under the influence of gravity and drag impacting the surface on a point depending only from conditions at the entry interface. This is the case of capsules as the Mercury [5].

Skip entry

The vehicle has median entry angle (45^o) and has a certain lift to drag ratio (L/D) and uses the lifting ability to first graze the atmosphere, then slow a bit, then pitch up such that the lift carries it back out of the atmosphere. This is repeated several times until the vehicle is slowed down appropriately and penetrates the atmosphere and landing. Entry mode has been used partially by the Apollo capsules [5].

Glide entry

The vehicle is essentially an airplane, generating a large L/D ratio. The vehicle enters the atmosphere at very small entry angle (0.5^o-10^o), flies to the surface, and land on a runway. This entry mode has been used partially by the space shuttle.

The choice of any entry strategies implies the choice of a type of vehicle configuration that can be characterized by two entry performance parameters: the lift to drag ratio (L/D) and the ballistic coefficient,

mg/CDS [5]. This parameter, is dimensional and is measure of the relative effect of the inertial force mg to the aerodynamic retarding force or drag CDS, where CD is the drag coefficient and S is the reference area. In this paper the reference area S will always be the maximum cross-sectional area. In the English system ballistic coefficient has the units of Ib/ft^2, while in the metric system it has the units of N/m^2 [6].

By means of these two parameters it is possible to compare the vehicles performances even though the vehicles have dramatically different masses, references area and aerodynamic characteristics [5].

Equation of motion

Only a fraction of the total kinetic energy need be transferred to the vehicle as heat. The approximate amount can be determined from the following analysis. The motion of vehicle is analytical by use the coordinate system shown in Fig. 1. The figure shows the forces acting on the vehicle, where D is the drag force; L is the lift force, mg gravity force and other force. The equation of motion simplified to consider only the most important term the drag is [7]:

$$m\frac{dV}{dt} = -\frac{1}{2}C_D\rho V^2 A \tag{1}$$

Where m is vehicle mass, V speed, t time, ρ air density, C_D drag coefficient based on A and A is the reference area [7].

The heating equation is:

$$\frac{dH}{dt} = \frac{1}{2}C_H\rho V^3 A \tag{2}$$

Where H is the heat input and C_H is the heat transfer coefficient. From these two equations one can readily show that the total heat input for the entire braking process is then [7]:

$$H = \frac{C_H}{C_D}\left(\frac{1}{2}mV_E^2\right) \tag{3}$$

It is clear the fraction of heat given to the vehicle is just determined by the ratio of the heat transfer coefficient to the drag coefficient [8].

The estimation of the velocity variation with altitude during atmosphere is given by:

$$V = Vo\, e^{-\frac{C_D A}{m\sin\theta}\frac{\rho_o}{2b}\sigma} \tag{4}$$

Where σ is density ratio:

$$\sigma = \frac{\rho}{\rho_o} = e^{-hb}$$

h and b is altitude and exponential coefficient in the density approximation respectively [8].

The laminar heat transfer rate per unit frontal can be approximated [2]:

$$\frac{q}{A}=\frac{3}{2}\frac{\rho_o V_o^3}{\sqrt{(\frac{R_{ed}}{M_d})d}}\sqrt{\sigma}(\frac{V}{V_o})^3 \tag{5}$$

Where d is the body diameter or thickness and (R_{ed}/M_d) is the Reynolds number per unit length per Mach number at sea level and is equal to about $7.0\text{x}10^8$ for the earth's atmosphere, and ρ_o is air density at sea level. The turbulent heating rates are roughly an order of magnitude larger than the corresponding laminar values and vary somewhat differently according to body size, gas, density and velocity. And can be computed as [2]:

$$\frac{q}{A}=\frac{\rho^{0.8}V^3}{d^{0.2}} \tag{6}$$

The relation for the heating rate as a function of velocity and altitude Eq.(5) may be used to estimate the variation of heating rate during descent, the maximum heating rate and the total heat load. For example Eq.(4)and Eq.(5) Indicate that for a relatively steep entry of nonlifting body, the maximum heating rate is [2]:

$$\left(\frac{q}{A}\right)_{\max}=\frac{0.371\rho_o V_o^3\sqrt{\sin\theta}}{\sqrt{(\frac{R_{ed}}{M_d})d}\sqrt{\frac{C_D A}{m}\frac{\rho_o}{2b}}} \tag{7}$$

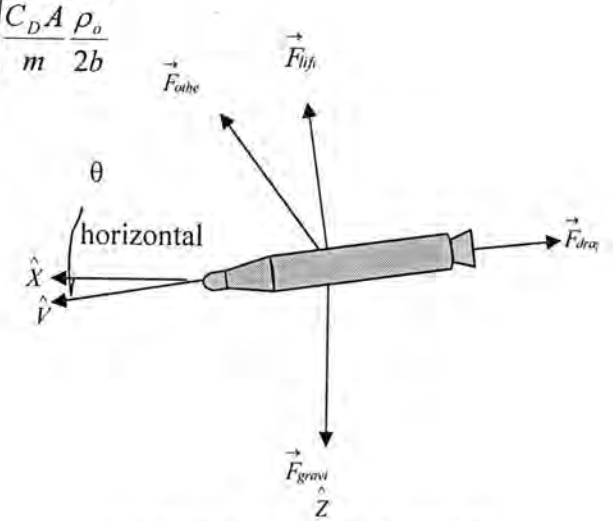

Fig.-1: the coordinate system for entry vehicle.

And the heating rate at any time in ratio to its maximum value is [2]:

$$\frac{q}{q_{\max}}=4.05\sqrt{\frac{\rho_o}{2b}\sigma\frac{C_D A}{m\sin\theta}}\exp\left[-3\frac{\rho_o}{2b}\sigma\frac{C_D A}{m\sin\theta}\right] \tag{8}$$

The total heat load obtained by integrating the heating rate over the time of heating is [2]:

$$\frac{q}{A} = 3\sqrt{\frac{\pi}{2}} V_o^3 \frac{\sqrt{\frac{\rho_o}{2b}}}{\sqrt{(\frac{R_{ed}}{M_d})d}\sqrt{\frac{C_D A}{m}\sin\theta}} \tag{9}$$

RESULT AND DESICCATION

The laminar boundary-layer condition is occur at high altitudes because of the atmosphere density is very low and the velocity is very large. But in lower altitudes where the density is very high and the velocity is very little. The turbulent boundary-layer condition is occurring. Also the heat-transfer rate per unit frontal is high at turbulent boundary-layer condition but it is very low in the laminar boundary-layer condition these because of the laminar and turbulent are depended on body size, gas density and velocity. As shown in Fig. 2.

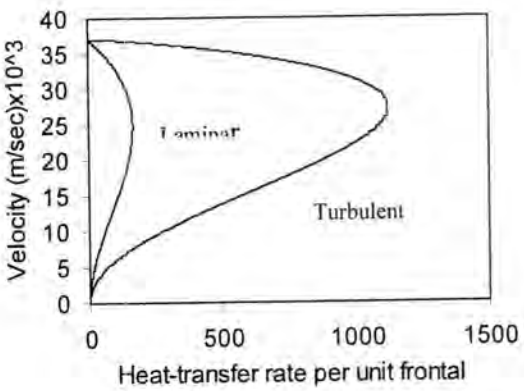

Fig.- 2: Variation of heat-transfer rate per unit frontal with velocity.

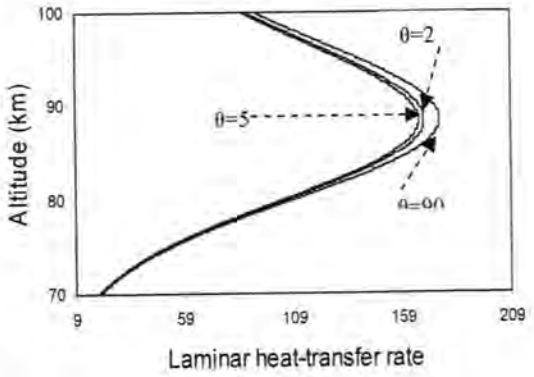

Fig.- 3: Variation of laminar heat-transfer rate per unit frontal with altitude for various entry angles.

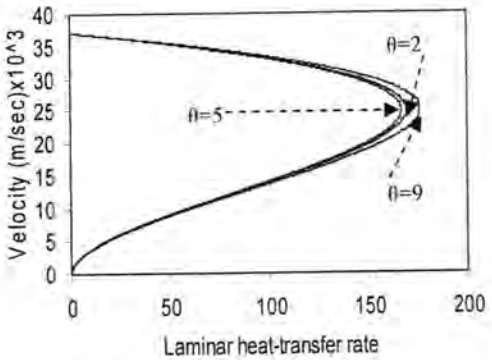

Fig. 4: Variation of laminar heat-transfer rate per unit frontal with velocity for various entry angles.

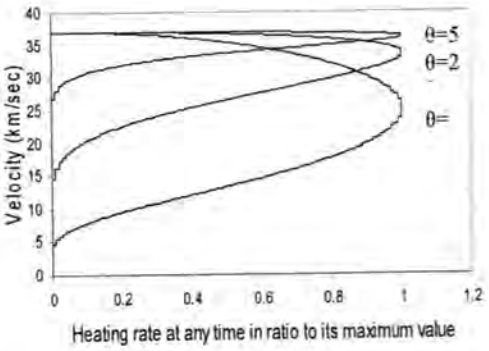

Fig. 5: Variation of heating rate at any time with velocity for various entry angles.

The behavior of laminar heat transfer rate per unit frontal with altitude is similar for many entry angles, with displacement to high heat transfer region for increases entry angle. Shown in Fig. 3.

The variation of laminar heat-transfer rate per unit frontal with velocity is illustrated in Fig.4. The laminar heat transfer rate per unit frontal is increases when the vehicle is start entry from high altitude where it has very large kinetic energy and gas density is very low in this region.

The laminar heat transfer is increases until the region, which decreasing velocity become grater than increasing density. The maximum laminar heat-transfer is occurring in this region.

The maximum heating rate at any time dependent on entry angles, where the maximum heating rate is displace to low velocity region when entry angle is increase. The flight time is dependent on the entry angle where, in case increasing of entry angle the flight time is decreases, this is illustrated in Fig. 5 and Fig. 6.

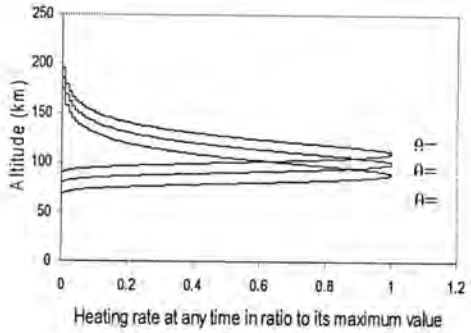

Fig. 6: Variation of heating rate at any time with altitude for various entry

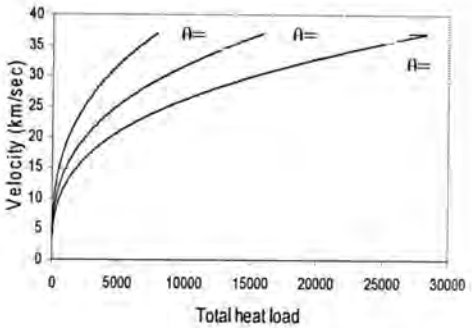

Fig. 7: variation of total heat load with velocity for various entry

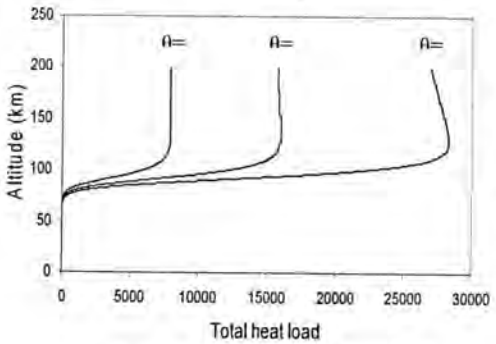

Fig. 8: variation of total heat load with altitude for various entry angles

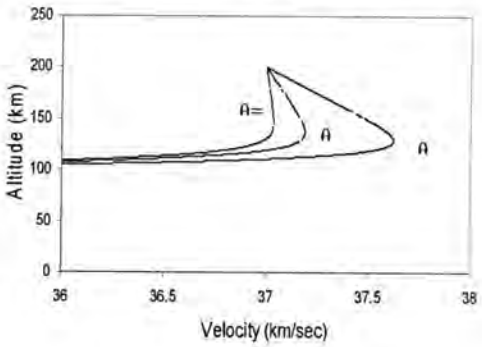

Fig. 9: Variation of velocity with altitude for various entry angles.

The total heat load is exponential decreases when velocity of vehicle is decreases. Also when the entry angle is grater than 45° the maximum total heat load is very large, but when it is lower than 45° the maximum total heat load is very low. These results appear when the velocity effect is grater than density effect.

While the variation of total heat load with altitude in the beginning is constant in maximum value after that, the total heat load at 100 km is began speedily decreases.

The entry angle is effect on the maximum total heat load where at large entry angle the maximum total heat load is displace to large values. These results illustrate in Fig. 7 and Fig. 8. The velocity of vehicle is decreases with altitude because of drag force which acting on the vehicle in inverse direction for velocity, shown Fig. 9. From these results the choosing entry angle is dependent on type mission and type vehicle. The Mercury capsule is designer for glide entry at low entry angle.

REFERENCES

1. Loh, W., Reentry and Planetary Entry Physics and Technology, Springer-Verlag New York, vol. 1, pp. 1-4, (1968).
2. Carl, G., Atmospheric Entry, Rand Corp, 10-20, (1958).
3. Loh, W., Reentry and Planetary Entry Physics and Technology, Springer-Verlag New York, vol. 3, 99, (1968).
4. Milne, L., Theoretical Aerodynamic, Dover Publications, Inc, New York, 2-17, (1973).
5. Mario, S., *A Study of A High Lift Wing-Body Configuration for Low Earth Orbit Re-Entry*, Universita Degli Studi Di Napoli, 19-21, (2006).
6. Frank, J., *Re-Entry Vehicle Dynamics*, American Institute of Aeronautics and Astronautics.Inc., 100,(1984).
7. Adimurthy, V., Re-Entry Trajectory Optimization for an Airbreathing Reusable Launch Vehicle, Aerospace Engineering Divisional Journal., vol. 85, 38,(2004).
8. Julian, H., Some Problems of Planetary Atmosphere Entry, Ames Research Center,NASA,California,813-815,(1967).

Temperature Rise Computation in the Human Head Exposed to Different Mobile Phone Models

Salah I. Al-Mously[1] and Rafa'a I. Yahya[2]
[1]Department of Electrical and Computer Engineering, Academy of Graduate Studies, Tripoli, Libya.
[2]Department of Computer Sciences, College of Sciences, Al-Mustansiriyah University

Received 14/4/2010 – Accepted 5/10/2010

الخلاصة

في هذا البحث تم حساب إرتفاع درجة حرارة رأس مستخدم الهاتف المحمول ولنماذج مختلفة حيث تم حل معادلة الحرارة الحيوية (Pennes Bioheat Equation) بأستخدام طريقة البعد المحدود – نطاق الزمن الأمتثالية (Conformal FDTD) وبمعاونة الحقيبة الحاسوبية (SEMCAD X).
وأثناء عملية المحاكات بأستخدام طريقة (FDTD) الرياضية تم حساب إرتفاع درجة الحرارة برأس مستخدم الهاتف المحمول بأستخدام نموذج رأس غير متجانس مصوّر بالرنين المغناطيسي يمثّل مكونات رأس أمرأة ذات (25) غشاء (HR-EFH). وقد عُملت تصاميم قريبة من الواقع وبمعاونة الحاسوب لأربعة أنواع مختلفة من الهواتف المحمولة - نوع السبيكة ذو هوائي خارجي ونوع السبيكة ذو هوائي داخلي ونوع الصدفة ذو هوائي خارجي ونوع الصدفة ذو هوائي داخلي - وإشراكها أثناء محاكاة عملية تفاعل الموجات الكهرومغناطيسية بين الهاتف المحمول وجسم المستخدم، علماً بأن جميع هذه الهواتف تعمل عند التردد 900) (MHz وبقدرة إشعاع قيمتها (600 mW).
وقد بينت النتائج قيم مختلفة لأرتفاع درجة حرارة رأس مستخدم الهاتف المحمول نتيجة لأختلاف نوع الهاتف.

ABSTRACT

In this paper, the temperature rise in the user's head due to different mobile phone models is computed for a realistic usage pattern, where the Pennes Bioheat Equation is solved using a conformal Finite-Difference Time-Domain (FDTD)-based electromagnetic solver, SEMCAD X. A heterogeneous High-Resolution European Female Head (HR-EFH) with twenty five different tissues is used to simulate the human head, whereas four semi-realistic CAD models, i.e., candy-bar with external antenna, candy-bar with internal antenna, clamshell with external antenna, and clamshell with internal antenna, operating at 900 MHz with antenna output power of 600 mW are used to simulate the commercially available mobile phone models. The results show different temperature rise values in the user's head due to the different mobile phone handset models.

INTRODUCTION

Tremendous use of wireless mobile telephony around the globe by people of every age and every walk has spontaneously given rise to the debate about health hazards associated with the use of these devices, thereby emerges a need for research on the EM coupling between mobile phone antennas and the human so as the anticipated hazards could be confined to the lowest level. Some scientific studies have linked use of mobile phones to headaches, memory loss and cancer, while the industry claims that they are perfectly safe. One well-understood effect of the mobile phone radiation is the thermal effect. Computations of temperature may be preferable to computations of the specific absorption rate (SAR) because of the

more direct relationship between temperature and safety. Thus, the effect of localized SAR for mobile phones should also be related to the temperature rise in the human head.

The temperature increase in anatomically based human head models due to handset antenna has been calculated in a number of studies [1]-[15], and a brief description of their exposure conditions and type of RF source model are given in Table I [16]. In these published works, the handset was simulated using either a dipole or monopole antenna over a rectangular metal box (dielectric covered or none-covered), or a simple metal chassis with a shorted-patch antenna. None of the previous works considered a realistic or semi-realistic handset model for evaluating their thermal effect on human tissues, but they are considered in this paper and in [15].

In this paper, the bioheat equation is solved using a Finite-Difference Time-Domain (FDTD)-based Electromagnetic (EM) solver, *SEMCAD X* [26], to compute the temperature-rise in an anatomically based human head model due to the deposited SAR in tissues, with handset antenna power of 600 mW at 900 MHz. The influence of heated handset is also considered in the temperature rise computation.

TABLE -1: BRIEF DESCRIPTION OF HEAD MODEL, RF SOURCE AND EXPOSURE CONDITIONS CONSIDERED IN THE LITERATURE [1]-[15] TO COMPUTE THE TEMPERATURE RISE IN THE MOBILE PHONE USER'S HEAD.

Publication	Head model	Handset model (RF source)	Exposure conditions
Wang and Fujiwara (1999) [1]	MRI-based anatomically correct Japanese adult head model [17]	Quarter-wavelength monopole antenna mounted on a dielectric covered rectangular metal box	Vertical alignment of monopole antenna with pressed and non-pressed ear
Van Leeuwen (1999) [2]	Adult female volunteer	Dipole Antenna	Vertical alignment of dipole
Wainwright (2000) [3]	Male adult [18]	Quarter-wavelength monopole antenna mounted on a rectangular metal box	Lateral irradiation with the antenna vertically (900MHz) or horizontally (1800MHz) aligned
Bernardi *et al.* (2000) [4]	Male adult [19]	Monopole, whip and PIFA mounted on a dielectric covered rectangular metal box	Tilted dipole by (60°) relative to vertical
Bernardi *et al.* (2001) [5]	VHP [20]	Dual-band monopole-helix antenna mounted on a dielectric covered rectangular metal box.	Vertical alignment of the antenna
Gandhi *et al.* (2001) [6]	Male adult [21]	Monopole mounted on a dielectric covered rectangular metal box (different size for the two frequencies)	Tilted dipole by (30°) relative to vertical
Hirata and Shiozawa (2003) [7]	Male adult [22]	Dipole antenna	Normal ear (none-pressed)
Ibrahim *et al.* (2005) [8]	MRI-based male adult (COMOBIO)	Quarter-wavelength monopole antenna mounted on a dielectric covered rectangular metal box.	Handset is lined up with the mouth and the ear at *cheek*- position as defined in [CENELEC]
Fujimoto *et al.* (2006) [9]	NIT and Osaka University models plus developed three and seven-year-old children	Dipole Antenna	Two polarizations with different ten feeding point positions
Xiang and Gandhi (2006) [10]	Utah and VHP [23]	Quarter-wavelength monopole antenna mounted on a rectangular metal box.	The handset is oriented at cheek and tilt positions in compliance with [IEEE]
Samaras *et al.* (2207)[11]	VHP [21] and EuFem [24]	Quarter-wavelength monopole antenna mounted on a rectangular metal box.	The handset is oriented at cheek position in compliance with [IEEE]
Rodrigues *et al.* (2007) [12]	MRI-based male adult	Half-wavelength dipole	Vertical alignment of the antenna
Rodrigues *et al.* (2008) [13]	Modified John3Doe [25]	Half-wavelength dipole	Vertical alignment of the antenna
Zygiridis and Tsiboukis (2008) [14]	Male adult	A simple metal chassis with shorted-Patch antenna [27]	Tilted handset by 0° and 30° relative to vertical
Al-Mously, *et al.* (2009) [15]	HR-EFH [26]	Semi-realistic mobile phone models	The handset is oriented at cheek and tilt positions in compliance with [IEEE]

Pennes Bioheat Equation (BHE)

Temperature ($T = T(x, y, z, t)$ [°C]) was modeled in the head with a finite difference implementation of bioheat transfer equation (BHE), developed by Pennes in 1948 [28]:

$$\rho c \frac{\partial T}{\partial t} = \nabla \cdot (k \nabla T) + \rho Q_{met} + \rho(\mathrm{SAR}) - B(T - T_{blood}) \quad (1)$$

$$B = \rho_{blood}\, c_{blood}\, \rho\omega \quad (2)$$

where the ρ [kg/m^3] is the material density, c [J/(kg · °C)] is the specific heat capacity, k [W/(m · °C)] is the thermal conductivity, Q_{met} [W/kg] is the metabolic heat generation rate, B [W/(m^3 · °C)] is the blood perfusion coefficient, ω [L/(s · kg)] is the blood perfusion rate, and T_{blood} is blood temperature. In (1), the term on the left represents the rate of change in the stored internal energy of the tissue; the term $\nabla \cdot (k \nabla T) = k \nabla^2 T$ is the heat transfer due to thermal associated with blood flow. The heat is distributed through the conduction, and the last term relates convection heat loss simulation domain by diffusion. It is generated by metabolic body processes and by the deposited radiation energy. A homogeneous 'heat-sink' term has a cooling effect and models the heat removal due to blood circulation.

Heat exchange at the tissue interface with the surrounding environment is modeled by imposing the continuity of heat flow perpendicular to the skin surface as the boundary condition. Various boundary conditions are commonly applied: the Dirichlet ($T = T_a$), the Neumann ($k\, \partial T/\partial n = q$) and the mixed boundary condition which is used and expressed as;

$$k \frac{\partial T}{\partial n}(x, y, z) = -H_a (T_{skin} - T_a) \left[\frac{\mathrm{W}}{\mathrm{m}^2}\right] \quad (3)$$

where n is the normal to the skin surface and the right hand expression models the heat losses from surface of the skin due to convection and radiation which are proportional to the difference between the skin temperature (T_{skin}) and external environment (ambient) temperature (T_a), H_{a} is the convection coefficient for heat exchange with the external temperature. In this study, the heating due to RF absorption is very small; therefore, the neglecting of sweating does not make any difference.

FDTD Modelling

A. Cellular Phone Handset Models

Four single-band mobile phone handset models working at 900 MHz with antenna output power of 600 mW are designed and simulated to find out the available commercial models design as follow;

1. Model-A: Candy-bar type mobile phone with left-side external antennas. The maximum physical dimensions (excluding the antenna) are 104 mm × 43 mm × 16.5 mm (length × width × thickness), whereas, the multilayer PCB dimensions are 97 mm × 37 mm × 1 mm, Fig. 1. The proposed external antenna is a single-band short-whip top loaded with a small cylinder [29], Fig. 2.
2. Model-B: Candy-bar type mobile phone with upper internal antennas. The maximum physical dimensions are 110 mm × 44 mm × 13 mm, whereas; the multilayer PCB dimensions are 97 mm × 37 mm × 1 mm, Fig. 3. The proposed internal antenna is a single-band probe-fed rectangular patch with shorting plate at the edge [29], Fig. 4.
3. Model-C: Clamshell type mobile phone with left-side external antennas. The maximum physical dimensions (excluding the antenna) when closed are 89 mm × 50 mm × 19 mm, whereas; the base-multilayer PCB dimensions are 67.5 mm × 43 mm × 1 mm, Fig. 5. Fig. 6 shows the external antenna structure and dimensions at 900 MHz [29].
4. Model-D: Clamshell type mobile phone with upper internal antennas. The maximum physical dimensions of model-D when closed are 90 mm × 45 mm × 18.5 mm, whereas; the base-multilayer PCB dimensions are 77 mm × 37 mm × 1 mm, Fig. 7.

The patch antenna in model-B is mounted on the back-side of the upper part of the PCB, whereas, in model-D the patch is mounted on the back-side of the upper part of the base-PCB. The dielectric components of the mobile phone models are represented within the FDTD simulation using the material parameters summarized in Table II.

TABLE -2: THE DIELECTRIC PARTS OF THE MOBILE PHONES MECHANICAL CAD DATA SETS AND THE CORRESPONDING MATERIAL PARAMETERS

Part	ε_r	σ (S/m)
Antenna cover and bushing	2.5	0.003
PCB dielectric	4.5	0.07
LCD glass	4.5	0.01
LCD dielectric	3.0	0.01
Housing and covers	3.5	0.02
Keypad/buttons	3.5	0.02
Battery case	3.5	0.02

B. Human-Hand Model

A homogeneous hand model consisting of three tissues (skin, muscle, and bone) [16] is designed. The hand model is gripping the mid-part of the handset and represents a realistic usage pattern of handheld set.

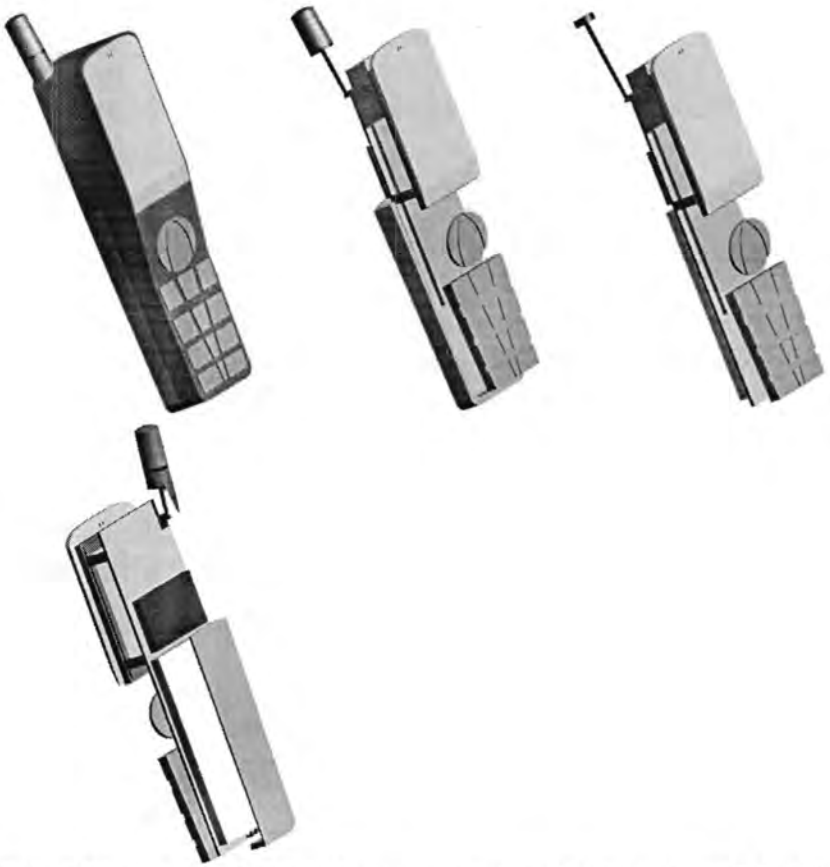

FIGURE-1: The *SEMCAD* representation of handset model-A in different views showing different components and parts.

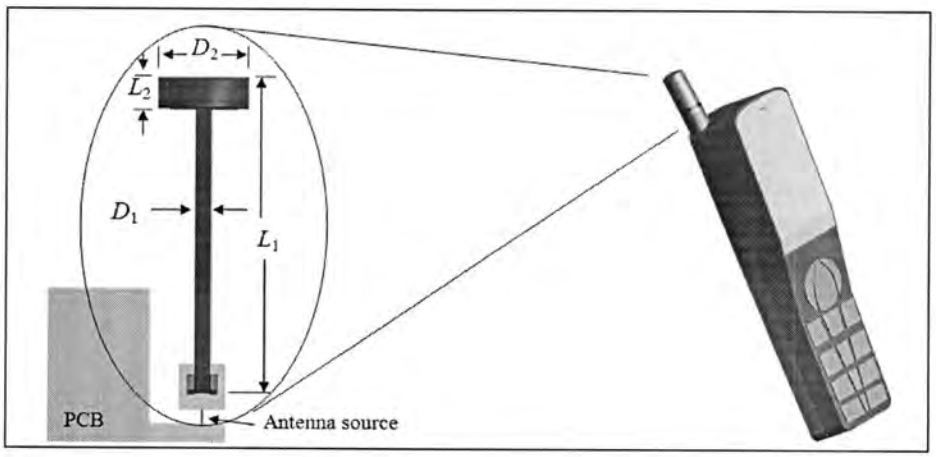

	900 MHz
L_1	31.0 mm
L_2	2.0 mm
D_1	1.0 mm
D_2	6.0 mm

FIGURE-2: The numerical antenna structure of model-A and its dimensions at 900 MHz.

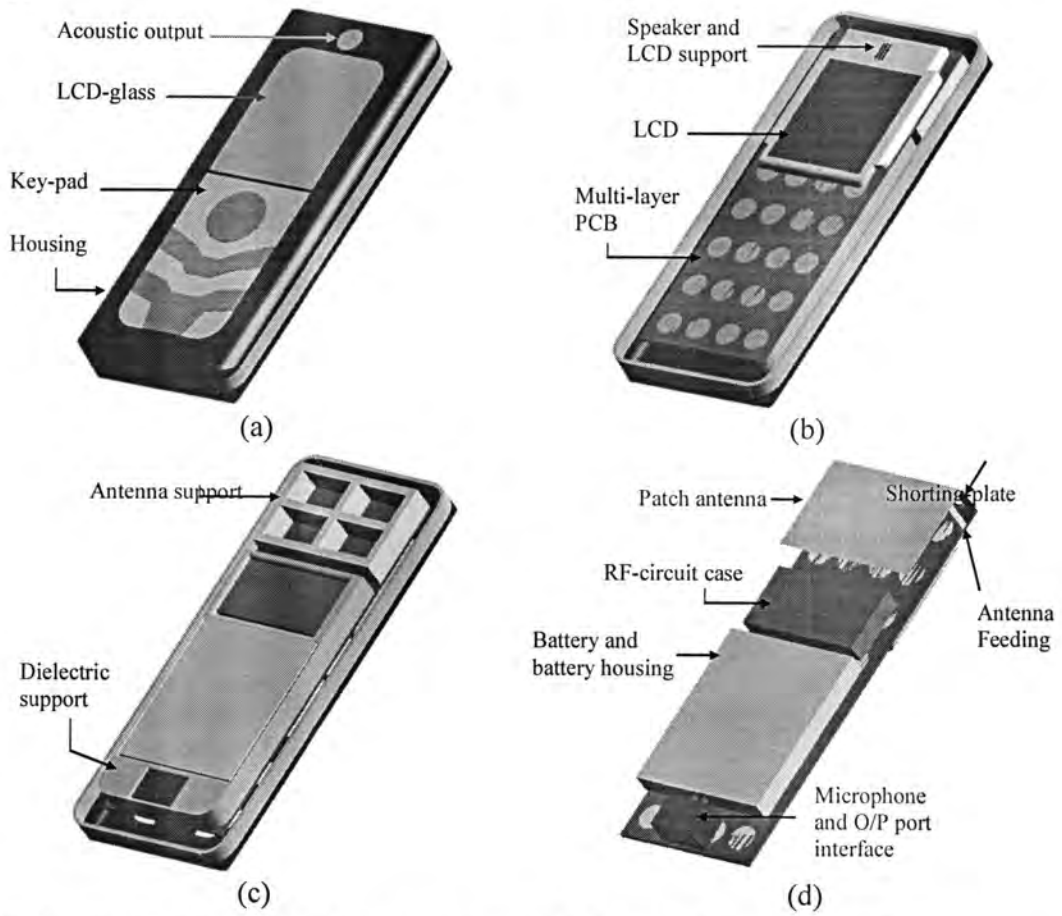

FIGURE 3: The SEMCAD representation of the handset with internal antenna (model-B) showing different components and parts in different views.

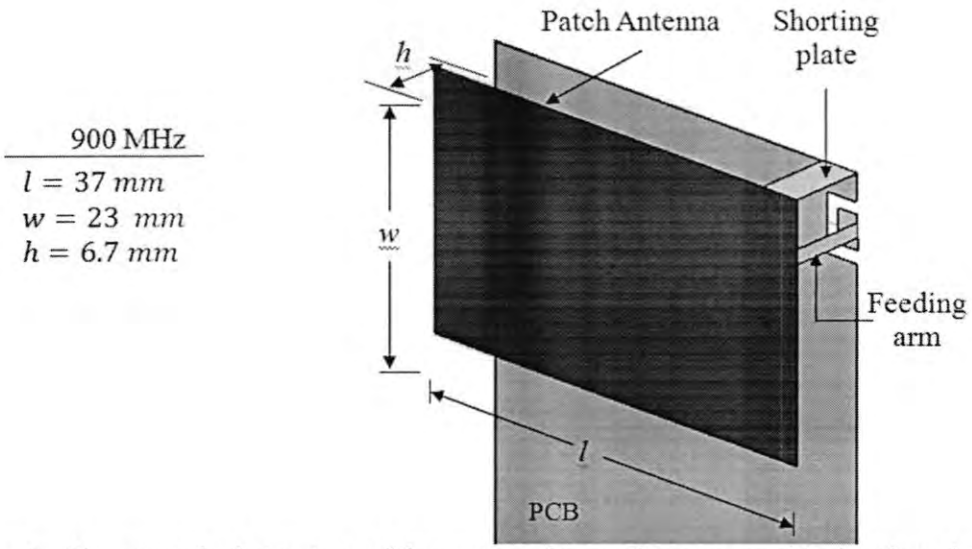

Figure-4: The numerical structure of the rectangular patch antenna with shorting plate, used for the handset model-B, and its dimensions at 900 MHz.

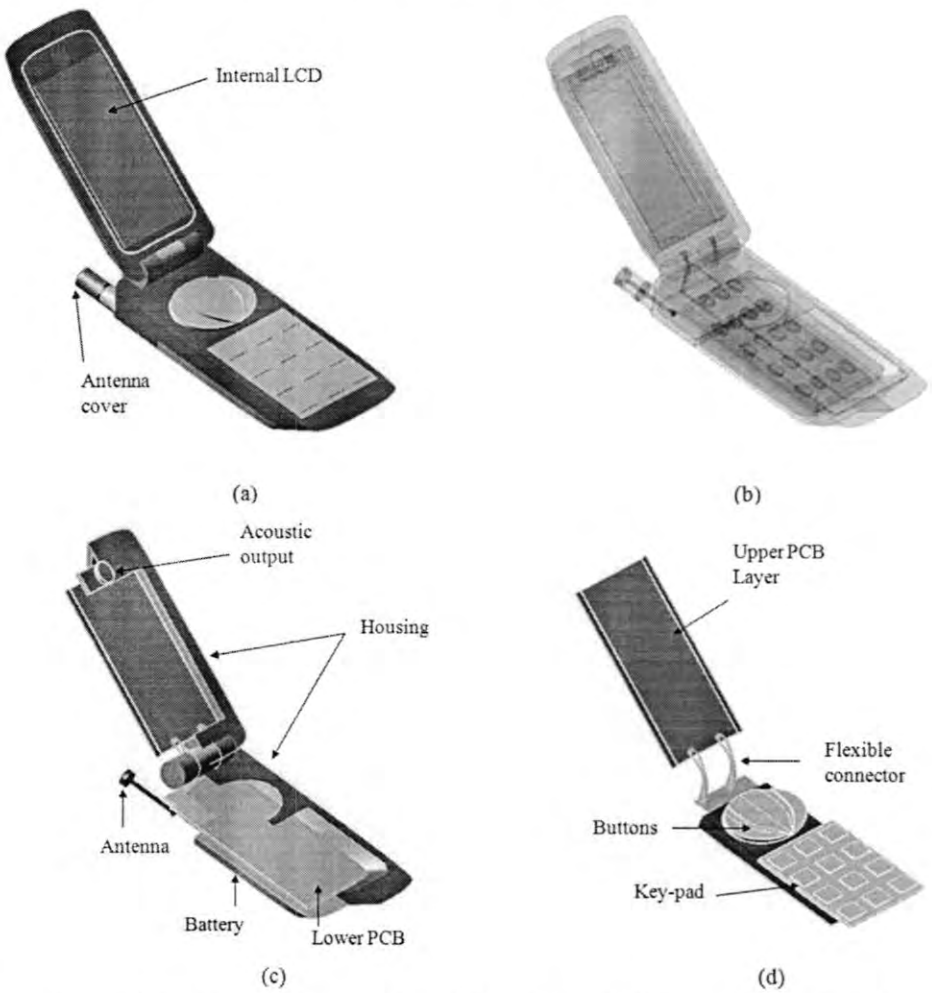

FIGURE-5: Numerical components structure of the clamshell-type handset model-C: (a) 3D view with all parts, (b) transparent 3D view, (c) 3D cut-view of the housing with PCB, antenna, speaker and battery, and (d) 3D view of PCB, key-pad and buttons.

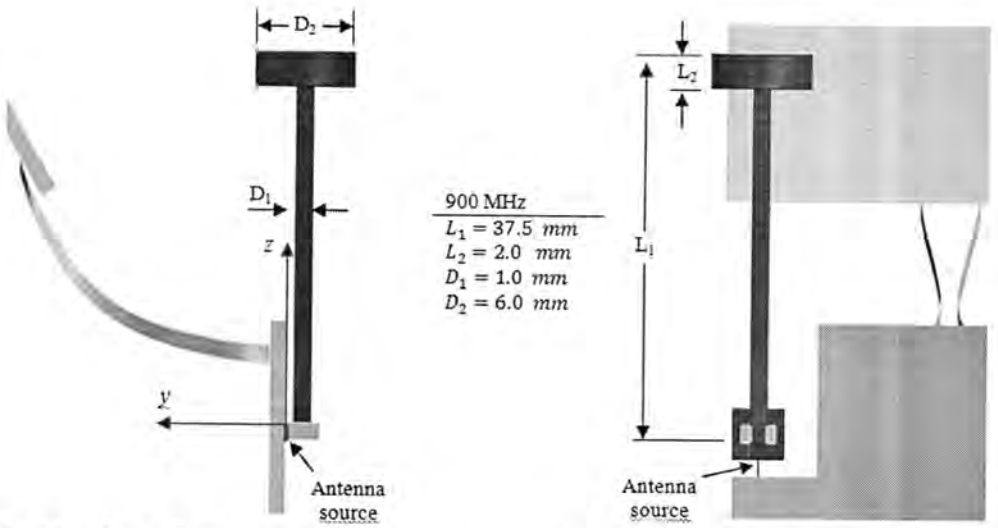

(a) A side-view of antenna structure with dimensions

(b) A Front-view of antenna structure with dimensions

FIGURE-6: Different views of the proposed loaded short-whip antenna attached to the PCB, used for the handset model-C, with its dimensions at the adopted frequencies.

C. Human-Head Model

The user's head is simulated using an MRI-based anatomically correct model, High-Resolution European Female Head (HR-EFH), available with SPEAG [26]. This heterogeneous head model has 25 different tissues with pressed ears. The electrical properties and densities of tissues are given in Table III [16], [30].

Temperature-Rise Computation in a Heterogeneous Head Model

Fig. 8 shows the mobile phone handset models A, B, C, and D setups that used for temperature rise computation in the user's head.

Solving the BHE using the conformal-FDTD method to compute the temperature-rise in handset user's head due to the SAR deposition needs accomplishment of two simulations; first, the EM-simulation to compute the deposited SAR in tissue, second, thermo-simulation to compute the temperature-rise in tissue.

In the EM-simulation achieved in this paper, the FDTD-grid for each handset setup has a minimum spatial resolution of $0.5 \times 0.5 \times 0.5$ mm^3 and maximum resolution of $10 \times 10 \times 10$ mm^3 in the x, y, and z directions with grading ratio of 1.2. The absorbing boundary conditions (ABCs) are set as U-PML mode with 10 layer thickness [26]. This FDTD-grid setting is also applied in thermo-simulation. A mixed boundary condition given in (3) involving skin plus ears is used with convection coefficient ($H_a = 2.7\ W/(m^2\ °C)$ and ambient temperature ($T_a = 25\ °C$). The core temperature is ($T_{blood} = 37\ °C$). The heat exchanged through the neck and the other remaining parts of the body has been approximated by means of setting the neck boundary temperature as the blood temperature.

Table III lists the hand and head tissues dielectric properties, whereas Table IV lists the mass, mass density, and thermal properties of the head tissues.

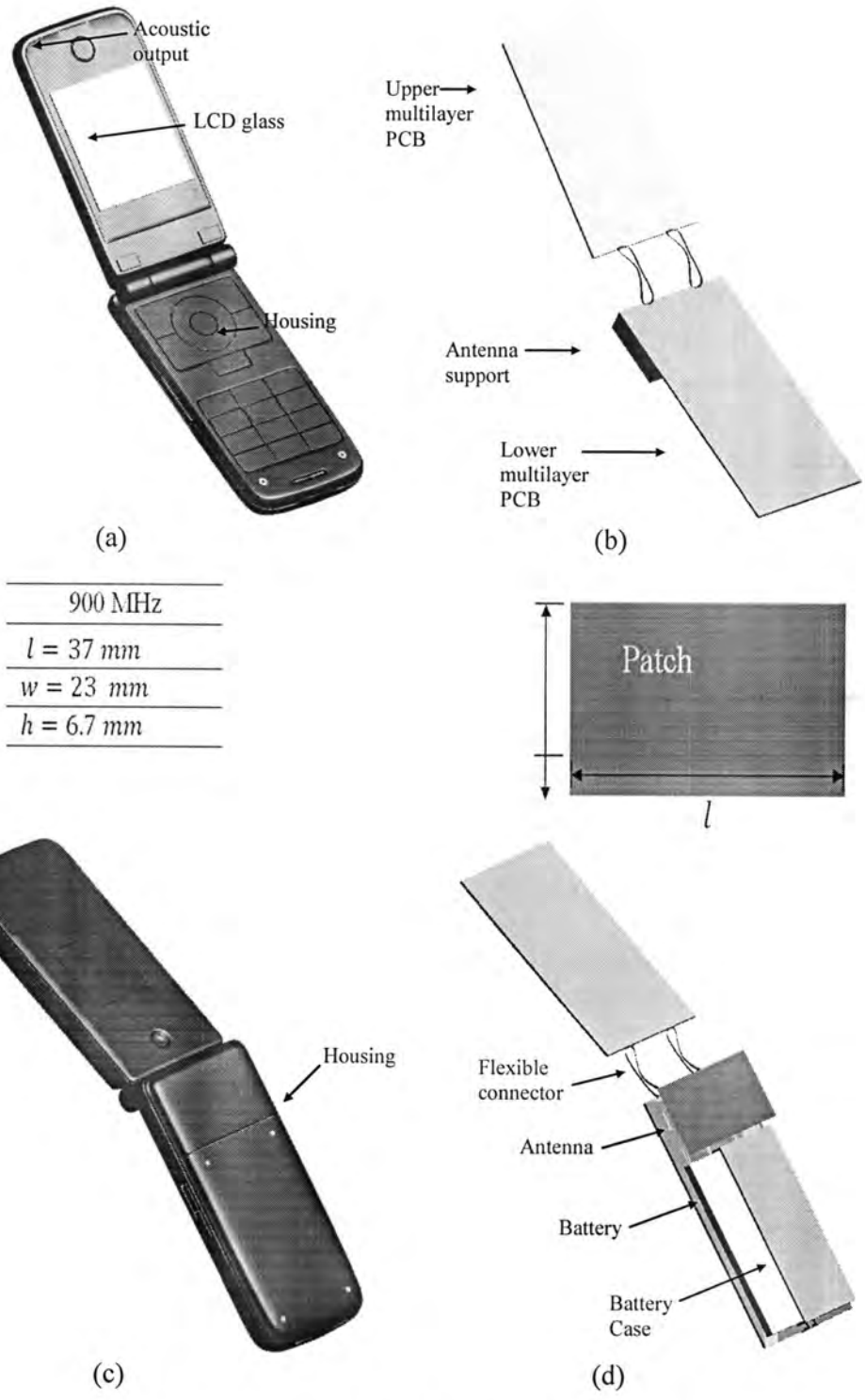

FIGURE-7: The *SMCAD* representation of handset model-D1 in different views showing different components and parts, and explaining antenna dimensions at the adopted frequencies.

It should be noticed that the results based on experiments involving animals are used for most of the thermal parameters required in the human-head model [7]. Since no solid relations describe the thermal parameters dependency on the minor expected temperature-rise in head of the handset user, in this paper the blood perfusion coefficient of the brain as well as the skin and ears is modeled to be linearly temperature dependent; based on the temperature distribution and blood perfusion response in rat brain during selective brain cooling presented by Diao and Zhu in [31]. In [31], a rat model was used to examine the transient temperature distribution and blood flow response in the brain during selective brain cooling (SBC) and re-warming. SBC was induced by a head cooling helmet with circulating water of 18 °C (moderate cooling) or 0 °C (deep cooling). It has been shown that the brain temperature reductions were 1.7±0.2 °C (5 mm beneath the brain surface) and 3.2±1.1 °C (2 mm beneath the brain surface) when the temperature of the water was 18 °C. The blood flow rate is dropped by up to 22% and 44% during the cooling from its baseline in the moderate cooling group and in the deep cooling group, respectively. The characteristic time that it took for the tissue temperatures to reach a new steady state after the initiation of cooling varied from 5 min to more than 35 min and it depended strongly on the blood flow response to the cooling.

Although the heat dissipation in the skin of rats differs from that of in the human skin, the experiment results presented in [31] are used to approximate per 1 °C blood perfusion in brain, skin and ears tissue at a rate value of 13%, while computing the temperature-rise in the head of handset user.

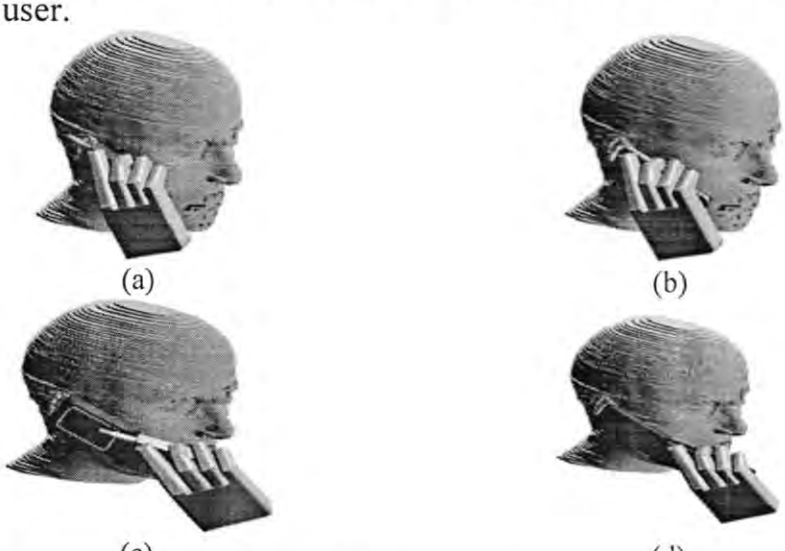

FIGURE 8. The adopted different mobile phone handset models, close to HR-EFH at *cheek*-position, for temperature-rise computation; (a) Model-A, (b) Model-B, (c) Model-C and (d) Model-D.

Table V depicts the number of generated voxels, the computed SAR_{1g} induced in HR-EFH tissues and their corresponding steady-state temperature after 60 min of using the handheld set models-A, B, C, and D, normalized to antenna radiated power of 600 mW at 900 MHz. Fig. 9 demonstrates the sliced-distribution of SAR_{1g} induced in HR-EFH tissues, and the corresponding steady-state temperature after 60 min of using handset models A and B at 900 MHz.

The 600 mW antenna radiated power is for the analogue phone, whereas, the radiated power of digital generation of GSM mobile phone is 250 mW at 900 MHz. That is because the main aim of the study is to calculate the maximum temperature-rise in human head due to the possible maximum RF emission for the purpose of comparison with previously published works on this subject.

Although the IEEE –Standard [32] and other standards apply the SAR limit for the extremities to the normal pinnae, and since the used MRI-based head model (HR-EFH) has pressed pinnae; in this paper the pinnae are subject to the same exposure limit, for peak spatial SAR, as the head. It has been observed that there are no substantial differences between the computed SAR values for the head with and without pressed pinnae, where the peak spatial SAR location is not at the pinna, instead the peak shift to region near the pinna.

TABLE -3: VALUES OF HAND AND HR-EFH TISSUES PARAMETERS (RELATIVE PERMITTIVITY ε_r, ELECTRICAL CONDUCTIVITY σ) USED FOR SIMULATIONS AT 900 MHZ [16], [30].

Hand Tissue		σ (S/m)
Hand skin	41.41	0.87
Hand muscle	55.03	0.94
Hand bone	12.45	0.14

HR-EFH Tissue		σ (S/m)	HR-EFH Tissue		σ (S/m)
Air	1.000	0.00	Mastoid cells (bones)	5.50	0.04
Blood vessel	44.78	0.70	Mid-brain (mesencephalon)	45.79	0.76
Bone (ramus of mandible)	12.45	0.14	Muscles	55.03	0.94
Brain /grey matter	52.73	0.94	Nasal cavity	46.08	0.84
Brain /white matter	38.89	0.59	Parotid Gland	59.68	1.04
Cerebellum	49.44	1.26	Skin	41.41	0.87
Cerebro Spinal Fluid (CSF)	68.64	2.41	Skull	16.62	0.24
Ear (cartilage)	42.65	0.78	Spinal cord	32.53	0.57
Eye-cornea	55.24	1.39	Spine	12.45	0.14
Eye-lens	46.57	0.79	Thalamus	45.79	0.76
Eye- vitreous body	68.90	1.64	Tongue	55.27	0.94
Fat (average infiltrated)	11.33	0.11	Ventricles (brain)	68.64	2.41
Jaw bone (mandible)	12.45	0.14			

TABLE -4:MASS, MASS DENSITY AND THERMAL PROPERTIES ASSUMED FOR THE VARIOUS TISSUES [5], [7], [9], [16].

HR-EFH Tissue	Mass (kg)	[illegible]	[illegible]	V	[illegible]	[illegible]
Air .1	0.000	1.16	1006	0.0263	0.00	0
Blood Vessel .2	0.005	1050	3553	0.46	1.52	1000
Bone .3	0.030	1990	1300	0.4	0.15	1000
Brain /grey matter .4	0.871	1039	3700	0.57	9.70	35000
Brain /white matter .5	0.367	1043	3600	0.50	9.70	35000
Cerebellum .6	0.125	1040	4200	0.58	9.70	35000
CSF .7	0.256	1007	4000	0.60	0.00	0
Ear (cartilage) .8	0.011	1100	3400	0.45	0.20	9100
Eye-cornea .9	0.002	1032	4200	0.58	0.00	0
Eye-lens .10	0.002	1090	3000	0.40	0.00	0
Eye- vitreous body .11	0.010	1009	4200	0.60	0.34	0
Fat .12	0.032	916	2500	0.25	0.15	520
Jaw bone .13	0.243	1990	1300	0.40	0.15	1000
Mastoid cells .14	0.027	980	2700	0.22	5.82	32000
Mid-brain .15	0.026	1039	3700	0.57	9.70	35000
Muscles .16	0.940	1041	3600	0.50	0.67	2700
Nasal cavity .17	0.063	1050	3300	0.43	1.523	9000
Parotid Gland .18	0.020	1050	3700	0.53	9.70	25000
Skin/dermis .19	0.760	1100	3500	0.42	1.07	9100
Skull .20	0.744	1645	1300	0.4	0.15	1000
Spinal cord .21	0.007	1038	3500	0.46	9.70	35000
Spine .22	0.120	1990	1300	0.40	0.15	1000
Thalamus .23	0.015	1039	3700	0.57	9.70	35000
Tongue .24	0.035	1041	3300	0.42	0.461	13000
Ventricles (brain) .25	0.005	1007	4200	0.60	0.00	0

TABLE -5:THE GENERATED VOXELS, PEAK SAR_{1g} IN HEAD (HR-EFH) AND THE CORRESPONDING PEAK TEMPERATURE (NOT ΔT) AFTER 60 MIN OF USING THE HANDHELD SET MODELS-A, B, C, AND D AT CHEEK-POSITION WITH ANTENNA OUTPUT POWER OF 600 MW AT 900 MHZ.

Handset Model	No. of FDTD Nodes/Voxels	SAR_{1g} in Head (W/kg)	Max. T in Head (°C)
Model-A (bar-type + external antenna)	276×250×276 / 18830625	4.70	37.43
Model-B (bar-type + internal antenna)	273×297×243 / 19483904	3.88	37.45
Model-C (clamshell-type + external antenna)	266×260×273 / 18668720	1.58	37.34
Model-D (clamshell-type + internal antenna)	256×300×251 / 19061250	0.93	37.31

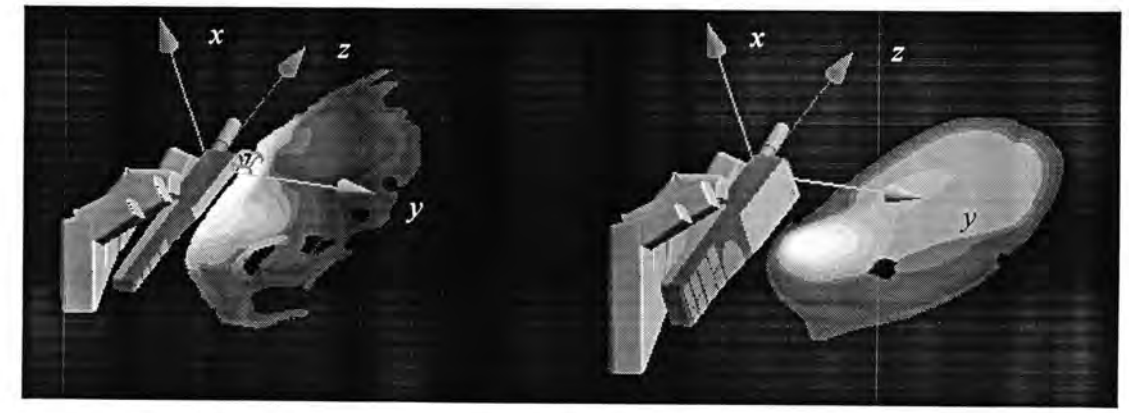

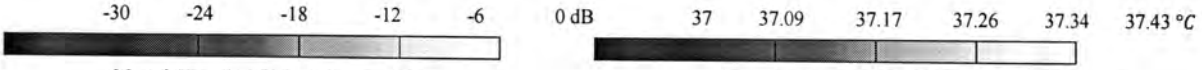

Max. SAR_{1g} (4.7 W/kg) at $x = -3.8$ mm

(a) Sliced distribution of SAR_{1g} induced in HR-EFH due to handset model-A at *cheek*-position operating at 900 MHz.

Max. temperature (37.43 °C) at $x = -22.2$ mm

(b) Sliced distribution of temperature inside HR-EFH due to the SAR_{1g} deposition in (a).

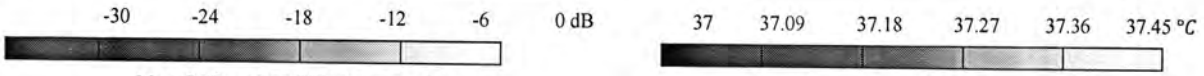

Max. SAR_{1g} (3.88 W/kg) at $x = -3.8$ mm

(c) Sliced distribution of SAR_{1g} induced in HR-EFH due to handset model-B at *cheek*-position operating at 900 MHz.

Max. temperature (37.45 °C) at $x = -20$ mm

(d) Sliced distribution of temperature inside HR-EFH due to the SAR_{1g} deposition in (c).

FIGURE-9: Sliced-distribution of SAR_{1g} and its corresponding steady-state temperature in HR-EFH tissues due to mobile phone handset model-A and model-B at 900 MHz with 600 mW antenna output power.

The results show that the global maximum field position of both SAR and its corresponding temperature are not identical; while the peak SAR occurs outside the pinna or skin surfaces depending on the handset position, the peak temperature occurs inside the head tissues and mostly in cheek muscle. Although Model-A induces higher SAR in head, as compared with other models, model-B causes higher temperature increase in head, since the handset shape plays an important role in convection.

Even though the core temperature of the head is considered as $T_{blood} = 37\ °C$, the initial basal temperature distribution in head tissues are different due to the ambient temperature of $T_a = 25\ °C$.
While the basal temperatures of head tissues are $36.4\ °C - 37\ °C$, the skin and pinnae basal temperature are around $34\ °C$. Thus, the maximum temperature rise (ΔT) will be occurred in pinna.

The steady-state temperature-rise due to practical use of cellular handsets may not give a realistic picture of the temperature-rise distribution within the head because of telephone call may not be very long. Thus, it is useful to consider how quickly the temperature in the head is elevated. To test our temperature computation reliability, the thermal time constants for tissue, i.e. brain tissue, was measured and found to be over 6 min. The thermal time constant, obtained from the intersection of the tangent line of the temperature-rise curve and the steady-state value (for a human), was over 6 min [33]. After 20 min of exposure time, 90% of the steady-state temperature was reached.

Influence of Heated Handset on the Temperature Rise in the User's Head

Besides the two causes of temperature increase in the head (namely, SAR deposition and handset contact with ear and cheek skin), a third additional cause for the temperature increase is the heating of the handset itself. This is due to the power dissipated in the circuitry and, in particular, in the power amplifier; this heating is transmitted to the head tissues via thermal conduction [5]. Some of the commercial mobile phones currently available in the market are manufactured with a metal case covering the back-side (except antenna zone) to accelerate the heat dissipation to air and the user's hand.

To examine the temperature increase of cellular handsets in a practical usage pattern, two commercially available models, the candy-bar type Motorola L71, and clamshell type Motorola RAZR V3i, were examined at *cheek*-position in continuous calling for 60 min duration. The temperature of the handset area touching the user's head was measured using a precise thermometer (erfi-MPL / GOSSEN 0421/207). A maximum temperature of $38.5\ °C$ was recorded for the Motorola L71-type, and, a maximum temperature of $37.5\ °C$ for the Motorola RAZR V3i-type. Simulating the heated handset with a temperature of $39°C$, as the worst case, temperatures of $38.36\ °C$ and $38.86\ °C$ were noticed in the ear tissue for handset model-A and model-B, as an example, at *cheek*-position, respectively. This occurred without any considerable temperature increase in the brain tissue. These results agreed with that given in [5].

Temperature increase in the mobile phone user's head due to different handset models was computed using a conformal-FDTD based EM solver. The temperature due to, firstly, the deposited SAR in head, and secondly, the heated handset, were both considered in this paper. Considerable differences in the temperature increase in head tissues were noticed due to the different handset models involved in simulations. The possible computed temperature increases in the head were found to be well within normal biological variations of temperature in humans.

REFERENCES

1. Wang, J. and Fujiwara, O., "FDTD computation of temperature rise in the human head for portable telephones," *IEEE Transaction on Microwave theory and Techniques*, 47,(8), pp. 1528–1534, Aug.(1999).
2. Van Leeuwen, G. M. J., Lagendijk, J. J. W., Van Leersum, B. J. A. M., Zwamborn, A. P. M., Hornsleth, S. N., and Kotte, A. N. T. J. "Calculation of change in brain temperatures due to exposure to a mobile phone," *Phys. Med. Biol.*, 44, pp. 2367–2379, (1999).
3. Wainwright, P., "Thermal effects of radiation from cellular telephones," *Phys. Med. Biol.*, (45), pp. 2363–2372,(2000).
4. Bernardi, P., Cavagnaro, M., Pisa, S., and Piuzzi, E., "Specific absorption rate and temperature increases in the head of a cellular-phone user," *IEEE Transaction on Microwave Theory and Techniques*, 48, (7), pp. 1118-1126,(2000).
5. Bernardi, P., Cavagnaro, M., Pisa, S., and Piuzzi, E., "Power absorption and temperature elevations induced in the human head by a dual-band monopole-helix antenna phone," *IEEE Transaction on Microwave Theory and Techniques*, 49, (12), pp. 1118–1126, Dec. (2001).
6. Gandhi, O. P., Li, Q.-X., and Kang, G., "Temperature rise for the human head for cellular telephones and for peak SARs prescribed in safety guidelines," *IEEE Transaction on Microwave theory and Techniques*, vol. 49, (9), pp. 1607–1613, Sep.(2001).
7. Hirata, A. and Shiozawa, T. "Correlation of maximum temperature increase and peak SAR in the human head due to handset antennas," *IEEE Transaction on Microwave theory and Techniques*, 51, (7), pp. 1834–1841, Jul. (2003).
8. Ibrahiem, A., Dale, C., Tabbara, W. and Wiart, J., "Analysis of the temperature increase linked to the power induced by RF source," *Progress In Electromagnetics Research*, PIER 52, 23-46,(2005).
9. Fujimoto, M., Hirata, A., Wang, J., Fujiwara, O., and Shiozawa, T.,

"FDTD-derived correlation of maximum temperature increase and peak SAR in child and adult head models due to dipole antenna," *IEEE Transactions on Electromagnetic Compatibility*, vol. 48, (1), pp. 240–247, Feb.(2006).

10. Li, Q-X., Gandhi, Om-P., "Thermal implications of the new relaxed IEEE RF safety standard for head exposures to cellular telephones at 835 and 1900 MHz," *IEEE Transaction on Microwave Theory and Techniques*, 54, (7), pp. 3146-3154, (2006).
11. Samaras, T., Kalampaliki, E. and Sahalos, J. "Influence of thermophysiological parameters on the calculations of temperature rise in the head of mobile phone users," *IEEE Transactions on Electromagnetic Compatibility*, 49, (4), pp. 936–939, Nov.(2007).
12. Rodrigues, A. O., Viana, J. J., Rodrigues, L. O., and Ramirez, J. A., "Calculation of temperature rise induced by cellular phones in the human head," *Journal of Microwaves and Optoelectronics*, 6, (1), pp. 310-322, Jun. (2007).
13. Rodrigues, A. O., Malta, L., Viana, J. J., Rodrigues, L. O. C., and Ramírez, J. A., "A head model for the calculation of SAR and temperature rise induced by cellular phones," *IEEE Transaction on Magnetics*, 44, (6), Jun. (2008).
14. Zygiridis, T. T. and Tsiboukis, T. D., "Assessment of the human head exposure to wireless communication devices: combined electromagnetic and thermal studies for diverse frequency bands," *Progress In Electromagnetics Research* B, (9), pp. 83-96,(2008).
15. Al-Mously, S. I. and Abousetta, M. M. "A definition of thermophysiological parameters of SAM materials for temperature rise calculation in the head of cellular handset user," in *Proceeding of the Progress in Electromagnetics Research Symposium* (PIERS), pp. 170-174, Moscow, Russia, 18-21 August(2009). [online]: http://www.piers.org.
16. Al-Mously, S. I., "Design and Performance Enhancement of Cellular Handset Antennas and Assessment of Their EM Interaction with a Human, Ph.D. thesis, School of Applied Sciences and Engineering, Academy of Graduate Studies, Tripoli, Libya, August, (2009). http://www.salahalmously.info.
17. Fujiwara, O., and Kato, A., "Computation of SAR inside eyeball for 1.5-GHz microwave exposure using finite-difference time-domain technique," *IEICE Transaction on Communication*, vol. E77-B, no. 6, pp. 732–737, (1994).
18. Dimbylow, P. J., and Mann, S. M., "SAR calculations in an anatomically realistic model of the head for mobile communication transceivers at 900 MHz and 1.8 GHz," *Phys. Med. Biol.*, vol. 39, pp. 1537–1553, (1994).

19. Zubal, I. G., Harrell, C. R., Smith, E. O., Rattner, Z., Gindi, G. R., and Hoffer, P. B., "Computerized three-dimensional segmented human anatomy," *Med. Phys.*, 21, (2), pp. 299-302, (1994).
20. National Library of Medicine (2006, Jul. 28). The visible human project [online]. Available: http:// www.nlm.nih.gov/research/visible/visible_human.html.
21. Gandhi, O. P., Lazzi, G., and Furse, C. M., "Electromagnetic absorption in the human head and neck for mobile telephones at 835 and 1900 MHz," *IEEE Transaction on Microwave Theory and Techniques*, 44, (10), pp. 1884–1897, Oct. (1996).
22. Hirata, A., Matsuyama, S., and Shiozawa, T., "Temperature rises in the human eye exposed to EM waves in the frequency range 0.6–6 GHz," *IEEE Transaction on Electromagnetic Computations*, vol. 42, no. 4, pp. 386–393, Nov. (2000).
23. National Library of Medicine (2006, Jul. 28). The visible human project [online]. Available: http:// www.nlm.nih.gov/research/visible/visible_human.html.
24. SEMCAD HR-EF-1. *High resolution European female head (compressed ears)* [Online]. Available: http:// www.semcad.com/simulation/catalog/ phantoms.php
25. "Chapel Hill Volume Rendering Test Data Set—Volume II" SoftLab Software Systems Laboratory, Dept. Computer Science, Univ. North Carolina, Chapel Hill, 1995 [Online]. Available: ftp://ftp.cs.unc.edu/pub/projects/image/CHVRTD/volII/
26. SEMCAD X, Reference Manual for the SEMCAD Simulation Platform for Electromagnetic Compatibility, Antenna Design and Dosimetry," SPEAG - Schmid & Partner Engineering. AG [http://www.semcad.com].
27. Kivekas, O., Ollikainen, J., Lehtiniemi, T., and Vainikainen, P., "Bandwidth, SAR, and efficiency of internal mobile phone antennas," *IEEE Transactions on Electromagnetic Compatibility,* 46, (1), pp. 71–86,(2004).
28. Pennes, H. H. "Analysis of tissue and arterial blood temperature in resting forearm," *J. Appl. Phys.*, (1), pp. 93–122,(1948).
29. Al-Mously, S. I. and, Abousetta, M. M. "Anticipated Impact of Hand-Hold Position on the Electromagnetic Interaction of Different Antenna Types/Positions and a Human in Cellular Communications," *International Journal of Antennas and Propagation* (IJAP), vol. 2008, Article ID 102759, 22 pages,(2008).
30. "Dielectric Properties of Body Tissue in the frequency range 10 Hz – 100 GHz," Italian National Research Council, Institute for Applied Physics, Florence, Italy, http://niremf.ifac .cnr.it/tissprop.
31. Diao, C. and Zhu, L. "Temperture distribution and blood

perfusion response in rat brain during selective brain cooling." *Med. Phys*. 33,(7), pp. 2565-2573, Jul. (2006).

32. Standard for Safety Levels with Respect to Human Exposure to Radiofrequency Electromagnetic Fields, 3 kHz to 300 GHz, IEEE Standards Coordinating Committee 28.4,(2006).
33. *American National Standard—Safety Levels with Respect to Exposure to Radio Frequency Electromagnetic Fields, 3 kHz to 300 GHz*, ANSI/IEEE C95.(1-1992).

Vol. 21
No. 4
2010

مجلة علوم المستنصرية

تصدر عن كلية العلوم الجامعة المستنصرية

Mobile: 07706289924
e-mail: mustjsci@yahoo.com

بسم الله الرحمن الرحيم

تعليمات النشر لمجلة علوم المستنصرية

1. تقوم المجلة بنشر البحوث الرصينة التي لم يسبق نشرها في مكان آخر بعد إخضاعها للتقويم العلمي من قبل مختصين وبأي من اللغتين العربية او الانكليزية .
2. يقدم الباحث طلبا تحريريا لنشر البحث في المجلة على أن يكون مرفقا بأربع نسخ من البحث مطبوعة على الحاسوب ومسحوب بطابعة ليزرية وعلى ورق ابيض قياس (A4) مع قرص مرن (Disk) محمل بأصل البحث ويكون عدد صفحات البحث 10 صفحات وبضمنها الاشكال والجداول على ان لايكون الحرف اصغر من قياس 12 .
3. يطبع عنوان البحث واسماء الباحثين (كاملة) وعناوينهم باللغتين العربية والانكليزية على ورقة منفصلة شرط ان لاتكتب اسماء الباحثين وعناوينهم في أي مكان اخر من البحث ، وتعاد كتابة عنوان البحث فقط على الصفحة الاولى من البحث .
4. تكتب اسماء الباحثين كاملة بحروف كبيرة وفي حالة استخدام اللغة الانكليزية وكذلك الحروف الاولى فقط من الكلمات (عدا حروف الجر والاضافة) المكونة لعنوان البحث ، وتكتب عناوين الباحثين بحروف اعتيادية صغيرة .
5. تقدم خلاصتان وافيتان لكل بحث ، احداهما بالعربية والاخرى بالانكليزية وتطبع على ورقتين منفصلتين بما لايزيد على (250) كلمة لكل خلاصة.
6. يشار الى المصدر برقم يوضع بين قوسين بمستوى السطر نفسه بعد الجملة مباشرة وتطبع المصادر على ورقة منفصلة ، ويستخدم الاسلوب الدولي المتعارف عليه عند ذكر مختصرات اسماء المجلات.
7. يفضل قدر الامكان تسلسل البحث ليتضمن العناوين الرئيسة الاتية : المقدمة ، طرائق العمل ،النتائج والمناقشة و الاستنتاجات، المصادر، وتوضع هذه العناوين دون ترقيم في وسط الصفحة ولا يوضع تحتها خط وتكتب بحروف كبيرة عندما تكون بالانكليزية .
8. يتبع الاسلوب الاتي عند كتابة المصادر على الصفحة الخاصة بالمصادر: ترقيم المصادر حسب تسلسل ورودها في البحث ، يكتب الاسم الاخير (اللقب) للباحث او الباحثين ثم مختصر الاسمين الاولين فعنوان البحث ، مختصر اسم المجلة ، المجلد او الحجم ، العدد ، الصفحات ، (السنة) . وفي حالة كون المصدر كتابا يكتب بعد اسم المؤلف او المؤلفين عنوان الكتاب ، الطبعة ، الصفحات ، (السنة) الشركة الناشرة ، مكان الطبع .
9. بخصوص اجور النشر يتم دفع مبلغ (25000) عشرون الف دينار عند تقديم البحث للنشر وهي غير قابلة للرد ومن ثم يدفع الباحث (25000) عشرون الف دينار اخرى عند قبول البحث للنشر وبهذا يصبح المبلغ الكلي للنشر خمسون الف دينار .

المـــحتـــويـات

دراسة بعض المعايير الحياتية و تأثير المنظفاتDetergents لنوعين من القراد الصلبHyalomma ana. anatolicum و *Ripicephlus turanicus*

أفكار مسلم هادي
مركز بحوث ومتحف التاريخ الطبيعي

تاريخ تقديم البحث 2009/7/28 - تاريخ قبول البحث 2010/5/10

ABSTRACT

The effect of detergent solutions (1, 2, 3)with concentrations 23.3 ,11.6 ,7.7 respectively; on two species of the hard ticks : *Hyalomma ana. anatolicum* and *Ripicephlus turanicus* were slow; taking several hours due to the sclerotized shields covered the body which contain cement and wax that prevent solution permeated. Females before mating died in less period than males because thick shield didn't cover all the body .Larvae died in less period that due to delicate and transparent body walls. Nymphs, compared with larvae, died in longer period due to hard sclerotized shields .The period of death was less in female full with eggs due to shield area are elongated and permeable.

It was found that the highest concentration of solution has the greatest activity. Highest concentration of Detergent stopped the embryonic development of eggs and hatching percentage was zero. The study recorded the highest ovulation at 31°C for the two species, and incubation period decreased with the increasing of temperature .Hatching percentage was recorded high differences among their averages.

الخلاصة

استغرق هلاك القراد الصلب بنوعيه *Hyalomma ana. anatolicum* و *Ripicephlus turanicus* عدة ساعات عند وضعه في المحلول المنظف (1،2،3) بالتراكيز 23,3، 11,6، 7,7 على التوالي، ويعزى ذلك إلى الأغلفة المتصلبة التي تغطي جسم القراد والمتكونة عادة من طبقة سمنتية وشمع ،تمنع تسرب المحلول إلى داخل الجسم،وبذلك فقد سجل هلاك الإناث قبل التزاوج في مدة اقل من الذكور لان الطبقة المتصلبة لاتغطي كل جسم الأنثى و سجلت اليرقات مدة اقصر وهذا يعزى الى الشفافية ورقة الطبقة المتصلبة في حين إن المدة ازدادت عند الحوريات لأنها أكثر تصلبا وقلت عند الإناث البالغات الممتلئات لان الأغلفة الجسمية متمددة وأكثر مسامية بسبب تطاولها وكبر حجمها وامتلائها بالدم.وظهر إن المحلول الأكثر تركيز هو أكثر فاعلية كما أظهرت النتائج هلاك الأجنة داخل البيوض المعرضة للمحلول المنظف وان نسبة الفقس كانت صفر.بينت النتائج أعلى معدل للاباضة عند درجة 31 م° للنوعين على حد سواء وان فترة الحضانة تقصر مع ازدياد درجة الحرارة وان نسب الفقس سجلت تفاوتا كبيرا في معدلاتها.

المقدمة

القراد طفيليات خارجية ماصة لدم الإنسان والحيوانات الاقتصادية وحيوانات الزينة وحتى الحيوانات البرية، وهي لاتقل أهمية عن أنواع الحشرات الناقلة للأمراض فهي تنقل الأمراض المعدية والسامة (1)لاسيما القراد الصلب الذي ينقل للإنسان أمراضا عديدة منها: مرض لايم Lyme disease(2) إضافة إلى الأمراض التي ينقلها للحيوانات الاقتصادية والبرية على حد سواء مثل البابيزيا والانابلازما Babesiosis&Anaplasmosis(3،4).فضلا عن تسجيل حالات البابيزيا في الإنسان مؤخرا(5،6)،كما إن مرض الثايليريا من الأمراض المتوطنة في العراق في الأبقار(7) فالقراد هو الناقل الرئيسي للمرض لاسيما في المناطق الحارة والدافئة(8)

استنبط الإنسان طرقا وأساليب شتى في القضاء على القراد وإبادتها ،فقد ذكر (9)عددا من الطرق تنحصر في: الطرق الآلية،والطرق الوقائية،والطرق الطبيعية ،والطرق الكيميائية،ثم

ذهب بعض الباحثين إلى المكافحة بواسطة أشعة كاما(10)،كما ذكر(11) إن بعض الطيور(الزر زور والعقعق وابوقردان) تعتبر أعداء طبيعية تفيد في التخلص من القراد وقد فسر(12) المكافحة الإحيائية على أنها قمع للآفات سواء كانت حيوانات أو نباتات بواسطة أعدائها الطبيعية لاسيما الحشرات فهي إذن النقيض المباشر للوسائل الصناعية في المكافحة.ولكن بعض الباحثين في هذا الموضوع ينظرون له نظرة أوسع ويضعون تحت المكافحة الإحيائية جميع العوامل الأخرى مثل المنافسة بين الأنواع المختلفة وإبادة العوائل المتبادلة،وتربية وتبني السلالات المنيعة وكذلك الدراسات الزراعية وتأثير الرعي وغيرها.
مهما قيل عن المواد المبيدة والمستعملة لقتل القراد او الحشرات في المنازل والمحلات الأخرى بأنها قليلة الضرر ومهما كانت أنواعها فانه يجب على سكنة المنازل أن يتخذوا الاحتياطات اللازمة وإتباع التوصيات والتعليمات المعطاة لأنها خطرة على الإنسان ويجب الاحتراس والاحتياط منها .أجريت هذه الدراسة لبيان تأثير المنظفات(مسحوق الغسيل) detergents في مكافحة بعض أنواع القراد مختبريا وبيان تأثيرها في مراحل حياته مع عوامل حياتية أخرى كتاثير درجة الحرارة على معدل الاباضة اليومي وفترة الحضانة ونسبة الفقس .

المواد وطرائق العمل

تحضير المحلول-
المادة الكيميائية المستعملة هي مسحوق الغسيل detergent ومكوناته هي : سيليكات الصوديوم،كربوكسي مثيل سليلوز الصوديوم ،كبريتات الصوديوم ،مواد متفلورة ،كبريتات تليونات الصوديوم. (الموضحة ادناه).
تركيز المادة الفعالة 50 غم / 10 لتر ماء.
تم وزن 7 غم من المسحوق وهو يساوي تقريبا ملعقة طعام .وتم تحضير ثلاث محاليل بتراكيز مختلفة كالأتي:
1- تم تحضير المحلول (1) : بإذابة 7غم من مسحوق الغسيل في 60 سم3 ماء بتركيز23.3.
2- تم تحضير المحلول(2): بإذابة 7غم من مسحوق الغسيل في 120 سم3 ماء بتركيز 11.6.

3- تم تحضير المحلول(3): بإذابة 7غم من مسحوق الغسيل في 180 سم3 ماء بتركيز7.7.
عينات القراد- جمعت عينات القراد من الحيوانات الاقتصادية(الأغنام والأبقار والماعز) بوساطة الملقط والقطن الطبي المحتوى على الكحول.
تضمن العمل الأجزاء الآتية:
الجزء الأول: تم جمع (21)عينة من القراد الصلب نوع *Hyalomma ana. anatolicum*(18 ذكور و 3 إناث) و (12)عينة قراد من نوع *Ripicephlus turanicus* (8 ذكور و 4 اناث) و (30) يرقة و(8) حورية و(9) أنثى ممتلئة.
وضعت مجاميع القراد الحية في صحن بتري ملى بالمحاليل المحضرة سابقا(1،2،3) لدراسة مدة الهلاك بواسطة عداد وقتي ثم فحصت العينات تحت المجهر الضوئيX2, 4X لتشخيص النوع في مختبر مركز بحوث ومتحف التاريخ الطبيعي للفترة من شهر أيار إلى نهاية شهر تشرين الاول2008 وهي فترة ارتفاع نسبة إصابة الحيوانات الاقتصادية بالقراد في العراق.وقد اختير النوعين *Hyalomma ana. anatolicum* و *Ripicephlus turanicus* للدراسة لانها اكثر الانواع شيوعا في الحيوانات الاقتصادية (11).
استخدم في تحليل البيانات إحصائيا اختبار مربع كاي Chi Square X2 وذلك لمعرفة الفروقات المعنوية في فعالية التراكيز الثلاثة للمحلول المنظف.
الجزء الثاني:تم جمع عينات أخرى من الإناث الممتلئة (10)عينة لكل نوع في شهر أيار حيث تتراوح درجات الحرارة 30- 40 مº للدراسة المختبرية ووضعت كل أنثى على حدة في قنينة زجاجية بارتفاع 5,5 سم وبقطر 2,5 سم ثم نقلت الإناث إلى صحن بتري وعزلت كل أنثى

على حدة في صحن بتري يحوي ورقة ترشيح ترطب يوميا بالماء المقطر لغرض مراقبة وضع البيض مع مراعاة قياس درجات الحرارة اليومي.وقد فحصت الأواني يوميا لتجديد الهواء ولرفع ما وضع من البيض في أطباق جديدة تحمل نفس المعلومات لحساب المعدل اليومي لوضع البيض ودراسة فترة الحضانة ونسبة الفقس .وقد كررت هذه العملية يوميا إلى انقطاع البيض.

الجزء الثالث:اخذت عزلة بيض واحدة(ما يقارب 360بيضة) من كل نوع في طبق منفصل وأضيف لها المحلول(1) مع الفحص اليومي تحت المجهر الضوئي لملاحظة تأثير المحلول المنظف في نمو الاجنة وقد تم تصوير البيوض خلال مراحل التطور .

النتائج و المناقشة

ظهر من وضع (21)عينة من القراد الصلب نوع *Hyalomma ana. anatolicum*(18 ذكور و 3 إناث) في المحلول المنظف(1،2،3) إن مدة هلاك الذكور تتراوح بين (4.5 – 5.5 ساعة) بينما مدة هلاك الإناث البالغة تتراوح بين(4-5 ساعة) .وظهر من وضع (12)عينة قراد من نوع *Ripicephlus turanicus* في المحلول المنظف (1،2،3) إن مدة هلاك الذكور تتراوح بين (5-6 ساعة) بينما مدة هلاك الإناث البالغة تتراوح بين (4-5 ساعة) .بينما ظهر إن مدة هلاك اليرقات (1.5 – 1.75 ساعة) والحوريات (2.5 – 3.5 ساعة) والإناث الممتلئات (2-2.5 ساعة) جدول 1 . اظهر التحليل الإحصائي وجود فرق معنوي $P<0.01$ بين التراكيز الثلاثة للمحلول المنظف،وإن المحلول الأول بالتركيز 23.3 هو أكثر فاعلية.شكل4.

سجلت نسبة الفقس (صفر) لعزلة البيض المعرضة للمحلول المنظف (1بالتركيز23.3) ولكلا النوعين جدول 2 .

معدل عدد البيض:

تبين إن اعلى معدل لعدد البيض الموضوع من الاناث نوع *Hyalomma ana. anatolicum*

،والإناث نوع *Ripicephalus turanicus* قد سجل عند درجة حرارة 31 م°.جدول(3)وجدول (4).

المعدل اليومي للاباضة:

عند ملاحظة فترة الاباضة وارتباطها بالمعدل اليومي للاباضة للنوعين قيد الدراسة نلاحظ إن أعلى إنتاجية سجلت في الأيام (3،5) للنوع *Hyalomma ana ana.* وأعلى إنتاجية سجلت في الأيام (3،4) للنوع *Ripicephalus turanicus* ثم يتدرج المعدل اليومي لإنتاج البيض بعد نهاية الأسبوع بالانحدار مع ارتفاع درجات الحرارة إلى انقطاع البيض في اليوم الثامن عند درجة حرارة 37 م°.

فترة الحضانة:

بدا فقس البيض في اليوم السادس عشر وانتهى في اليوم السابع والعشرين في فترتين تراوحت فترة الحضانة القصيرة بين (16 - 20) يوم وفترة الحضانة الطويلة (20 -27) يوم لكلا النوعين في درجة حرارة المختبر 30- 32 م°ليلا و40 - 42 م° نهارا.

نسبة الفقس:

ظهرت نسب الفقس تفاوتا كبيرا في معدلاتها ولكلا النوعين قيد الدراسة فقد تراوحت بين 77% -4 % في النوع*Hyalomma ana. anatolicum* و82.8% - 8.6% في النوع *Ripicephalus turanicus*في درجة حرارة المختبر.

أظهرت النتائج بطيء هلاك نوعي القراد الصلب قيد الدراسة عند وضعهما في المحلول المنظف(1،2،3) بشكل عام وهذا قد يعزى إلى الأغلفة المتصلبة Sclerotized

shieldsالتي تغطي جسم القراد والمتكونة عادة من طبقة سمنتية وشمع cement and waxتمنع تسرب المحلول الى داخل الجسم، لكن قد يتسرب الى الجسم عن طريق الفتحات الطبيعية(فم،مخرج) والمجاري التنفسية او من خلال جدار الجسم نفسه لكن يستغرق ذلك بضع ساعات ثم يبدا عمله فآلية عمله في إزالة الدهون هي آلية فيزياوية .(13)
وهذا ينسجم مع ماسجلته الاناث من قصر مدة الهلاك (4-5 ساعة) مقارنة بالذكور لان الطبقة المتصلبة لاتغطي كل جسم الانثى و سجلت اليرقات مدة اقصر (1.5 -3.5 ساعة)لكل التراكيز، وهذا يعزى الى الشفافية ورقة الطبقة المتصلبة في حين ان المدة ازدادت عند الحوريات (2.5 -3.5 ساعة) لانها اكثر تصلبا وتقل عند الاناث البالغات الممتلئات (2 -2.5 ساعة) لان الاغلفة الجسمية متمددة واكثر مسامية بسبب تطاولها وكبر حجمها وامتلائها بالدم.وهذا يتفق مع ماذكره (14) حول المبيدات فان كمية المبيد التي توجد داخل الجسم تتوقف على سرعة نفاذ المبيد الى داخل الجسم وسرعة هدمه داخل الجسم وافرازه منه. .
اظهر التحليل الإحصائي وجود فرق معنوي $P<0.01$ بين التراكيز الثلاثة للمحلول المنظف،وإن المحلول الأول هو أكثر فاعلية في هلاك القراد بمختلف ادوار حيا ته لأنه الأكثر تركيز(23.3)،ولكن طبقا لهذه النتائج لايمكن اعتبار المنظفات كمبيدات فعالة للقراد وأطواره اليرقية لبطء هلاك العينات التي استغرقت عدة ساعات . كما اظهرت النتائج انبعاج البيوض المعرضة للمحلول المنظف الاول الاكثر تركيزمنذ الايام الأولى (شكل1) و هلاك الأجنة داخل البيوض في الايام الاخيرة من الحضانة (شكل 2) مقارنة بالحالة الطبيعية للبيوض (شكل 3) وهذا ماأثبتته نسبة الفقس حيث كانت صفر%ولكلا النوعين وهذا يعني ان المحلول المنظف فعال لمكافحة البيوض وقتل الأجنة وهذا يفيد في تنظيف جدران وأرضيات حظائر الحيوانات حيث تضع إناث القراد البيض.

معدل عدد البيض:

بينت النتائج اعلى معدل للاباضة كان عند درجة 31 مºللنوعين على حد سواء وهذا يمثل تكيفا في هذه العملية من قبل هذين النوعين للدرجات الحرارية العالية وهذا يتفق مع ماذكره(11) بان جميع الأنواع توضع الغالبية العظمى من البيض عند الدرجات(22 – 32 مº) فيما يشكل البيض الموضوع في باقي الدرجات الحرارية نسبة ضئيلة.

المعدل اليومي للاباضة:

ان المعدل اليومي للاباضة يكون مرتفعا ضمن معدلات الحرارة المناسبة كما في العمليات الحياتية الأخرى بينما يضطرب كثيرا عند الدرجات الحرارية المتطرفة 37 مº. ان تسجيل اعلى المعدلات عند 31 مºيرتبط مباشرة بكونها الدرجة الاكثر ملائمة لسير العمليات الحياتية.

فترة الحضانة:

سجلت فترة الحضانة القصيرة(16 -20)يوم أعلى نسب فقس للبيوض 77 – 70,3 % للنوع *H.ana.anatolicum*و82,8 – 70,5 % للنوع *R. turanicus* بالرغم من اختلاف أحجام كتل البيض وإنها ليست الكتل الأكبر وقد يعزى هذا الى اختلاف درجات الحرارة للعينات الموضوعة في المختبر بدرجة 30 - 32 مº ليلا و40 – 42 مº نهارا يدل على ان زيادة الحرارة تقلل من الفترة اللازمة لحضانة البيض وهذا يتفق مع(15) عند حديثه عن النويع *Hyalomma ana. anatolicum.* فقد سجل اقصر الفترات بين 22-32 مº ولغرض المقارنة فان النتائج الحالية تتفق مع(16) الذي سجل 23-26 يوما في الظروف المختبرية 20 مº مقابل 9 - 12 يوما في درجة حرارة 27 مº.

نسبة الفقس:

تعتمد نسبة الفقس على بعض العوامل منها درجات الحرارة و حجم كتلة البيض فكلما ازداد حجم كتلة البيض ازدادت نسب الفقس (17).سجلت نسب الفقس تفاوتا كبيرا في معدلاتها تراوحت بين 77% -4 % في النوع *H. ana.anatolicum* و82.8 % - 8.6%في النوع

R. turanicus ،وهذا قد يعزى إلى تفاوت درجات الحرارة في منتصف شهر أيار إلى منتصف شهر حزيران حيث تراوحت درجات حرارة المختبر بين 30 -32 مº ليلا و 40 – 42 مº نهارا ، لاسيما وان درجات الحرارة المثلى لسرعة تطور اليرقات داخل البيوض وفقسها غير متماثلة، ويعزى ذلك إلى بعض المشاكل العملية التي غالبا ماتواجه عند إجراء الدراسات الحياتية في درجة حرارة المختبر لكن هذا التفاوت قد يفسر لنا ظهور الثورات المرضية لمرض الثايليريا في الحيوانات الحقلية لاسيما في الأبقار في أشهر الربيع والخريف لاسيما وان القراد الناقل الرئيسي للمرض وان ارتفاع إصابة الحيوانات الحقلية بالقراد يزداد في (أيار وحزيران)ثم (أيلول وتشرين الأول) . (7)

جدول 1-: مدة هلاك بعض أنواع من القراد الصلب عند وضعها في المحلول المنظف.

الاسم العلمي	الجنس	مدة الهلاك بالساعة المحلول(1)	المحلول(2)	المحلول(3)
Hyalomma ana. anatolicum	♂	5 - 4.5	5.5 - 5	5.5- 5
	♀	4.5 -4	5 - 4.5	5 – 4.5
	♂	5.5 – 5	6 – 5.5	6 - 5.5
	♀	4.5 – 4	5 – 4.5	5 – 4.5
Ripicephlus turanicus	يرقة	1.75 – 1.5	3.5 – 3.25	3.5 – 3.25
	حورية	2 – 1.5	2.5 – 2	2.5 – 2
	ممتلنة	2.5 – 2	2.5 – 2	2.5 – 2

***يوجد فرق معنوي P<0.01 بين التراكيز الثلاثة للمحلول المنظف.**

جدول -2: نسبة الفقس بعد تعرض البيض للمحلول المنظف الأول ولكلا النوعين.

عدد البيض	نسبة الفقس
360بيضة	صفر%

جدول-3:بعض المعايير الحياتية للقراد نوع*Hyalomma ana. anatolicum* مختبريا لشهري أيار وحزيران 2008 .

المعيار الحياتي	اليوم الأول	اليوم الثاني	اليوم الثالث	اليوم الرابع	اليوم الخامس	اليوم السادس	اليوم السابع	اليوم الثامن
درجة الحرارةمº	30	31	31	32	33	34	36	37
عدد البيض	324	391	1056	80	552	65	25	0
فترة الحضانة يوم	16 – 20	20 – 16	27 - 20	27 – 20	27– 20	27 – 20	27 – 20	0
نسبة الفقس%	77	70.3	68.5	3.75	64	18.4	4	0

جدول-4:بعض المعايير الحياتية للقراد نوع *Ripicephalus turanicus* مختبريا لشهري أيار وحزيران2008.

المعيار الحياتي	اليوم الأول	اليوم الثاني	اليوم الثالث	اليوم الرابع	اليوم الخامس	اليوم السادس	اليوم السابع	اليوم الثامن
درجة الحرارة م°	30	31	31	32	33	34	36	37
عدد البيض	320	390	1072	424	95	54	23	0
فترة الحضانة يوم	20 – 16	20 – 16	27- 20	27 – 20	27– 20	27 – 20	27 – 20	0
نسبة الفقس%	82.8	70.5	68.3	67.6	17.8	14.8	8.6	0

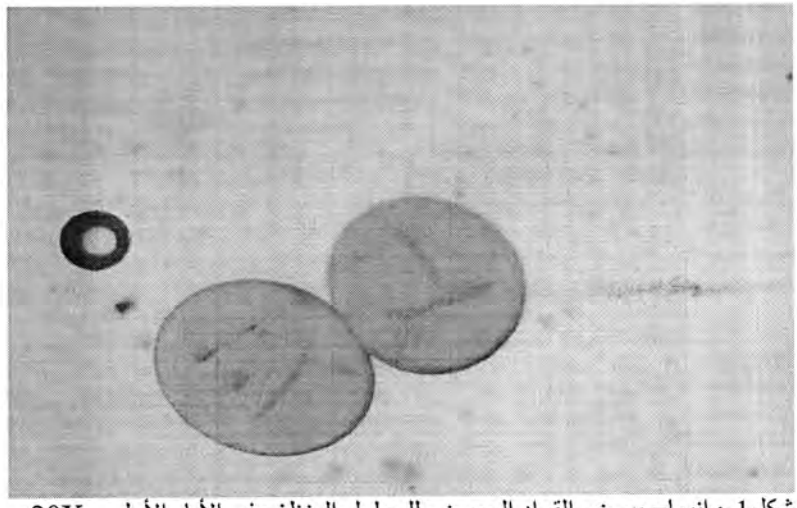

شكل1-: انبعاج بيوض القراد المعرض للمحلول المنظف في الأيام الأولى . 20X
للنوعين *Hyalomma ana. anatolicum* و *Ripicephalus turanicus* .

شكل-2 : انبعاج بيوض القراد المعرض للمحلول المنظف في الأيام الأخيرة .20X
للنوعين *Hyalomma ana. anatolicum* و *Ripicephalus turanicus* .

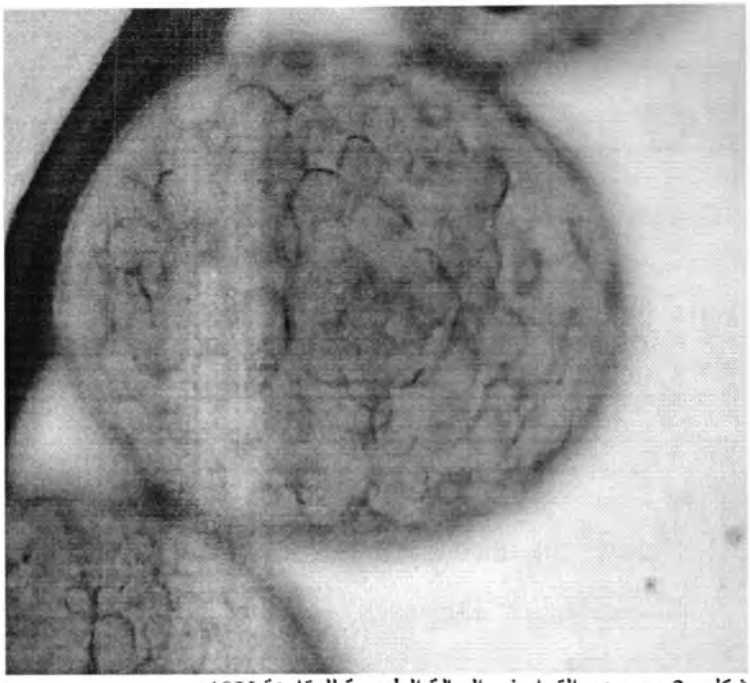

شكل -3 : بيوض القراد في الحالة الطبيعية للمقارنة.40X
للنوعين *Hyalomma ana. anatolicum.* و*Ripicephalus turanicus* .

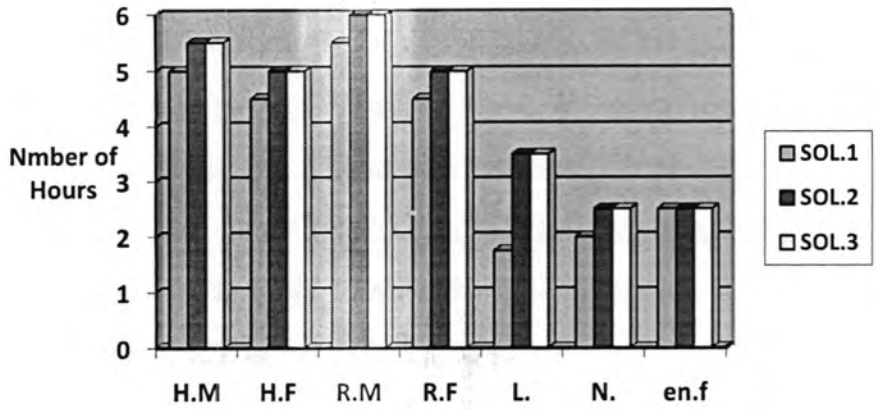

شكل- 4 : تأثير المحاليل الثلاثة على الأطوار المختلفة للقراد الصلب للنوعين
Hyalomma ana. anatolicum و*Ripicephlus turanicus* .

H. Male - *Hyalomma ana. anatolicum*
H. Female - *Hyalomma ana. anatolicum*
R. Male- *Ripicephlus turanicus*
R. Female- *Ripicephlus turanicus*
L. – Larvae
N. - Nymph
en. f. – engorged female

النشرة المرفقة للمحلول المنظف.

daryar multipurpose Detergent whiter and brighter
المحتويات: مواد فعالة STPP ،سيليكات الصوديوم ، كربوكسي مثيل سليلوز الصوديوم، كبريتات الصوديوم،مواد متفلورة، رائحة، كبريتات تليونات الصوديوم. صنع في إيران شركة تولى برس(مساهمة عامة) فزوين – المدينة الصناعية البرز WWW.tolypers.com

المصادر

1. Edlow, Jonathon A. Tick-Borne Diseases. Emergency Medicine - Infectious Diseases. www.emedicine.com. Retrieved on 2006-03-14(2005).
2. Rand, P.W. Abundance of *Ixodes scapularis* (acari:Ixodidae) after complete removal of deer from an isolated offshore island, endemic for Lyme disease. Journal of Medical Entomology 41:779-784(2004).
3. Wielinga, P. R., Gaasenbeek, C., Fonville, M., de Boer, A., de Vries, A., Dimmers, W., Akkerhuis Op Jagers, G., Schouls, L. M., Borgsteede, F., van der Giessen, J. W. B. Longitudinal Analysis of Tick Densities and Borrelia, Anaplasma, and Ehrlichia Infections of Ixodes ricinus Ticks in Different Habitat Areas in The Netherlands. *Appl. Environ. Microbiol.* 72: 7594-7601(2006).
4. Tsuji, N., Battsetseg, B., Boldbaatar, D., Miyoshi, T., Xuan, X., Oliver, J. H. Jr., Fujisaki, K. Babesial Vector Tick Defensin against Babesia sp. Parasites. *Infect. Immun.* 75: 3633-3640(2007).
5. Tsuji, M., Wei, Q., Zamoto, A., Morita, C., Arai, S., Shiota, T., Fujimagari, M., Itagaki, A., Fujita, H., Ishihara, C. Human Babesiosis in Japan: Epizootiologic Survey of Rodent Reservoir and Isolation of New Type of Babesia microti-Like Parasite. *J. Clin. Microbiol.* 39: 4316-4322(2001).

6. Kim, J.-Y., Cho, S.-H., Joo, H.-N., Tsuji, M., Cho, S.-R., Park, I.-J., Chung, G.-T., Ju, J.-W., Cheun, H.-I., Lee, H.-W., Lee, Y.-H., Kim, T.-S. First Case of Human Babesiosis in Korea: Detection and Characterization of a Novel Type of Babesia sp. (KO1) Similar to Ovine Babesia. *J. Clin. Microbiol.* 45: 2084-2087(2007).

7. Tarish H. Raheem A study of the role of the ticks in the epidemiology of the Theileria disease. MSC. Thesis submitted to the department of parasitology college of Veterinary Medicine University of Baghdad(1982).

8. Martin-Davila, P., Fortun, J., Lopez-Velez, R., Norman, F., Montes de Oca, M., Zamarron, P., Gonzalez, M. I., Moreno, A., Pumarola, T., Garrido, G., Candela, A., Moreno, S. Transmission of Tropical and Geographically Restricted Infections during Solid-Organ Transplantation. *Clin. Microbiol. Rev.* 21: 60-96(2008).

9. أبو الحب ،جليل كريم 1972 .الحشرات المنزلية ومكافحتها .مطبعة الايمان .العراق – بغداد شارع المتنبي رقم الايداع في المكتبة الوطنية -251 لسنة 220 صفحة(1972).

10. حمندي ،عدنان كاظم جواد امكانية استخدام اشعة كاما في السيطرة على القراد من نويع هايلوما انتولكم انتولكم . رسالة ماجستير كلية الطب البيطري – جامعة بغداد 53 صفحة(1978).

11. محمد ، محمد كاظم 1996 .دراسة حياتية – تصنيفية على القراد الصلب لبعض الحيوانات الاليفة والبرية من العراق.رسالة دكتوراه .كلية العلوم .جامعة بغداد114 صفحة.

12. امز .ا.د. ترجمة الدكتورة سميرة الزبادي . حياة الحشرات.دار الفكر العربي باشراف الادارة العامة للثقافة وزارة التعليم العالي 437 صفحة(1963).

13. Shreve R.N.orris Chenical process Industries .Third Edition International student edition.Toshp printing co., LTD. , Tokyo ,Japan 905 pages(1967).

14. طبوزاده ،اميرة حسين مقاومة الحشرات والقراد والحلم لمبيدات الافات .المكتبة الزراعية.دار المعرف 1119 كورنيش النيل .فرع الاسكندرية 42 شارع سعد زغلول -2 ميدان التحرير (المنشية).566 صفحة(1966).

15. Snow, K.R. The life history of *Hyalomma anatolicum anatolicum* koch 1844 (Arach.Aran.Ixodidae) under laboratory conditions .Parasitology ;59:105-122(1969).
16. Pomerantsev, B.I. Fauna of USSR Arachnida, 4.no.2 pp.224 Acad.USSR, MOSCOW(1950).
17. Martho ,J.A.R.,Rooha, U.F.,Moraes,F.R.,Ferrari, O.,Costa, A.J. Ecology of ticks XVI- aportable wet chamber of outdoor observations of tick egg laying and egg hatching . Ars.Vet. 2(2):221-231(1988).

حزم الطاقة و عزم القصور الذاتي لنواة Er(A=170) شديدة التشوه ذات التناظر الديناميكي SU(3)

إيمان طارق العلوي و عطاء علي حسن
قسم الفيزياء/ كلية العلوم /الجامعة المستنصرية

تاريخ تقديم البحث 2009/6/20 - تاريخ قبول البحث 2010/10/5

ABSTRACT

In this work,the energy bands and the moment of inertia for strongly deformed even-even Er(A=170) nucleus have been studied , the dynamical symmetry SU(3) has been predicated for this nucleus, using the Interacting Boson Model (IBM-1) and the Variable Moment of Inertia (VMI).
In this research the rotational energy and the moment of inertial, the softness coefficient; the cross bands; the back bending have been calculated for this nucleus and their dependence on the angular momentum and their relation with angular momentum .The calculated results have been compared with the available experimental data.

الخلاصة

تم خلال البحث الحالي دراسة حزم الطاقة و عزم القصور الذاتي لنواة Er(A=170) الزوجية- زوجية الشديدة التشوه ذات التناظر الديناميكي SU(3) باستخدام نموذج البوزونات المتفاعلة الأول (IBM-1) ونموذج عزم القصور الذاتي المتغير (VMI) وقد تم خلال البحث أيضا حساب الطاقة الدورانية لعزم القصور الذاتي ومعامل الليونة وتقاطع الحزم وظاهرة الانحناء الخلفي وعلاقتها بالزخم الزاوي .لقد تم مقارنة نتائج الحسابات مع النتائج العملية المتوفرة.

المقدمة

أاقترح نموذج البوزونات المتفاعلة (Interacting Boson Model) (IBM) في عام (1974) من قبل (Arima and Iachello)[1]. في هذا النموذج يتم وصف المستويات التجميعية الواطئة (Low Lying Collective States) للنوى المتوسطة والثقيلة (الزوجية-زوجية) والبعيدة عن المدارات المغلقة والمسيطر عليها بواسطة تهيجات البروتونات والنيوترونات التكافؤية (Valance Nucleons) أي النيوكليونات التي تقع خارج ابعد مدار مغلق في النواة، لتكون جسيمات مزدوجة متماثلة من البروتونات أو النيوترونات والتي تسمى بالبوزونات ذات زخوم زاوية 0 او 2 (j=0,2) حسب الحالة التي يكون فيها البوزون، فالبوزون ذو الزخم الزاوي (j=0) يسمى بـ (s-boson) ويرمز له (N_π)، بينما الذي يمتلك زخماً زاوياً (j=2) يرمز له (N_υ) ويسمى بـ (d-boson) وان العدد الكلي للبوزونات هو ($N=N_\pi+N_\upsilon$) [1,2,3].

حيث ان N_π تمثل عدد البوزونات من نوع بروتون-بروتون.
و N_υ تمثل عدد البوزونات من نوع نيوترون-نيوترون.

اما نموذج عزم القصور الذاتي المتغير فقد تم اقتراحه من قبل (Mariscotti) وجماعته عام (1969)[4] لمعالجة الاختلاف بين قيم مستويات الطاقة العملية والنظرية للنوى الدورانية اذ افترضوا ان قيمة عزم القصور الذاتي تزداد بزيادة قيمة الزخم الزاوي (L) وتم الحصول "من خلال استخدام هذا النموذج" على قيم مقاربة لقيم مستويات الطاقة العملية لهذا النوع من النوى التي تمتلك عزم قصور ذاتي عالي وليونة (Softness) نووية صغيرة عندما تكون في حالتها الأرضية[2].

لقد تم اكتشاف ظاهرة الانحناء الخلفي (Back Bending) من قبل (Johnson) وجماعته عام (1971)[5] اذ وجدوا ان عزم القصور الذاتي عند زخوم معينة تزداد بشكل واضح

ويرافق ذلك نقصان في قيمة الطاقة الدورانية في بعض النوى. وفي حالة عدم ظهور الانحناء الخلفي فهذا يعني انه لا تأثير لعزم القصور الذاتي على تشوهها. وهناك تفسيرات لسبب حدوث هذه الظاهرة:

1. تقاطع الحزم Band Crossing

تتلخص ظاهرة تقاطع الحزم على انه اذا كان لدينا حزمة طاقة مثل حزمة بيتا (β-band) او حزمة كاما (γ-band) ذات عزم قصور ذاتي ϑ_2، وكانت حزمة الحالة الأرضية (g-band) ذات عزم قصور ذاتي ϑ_1 بحيث ان $(\vartheta_2 > \vartheta_1)$ فسينتج عن ذلك تقاطع بين الحزمتين عند زخم زاوي معين L_c (L_{cross}) والمقصود بهذا التقاطع هو ان حزمة الطاقة ذات عزم قصور ذاتي عالي سوف تحل محل طاقة ذات عزم قصور ذاتي واطئ عند زيادة الزخم الزاوي عن L_c [6].

2. تأثير قوة كوريولس Corielis Force Effect

يزداد تأثير قوة كوريولس عند الزخوم الزاوية العالية على النيوكليونات التي لها زخم زاوي كبير، وهذا يؤدي إلى فك الازدواج (Depairing) بين زوج أو أكثر من هذه النيوكليونات وان فك ازدواج الزوج الاول يكافئ ظهور حزمة جديدة هي حزمة شبيهي الجسيمات (Two Quasi Particles) التي يحتمل ان تقطع الحزمة الأرضية (g-band) عند زخم زاوي معين وتبقى حزمة الحالة الأرضية (g-band) كاملة الازدواج (Completely Paired)[7]. في عام (2007) قام كل من (Turkan and Maras)[8] بدراسة نموذج البوزونات المتفاعلة (IBM) ووصف الخواص النووية التجميعية عبر مدى واسع للنوى والذي يعتمد أساسه على تقنيات الجبر العام لنظرية الزمر (Group Theory). ونموذج (IBM) يكون استعماله واسعاً لوصف مستويات رباعي القطب التجميعية للنوى المتوسطة والثقيلة وان الصيغة الأولى لنموذج (IBM-1) لا تميز بين بوزونات البروتونات والنيوترونات، ولاحظوا ان النوى الزوجية-زوجية (Even-Even) تكون متميزة بدراسة الحزم المشوهة بشدة (Strongly Deformed Bands). وفي عام (2008) قام (Sönmezoğlu) وجماعته[9] بتفسير خواص التناظر للنوى المشوهة (Deformed Nuclei) الزوجية-زوجية (Even-Even) ضمن إطار نموذج البوزونات المتفاعلة (IBM) واستخدموا نموذج عزم القصور الذاتي المتغير (VMI) (Variable Moment Inertia) لوصف خواص التناظر واعتمدوا في الحسابات على حزمة المستوي الأرضي للنوى المشوهة الزوجية-زوجية.

الاسس النظرية

يمكن كتابة مؤثر دالة هاملتون بدلالة المولدات الثمانية للزمرة الوحدوية الخاصة لـ SU(3) (SU(3) Special Unitary Group)، حيث تأخذ مصفوفة هذا المؤثر شكلا قطرياً في هذه الزمرة، وقد بين (Elliott) ان مؤثر دالة هاملتون يكتب بالصيغة الآتية [1,2,3,10]:

$$\hat{H} = a_1(\hat{L}.\hat{L}) + a_2(\hat{Q}.\hat{Q}) + a_3(\hat{U}.\hat{U}) + a_4(\hat{V}.\hat{V}) \qquad ...(1)$$

حيث أن $\hat{L}, \hat{Q}, \hat{U}, \hat{V}$ هي مؤثرات دالة هاملتون وأن a_1, a_2, a_3, a_4 هي الاعلومات يمكن الحصول عليها عند أفضل تطابق (Fitting).

وبالإمكان إيجاد القيم الذاتية (Eigen Values) بصورة تحليلية (Analytically) وتأخذ الحالات الذاتية (Eigen States) الصيغة الآتية [2,10]:

$$\left| \begin{array}{cccc} U(6) \supset & SU(3) \supset & O(3) \supset & O(2) \\ \downarrow & \downarrow & \downarrow & \downarrow \\ [N] & (\lambda,\mu)\tilde{\chi} & \mathrm{L} & \mathrm{M_L} \end{array} \right\rangle \qquad ...(2)$$

حيث ان:

N: العدد الكلي للبوزونات (Total Number of Bosons) = (N_π+N_υ).
N_π: عدد بوزونات البروتونات (Proton Bosons Number).
N_υ: عدد بوزونات النيوترونات (Neutron Bosons Number).
ان N تشير الى التمثيل غير القابل للاختزال المتناظر كليا للزمرة الوحدوية U(6) (Totally Symmetric Irreducible Representation of U(6)).
التمثيل المتناظر تعني ان البوزونات تتميز بدوال موجية متناظرة (Symmetrical Wave Functions). اما (λ,μ) فهي عبارة عن تمثيلات غير قابلة للاختزال للزمرة SU(3) (Irreducible Representation of SU(3)). وان L و M_L تمثلان الزخم الزاوي ومسقطه على المحور z على التوالي، وان $\tilde{\chi}$ هو عدد كمي اضافي لـ Vergados [2,3] له علاقة بمسقط الزخم الزاوي.
ان معادلة الطاقة لحزمة الحالة الأرضية (Ground State Band) للنوى الدورانية تكتب بالصيغة التالية[2]:

$$E(L)=\frac{L(L+1)}{2\vartheta} \qquad ...(3)$$

حيث ان:L : هو الزخم الزاوي للنواة ، ϑ : هو عزم القصور الذاتي للنواة بوحدة $(MeV)^{-1}$ وحسبت من وحدات $\vartheta/\hbar^2$.
لم يتمكن نموذج عزم القصور الذاتي للنوى الدورانية من وصف مستويات الطاقة بشكل جيد لافتراضه ثبات مقدار عزم القصور الذاتي، لذلك تم افتراض نموذج عزم القصور الذاتي المتغير (VMI) (Variable Moment of Inertia Model) [9,11,12,13]، وقد تم في هذا النموذج ادخال مفهوم تغير عزم القصور الذاتي للنواة واعتباره كدالة للزخم الزاوي للنواة وذلك باضافة حد ثاني للمعادلة (3) من قبل (Mariscotti)[14] وكالاتي:

$$E(L)=\left[\frac{L(L+1)}{2\vartheta(L)}+\frac{1}{2}C(\vartheta(L)-\vartheta_o)^2\right] \qquad ...(4)$$

حيث ان:
$\vartheta(L)$: عزم القصور الذاتي للنواة كدالة للزخم الزاوي (L).
ϑ_o : عزم القصور الذاتي للنواة في الحالة الارضية.
وان كل من C و ϑ_o اعلومات (Parameters) تتلائم قيمها مع القيم العملية لمستويات الطاقة.
اما معامل الليونة (Softness Coefficient) للنواة فيكتب بالشكل الاتي [3,9,11,14]:

$$\sigma=\frac{1}{2C\vartheta_o^3} \qquad ...(5)$$

لقد نجح هذا النموذج في وصف مستويات الطاقة للنوى الدورانية وحتى للنوى الاهتزازية.
ان ظاهرة الانحناء الخلفي (Back Bending) تحدث بسبب زيادة في عزم القصور الذاتي والتي يرافقها نقصان في الطاقة الدورانية عند زخوم زاوية معينة في بعض النوى. ان مربع الطاقة الدورانية وعزم القصور الذاتي تكتب بالشكل الاتي [9,11,12,13]:

$$(\hbar\omega)^2=\left[\frac{E(L)}{\sqrt{L(L+1)}}\right]^2 \qquad ...(6)$$

$$\frac{2\vartheta}{\hbar^2}=\frac{L(L+1)}{E(L)} \qquad ...(7)$$

$$(\hbar\omega)^2=\left[\frac{E(L\rightarrow L-2)}{\sqrt{L(L+1)}-\sqrt{(L-2)(L-2+1)}}\right]^2 \qquad ...(8)$$

ان الحد L(L+1) يقلل الى حدين L(L+1) و (L-1) (L-2) لذلك فان المعادلة (6) تصبح كالاتي للانتقالات الكامية لحزمة g وحزم β [11,12]:

$$(\hbar\omega)^2 = \left[\frac{E_\gamma}{\sqrt{L(L+1)} - \sqrt{(L-2)(L-1)}}\right]^2 \qquad ...(9)$$

$$(\hbar\omega)^2 = \left[\frac{E(L \to L-1)}{\sqrt{L(L+1)} - \sqrt{L(L-1)}}\right]^2 \qquad ...(10)$$

وبالمثل لحزم γ.

ومن المعادلة (7) نحصل على عزم القصور الذاتي لحزمة الحالة الأرضية (g-band) وحزم بيتا (β-bands)

$$\frac{2\vartheta}{\hbar^2} = \frac{L(L+1) - (L-2)(L-2+1)}{E(L \to L-2)} \qquad ...(11)$$

$$\frac{2\vartheta}{\hbar^2} = \frac{4L-2}{E_\gamma} \qquad ...(12)$$

وبالمثل لحزم γ

$$\frac{2\vartheta}{\hbar^2} = \frac{L(L+1) - L(L-1)}{E(L \to L-1)} = \frac{2L}{E_\gamma} \qquad ...(13)$$

حيث إن E(L→L-2) تمثل فرق الطاقة بين مستويين لهما زخم زاوي L و (L-2) في كل من حزمة الحالة الأرضية (g-band)، وحزم بيتا (β-band) اما E(L→L-1) فتمثل فرق الطاقة في حزمة كاما (γ-band) بين مستويين لهما زخم زاوي L و (L-1).

لقد تمت برمجة المعادلة (4) من خلال كتابة البرنامج (VMI.for) بلغة (Fortran 90) وباستخدام البرنامج التشغيلي (Compaq Visual Fortran V6.6) لتنفيذه، وذلك لغرض حساب عزم القصور الذاتي للنواة(L) ϑ.كما وظف هذا البرنامج لحساب مربع الطاقة الدورانية $(\hbar\omega)^2$ وعزم القصور الذاتي $\left(\frac{2\vartheta}{\hbar^2}\right)$ للحزمة الأرضية (g-band) وكل من حزمة بيتا (β-band) وحزمة كاما (γ-band) وذلك ببرمجة المعادلات (8 ← 13). كما وظف هذا البرنامج أيضا لحساب معامل الليونة (Softness Coefficient) للنواة ببرمجة المعادلة (5). حيث يتم تغذية برنامج (VMI.for) بالاعلومات C, ϑ_o, K كمدخلات لإجراء الحسابات إضافة لإدخال قيم مستويات الطاقة العملية والنظرية المحسوبة باستخدام (IBM-1) لغرض المقارنة.

وقد تم حساب معدل الجذر التربيعي للانحراف المعياري (Standard Deviation) من المعادلة الآتية[15,16]:

$$\text{Standard Deviation} = \left[\frac{1}{N}\sum_{i=1}^{N}\left|\left(E_{cal.} - E_{\exp.}\right)_i\right|^2\right]^{\frac{1}{2}} \qquad ...(14)$$

اما مربع كاي (Chi-Squared) الذي يمثل مدى ملائمة النموذج فقد تم حسابه من المعادلة الآتية[16]:

$$\chi^2 = \frac{(E_{cal.} - E_{\exp.})^2}{E_{cal.}^2} \qquad ...(15)$$

الحسابات و النتائج

ان معظم المستويات النووية المتهيجة والتي تمتلك زخماً زاوياً عالياً تنحل عن طريق انبعاث أشعة كاما وهنا تكمن إمكانية دراسة حقائق جيدة للتركيب النووي للانوية قيد الدراسة، إن الحركة الدورانية الجماعية (Collective Rotation Motion) للنواة تعتمد على حركة النيوكليونات بشكل متشاكهة (Coherently) لحركة النواة مسبباً بذلك دوران النيوكليونات حول محور يختلف عن محور التناظر النووي (Nuclear Symmetry Axis). هذا النوع من التهيجات يحدث في النوى المشوهة إذ إن النوى المشوهة لها عزم قصور ذاتي (Moment of Inertia) عالي مع محافظة حركة النيوكليونات المنفردة على عدم اضطرابها أثناء عملية الدوران المشوهة، ويبين الشكل (1) نوعين من النوى الدورانية الاول من نوع النواة المتطاولة (Prolate Nucleus) والتي تدور حول محور عمودي على محور التناظر النووي ويسمى بالدوران الجماعي (Collective Rotation) اما النوع الثاني من النوى الدورانية فتسمى بالنواة المفلطحة (Oblate Nucleus) فتدور حول محور موازي لمحور التناظر النووي والتي تظهر في ميكانيكيتها زخوم زاوية عالية ويسمى هذا النوع من الحركة النووية بالدوران غير الجماعي (Non-Collective Rotation).

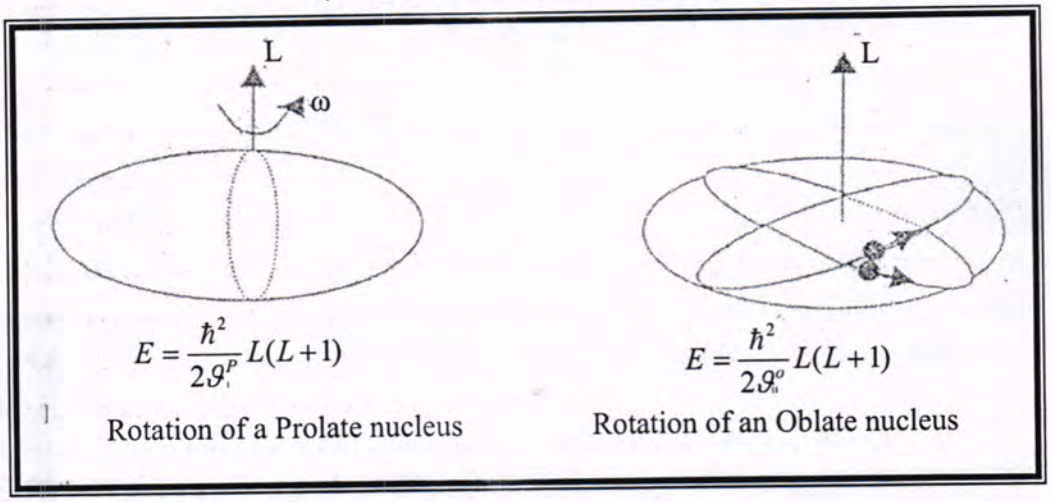

شكل -1: الحركة الدورانية الجماعية للنواة المتطاولة والحركة الدورانية غير الجماعية للنواة المفلطحة، حيث ان $\vartheta_{\parallel}^{o}, \vartheta_{\perp}^{o}$ تمثل عزم القصور الذاتي للنوعين على الترتيب[17].

وفي كلا النوعين عندما تكون الحركة الدورانية سريعة فان قوة كورلويس تحطم الازدواج (Pairing) الحاصل بين عدد من أزواج النيوكليونات مسببة بذلك ظهور حزمة شبيهي الجسيمات (Two-Quasi Particles) ومسببة شذوذاً عند زخوم زاوية معينة ($L^{\pi}>10^{+}$) في بعض النوى والتي تسبب ظاهرة الانحناء الخلفي (Back Bending)[17].

لقد تم حساب مستويات الطاقة وقيم عزم القصور الذاتي والطاقة الدورانية وفق نموذج عزم القصور الذاتي (VMI) ونموذج تفاعل البوزونات الاول (IBM-1) على اعتبار ان الحسابات الحالية لنواة Er(A=170) قيد البحث قد اعتمدت على ما يلي:

1. معادلة مؤثر دالة هاملتون في نموذج (IBM-1) معادلة (1).
2. معادلة الطاقة في نموذج عزم القصور الذاتي المتغير (VMI) معادلة (4).
3. معادلة مربع الطاقة الدورانية $(\hbar\omega)^2$ معادلة (9) و (10).

4. معادلة عزم القصور الذاتي $(2\vartheta/\hbar^2)$وفق نموذج (VMI) التي تفترض ان النواة جسم صلد معادلة (12) و (13) وحساب معامل الليونة σ معادلة(5).

ويبين الجدول (1) قيم اعلومات مؤثر دالة هاملتون لنموذج البوزونات المتفاعلة الاول (IBM-1) لأفضل تطابق (Fitting) مع القيم العملية للنواة قيد الدراسة $(^{170}_{68}Er_{102})$. ويبين هذا الجدول كذلك عدد بوزونات البروتونات (N_π) وعدد بوزونات النيوترونات (N_υ) والعدد الكلي للبوزونات (N) والاعلومات الخاصة بنموذج عزم القصور الذاتي المتغير (VMI) لأفضل تطابق أيضا والذي استخدم في الحسابات الحالية وذلك حسب حزم الطاقة الخاصة للنواة قيد الدراسة. كما تضمن هذا الجدول الاعلومات (Parameters) $C,(\vartheta_o/\hbar^2)$ وطاقة رأس الحزمة K (Band-Head Energy K) ومعامل الليونة σ (Softness σ) وقيم الانحراف المعياري (Standard Deviation) لكلا النموذجين (VMI) و (IBM-1) وفقاً للمعادلة (14) وكذلك قيم مربع كاي (Chi-Square) لكلا النموذجين (VMI)و (IBM-1) وفقاً للمعادلة (15) للنواة قيد الدراسة وحسب ترتيب الحزم.

ان معامل الليونة(σ) يتناسب عكسياً مع مكعب عزم القصور الذاتي بثبوت الاعلومة C أي انه كلما ازداد عزم القصور الذاتي قل معامل الليونة وان اقل عامل ليونة يعطي أعلى تشوه للنواة. كما ونلاحظ عند زيادة الزخم الزاوي L يؤدي الى زيادة في السرعة الدورانية للنواة $(\hbar\omega)^2$، حيث $L = \vartheta\omega$ ، وعندما تكون السرعة الدورانية للنواة $(\hbar\omega)^2$ كبيرة سيحصل زيادة في القوة الطاردة المركزية (Centrifugal Force) عندها ستبتعد الجسيمات عن مركز النواة ويحصل تشوه شديد في النواة يرافقه كبر في حجمها بشكل اهليليجي متطاول أو مفلطح. هذا من ناحية ومن ناحية أخرى نلاحظ ان عزم القصور الذاتي ϑ_o يزداد أيضا، هذا يؤدي إلى زيادة في الطاقة الدورانية، انظر المعادلة (4). وان هذا دليل على ان النواة تقع في المنطقة الدورانية لزمرة التناظر الديناميكي SU(3).

ونلاحظ من نتائج حسابات معامل الليونة لنواة $^{170}_{68}Er_{102}$ والمبينة في الجدول (1). ان النواة $^{170}_{68}Er_{102}$ تكون اقل تشوها في الحزمة الأرضية (g-band) منه في حزمتي بيتا و كاما (β,γ-bands) في حين ان عزم القصور الذاتي ϑ_o اقل ما يمكن في حزمة كاما (γ-band) ويزداد في الحزمة الأرضية وتليها حزمة بيتا ويعزى السبب إلى تأثير الاعلومة C في جعل عزم القصور الذاتي في حزمة كاما اقل منه في الحزمة الأرضية.

لقد تم حساب قيم مستويات الطاقة حسب ترتيب الحزم والتي تم الحصول عليها باستخدام كل من نموذج (VMI) ونموذج (IBM-1) وكذلك حساب مربع الطاقة الدورانية $(\hbar\omega)^2$ وعزم القصور الذاتي $(\vartheta/\hbar^2)$لطاقات الانتقالات الكامية (E_γ) لنواة قيد الدراسة $(^{170}_{68}Er_{102})$،والمبينة في الجدول (2) ويظهر من مقارنة النتائج التي حصلنا عليها توافقاً جيداً مع القيم العملية [18,19] وذلك من خلال قيم الانحراف المعياري ومربع كاي المحسوبة في العمل الحالي والتي ورد ذكرها في الجدول (1).

يبين الشكل (2) العلاقة بين عزم القصور الذاتي $(\vartheta/\hbar^2)$ للحزمة الأرضية (g-band) وحزمة بيتا (β-band) وحزمة كاما (γ-band) كدالة لتغيير الزخم الزاوي لنواة $(^{170}_{68}Er_{102})$ وفق كل من نموذج (VMI) ونموذج (IBM-1) المحسوبة في العمل الحالي مقارنة مع قيم عزم القصور الذاتي المحسوبة من قيم الطاقات العملية المتوفرة[20] ويلاحظ من الشكل (2) تطابق قيم عزم القصور الذاتي بشكل جيد لنموذج (VMI) مع القيم العملية للحزمة الأرضية وحزمة بيتا، في حين لا يعطي نموذج (IBM-1) تطابق ملحوظ لهاتين الحزمتين. لذلك يكون نموذج (VMI) اكثر ملائمة لحساب عزم القصور الذاتي من نموذج (IBM-1). اما قيم عزم القصور الذاتي لحزمة كاما فيوجد توافق ضعيف بين القيم العملية ونموذج (VMI) وذلك لقلة

وفرة القيم العملية لعزم القصور الذاتي (حيث توفرت قيمتان لنواة $^{170}_{68}Er_{102}$ فقط) وهذا لا يكفي لعملية تطابق حسابات حزمة كاما بأكملها مما جعل اختلاف واضح بالنتائج.
اما قيم عزم القصور الذاتي باستخدام (IBM-1) للشكل أعلاه ولحزمة كاما أيضا نلاحظ وجود توافق ضعيف بين القيم العملية والقيم المحسوبة في العمل الحالي. إضافة إلى ذلك نلاحظ تعرجاً واضحاً نتيجة تذبذب قيم عزم القصور الذاتي باستخدام (IBM-1)وهذا يعزى للأسباب الآتية:

1. عدم توفر القيم العملية الكافية لحزمة كاما لمستويات الطاقة ولعزم القصور الذاتي.
2. عدم التمييز بين بوزونات البروتونات (N_π) وبوزونات النيوترونات (N_υ) في نموذج (IBM-1) مما جعل اختلاف واضح بين القيم العملية والنظرية لمستويات الطاقة في حزمة كاما وهذا بالتالي يؤثر على نتائج حسابات عزم القصور الذاتي لنفس النموذج.
3. ان نواة ($^{170}_{68}Er_{102}$) تكون اشد تشوهاً في المستويات العالية وخصوصاً في حزمة كاما مما يجعل النواة تتذبذب بين الشكل الاهليليجي المتطاول والمفلطح أي بين التناظر الديناميكي SU(3) بشكلها المتطاول وبين التناظر الديناميكي SU(3) بشكلها المفلطح مروراً بالتناظر الديناميكي O(6)، وهذا مما يجعل عزم القصور الذاتي يتغير بشكل متعرج في هذه الحزمة.

الشكل (3) يبين حزم الطاقة كدالة للزخم الزاوي لنواة $^{170}_{68}Er_{102}$ حيث تظهر القيم العملية للطاقة مع نتائج الطاقة المحسوبة من نموذج عزم القصور الذاتي المتغير (VMI) تطابقاً جيداً.
ان ظاهرة تقاطع الحزم تحدث عند زخم زاوي معين L_c (L_{cross}) حيث تحل حزمة الطاقة ذات القيم العالية محل حزمة الطاقة ذات القيم الواطئة واللتان تمتلك نفس البرم للحزمتين. فعند تقاطع حزمتين فان جميع النيوكليونات يكون لها برم يساوي صفراً تحت تاثير تفاعل الارتباط المزدوج (Pairing Correlation Interaction) وفي هذه الحالة تعتبر النواة فائقة الميوعة وطاقتها الذاتية تكون اقل من طاقة الارتباط المزدوج ويكون للنواة عزم قصور ذاتي قليل. كما ان قوة كوريولوس (Coriolois Force) عند زيادة السرعة الزاوية (زيادة الطاقة الدورانية ($\hbar^2\omega^2$)) تعمل على فك الازدواج بين زوج او اكثر من ازواج النيوكليونات في بعض النوى مكونة حزمة طاقة متهيجة نتيجة انفصال نيوكليونين اواكثر في النواة (تسمى هذه الحزمة بحزمة شبيهي الجسيمات) فيكون زخمها الزاوي باتجاه محور الدوران وباقل طاقة دورانية واعظم زخم زاوي ليكونان مستوى دوران ذاتي يكون اساساً للحزم الدورانية ان عدم استقرار هذين المستويين يؤدي الى تقاطع الحزم المتهيجة للجسيمين مع الحزمة الارضية او حزمة بيتا او حزمة كاما[17].
اوضحت نتائج نموذج عزم القصور الذاتي المتغير (VMI) الموضحة في الشكل (3) ان نواة $^{170}_{68}Er_{102}$ لايوجد فيها تقاطع بين الحزم لانها تنتمي الى زمرة التناظر الديناميكي SU(3).
يبين الشكل (4) علاقة تغيير عزم القصور الذاتي كدالة لمربع الطاقة الدورانية، التي تم عرض نتائجها في الجدول (2)، حيث نلاحظ عدم وجود انحناءات في الحزمة الارضية وحزمة بيتا وحزمة كاما لكون التناظر الديناميكي من نوع SU(3).
اما التعرجات الواضحة في حزمة كاما لنواة $^{170}_{68}Er_{102}$ فتعزى الى نفس الاسباب التي تم مناقشتها.

الاستنتاجات

أثبت نتائج هذا البحث بأنه لايوجد أي تأثير عزم القصور الذاتي على التركيب النووي لنواة Er(A=170) شديدة التشوه ذات التناظر الديناميكي SU(3) ،وذلك يسبب عدم ظهور ظاهرة الانحناء الخلفي في حزم الطاقة لهذه النواة و احتوائها على قيم عالية لعزم القصور الذاتي و ما يقابلها من قيم واطئة جداً لمعامل الليونة (σ) و هذا مايؤكد بان هذه النواة شديدة التشوه.لقد نجح نموذج (VMI) في حسابات عزم القصور لنواة Er(A=170) ولكافة الحزم مقارنتاً مع القيم العملية، في حين لم يوفق نموذج (IBM-1) في ذلك.

جدول -1: قيم اعلومات مؤثر دالة هاملتون لنموذج البوزونات المتفاعلة الاول وقيم اعلومات نموذج عزم القصور الذاتي المتغير (VMI) لنواة Er(A=170).

Nuclei	Dynamical symmetry	Nπ	Nυ	N	Parameters		ε (MeV)	$\hat{P}\cdot\hat{P}$ (MeV)	$\hat{L}\cdot\hat{L}$ (MeV)	$\hat{Q}\cdot\hat{Q}$ (MeV)	$\hat{U}\cdot\hat{U}$ (MeV)	$\hat{T}\cdot\hat{T}$ (MeV)	CHI
$^{170}_{68}Er_{102}$	SU(3)	7	10	17	IBM-1		0.0000	0.0000	0.0150	-0.0110	0.0000	0.1002	-1.322785
					VMI Model	Bands	Parameters						
						g	$\vartheta_\sigma/\hbar^2$ (MeV)$^{-1}$	C (MeV)^3	K (MeV)	σ		Standard Deviation	χ^2
												Model	Model
												VMI IBM-1	VMI IBM-1
						g	39.0000	0.0090	0.0000	0.0009	0.0163 0.2269		0.001300 0.0137
						β	43.0000	0.0069	0.8909	0.0010	0.0017 0.0914		0.000002 0.0054
						γ	33.9500	0.0400	0.8325	0.0032	0.0114 0.0290		0.000100 0.0006

جدول -2: قيم مستويات الطاقة وطاقات الانتقال (النظرية والعملية) وقيم عزم القصور الذاتي ومربع الطاقة الدورانية لنواة Er(A=170) الزوجية-زوجية باستخدام نموذج عزم القصور الذاتي التمغير (VMI) ونموذج (IBM-1) ولكافة الحزم

Nucleus			Band		N_g	N_γ	N	Dynamical symmetry								
$^{170}_{68}Er_{102}$			g		7	10	17	SU(3)								
	Experimental		IBM-1 (pw)		VMI(pw)			Experimental			IBM-1 (pw)			VMI(pw)		
L^+	Energy (MeV) [18,19]	$\vartheta/\hbar^2$ (MeV) [20]	Energy (MeV) [18,19]	$\vartheta/\hbar^2$ (MeV) [20]	Energy (MeV) [18,19]	$\vartheta/\hbar^2$ (MeV) [20]	$L_i^+ - L_f^+$	E_γ (MeV) [18,19]	$(\hbar\omega)^3$ $(MeV)^3$ (pw)	$2\vartheta/\hbar^2$ $(MeV)^{-1}$ (pw)	E_γ (MeV) [18,19]	$(\hbar\omega)^3$ $(MeV)^3$ (pw)	$2\vartheta/\hbar^2$ $(MeV)^{-1}$ (pw)	E_γ (MeV) [18,19]	$(\hbar\omega)^3$ $(MeV)^3$ (pw)	$2\vartheta/\hbar^2$ $(MeV)^{-1}$ (pw)
0_1^+	0.0000	37.8300	0.0000	32.9977	0.0000	39.0000	$2_1^- - 0_1^+$	0.0785	0.0010	76.4331	0.0786	0.0010	76.2873	0.0767	0.0009	78.2173
2_1^+	0.0785	38.2166	0.0786	36.1437	0.0767	39.2167	$4_1^- - 2_1^+$	0.1816	0.0080	77.0925	0.1900	0.0088	73.6803	0.1774	0.0076	78.9244
4_1^+	0.2601	38.5463	0.2686	36.8402	0.2541	39.7048	$6_1^- - 4_1^+$	0.2810	0.0196	78.2918	0.3169	0.0249	69.4072	0.2745	0.0187	80.1386
6_1^+	0.5411	39.1459	0.5856	34.7036	0.5286	40.4276	$8_1^- - 6_1^+$	0.3719	0.0344	80.6668	0.4588	0.0524	65.3794	0.3668	0.0335	81.7774
8_1^+	0.9130	40.3334	1.0444	32.6897	0.8954	41.3405	$10_1^+ - 8_1^+$	0.4610	0.0529	82.4295	0.6167	0.0929	62.2214	0.4537	0.0513	83.7515
10_1^+	1.3740	41.2148	1.6552	31.1108	1.3492	42.3993	$12_1^+ - 10_1^-$	0.5376	0.0721	85.5654	0.7684	0.1473	59.8607	0.5350	0.0714	85.9789
12_1^+	1.9115	42.7865	2.4236	29.8608	1.8842	43.5661	$14_1^+ - 12_1^+$	-	-	-	0.9296	0.2157	58.0895	0.6109	0.0932	88.3905
14_1^+	-	-	3.3532	29.0448	2.4951	44.8102	$16_1^+ - 14_1^+$	-	-	-	1.0927	0.2982	56.7381	0.6818	0.1161	90.9325
16_1^+	-	-	4.4460	28.3691	3.1769	46.1079	$18_1^+ - 16_1^+$	-	-	-	1.2571	0.3947	55.6819	0.7481	0.1398	93.5639
18_1^+	-	-	5.7031	27.8409	3.9251	47.4417	$20_1^+ - 18_1^+$	-	-	-	1.4223	0.5054	54.8384	0.8103	0.1641	96.2542
20_1^+	-	-	7.1255	27.4192	4.7354	48.7985	$22_1^+ - 20_1^+$	-	-	-	1.5881	0.6302	54.1524	0.8688	0.1886	98.9807
22_1^+	-	-	8.7136	27.0762	5.6043	50.1688	$24_1^+ - 22_1^+$	-	-	-	1.7542	0.7689	53.5847	0.9240	0.2133	101.7276
24_1^+	-	-	10.4678	26.7924	6.5283	51.5459	-	-	-	-	-	-	-	-	-	-

جدول -2: (2/3)

Nucleus		Band		N	N	N	Dynamical symmetry											
$^{170}_{68}Er_{102}$		β		π	ν		SU(3)											
		IBM-1 (pw)		VMI(pw)		17			Experimental			IBM-1 (pw)			VMI(pw)			
L^+	Energy (MeV) [18,19]	$\vartheta/\hbar^2$ (MeV) [20]	Energy (MeV) [18,19]	$\vartheta/\hbar^2$ (MeV) [20]	Energy (MeV) [18,19]]	$\vartheta/\hbar^2$ (MeV) [20]	$L_i^+ - L_f^+$	E_γ (MeV) [18,19]	$(\delta re)^2$ (MeV)^2 (pw)	$2\vartheta/\hbar^2$ (MeV)^2 (pw)	E_γ (MeV) [18,19]	$(\delta re)^2$ (MeV)^2 (pw)	$2\vartheta/\hbar^2$ (MeV)^2 (pw)	E_γ (MeV) [18,19]	$(\delta re)^2$ (MeV)^2 (pw)	$2\vartheta/\hbar^2$ (MeV)^2 (pw)
0_2^+	0.8969		0.9069	42.5675	0.8969	43.0000	$2_3^+ - 0_2^+$	0.0689	0.0008	87.0827	0.0909	0.0014	66.0066	0.0696	0.00381	86.2679
2_3^+	0.9598	43.5414	0.9979	33.0033	0.9605	43.2671	$4_3^+ - 2_3^+$	0.1642	0.0066	85.2619	0.2789	0.0190	50.1846	0.1607	0.0063	87.1372
4_3^+	1.1240	42.6309	1.2769	25.1846	1.1211	43.8661	$6_3^+ - 4_3^+$	-	-	-	0.4776	0.0563	46.0665	0.2482	0.01528	886233
6_3^+	-	-	1.7544	23.0333	1.3693	44.7479	$8_3^+ - 6_3^+$	-	-	-	0.6637	0.1096	45.2025	0.3311	0.0273	90.6138
8_3^+	-	-	2.4181	22.6013	1.7004	45.8537	$10_3^+ - 8_3^+$	-	-	-	0.8398	0.1757	45.2547	0.4086	0.0416	92.9462
10_3^+	-	-	3.2578	22.6271	2.1091	47.1273	$12_3^+ - 10_3^+$	-	-	-	1.0082	0.2536	45.6281	0.4808	0.0577	95.6658
12_3^+	-	-	4.2659	22.8141	2.5899	48.5217	$14_3^+ - 12_3^+$	-	-	-	1.1686	0.3409	46.2076	0.5480	0.0749	98.5394
14_3^+	-	-	5.4346	23.1038	3.1379	50.0000	$16_3^+ - 14_3^+$	-	-	-	1.3198	0.4350	46.9764	0.6105	0.0931	101.5524
16_3^+	-	-	6.7544	23.4882	3.7484	51.5347	$18_3^+ - 16_3^+$	-	-	-	1.4638	0.5352	47.8207	0.6689	0.1117	104.6577
18_3^+	-	-	8.2182	23.9104	4.4173	53.1056	$20_3^+ - 18_3^+$	-	-	-	1.6119	0.6491	48.3916	0.7234	0.01307	107.820
20_3^+	-	-	9.8301	24.1956	5.1406	54.6982	$22_3^+ - 20_3^+$	-	-	-	1.7296	0.7475	49.7217	0.7747	0.1499	111.0164
22_3^+	-	-	11.596 8	24.8609	5.9153	56.3021	$24_3^+ - 22_3^+$	-	-	-	1.9637	0.9636	47.6678	0.8229	0.1692	114.2369
24_3^+	-	-	13.523 4	23.9339	6.7383	57.9097	-	-	-	-	-	-	-	-	-	-

جدول -2: (3/3)

Nucleus			Band		N_π	N_ν	N	Dynamical symmetry									
$^{170}_{68}Er_{102}$			7		7	10	17	SU(5)									
	Experimental		IBM-1 (pw)		VMI(pw)			Experimental				IBM-1 (pw)			VMI(pw)		
L^+	Energy (MeV) [18,19]	$\vartheta/\hbar^2$ (MeV) [20]	Energy (MeV) [18,19]	$\vartheta/\hbar^2$ (MeV) [20]	Energy (MeV) [18,19]]	$\vartheta/\hbar^2$ (MeV) [20]	$L_i^+ - L_f^+$	E_γ (MeV) [18,19]	$(\hbar\omega)^2$ (MeV)^2 (pw)	$2\vartheta/\hbar^2$ (MeV)$^{-1}$ (pw)	E_γ (MeV) [18,19]	$(\hbar\omega)^2$ (MeV)^2 (pw)	$2\vartheta/\hbar^2$ (MeV)$^{-1}$ (pw)	E_γ (MeV) [18,19]	$(\hbar\omega)^2$ (MeV)^2 (pw)	$2\vartheta/\hbar^2$ (MeV)$^{-1}$ (pw)
2_2^+	0.9320	-	0.9328	36.5474	0.9200	34.5773	$3_1^- - 2_2^+$	0.0785	0.059	76.4332	0.0909	0.0089	65.9848	0.0860	0.0072	69.745
3_1^+	1.0105	38.2166	1.0238	32.9924	0.0061	35.1632	$4_2^+ - 3_1^+$	0.0930	0.0085	86.0214	0.1282	0.0161	62.3879	0.1126	0.0125	71.0608
4_2^+	1.1035	43.0107	1.1520	31.1939	1.1187	35.8908	$5_1^- - 4_2^+$	-	-	-	0.1816	0.0326	55.0812	0.1377	0.0188	72.6290
5_1^+	-	-	1.3336	27.5406	1.2563	36.7297	$6_2^- - 5_1^+$	-	-	-	0.1819	0.0328	65.9413	0.1613	0.0258	74.3925
6_2^+	-	-	1.5155	32.5706	1.4176	37.6530	$7_1^- - 6_2^+$	-	-	-	0.2906	0.0840	48.1762	0.1835	0.0335	76.3022
7_1^+	-	-	1.8061	24.0881	1.6011	38.6387	$8_2^+ - 7_1^+$	-	-	-	0.2259	0.0508	70.8372	0.2042	0.0416	78.3186
8_2^+	-	-	2.0320	35.4186	1.8054	39.6692	$9_1^- - 8_2^+$	-	-	-	0.4115	0.1688	43.7382	0.2239	0.0499	80.4109
9_1^+	-	-	2.4435	21.8690	2.0297	40.7311	$10_2^+ - 9_1^+$	-	-	-	0.2637	0.0694	75.8237	0.2423	0.0585	82.5558
10_2^+	-	-	2.7073	37.9118	2.2715	41.8142	$11_1^+ - 10_2^+$	-	-	-	0.5395	0.2904	40.7807	0.2596	0.0672	84.7353
11_1^+	-	-	3.2468	20.3904	2.5312	42.9108	$12_2^+ - 11_1^+$	-	-	-	0.2978	0.0885	80.5856	0.2761	0.0760	86.9359
12_2^+	-	-	3.5446	40.2928	2.8072	44.0153	$13_1^+ - 12_2^+$	-	-	-	0.6718	0.0891	38.7019	0.2916	0.0849	89.1479
13_1^+	-	-	4.2164	19.35099	3.0989	45.1232	$14_2^+ - 13_1^+$	-	-	-	0.3292	0.1082	85.0651	0.3065	0.0938	91.3636
14_2^+	-	-	4.5456	19.1928	3.4053	46.2315	-	-	-	-	-	-	-	-	-	-

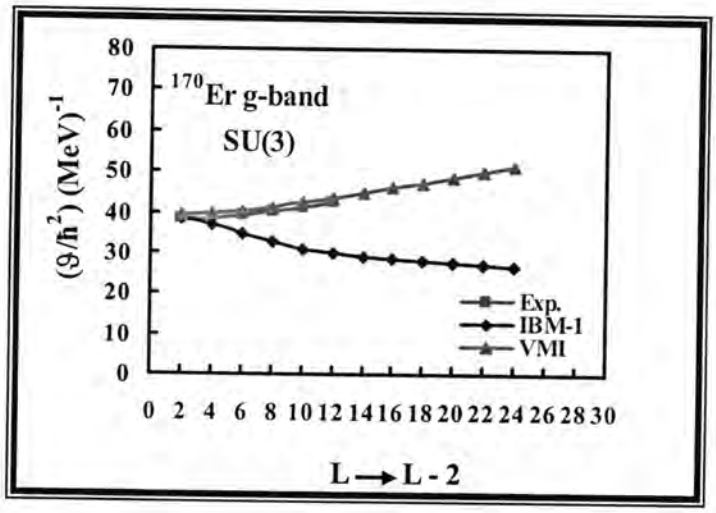

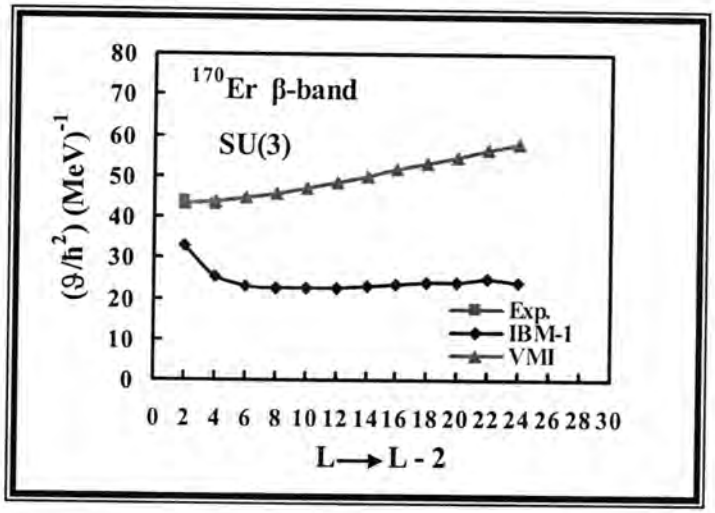

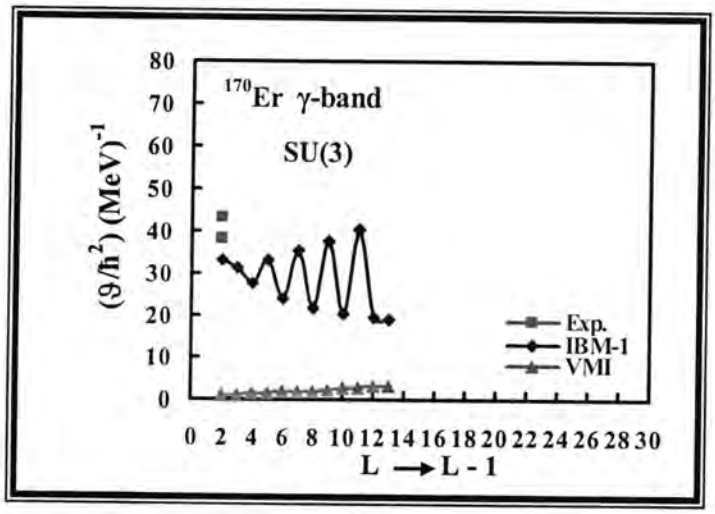

شكل -2 : عزم القصور الذاتي كدالة لتغير الزخم الزاوي للحزم(g,β,γ) لنواة(A=170) Er.

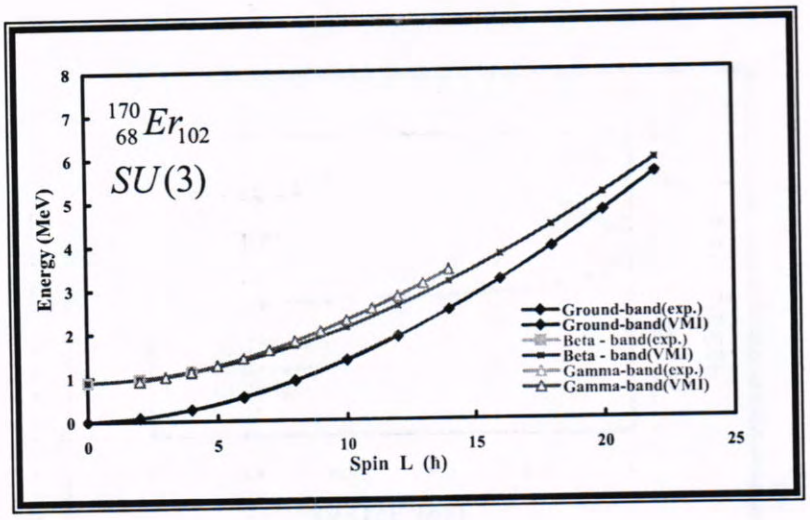

شكل -3 : تقاطع الطاقة كدالة للزخم الزاوي للانوية Er(A=170) باستخدام نموذج (VMI)

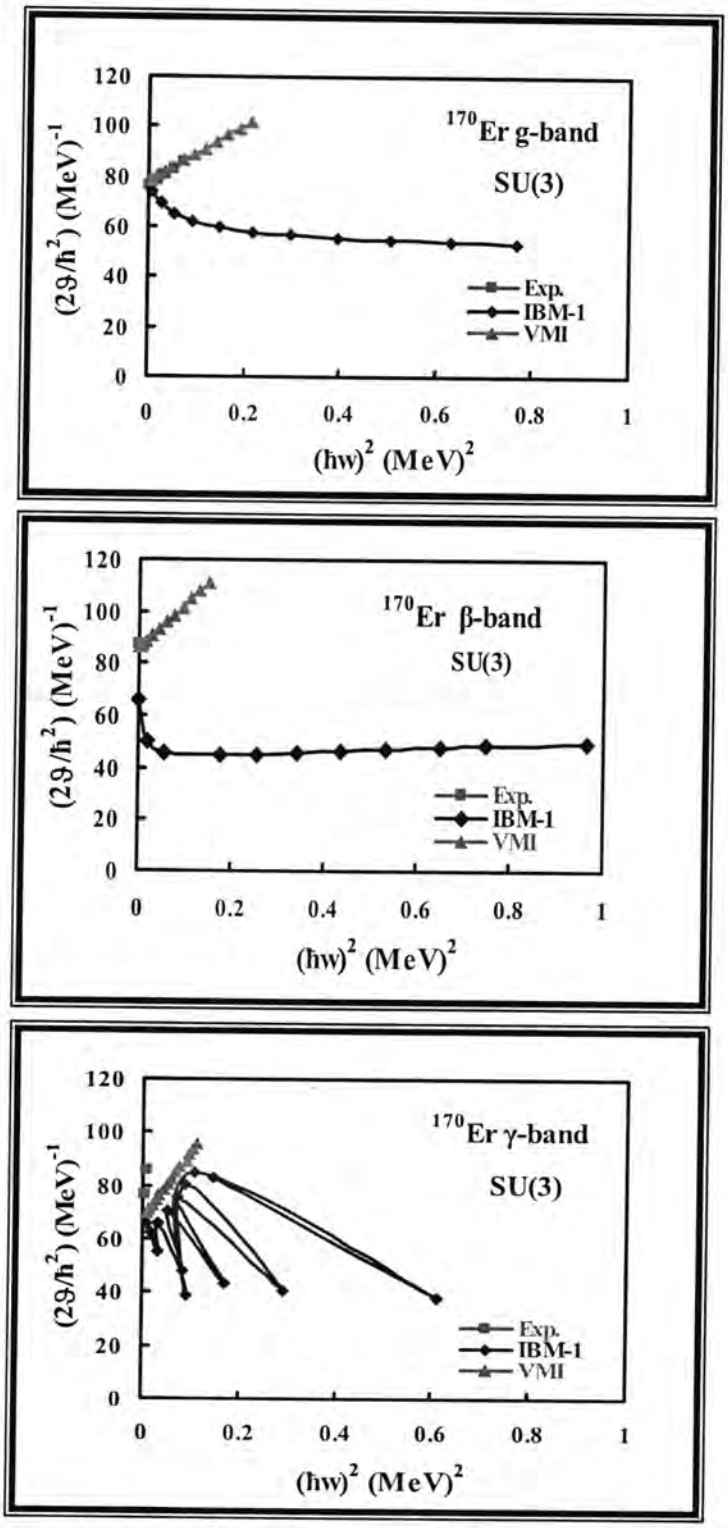

شكل -4 : عزم القصور الذاتي كدالة لمربع الطاقة الدورانية لنواة Er(A=170) ولكافة الحزم.

المصادر

1. Arima A. and Iachello F., " The Interacting Boson Model", The Syndicate Press of the University of Cambridge,England,PP.3-127(1987).
2. Bonatsos D. " Interacting Boson Model of Nuclear Structure" Oxford University Press, New York,PP.1- 271 (1988).
3. Casten R.F and Warner D.D., "The Interacting Boson Approximation",Rev.Mod.Phys.,Vol.60,P. 389 (1988).
4. Mariscotti M.A.J., Seharff-Goldhaber G. and Branin B., "Study of Variable Moment of Intertia Model (VMI) for Rotation Nuclei",Phys. Rev., Vol.178,P. 1864 (1969).
5. Nyako B.M.,Cresswell J.R.,Forsyth P.D.,Howe D.,Nolan P.N.,Riley M.A. and Twin P.J., "Observation of Super Deformation in ^{152}Dy",Phys.Rev.Lett., Vol.52,P. 507(1984).
6. Ward D., Graham R.L.,Geijer J.S. and Androws H.R., "Experimental Evidence of Band Crossing Spins for Even-Even Nuclei",Phys.Lett. B,Vol.44, P.39(1973).
7. Bohr A., and Mottelson B.R, "Symmetry and Shape of Nuclear Equilibrium Deformation", Mat. Fys. Medd. Dan.Vid. Selsk, Vol.27, P.16(1953).
8. Turkan N. and Maras I., "Microscopic Interacting Boson Model Calculation for Even- Even $^{128-138}$Ce Nuclei ",Pramana Journal of Physics, Vol. 68,P.769 (2007).
9. Sönmezoğlu S.,Okuducu S. and Eser E., "Investigation of Symmetry Properties in Deformed Light Even-Even Nuclei", International Journal and Engineering Sciences. Vol.2, P.1 (2008).
10. Talmi I . , "Simple Models of Complex Nuclei ,The Shell Model and Interacting Boson Model ",Harwood Academic Publishers, PP.187-198(1993).
11. Nojarov R. and Nodjakov E., "Band Coupling and Crossing in Nuclei", Nucl. Phys.A, Vol.397,P.29(1983).
12. Lian A.W. and Toki H., "Evidence on $\Delta I=4$ Bifurcation in Ground Bands of Even- Even and the Theoretical Explanation with the Interacting Boson Model",Phys.Rev.C, Vol.56, P.1821(1997).

13. Banatsos D.,Daskaloyannis C.,Drenska S.B. and Karoussos N., "ΔI=2 Staggering in Rotational Bands of Diatomic Molecules as a Manifestation of Interband Interactions", Phys. Rev. A, Vol.60, P.253 (1999).
14. Mariscatti M.A.J., "Description of Variable Moment of Inertia Model for Heavy Even-Even Nuclei", Phys.Rev., Vol.172, P.1742 (1970).
15. Xu F.X.,Wu C.S., and Zeng J.Y., "Relations for the Coefficients in the L(L+1) Expansion for Rotational Spectra", Phys.Rev.C, Vol.40, P.2337(1989).
16. Stephons J., "Schoum' Murray R., Spiegel T.and Stephons J. Outlines Statistics", Mc Graw-Hill, PP.100-105(1999).
17. Arima A. and Iachello F., "In advance in Nuclear Physics ", Plenum, New York, PP.139-145(1984).
18. Sakai M., "Quasi-Band in Even- Even Nuclei " ,Atomic Data and Nuclear Data Tables,Vol.31, P399 (1984).
19. Lederer C. M. and Shirley V. S., "Table of Isotopes 7th Edition", John Wiley and Sons, New York, PP.1078-1148 (1978).
20. Venkova T. and Andrejtscheff W., "Transition Strengths B(E2) in the Yrast Band of Doubly Even Nuclei ", Atomic Data and Nuclear Data Tables,Vol.26, P.93 (1981).

تحليل محسّن للتوزيع الزاوي لأشعة كاما الناتجة من التفاعل $^{158}_{64}Gd\,(\alpha,2n\gamma)^{160}_{66}Dy$

ماهر ناصر سرسم[1] و هرمزموشي يوحنا[2] و إنعام نوري إبراهيم[3]
[1,2]جامعة بغداد - كلية التربية ابن الهيثم
[3]وزارة التربية

تاريخ تقديم البحث 2010/4/13 - تاريخ قبول البحث 2010/10/5

ABSTRACT

The $\delta-$ Mixing ratios of $\gamma-$ transitions from low and high Spin states populated from the nuclear reaction $^{158}_{64}Gd\,(\alpha,2n\gamma)^{160}_{66}Dy$ are calculated using a new method which we can called it as Improved Analysis Method. The comparison of the results of experimental values,CST method, LST and adopted $\delta-$ mixing ratios with the results Of the presented work confirm the validity of this method.

الخلاصة

تم حساب نسب الخلط (δ) لانتقالات كاما من المستويات ذات البروم الواطنة والعالية المتولدة من التفاعل النووي $^{158}_{64}Gd\,(\alpha,2n\gamma)^{160}_{66}Dy$ وذلك باستعمال طريقة (مستحدثة) جديدة يمكن ان يطلق عليها تسمية طريقة التحليل المحسن وتؤكد النتائج التي تم الحصول عليها صحة هذه الطريقة في حساب نسب الخلط وتوافقها على نحوٍ جيد مع القياسات العملية وطريقة CST و LSF ونسب الخلط للقيم المتبناة.

المقدمة

التوزيع الزاوي لأشعة كاما : يعرف التوزيع الزاوي لأشعة كاما المنبعثة من تفاعل نووي $X(a,b)Y$ بأنه توزيع لشدة اشعة كاما كدالة للزاوية θ بين اتجاه انبعاث أشعة كاما واتجاه الجسيم الساقط ، ويعبر عنها بالعلاقة الآتية :

$$W(\theta)=\sum_k A_k P_k(\cos\theta)=\sum \rho_k(J_i)\,F_k(J_iJ_f\delta)\,P_k(\cos\theta).....(1)$$

حيث إن:-

A_k معامل التوزيع الزاوي (Angular Distribution Coefficient)

$P_k(\cos\theta)$ متعدد حدود لاجندر (Legender Polynomial)

$\rho_k(J_i)$ التنسّرات الاحصائية التي تصف تراصف المستوى الابتدائي للنواة الناتجة عن التفاعل والباعثة لأشعة كاما. و(J_i)البرم النووي للمستوى الابتدائي

(J_f)البرم النووي للمستوى النهائي

إن $F_k(J_iJ_f\delta)$ هي معاملات تتضمن معلومات عن تغيرات الزخم الزاوي ونسب الخلط (δ) وتعطى بالعلاقة الآتية [1] :-

$$F_k(J_iJ_f\delta)=\frac{[F_k(J_fL_1L_1J_i)+2\delta F_k(J_fL_1L_2J_i)+\delta^2F_k(J_fL_2L_2J_i)]}{(1+\delta^2)}\text{.....(2)}$$

حيث إن :- L يمثل الزخم الزاوي
L_1 يمثل الزخم الزاوي الابتدائي.و L_2 الزخم الزاوي الثانوي

$$L_2=L_1+1\text{ .....(3)}$$
$$L_1=|J_i-J_f|\neq 0\text{ .....(4)}$$

وبصورة عامة تعطى المعاملات $F_k(J_fL_1L_2J_i)$ بالعلاقة الآتية

$$F_k(J_fL_1L_2J_i)=(-1)^{J_f-J_i-1}\left[(2L_1+1)(2L_2+1)(2J_i+1)\right]^{1/2}(L_1 1L_2-1|K0)$$
$$*\,W(J_iJ_iL_1L_2,KJ_f)\text{.....(5)}$$

تمثل $(L_1 1L_2-1|K_0)$ معاملات كلابش – كوردن (Clebsch–Gordan) و $W(J_iJ_iL_1L_2,KJ_f)$ معاملات راكاه (Racah Coefficient) وهذه المعاملات تحدد قيمة K (ان K تاخذ القيم 0,2,4,.....) والقيم العظمى تحدد على النحو الآتي [2] :-

$$0\le K\le\min(2L_1,2L_2,2J_i)\text{.....(6)}$$

وفي حالة $K=0$ فإن :-

$$F_o(J_fL_1L_2J_i)=\delta_{L_1L_2}=\begin{cases}1 & if\ L_1=L_2\\ 0 & if\ L_1\neq L_2\end{cases}\text{.....(7)}$$

أما التنسرات الاحصائية $\rho_k\ (J_i)$ فإنها تعطى بالجمع المعدل (Weighted Sum) عبر معاملات التولد $P(m_i)$ (population Parameters) لـ $(2J_i+1)$ من المستويات الثانوية المغناطيسية المرافقة لـ J_i وعلى النحو الآتي :-

$$\rho_k\ (J_i)=\sum_{\substack{m_i=0\\ 0r\,m_i=\frac{1}{2}}}^{J_i}\rho_k\ (J_i,m_i)\,P(m_i)\text{.....(8)}$$

مع أعتمادشرط التعيير (Normalization condition) الآتي :-

$$\sum_{m_i=-J_i}^{J_i}P(m_i)=1\text{.....(9)}$$

تم استخدام معاملات F_4 , F_2 التي قام الزهيري بحسابها [3] لاعداد البروم الصحيحة لغاية $J_i = 20$ وللمضاعفات نصف فردية لغاية $J_i = \frac{51}{2}$. كما استخدمت معاملات التنسّر الاحصائي $\rho_k\ (J_i , m_i)$ المجدولة في المصدر [1]

معاملات توهين الترصيف α_k :-

The Alignment Attenuation Coefficients (α_k)

إن درجة الترصيف (Degree of Alignment) للحالة الابتدائية التي تمتلك برم (J_i) يمكن تحديدها بمعرفة ثوابت التولد $P(m)$ (Population Parameters) ويمكن أن يعطى بدلالة التنسر الاحصائي $\rho_k\ (J_i)$ (Statistical Tensor).

إن $\rho_k\ (J_i)$ يحوي معلومات عن معاملات التولد ، وتعطى بالعلاقة الآتية [2,4] .

$$\rho_k\ (J_i) = \sqrt{2J_i + 1} \sum_m (-1)^{J_i - m}\ (J_i\, m\, J_i - m \,|\, k_0)\ P_m\ (J_i) \qquad \ldots\ldots\ldots (10)$$

إذ يمثل $(J_i\, m\, J_i - m \,|\, k_0)$ معامل كلبش كوردن (Clebsch Gorden Coefficient) و $P(m)$ معاملات التولد (Population Parameters)، وهي الاحتمالية النسبية لتوليد الحالات الثانوية (m) $(m = -J_i , \ldots\ldots , +J_i)$ (Population of Magnetic substate) للحالات الابتدائية وتسمى - أيضا - ثوابت التولد (Generation Constants) .

إن $P(m)$ يمكن التعبير عنها كتوزيع كاوسي (Gaussian Distribution) بالمعادلة الآتية :-

$$p_m = \frac{e^{-\left(m^2 / 2\sigma^2 \right)}}{\sum_{m=-J_i}^{J_i} e^{-\left(m^2 / 2\sigma^2 \right)}} \qquad \ldots\ldots\ldots (11)$$

إذ يمثل σ نصف اتساع (Half Width) التوزيع الكاوسي ، وفي حالة الترصيف التام (Complete Alignment) تكون $\sigma = 0$ و $\alpha_2\ (J_i) = 1$.

إن التوزيع الكاوسي (Gaussian Distribution) للمستويات الثانوية (Substates) يتلاءم مع تجارب التوزيع الزاوي [2].

تعرف $\alpha_k\ (J_i)$ بأنها معاملات التوهين (Attenuation coefficients).

إن معاملات التوهين α_k للمستويات ذات الترصيف الجزئي غير المكتمل (Partiallly Aligned States) يعطى بالعلاقة الآتية .

$$\alpha_k(J_i)=\frac{\rho_k(J_i)}{B_k(J_i)} \qquad ;\ k=2,4,6 \qquad \text{.....(12)}$$

اما في حالة الترصيف التام (Complete Alignment) فيعطى التنسّر الاحصائي (Statistical Tensor) $B_k(J_i)$ بالعلاقة الآتية :

$$B_k(J_i)=\begin{cases}\sqrt{(2J_i+1)}\,(-1)^{J}\ (J_0\,J_0\,|\,k_0) & \text{for integral spin}\\ \sqrt{(2J_i+1)}\,(-1)^{J-\frac{1}{2}}\ (J\ \tfrac{1}{2}\ J\ -\tfrac{1}{2}\,|\,k_0) & \text{for half integral spin}\end{cases} \qquad \text{.....(13)}$$

وقد تم اعتماد قيم جداول B_2 و B_4 في المصدر [2,4].

المواد وطرائق العمل

طريقة نسبة a_2 :- $(a_2$ −Ratio Method) تعتمد هذه الطريقة على شرطين هما :-

1-أن يكون في الاقل هناك انتقالان لكاما من مستوى الطاقة الابتدائية نفسه (J_i) (أي الانبعاث من المستوى (J_i) نفسه الى مستويات مختلفة لـ (J_f)).

2-إن أحد الانتقالات يجب أن يكون نقيا أو يفترض أن يكون نقيا.

تعتمد حسابات نسبة a_2 $(a_2$ Ratio) ـ اعتماداً كلياً ـ علىالزخم الزاوي لتعاقب البرم (J_i-J_f) لكل انتقال من انتقالات كاما وعلى L_1L_1, L_1L_2, L_2L_2 معاملات التوزيع الزاوي a_2 وعلى معاملات F_2 لكل انتقال ، أي إن طريقة نسبة a_2 لا تعتمد على طاقات المستويات ولا على طاقات كاما ولا على التماثل . إن الشرط الاول يجعل هذه الطريقة غير قادرة على حساب نسب الخلط لكل انتقالات كاما.

لقد تم تطبيق هذه الطريقة بنجاح من قبل Youhana[5,6,7] ليس لحساب قيم δ للانتقال المختلط وإنما لاختبار صحة النتائج التجريبية.

طريقة التنسّر الاحصائي الثابت (CST)

Constant Statistical Tensor Method

تعتمد هذه الطريقة على شرطين أساسيين :-

1- وجود انتقالات نقية مثل $(2-0)$ أو $(1-0)$ ، أو انتقالات يمكن عدها نقية مثل $\bar{3}-(2,3,4)^{+}$ ، $\bar{5}-(4,5,6)^{+}$ ، $\overset{+}{7}-(6,7,8)^{-}$.

إن قيمة a_k يمكن حسابها من القانون الآتي [8,9]:-

$$a_k(J_i - J_f) = \rho_k \times \frac{F_k(J_f L_1 L_1 J_i) + 2\delta F_k(J_f L_1 L_2 J_i) + \delta^2 F_k(J_f L_2 L_2 J_i)}{(1+\delta^2)} \quad .....(14)$$

حيث ان $(a_k = a_2, a_4, a_6 .....)$ تمثل معاملات التوزيع الزاوي

وعندما يكون الانتقال نقي فان نسب الخلط $(\delta = 0)$ وبالتالي يتم الاستفادة من $\rho_k(J_i)$ في حساب نسب الخلط للانتقالات من المستوى (J_i) نفسه .

2- وجوب تحقيق الشرط الآتي :- $\alpha_2(J_i) < 1$ حيث ان ($\alpha_2(J_i)$ هي معاملات التوهين للمستويات ذات الترصيف الجزئي غير المكتمل)

طريقة مطابقة المربعات الدنيا (LSF)

Least Squares Fitting *(LSF)* Method

إن طريقة مطابقة المربعات الدنيا $(LSF - Method)$ هي طريقة تحليلية تستعمل لحساب قيم الثابت الاحصائي التنسّوري $\rho_2(J_i)$ عند أقل خطأ (χ^2) لقيم $\rho_2(J_i)$ التي يتم حسابها بطريقة (CST) .كذلك فإن هذه الطريقة تحسب $\rho_2(J_i)$ للمستويات الابتدائية (J_i) مع اختلاف قيم البرم لها التي تكون مطابقة لحساب متعددة الحدود (polynomial series) بالصيغة الآتية:

$$\rho_2(J_i) = \sum_{x=0}^{x=n} C_x J_i^x \quad ; \quad n = 0,1,2,3,4 .....(15)$$

إن استخدام طريقة (LSF) يهدف إلى إيجاد معاملات (C_x) لكل قيم n وايجاد مربعات كاي (χ^2) لكل n.

طريقة التحليل المحسَّن:-

تعتمد هذه الطريقة على الانتقالات النقية او الانتقالات التي يمكن اعتبارها نقية $(E_2$ أو $E_1)$ ، إذ يتم حساب $\alpha_2(J_i)$ لهذه الانتقالات من العلاقة[9]:

$$\alpha_2(J_i) = \frac{\rho_2(J_i)}{B_2(J_i)} \quad .....(16)$$

ويجب ان تحقق $\alpha_2(J_i)$ الشرط : $\alpha_2(J_i) < 1$.

ويتم - بعد ذلك - إيجاد المناظرة لـ $\alpha_2(J_i)$ لكل (J_i) باستخدام الجداول في المصدر [4]، وايجاد نصف الاتساع (Half width) له ومن ثم ايجاد قيم $\alpha_4(J_i)$ المناظرة لكل من $\alpha_2(J_i)$ و $(\frac{\sigma}{J_i})$ باستعمال الجداول أنفسها ، وتتم الاستعانة بطريقة (CST) لايجاد معاملات التولد $P(m_i)$ وايجاد قيم $\rho_2(J_i)$ و $\rho_4(J_i)$ و معاملات التوزيع الزاوي

للانتقالات النقية ومقارنتها بالنتائج المنشورة.كذلك اجريت حسابات التوزيع الزاوي لأشعة كاما $\omega(\theta)$ عند $\theta = 90^\circ$ والإفادة منها في حساب نسب الخلط لجميع الانتقالات النقية والمختلطة للتفاعل $^{158}_{64}Gd\,(\alpha,2n\gamma)^{160}_{66}Dy$ ومقارنتها مع نسب الخلط المعتمدة [10],[11] ونسب الخلط المحسوبة من قبل الزهيري[3] كما موضح في الجداول (4)و(5) .

ومن ثم تم حساب معاملات التوزيع الزاوي a_4, a_2 بالاعتماد على قيم δ المحسوبة من قبل Riezebos[10] ومقارنتها بالنتائج التجريبية المنشورة. وكذلك تتم الاستعانة بطريقة (LSF) في ايجاد قيم $\rho_2(J_i)$ للمستويات التي لا تمتلك انتقالات نقية أو التي لا تحقق الشرط $(\alpha_2(J_i)<1)$.

أن هذه الطريقة تعتمد على الطرائق الثلاث ($(\frac{\sigma}{J_i})$ و (CST) و (LSF)) وعلى القوانين الرئيسة للتوزيع الزاوي.

إن الطرائق الثلاث التي تم الاعتماد على قوانينها أعتُمِد عليها ضمنيا، أي تم تكوين طريقة واحدة تعتمد على ثلاث طرائق .

النتائج والمناقشة

تم في هذه الدراسة حساب نسب الخلط (δ) لانتقالات كاما من المستويات ذات البرم الواطئة والعالية المتولدة من التفاعل النووي $^{158}_{64}Gd\,(\alpha,2n\gamma)^{160}_{66}Dy$ باستعمال طريقة جديدة أطلقنا عليها تسمية طريقة التحليل المحسَّن ، ذلك لأن نتائجها متوافقة على نحوٍ كبير جدا مع القياسات العملية وطرائق CST ، و LSF فضلاً عن إمكانيتها تحديد مواقع الأخطاء التجريبية او الحسابية الناتجة من أخطاء المعطيات .

طُبِقت هذه الطريقة على هذا ألانموذج من التفاعل النووي الذي سبق وأن دُرس من قبل عدد من الباحثين باستعمال الطرائق الثلاث المذكورة في أعلاه.كانت نتائج حسابات نسب الخلط (δ) لانتقالات كاما لـ $^{160}_{66}Dy$ كما هو مؤشر في جدول(4)وجدول (5) كالاتي :

من أصل (37) انتقالاً كامياً نقياً اظهرت النتائج توافقاً كاملاً لـ (25) انتقالاً كامياً وتقارباً في النتائج لـ (4) انتقالات وعدم توافق في (8) انتقالات .

يعود سبب التقارب في النتائج او عدم التوافق إلى تأثير قيم a_4 التجريبية . لقد استُعمِلت قيم a_4 و a_2 التجريبية لإيجاد نسب الخلط في هذه الدراسة، أما في الحسابات السابقة فكان الاعتماد على قيم a_2 فحسب وإهمال قيم a_4 اعتقاداً بعدم تأثيرها وذلك بسبب صغر قيمتها مقارنة بقيم a_2.

تم حساب قيم معاملات a_2 و a_4 ومقارنتها بالقيم التجريبية بالاعتماد على نسب الخلط المنشورة ،وقد اتضح أن حسابات معاملات التوزيع الزاوي a_2 لجميع انتقالات كاما النقية

والتي عدت نقية لـ ^{160}Dy يتوافق على نحوٍ متميز مع القياسات التجريبية إلا أن نتائج حسابات معاملات التوزيع الزاوي a_4 للانتقالات الكامية بعدد (37) ظهرت كما يأتي :

هنالك توافق كامل لـ (26) انتقالاً كامياً.
هنالك شبه توافق لـ (6) انتقالات كامية.
وهنالك عدم توافق في (5) انتقالات كامية.

يعود سبب ذلك بالتأكيد إلى الأخطاء في القياسات التجريبية وكما موضح في هذه الدراسة كذلك حُدِدت مواقع الأخطاء التجريبية في انتقالات كاما المختلطة لـ ^{160}Dy إذ تم ـ بعد دراسة (16) انتقالاً كامياً مختلطاً ـ التأكد من توافق نتائج (10) انتقالات وتحديد (6) انتقالات تكون فيها قيم a_4 المحسوبة في هذه الدراسة غير متفقة مع القياسات التجريبية التي نعتقد بأنها غير دقيقة، وكما موضح ايضاً في هذه الدراسة.

ملاحظة: تم استخدام (exp) مختصر (experimental) و (th) مختصر (theoretical)

جدول -1: **قيم معاملات توهين الترصيف للانتقالات التي عدت نقية (E_1 او E_2) وقيم $\frac{\sigma}{J_i}$ وقيم التنسر الاحصائي الثابت $\rho_2(J_i)$ التي تم حسابها بالطريقة الحالية لـ ^{160}Dy .**

J_i exp	J_f exp	$\alpha_2(J_i)$ th	$(\frac{\sigma}{J_i})$ th	σ $p.w$	$\rho_2(J_i)$ $P.W$ $\rho_2(J_i)$ [3]	$\rho_2(J_i)_{ave}$ $p.w$
2	0	0.1967	0.9204	1.8408	-0.2352 -0.23515	-0.2352
3	2	0.3663	0.6213	1.8639	-0.4232 -0.42297	-0.4231
4	2	0.4867	0.4993	1.9972	-0.5545 -0.55463	-0.5545
5	4	0.5729	0.4297	2.1485	-0.6491 -0.6487	-0.6489
6	4	0.6382	0.3830	2.2980	-0.7196 -0.72003	-0.7198
7	5	0.6925	0.3461	2.4227	-0.7786 -0.77945	-0.7790
8	6	0.7421	0.3124	2.4992	-0.8335 -0.83407	-0.8338
9	8	0.7902	0.2806	2.5254	-0.8847 -0.88713	-0.8859
10	8	0.8361	0.2475	2.475	-0.9347 -0.93803	-0.9364
11	9	0.8761	0.2132	2.3452	-0.9812 -0.98233	-0.9818
12	10	0.9028	0.1863	2.2356	-1.0129 -1.01175	-1.0123

جدول - 2 :- قيم $\rho_4(J_i)$ بدلالة J_i التي حُسبت بطريقتين مختلفتين للنظير ^{160}Dy .

حيث يستفاد منها بشكل اساسي لايجاد معاملات التوزيع الزاوي a_4 والتي تم اعتمادها في البحث الحالي حيث كان يتم اهمالها سابقا

J_i exp	J_f exp	$\frac{\sigma}{J_i}$ *th*	$\alpha_4(J_i)$ *p.w*	$\rho_4(J_i)$ *p.w*	$\rho_4(J_i)_2$ *p.w*	$\rho_4(J_i)_{ave}$ *p.w*
2	0	92040.	01430.	01430.	40140.	01440.
3	2	0.6213	0.0567	0.0725	0.0727	0.0726
4	2	0.4993	0.1219	0.1471	0.1469	0.1470
5	4	0.4297	0.1888	0.2222	0.2221	0.2222
6	4	0.3830	0.2533	0.2940	0.2928	0.2934
7	5	0.3461	0.3182	0.3663	0.3633	0.3648
8	6	0.3124	0.3865	0.4427	0.4415	0.4421
9	8	0.2806	0.4619	0.5271	0.5260	0.5266
10	8	0.2475	0.5490	0.6248	0.6231	0.6240
11	9	0.2132	0.6418	0.7290	0.7286	0.7288
12	10	0.1863	0.7126	0.8094	0.8093	0.8094

جدول - 3 : قيم a_2 و a_4 لانتقالات كاما النقية والانتقالات التي عدت نقية (E_1 أو E_2) من مستويات ^{160}Dy بطريقة التحليل المحسن ومقارنتها مع النتائج العملية.

$E_{Level}(keV)$ exp	$E_\gamma(keV)$ exp	$J_i^\pi - J_f^\pi$ exp	$\frac{a_2}{a_4}[10]$ exp	$\frac{a_2}{a_4}$ p.w.
86.8	86.8	$2^+ - 0^+$	0.140(5) - 0.028(7)	0.14 - 0.015
966.2	966.2	$2^+ - 0^+$	0.17(3) - 0.01(4)	
1286.7	1200.5	$3^- - 2^+$	-0.02(2) 0.00(4)	-0.147 0.00
1398.9	1312.1	$3^- - 2^+$	-0.14 (4) - 0.03(6)	
	1115.7	$3^- - 4^+$	0.01(11) - 0.31(16)	-0.06 0.00
283.8	197.0	$4^+ - 2^+$	0.247(8) 0.05(1)	0.248 - 0.04
1155.8	1069.0	$4^+ - 2^+$	0.20(4) - 0.07(5)	
1386.4	1102.6	$4^- - 4^+$	0.37(3) 0.02(4)	0.24 0.00
	337.3	$4^- - 3^+$	- 0.36(4) - 0.08(6)	- 0.17 0.00
1407.7	1125.0	$(5)^- - 4^+$	0.25(3) 0.03(4)	-0.19 0.00

ملاحظة : $\frac{a_2}{a_4}$ p.w. تشير الى قيم a_2 لبعض انتقالات اشعة كاما والتي تم حسابها بطريقة التحليل المحسن اعتمادا على قيم $\rho_2(J_i)$ و $\rho_4(J_i)_{ave}$ واعتمادا على نسب الخلط (δ) الخاط للقيم المتبناة (Adopted Values) وهي ناتجة عن ثلاثة قياسات لنسب الخلط (طريقة a_2 وطريقة LSF وطريقة CST)

تابع للجدول - 3:

$E_{Level}(keV)$ exp	$E_\gamma(keV)$ exp	$J_i^\pi - J_f^\pi$ exp	$\frac{a_2}{a_4}[10]$ exp	$\frac{a_2}{a_4}$ p.w.
581.2	297.4	$6^+ - 4^+$	0.283(5) - 0.07(1)	0.29 - 0.06
1438.6	1154.8	$6^+ - 4^+$	0.36(3) 0.01(5)	
1594.6	208.2	$6^- - 4^-$	0.17(2) - 0.15(6)	
1726.5	1442.7	$6^+ - 4^+$	0.07 (5) - 0.10(7)	
1787.5	252.3	$(6)^- - 4^-$	0.17(4) - 0.15(6)	
1594.6	1013.4	$6^- - 6^+$	0.19(3) 0.02(4)	0.32 0.00
	306.0	$6^- - 5^+$	-0.16(2) 0.00(2)	-0.20 0.00
1787.5	498.6	$(6)^- - 5^+$	-0.22(5) 0.05(7)	
1614.0	1032.8	$(7^-) - 6^+$	-0.24(2) 0.03(3)	-0.21 0.00
1617.6	328.5	$7^+ - 5^+$	0.23(3) -0.10(5)	0.30 -0.07
967.2	386.0	$8^+ - 6^+$	0.305(10) -0.068(15)	0.32 -0.08
1801.2	362.6	$8^+ - 6^+$	0.33(2) -0.08(3)	
1882.6	288.0	$8^- - 6^-$	0.35(11) -0.08(2)	
1978.3	1397.1	$8^+ - 6^+$	0.29(4) 0.13(6)	
2112.7	325.2	$(8)^- - (6)^-$	0.28(5) -0.12(7)	

جدول - 4 : قيم نسب الخلط (δ) لانتقالات كاما النقية والتي عدت نقية من مستويات ^{160}Dy

$E\ level(keV)$	$E_\gamma(keV)$	$J_i^\pi - J_f^\pi$	$\frac{a_2}{a_4}[10]$	δ			
				Ref [10]	Ref [11]	Ref [3]	*P.w.*
86.8	86.8	$2^+ - 0^+$	0.140(5) -0.028(7)	–	E_2	E_2	E_2
283.8	197.0	$4^+ - 2^+$	0.247(8) 0.05(1)	–	E_2	0.00(1)	- 0.19(2)*
581.2	297.4	$6^+ - 4^+$	0.283 (5) - 0.07(1)	–	E_2	- (1)10.0	-0.00(1)
966.2	966.2	$2^+ - 0^+$	0.17(3) - 0.01(4)	E_2	E_2	E_2	E_2
967.2	386.0	$8^+ - 6^+$	0.305(10) - (15)60.08	E_2	E_2	(11-0.0	1-0.0
1155.8	1069.0	$4^+ - 2^+$	0.20(4) -0.07(5)	E_2	- 0.022(36)	- 0.08(7)	-0.08(1)
1288.8	1285.8	$1^- - 0^+$	(3)390.)40.07(	–	E_1	E_1	E_1
1288.8	1199.0	$1^- - 2^+$	-0.02(2) 0.00(4)	–	–	–	–

تابع للجدول (4):

$E\ level(keV)$	$E_\gamma\,(keV)$	$J_i^\pi - J_f^\pi$	$\frac{a_2}{a_4}[10]$	δ			
				Ref [10]	Ref [11]	Ref [3]	*P.w.*
1286.7	1200.5	$3^- - 2^+$	(2)02-0. 0.00(4)		)3(08-0.0	–	(1)*160.
1386.4	1102.6	$4^- - 4^+$	0.37(3) 0.02(4)	(12)50.0	(1)50.0	Imaginary Root	Imaginary Root
	337.3	$4^- - 3^+$	(4)36-0. - 0.08(6)	1.2(12)	0.028(13)	-0.20(5)	-0.12(1)
1398.9	1312.1	$3^- - 2^+$	-0.14(4) (6)3- 0.0	-2.8(30)	)3(15-0.0	(5)10.0	0.04(1)
	1115.7	$3^- - 4^+$	0.01(11) -0.31(16)	-2.5(27)	0.001(3)	$-\left(0.12^{+0.20}_{-0.17}\right)$	Imaginary * Root
1407.7	0.1251	$(5)^- - 4^+$	0.25(3) 0.03(4)	-2.5(26)	E_1	0.40(4)	0.39
1428.2	461.0	$10^+ - 8^+$	)15(3350.)4-0.10(	E_2	E_2	-0.01(2)	-0.01
1438.6	1154.8	$6^+ - 4^+$	0.36(3) 0.01(5)	E_2	–	0.09(5)	0.03(2)

ملاحظة : تشير علامة النجمة*الى عدم توافق قيم نسب الخلط المحسوبة مع قيم نسب الخلط في المصدر[3] ؛ كون نسب الخلط (δ) التي تتم المقارنة معها هي نسب الخلط للقيم المتبناة (Adopted Value) وهي ناتجة من ثلاثة قياسات لنسب الخلط (طريقة a_2 وطريقة LSF وطريقة CST).

جدول - (5): بعض قيم نسب الخلط لانتقالات كاما المختلطة من مستويات ^{160}Dy والتي تم حسابها حسب طريقة التحليل المحسن

$E\ level(keV)$	$E_\gamma\,(keV)$	$J_i^\pi - J_f^\pi$	$\frac{a_2}{a_4}[10]$	δ			
				Ref [10]	Ref [11]	Ref [3]	*P.w.*
966.2	879.4	$2^+ - 2^+$	-0.08(2) 0.01(3)	$<(-0.5)$	-16.6(5)	-0.67(9) -16.2(5) -5.3(27)	$-0.76^{+0.07}_{-0.05}$ -4.0(2)
1049.1	962.3	$3^+ - 2^+$	0.009(9) 0.040(13)	$<(-11.0)$	-13.8(3)	0.19(1) $-(18.7^{+4.9}_{-3.2})$	0.155(1) -21.9(5)
	765.3	$3^+ - 4^+$	-0.09 (3) - 0.009(5)	0.05(5)	-13.7(9)	0.05(3) -13.7(9)	0.04 $-11.0^{+2.6}_{-3.9}$
1155.8	872.0	$4^+ - 4^+$	-0.197(12) - 0.063(18)	$-1<\delta<8$	$-0.95^{+0.08}_{-0.11}$	-1.5(2) -5.6(17)	- 1.3(1) - 5.1(2)
1288.6	1004.8	$5^+ - 4^+$	-0.123(7) 0.133(10)	$-8<\delta<14$	$-(7.1^{+0.8}_{-1.0})$	0.06(1) - 9.9(6)	-0.03 - 9.4
	707.4	$5^- - 6^-$	-0.12(1) 0.06(5)	$<(-10)$	E_2	0.01(1) - 19(4)	0.05(1) $-22.2^{+2.2}_{-2.8}$
1438.6	875.4	$6^+ - 6^-$	-0.255(12) -0.19(2)	$<(-1.4)$	$<(-1.4)$	- 1.5(3)	- 1.41(3)

تابع للجدول - (5)

$E\ level(keV)$	$E_\gamma(keV)$	$J_i^\pi - J_f^\pi$	$\frac{a_2}{a_4}[10]$	δ			
				Ref [10]	Ref [11]	Ref [3]	P.W.
1617.6	1036.4	$7^- - 6^-$	-0.237(19) 0.185(15)	- 7.2(10)	- 7.2(1)	-7.2(1) - 0.03(1)	- 7.1(3) - 0.12(1)
	650.4	$7^- - 8^-$	0.01 (3) 0.21(5)	-5(8)	-5(8)	-5.9(5) - 0.09(2)	- 11.0(8) * 0.00(1) *
1726.5	1145.3	$6^- - 6^-$	0.27(13) 0.02(18)-	–	$M_1 + E_2$	$-0.11^{+0.19}_{?}$ $0.8^{+0.4}_{?}$	- 0.09(2) 0.97(2)
1801.2	834.2	$8^- - 8^-$	-0.191(9) -0.125(9)	<(-1.5)	<(-1.5)	-1.5(1) 6.1(6)	-1.9(1) - 9.3(11)
2022.4	1055.2	$(9^-) - 8^+$	-0.30(2) 0.30(3)	-7.0 (12)	-7.0 (12)	-7.0 (1) -0 05(1)	- 5.8(1) * -0.19 *
2222.9	794.7	$10^+ - 10^+$	-0.18 (5) -0.27(7)	-1.2<δ<2.7	<2.7	-1. 4(2) 3. 8(13)	-1.2 6. 5(3)
2487.4	1059.2	$(11^-) - 10^+$	-0.36 (14) 0.2(2)	<0.0	<0.0	-0.07(6) - 5.0 (33)	- 0.15(1) - 10.6(7)
2698.3	746.6	$(12^+) - 12^+$	0.30(6) 0.04(9)	--	--	$-(2.6^{+?}_{-0.6})$ $16.7^{+?}_{-8.7}$	Imaginary Roots *

ملاحظات حول الجدول 5:

ان نتائج حسابات نسب الخلط (δ) لانتقالات كاما المختلطة لـ ^{160}Dy قد نُفِذت باستعمال البرنامج الحاسوبي (Matlab) من دون الاعتماد على طاقة المستوى أو التماثل.

أولا:- إن اغلب انتقالات كاما المختلطة لـ ^{160}Dy تكون فيها نتائج نسب الخلط (δ) للقيمتين متوافقة مع القياسات السابقة ضمن نسب الخطأ او ان نسب الخلط (δ) (لإحدى القيمتين) متوافقة على نحوٍ جيد جدا مع القياسات في المصدر[3]

ثانيا:- إن بعض انتقالات كاما المختلطة لـ $^{160}_{66}Dy$ تكون فيها نتائج نسب الخلط (δ) قريبة من الحسابات في المصدر [3]. وهذه الانتقالات هي:

- انتقال كاما $(8^+ - 8^+)$ ذو الطاقة $(834.2\ keV)$
- انتقال كاما $10^+ - (11^+)$ ذو الطاقة $(1059.2\ keV)$

ثالثا :- بعض انتقالات كاما المختلطة لـ ^{160}Dy تكون فيها نتائج نسب الخلط (δ) غير متوافقة مع القياسات السابقة والتي اشير اليها بعلامة النجمة(*)والسبب يعود لتأثير قيم a_4 التجريبية التي استُعمِلت في إيجاد نسب الخلط (δ) إذ إن قيم a_4 التجريبية لهذه الانتقالات غير دقيقة لـ $^{160}_{66}Dy$ ،وسبب ظهور الاختلافات في قيم نسب الخلط لبعض الانتقالات ؛ كون نسب الخلط (δ) التي تتمم المقارنة معها هي نسب الخلط للقيم المتبناة (Adopted Value) وهي ناتجة من ثلاثة قياسات لنسب الخلط (طريقة a_2 وطريقة LSF وطريقة CST) .

المصادر

1. Inaam Nouri, Improved Analysis of Angular Distribution of γ-Rays From Heavy Ions and $(\alpha, xn\gamma)$ Reaction, M.Sc. Thesis Submitted to the College Of Ibn Al-Haythem, Baghdad University (2007).
2. Morinaga Yamazaki, In Beam γ-Ray Spectroscopy, North- Holland publishing company, (1976)
3. Al-Zuhairy M.H.M., Multipole Mixing Ratio and transition Strengths Of Gamma rays from levels of ^{80}Y, ^{84}Y, ^{160}Dy, ^{99}pd ,Ph.D Thesis, University of Baghdad (2002).
4. Krane K.S., Atomic Data Nucl. Data Tables, 25, 29, (1980).
5. Youhana H.M.; Al-Obeidi S.R and Al-Amili M.A ;Iraqi J.Sci.37 ,2,775 (1996).
6. Youhana H.M.; Ibn AL-haitham J.for pure and App.Sci.14,4A,45 (2001).
7. Youhana H.M.; Al-Obeidi S.R and Al-Amili M.A., Abid H.E. and Abdulla A.A.; Nucl.Phys.A458, 51 (1986).
8. Mohammed-Karim A.; Multipole Mixing Ratio and transition Strengths Of Gamma rays From Excited states of $^{112}_{48}cd$ and $^{113}_{48}cd$, Ph.D Thesis, University of Salahaddin, Erbil (2006).
9. Poletti A.R. and Warburton E.K.; Phys.Rev.c. vol. 137, p.595 (1965).
10. Riezebos H.J., DE Voigt M.J.A, Fields C.A. and Cheng X.W. Nucl.Phys.A 465, 1 (1987).
11. Firestone R.B. and Shirley V.S 'Tables of Isotopes", Eighth edition, John Wiley and Sons, New York (1999).

حزم الطاقة و عزم القصور الذاتي لنواة Hf(A=174) شديدة التشوه ذات التناظر الديناميكي SU(3)

ايمان طارق العلوي
عطاء علي حسن
قسم الفيزياء/ كلية العلوم /الجامعة المستنصرية
تاريخ تقديم البحث 2009/6/20 - تاريخ قبول البحث 2010/10/5

ABSTRACT

In this work, the energy bands and the moment of inertia for strongly deformed
even-even Hf(A=174) nucleus have been studied , the dynamical symmetry SU(3) has been predicated for this nucleus, using the Interacting Boson Model (IBM-1) and the Variable Moment of Inertia (VMI).

In this research the rotational energy and the moment of inertial, the softness coefficient; the cross bands; the back bending have been calculated for this nucleus and their dependence on the angular momentum and their relation with angular momentum .The calculated results have been compared with the available experimental data.

الخلاصة

تم خلال البحث الحالي دراسة حزم الطاقة و عزم القصور الذاتي لنواة Hf(A=174) الزوجية-زوجية الشديدة التشوه ذات التناظر الديناميكي SU(3) باستخدام نموذج البوزونات المتفاعلة الأول (IBM-1) ونموذج عزم القصور الذاتي المتغير (VMI) وقد تم خلال البحث أيضا حساب الطاقة الدورانية لعزم القصور الذاتي ومعامل الليونة وتقاطع الحزم وظاهرة الانحناء الخلفي وعلاقتها بالزخم الزاوي .لقد تم مقارنة نتائج الحسابات مع النتائج العملية المتوفرة.

المقدمة

أاقترح نموذج البوزونات المتفاعلة (Interacting Boson Model) (IBM) في عام (1974) من قبل (Arima and Iachello)[1]. في هذا النموذج يتم وصف المستويات التجميعية الواطئة (Low Lying Collective States) للنوى المتوسطة والثقيلة (الزوجية-زوجية) والبعيدة عن المدارات المغلقة والمسيطر عليها بواسطة تهيجات البروتونات والنيوترونات التكافؤية (Valance Nucleons) اي النيوكليونات التي تقع خارج ابعد مدار مغلق في النواة، لتكون جسيمات مزدوجة متماثلة من البروتونات او النيوترونات والتي تسمى بالبوزونات ذات زخوم زاوية 0 او 2 (j=0,2) حسب الحالة التي يكون فيها البوزون، فالبوزون ذو الزخم الزاوي (j=0) يسمى بـ (s-boson) ويرمز له (N_π)، بينما الذي يمتلك زخماً زاوياً (j=2) يرمز له (N_υ) ويسمى بـ (d-boson) وان العدد الكلي للبوزونات هو ($N=N_\pi+N_\upsilon$) [1,2,3].

حيث ان N_π تمثل عدد البوزونات من نوع بروتون-بروتون.

و N_υ تمثل عدد البوزونات من نوع نيوترون-نيوترون.

اما نموذج عزم القصور الذاتي المتغير فقد تم اقتراحه من قبل (Mariscotti) وجماعته عام (1969)[4] لمعالجة الاختلاف بين قيم مستويات الطاقة العملية والنظرية للنوى الدورانية اذ افترضوا ان قيمة عزم القصور الذاتي تزداد بزيادة قيمة الزخم الزاوي (L) وتم الحصول "من خلال استخدام هذا النموذج" على قيم مقاربة لقيم مستويات الطاقة العملية لهذا النوع من النوى التي تمتلك عزم قصور ذاتي عالي وليونة (Softness) نووية صغيرة عندما تكون في حالتها الارضية[2].

لقد تم اكتشاف ظاهرة الانحناء الخلفي (Back Bending) من قبل (Johnson) وجماعته عام (1971)[5] اذ وجدوا ان عزم القصور الذاتي عند زخوم معينة تزداد بشكل

واضح ويرافق ذلك نقصان في قيمة الطاقة الدورانية في بعض النوى. وفي حالة عدم ظهور الانحناء الخلفي فهذا يعني انه لا تاثير لعزم القصور الذاتي على تشوهها. وهناك تفسيرات لسبب حدوث هذه الظاهرة:

1. تقاطع الحزم Band Crossing

تتلخص ظاهرة تقاطع الحزم على انه اذا كان لدينا حزمة طاقة مثل حزمة بيتا (β-band) او حزمة كاما (γ-band) ذات عزم قصور ذاتي ϑ_2 ، وكانت حزمة الحالة الارضية (g-band) ذات عزم قصور ذاتي ϑ_1 بحيث ان $(\vartheta_2 > \vartheta_1)$ فسينتج عن ذلك تقاطع بين الحزمتين عند زخم زاوي معين L_c (L_{cross}) والمقصود بهذا التقاطع هو ان حزمة الطاقة ذات عزم قصور ذاتي عالي سوف تحل محل طاقة ذات عزم قصور ذاتي واطيء عند زيادة الزخم الزاوي عن L_c [6].

2. تاثير قوة كوريولس Corielis Force Effect

يزداد تاثير قوة كوريولس عند الزخوم الزاوية العالية على النيوكليونات التي لها زخم زاوي كبير، وهذا يؤدي الى فك الازدواج (Depairing) بين زوج أو أكثر من هذه النيوكليونات وان فك ازدواج الزوج الاول يكافئ ظهور حزمة جديدة هي حزمة شبيهي الجسيمات (Two Quasi Particles) التي يحتمل ان تقطع الحزمة الارضية (g-band) عند زخم زاوي معين وتبقى حزمة الحالة الارضية (g-band) كاملة الازدواج (Completely Paired) [7]. في عام (2007) قام كل من (Turkan and Maras)[8] بدراسة نموذج البوزونات المتفاعلة (IBM) ووصف الخواص النووية التجميعية عبر مدى واسع للنوى والذي يعتمد اساسه على تقنيات الجبر العام لنظرية الزمر (Group Theory). ونموذج (IBM) يكون استعماله واسعاً لوصف مستويات رباعي القطب التجميعية للنوى المتوسطة والثقيلة وان الصيغة الاولى لنموذج (IBM-1) لا تميز بين بوزونات البروتونات والنيوترونات، ولاحظوا ان النوى الزوجية-زوجية (Even-Even) تكون متميزة بدراسة الحزم المشوهة بشدة (Strongly Deformed Bands). وفي عام (2008) قام (Sönmezoğlu) وجماعته[9] بتفسير خواص التناظر للنوى المشوهة (Deformed Nuclei) الزوجية-زوجية (Even-Even) ضمن اطار نموذج البوزونات المتفاعلة (IBM) واستخدموا نموذج عزم القصور الذاتي المتغير (Variable Moment Inertia) (VMI) لوصف خواص التناظر واعتمدوا في الحسابات على حزمة المستوي الارضي للنوى المشوهة الزوجية-زوجية.

الاسس النظرية

يمكن كتابة مؤثر دالة هاملتون بدلالة المولدات الثمانية للزمرة الوحدوية الخاصة لـ SU(3) (SU(3) Special Unitary Group)، حيث تأخذ مصفوفة هذا المؤثر شكلا قطرياً في هذه الزمرة، وقد بين (Elliott) ان مؤثر دالة هاملتون يكتب بالصيغة الآتية [1,2,3,10]:

$$\hat{H} = a_1(\hat{L}.\hat{L}) + a_2(\hat{Q}.\hat{Q}) + a_3(\hat{U}.\hat{U}) + a_4(\hat{V}.\hat{V}) \qquad ...(1)$$

حيث أن $\hat{L},\hat{Q},\hat{U},\hat{V}$ هي مؤثرات دالة هاملتون وأن a_1,a_2,a_3,a_4 هي الاعلومات يمكن الحصول عليها عند أفضل تطابق (Fitting).

وبالإمكان إيجاد القيم الذاتية (Eigen Values) بصورة تحليلية (Analytically) وتأخذ الحالات الذاتية (Eigen States) الصيغة الآتية [2,10]:

$$\left|\begin{array}{cccc} U(6) \supset & SU(3) \supset & O(3) \supset & O(2) \\ \downarrow & \downarrow & \downarrow & \downarrow \\ [N] & (\lambda,\mu)\tilde{\chi} & \mathrm{L} & \mathrm{M}_{\mathrm{L}} \end{array}\right\rangle \qquad ...(2)$$

حيث ان:

N: العدد الكلي للبوزونات (Total Number of Bosons) = ($N_\pi+N_\upsilon$).

N_π: عدد بوزونات البروتونات (Proton Bosons Number).

N_υ: عدد بوزونات النيوترونات (Neutron Bosons Number).

ان N تشير الى التمثيل غير القابل للاختزال المتناظر كليا للزمرة الوحدوية U(6) (Totally Symmetric Irreducible Representation of U(6)). المتناظر تعني ان البوزونات تتميز بدوال موجية متناظرة (Symmetrical Wave Functions). اما (λ,μ) فهي عبارة عن تمثيلات غير قابلة للاختزال للزمرة SU(3) (Irreducible Representation of SU(3)). وان L و M_L تمثلان الزخم الزاوي ومسقطه على المحور z على التوالي، وان $\tilde{\chi}$ هو عدد كمي اضافي لـ Vergados [2,3] له علاقة بمسقط الزخم الزاوي.

ان معادلة الطاقة لحزمة الحالة الارضية (Ground State Band) للنوى الدورانية تكتب بالصيغة التالية[2]:

$$E(L)=\frac{L(L+1)}{2\vartheta} \qquad ...(3)$$

حيث ان:L : هو الزخم الزاوي للنواة ، ϑ: هو عزم القصور الذاتي للنواة بوحدة $(MeV)^{-1}$ وحسبت من وحدات $\vartheta/\hbar^2$.

لم يتمكن نموذج عزم القصور الذاتي للنوى الدورانية من وصف مستويات الطاقة بشكل جيد لافتراضه ثبات مقدار عزم القصور الذاتي، لذلك تم افتراض نموذج عزم القصور الذاتي المتغير (Variable Moment of Inertia Model) (VMI) [9,11,12,13]، وقد تم في هذا النموذج ادخال مفهوم تغير عزم القصور الذاتي للنواة واعتباره كدالة للزخم الزاوي للنواة وذلك باضافة حد ثاني للمعادلة (3) من قبل (Mariscotti)[14] وكالاتي:

$$E(L)=\left[\frac{L(L+1)}{2\vartheta(L)}+\frac{1}{2}C(\vartheta(L)-\vartheta_o)^2\right] \qquad ...(4)$$

حيث ان:

$\vartheta(L)$: عزم القصور الذاتي للنواة كدالة للزخم الزاوي (L).

ϑ_o: عزم القصور الذاتي للنواة في الحالة الارضية.

وان كل من C و ϑ_o اعلومات (Parameters) تتلائم قيمها مع القيم العملية لمستويات الطاقة.

اما معامل الليونة (Softness Coefficient) للنواة فيكتب بالشكل الاتي [3,9,11,14]:

$$\sigma=\frac{1}{2C\vartheta_o^3} \qquad ...(5)$$

لقد نجح هذا النموذج في وصف مستويات الطاقة للنوى الدورانية وحتى للنوى الاهتزازية.

ان ظاهرة الانحناء الخلفي (Back Bending) تحدث بسبب زيادة في عزم القصور الذاتي والتي يرافقها نقصان في الطاقة الدورانية عند زخوم زاوية معينة في بعض النوى. ان مربع الطاقة الدورانية وعزم القصور الذاتي تكتب بالشكل الاتي [9,11,12,13]:

$$(\hbar\omega)^2 = \left[\frac{E(L)}{\sqrt{L(L+1)}}\right]^2 \qquad ...(6)$$

$$\frac{2\vartheta}{\hbar^2} = \frac{L(L+1)}{E(L)} \qquad ...(7)$$

$$(\hbar\omega)^2 = \left[\frac{E(L \to L-2)}{\sqrt{L(L+1)} - \sqrt{(L-2)(L-2+1)}}\right]^2 \qquad ...(8)$$

ان الحد L(L+1) يقلل الى حدين L(L+1) و (L-1) (L-2) لذلك فان المعادلة (6) تصبح كالاتي للانتقالات الكامية لحزمة g وحزم β [11,12]:

$$(\hbar\omega)^2 = \left[\frac{E_\gamma}{\sqrt{L(L+1)} - \sqrt{(L-2)(L-1)}}\right]^2 \qquad ...(9)$$

$$(\hbar\omega)^2 = \left[\frac{E(L \to L-1)}{\sqrt{L(L+1)} - \sqrt{L(L-1)}}\right]^2 \qquad ...(10)$$

وبالمثل لحزم γ.

ومن المعادلة (7) نحصل على عزم القصور الذاتي لحزمة الحالة الارضية (g-band) وحزم بيتا (β-bands)

$$\frac{2\vartheta}{\hbar^2} = \frac{L(L+1) - (L-2)(L-2+1)}{E(L \to L-2)} \qquad ...(11)$$

$$\frac{2\vartheta}{\hbar^2} = \frac{4L-2}{E_\gamma} \qquad ...(12)$$

وبالمثل لحزم γ

$$\frac{2\vartheta}{\hbar^2} = \frac{L(L+1) - L(L-1)}{E(L \to L-1)} = \frac{2L}{E_\gamma} \qquad ...(13)$$

حيث ان E(L→L-2) تمثل فرق الطاقة بين مستويين لهما زخم زاوي L و (L-2) في كل من حزمة الحالة الارضية (g-band)، وحزم بيتا (β-band) اما E(L→L-1) فتمثل فرق الطاقة في حزمة كاما (γ-band) بين مستويين لهما زخم زاوي L و (L-1).

لقد تمت برمجة المعادلة (4) من خلال كتابة البرنامج (VMI.for) بلغة (Fortran 90) وباستخدام البرنامج التشغيلي (Compaq Visual Fortran V6.6) لتنفيذه، وذلك لغرض حساب عزم القصور الذاتي للنواة(L) ϑ.كما وظف هذا البرنامج لحساب مربع الطاقة الدورانية $(\hbar\omega)^2$ وعزم القصور الذاتي $\left(\frac{2\vartheta}{\hbar^2}\right)$ للحزمة الارضية (g-band) وكل من حزمة بيتا (β-band) وحزمة كاما (γ-band) وذلك ببرمجة المعادلات (8 ← 13). كما وظف هذا

البرنامج أيضا لحساب معامل الليونة (Softness Coefficient) للنواة ببرمجة المعادلة (5). حيث يتم تغذية برنامج (VMI.for) بالاعلومات C, ϑ_o, K كمدخلات لإجراء الحسابات إضافة لإدخال قيم مستويات الطاقة العملية والنظرية المحسوبة باستخدام (IBM-1) لغرض المقارنة . وقد تم حساب معدل الجذر التربيعي للانحراف المعياري (Standard Deviation) من المعادلة الآتية[15,16]:

$$\text{Standard Deviation} = \left[\frac{1}{N}\sum_{i=1}^{N}\left|\left(E_{cal.} - E_{\exp.}\right)_i\right|^2\right]^{\frac{1}{2}} \quad ...(14)$$

اما مربع كاي (Chi-Squared) الذي يمثل مدى ملائمة النموذج فقد تم حسابه من المعادلة الاتية[16]:

$$\chi^2 = \frac{(E_{cal.} - E_{\exp.})^2}{E_{cal.}^2} \quad ...(15)$$

الحسابات والنتائج

ان معظم المستويات النووية المتهيجة والتي تمتلك زخماً زاوياً عالياً تنحل عن طريق انبعاث اشعة كاما وهنا تكمن امكانية دراسة حقائق جيدة للتركيب النووي للانوية قيد الدراسة، ان الحركة الدورانية الجماعية (Collective Rotation Motion) للنواة تعتمد على حركة النيوكليونات بشكل متشاكهة (Coherently) لحركة النواة مسبباً بذلك دوران النيوكليونات حول محور يختلف عن محور التناظر النووي (Nuclear Symmetry Axis). هذا النوع من التهيجات يحدث في النوى المشوهة اذ ان النوى المشوهة لها عزم قصور ذاتي (Moment of Inertia) عالي مع محافظة حركة النيوكليونات المنفردة على عدم اضطرابها اثناء عملية الدوران المشوهة، ويبين الشكل (1) نوعين من النوى الدوارنية الاول من نوع النواة المتطاولة (Prolate Nucleus) والتي تدور حول محور عمودي على محور التناظر النووي ويسمى بالدوران الجماعي (Collective Rotation) اما النوع الثاني من النوى الدورانية فتسمى بالنواة المفلطحة (Oblate Nucleus) فتدور حول محور موازي لمحور التناظر النووي والتي تظهر في ميكانيكيتها زخوم زاوية عالية ويسمى هذا النوع من الحركة النووية بالدوران غير الجماعي (Non-Collective Rotation).

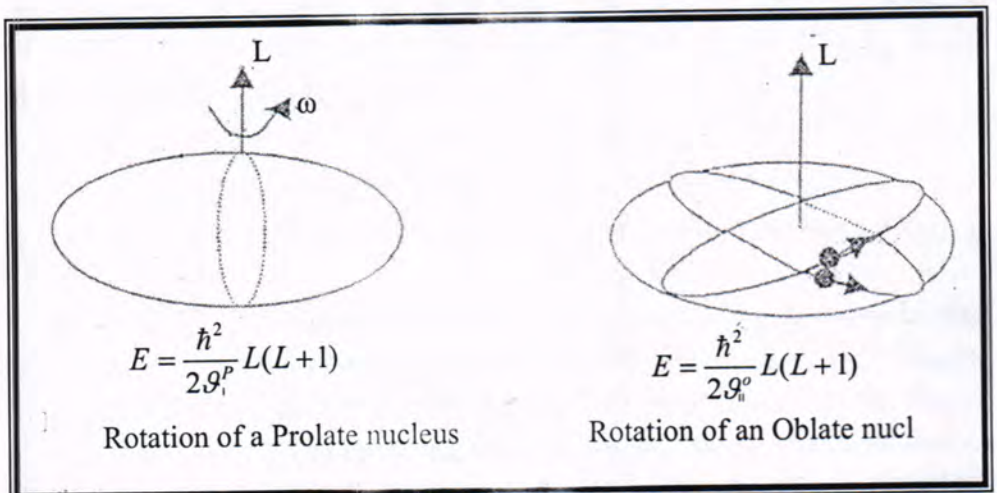

شكل -1: الحركة الدورانية الجماعية للنواة المتطاولة والحركة الدورانية غيرالجماعية للنواة المفلطحة، حيث ان $\vartheta_{\parallel}^{o}, \vartheta_{\perp}^{o}$ تمثل عزم القصور الذاتي للنوعين على الترتيب[17].

وفي كلا النوعين عندما تكون الحركة الدورانية سريعة فان قوة كورلويس تحطم الازدواج (Pairing) الحاصل بين عدد من أزواج النيوكليونات مسببة بذلك ظهور حزمة شبيهي الجسيمات (Two-Quasi Particles) ومسببة شذوذاً عند زخوم زاوية معينة ($L^{\pi}>10^{+}$) في بعض النوى والتي تسبب ظاهرة الانحناء الخلفي (Back Bending)[17].

لقد تم حساب مستويات الطاقة وقيم عزم القصور الذاتي والطاقة الدورانية وفق نموذج عزم القصور الذاتي (VMI) ونموذج تفاعل البوزونات الاول (IBM-1) على اعتبار ان الحسابات الحالية لنواة Hf(A=174) قيد البحث قد اعتمدت على مايلي:

1. معادلة مؤثر دالة هاملتون في نموذج (IBM-1) معادلة (1).
2. معادلة الطاقة في نموذج عزم القصور الذاتي المتغير (VMI) معادلة (4).
3. معادلة مربع الطاقة الدورانية $(\hbar\omega)^2$ معادلة (9) و (10).
4. معادلة عزم القصور الذاتي $(2\vartheta/\hbar^2)$وفق نموذج (VMI) التي تفترض ان النواة جسم صلد معادلة (12) و (13) وحساب معامل الليونة σ معادلة(5).

ويبين الجدول (1) قيم اعلومات مؤثر دالة هاملتون لنموذج البوزونات المتفاعلة الاول (IBM-1) لافضل تطابق (Fitting) مع القيم العملية للنواة قيد الدراسة $^{174}_{72}Hf_{102}$. ويبين هذا الجدول كذلك عدد بوزونات البروتونات (N_π) وعدد بوزونات النيوترونات (N_υ) والعدد الكلي للبوزونات (N) والاعلومات الخاصة بنموذج عزم القصور الذاتي المتغير (VMI) لافضل تطابق ايضاً والذي استخدم في الحسابات الحالية وذلك حسب حزم الطاقة الخاصة للنواة قيد الدراسة. كما تضمن هذا الجدول الاعلومات (Parameters) $C,(\vartheta_o/\hbar^2)$ وطاقة راس الحزمة K (Band-Head Energy K) ومعامل الليونة σ (Softness σ) وقيم الانحراف المعياري (Standard Deviation) لكلا النموذجين (VMI) و (IBM-1) وفقاً للمعادلة (14) وكذلك قيم مربع كاي (Chi-Square) لكلا النموذجين (VMI)و (IBM-1) وفقاً للمعادلة (15) للنواة قيد الدراسة وحسب ترتيب الحزم.

ان معامل الليونة(σ) يتناسب عكسياً مع مكعب عزم القصور الذاتي بثبوت الاعلومة C اي انه كلما ازداد عزم القصور الذاتي قل معامل الليونة وان اقل عامل ليونة يعطي اعلى تشوه للنواة. كما ونلاحظ عند زيادة الزخم الزاوي L يؤدي الى زيادة في السرعة الدورانية للنواة $(\hbar\omega)^2$، حيث $L=\vartheta\omega$ ، وعندما تكون السرعة الدورانية للنواة $(\hbar\omega)^2$ كبيرة سيحصل زيادة في القوة الطاردة المركزية (Centrifugal Force) عندها ستبتعد الجسيمات عن مركز النواة ويحصل تشوه شديد في النواة يرافقه كبر في حجمها بشكل اهليليجي متطاول او مفلطح. هذا من ناحية ومن ناحية اخرى نلاحظ ان عزم القصور الذاتي ϑ_o يزداد ايضاً، هذا يؤدي الى زيادة في الطاقة الدورانية، انظر المعادلة (4). وان هذا دليل على ان النواة تقع في المنطقة الدورانية لزمرة التناظر الديناميكي SU(3).

ونلاحظ من نتائج حسابات معامل الليونة لنواة $^{174}_{72}Hf_{102}$ والمبينة في الجدول (1). ان نواة $^{174}_{72}Hf_{102}$ تكون اشد تشوهاً في الحزمة الارضية ويقل مقدار تشوهها في كل من حزمة γ,β_2,β_1 على الترتيب مع الاخذ بنظر الاعتبار تاثير الاعلومة C على عزم القصور الذاتي ϑ_o

لقد تم حساب قيم مستويات الطاقة حسب ترتيب الحزم والتي تم الحصول عليها باستخدام كل من نموذج (VMI) ونموذج (IBM-1) وكذلك حساب مربع الطاقة الدورانية $(\hbar\omega)^2$ وعزم القصور الذاتي $(\vartheta/\hbar^2)$لطاقات الانتقالات الكامية (E_γ) لنواة قيد الدراسة $^{174}_{72}Hf_{102}$،والمبينة في الجدول (2) ويظهر من مقارنة النتائج التي حصلنا عليها توافقاً جيداً مع القيم العملية [18,19] وذلك من خلال قيم الانحراف المعياري ومربع كاي المحسوبة في العمل الحالي والتي ورد ذكرها في الجدول (1).

يبين الشكل (2) العلاقة بين عزم القصور الذاتي ($\vartheta/\hbar^2$) للحزمة الأرضية (g-band) وحزمة بيتا (β-band) وحزمة كاما (γ-band) كدالة لتغيير الزخم الزاوي لنواة $^{174}_{72}Hf_{102}$ وفق كل من نموذج (VMI) ونموذج (IBM-1) المحسوبة في العمل الحالي مقارنة مع قيم عزم القصور الذاتي المحسوبة من قيم الطاقات العملية المتوفرة[20] ويلاحظ من الشكل (2) تطابق قيم عزم القصور الذاتي بشكل جيد لنموذج (VMI) مع القيم العملية للحزمة الأرضية وحزمة بيتا، في حين لا يعطي نموذج (IBM-1) تطابق ملحوظ لهاتين الحزمتين. لذلك يكون نموذج (VMI) اكثر ملائمة لحساب عزم القصور الذاتي من نموذج (IBM-1). اما قيم عزم القصور الذاتي لحزمة كاما فيوجد توافق ضعيف بين القيم العملية ونموذج (VMI) وذلك لقلة وفرة القيم العملية لعزم القصور الذاتي (حيث توفرت ثلاثة قيم لنواة $^{174}_{72}Hf_{102}$ فقط) وهذا لا يكفي لعملية تطابق حسابات حزمة كاما بأكملها مما جعل اختلاف واضح بالنتائج. ما قيم عزم القصور الذاتي باستخدام (IBM-1) للشكل أعلاه ولحزمة كاما أيضا نلاحظ وجود توافق ضعيف بين القيم العملية والقيم المحسوبة في العمل الحالي. إضافة إلى ذلك نلاحظ تعرجاً واضحاً نتيجة تذبذب قيم عزم القصور الذاتي باستخدام (IBM-1)وهذا يعزى للأسباب الآتية:

1. عدم توفر القيم العملية الكافية لحزمة كاما لمستويات الطاقة ولعزم القصور الذاتي.
2. عدم التمييز بين بوزونات البروتونات (N_π) وبوزونات النيوترونات (N_υ) في نموذج (IBM-1) مما جعل اختلاف واضح بين القيم العملية والنظرية لمستويات الطاقة في حزمة كاما وهذا بالتالي يؤثر على نتائج حسابات عزم القصور الذاتي لنفس النموذج.
3. ان نواة $^{174}_{72}Hf_{102}$ تكون اشد تشوهاً في المستويات العالية وخصوصاً في حزمة كاما مما يجعل النواة تتذبذب بين الشكل الاهليليجي المتطاول والمفلطح أي بين التناظر الديناميكي SU(3) بشكلها المتطاول وبين التناظر الديناميكي SU(3) بشكلها المفلطح مروراً بالتناظر الديناميكي $O(6)$، وهذا مما يجعل عزم القصور الذاتي يتغير بشكل متعرج في هذه الحزمة.

الشكل (3) يبين حزم الطاقة كدالة للزخم الزاوي لنواة $^{174}_{72}Hf_{102}$ حيث تظهر القيم العملية للطاقة مع نتائج الطاقة المحسوبة من نموذج عزم القصور الذاتي المتغير (VMI) تطابقاً جيداً.

ان ظاهرة تقاطع الحزم تحدث عند زخم زاوي معين L_c (L_{cross}) حيث تحل حزمة الطاقة ذات القيم العالية محل حزمة الطاقة ذات القيم الواطئة واللتان تمتلك نفس البرم للحزمتين. فعند تقاطع حزمتين فان جميع النيوكليونات يكون لها برم يساوي صفراً تحت تاثير تفاعل الارتباط المزدوج (Pairing Correlation Interaction) وفي هذه الحالة تعتبر النواة فائقة الميوعة وطاقتها الذاتية تكون اقل من طاقة الارتباط المزدوج ويكون للنواة عزم قصور ذاتي قليل. كما ان قوة كوريولوس (Coriolis Force) عند زيادة السرعة الزاوية (زيادة الطاقة الدورانية ($\hbar^2\omega^2$)) تعمل على فك الازدواج بين زوج او اكثر من ازواج النيوكليونات في بعض النوى مكونة حزمة طاقة متهيجة نتيجة انفصال نيوكليونين اواكثر في النواة (تسمى هذه الحزمة بحزمة شبيهي الجسيمات) فيكون زخمها الزاوي باتجاه محور الدوران وباقل طاقة دورانية واعظم زخم زاوي ليكونان مستوى دوران ذاتي يكون اساساً للحزم الدورانية ان عدم استقرار هذين المستويين يؤدي الى تقاطع الحزم المتهيجة للجسيمين مع الحزمة الارضية او حزمة بيتا او حزمة كاما[17].

اوضحت نتائج نموذج عزم القصور الذاتي المتغير (VMI) الموضحة في الشكل (3) ان نواة $^{174}_{72}Hf_{102}$ لايوجد فيها تقاطع بين الحزم لانها تنتمي الى زمرة التناظر الديناميكي SU(3).

يبين الشكل (4) علاقة تغيير عزم القصور الذاتي كدالة لمربع الطاقة الدورانية، التي تم عرض نتائجها في الجدول (2)، حيث نلاحظ عدم وجود انحناءات في الحزمة الارضية وحزمة بيتا وحزمة كاما لكون التناظر الديناميكي من نوع SU(3).

اما التعرجات الواضحة في حزمة كاما لنواة $^{174}_{72}Hf_{102}$ فتعزى الى نفس الاسباب التي تم مناقشتها.

الاستنتاجات

أثبت نتائج هذا البحث بأنه لا يوجد أي تأثير عزم القصور الذاتي على التركيب النووي لنواة Hf(A=174) شديدة التشوه ذات التناظر الديناميكي SU(3) ،وذلك بسبب عدم ظهور ظاهرة الانحناء الخلفي في حزم الطاقة لهذه النواة و احتوائها على قيم عالية لعزم القصور الذاتي و ما يقابلها من قيم واطئة جداً لمعامل الليونة (σ) و هذا ما يؤكد بان هذه النواة شديدة التشوه.لقد نجح نموذج (VMI) في حسابات عزم لقصور لنواة Hf(A=174) ولكافة الحزم مقارنتاً مع القيم العملية، في حين لم يوفق نموذج (IBM-1) في ذلك.

جدول -1: قيم اعلومات مؤثر دالة هاملتون لنموذج البوزونات المتفاعلة الاول وقيم اعلومات نموذج عزم القصور الذاتي المتغير (VMI) لنواة Hf(A=174).

Nuclei	Dynamical symmetry	Nπ	Nυ	N	Parameters		ε (MeV)	$\hat{P}^{\dagger}.\hat{P}$ (MeV)	$\hat{L}.\hat{L}$ (MeV)	$\hat{Q}.\hat{Q}$ (MeV)	$\hat{U}.\hat{U}$ (MeV)	$\hat{V}.\hat{V}$ (MeV)	CHI
$^{174}_{72}Hf_{102}$	SU(3)	5	10	15	IBM-1		0.0000	0.0000	0.0170	-0.0099	0.0000	0.0900	-1.322875
					Bands	VMI Model	Parameters						
							$\vartheta_o/\hbar^2$ (MeV)$^{-1}$	C (MeV)^3	K (MeV)	σ	Standard Deviation Model		χ^2 Model	
											VMI	IBM-1	VMI	IBM-1
					g_g		32.4101	0.0039	0.0000	0.0037	0.0361	0.7514	0.00010	0.0406
					β_1		41.0000	0.0020	0.8274	0.0028	0.0160	1.1827	0.00003	0.0654
					β_2		37.0000	0.0000	1.2390	0.0011	0.0018	0.1231	0.00001	0.0064
					γ		43.7999	0.0000	1.1600	0.0008	0.0714	0.3052	0.00220	0.0825

جدول -2: قيم مستويات الطاقة وطاقات الانتقال (النظرية والعملية) وقيم عزم القصور الذاتي ومربع الطاقة الدورانية لنواة Hf(A=174) ولكافة الحزم.(IBM-1) ونموذج (VMI) الزوجية-زوجية باستخدام نموذج عزم القصور الذاتي التمغير

Nucleus			Band		N_π	N_ν	N	Dynamical symmetry									
$^{174}_{72}Hf_{102}$			g		5	10	15	SU(3)									
	Experimental		IBM-1 (pw)		VMI(pw)				Experimental			IBM-1 (pw)			VMI(pw)		
L^+	Energy (MeV) [18,19]	$\vartheta/\hbar^2$ (MeV) [20]	Energy (MeV) [18,19]	$\vartheta/\hbar^2$ (MeV) [20]	Energy (MeV) [18,19]	$\vartheta/\hbar^2$ (MeV) [20]	$L_i^+ - L_f^+$	E_γ (MeV) [18,19]	$(\hbar c)^2$ (MeV)^2 (pw)	$2\vartheta/\hbar^2$ (MeV)^4 (pw)	E_γ (MeV) [18,19]	$(\hbar c)^2$ (MeV)^2 (pw)	$2\vartheta/\hbar^2$ (MeV)^4 (pw)	E_γ (MeV) [18,19]	$(\hbar c)^2$ (MeV)^2 (pw)	$2\vartheta/\hbar^2$ (MeV)^4 (pw)
0_1^+	0.0000	32.8900	0.0000	32.5162	0.0000	32.4101	$2_1^+ - 0_1^+$	0.0910	0.0014	65.9341	0.0919	0.0014	65.2458	0.0916	0.0014	65.5293
2_1^+	0.0910	32.9670	0.0919	32.6228	0.0915	33.1117	$4_1^+ - 2_1^+$	0.2064	0.0104	67.8295	0.2203	0.0119	63.5526	0.2068	0.0105	67.6975
4_1^+	0.2974	33.9147	0.3123	31.7763	0.2983	34.5572	$6_1^+ - 4_1^+$	0.3109	0.0239	70.7623	0.3624	0.0326	60.6947	0.3096	0.0238	71.0613
6_1^+	0.6083	35.3812	0.6747	30.3473	0.6079	36.4606	$8_1^+ - 6_1^+$	0.4007	0.0399	74.8689	0.5181	0.0668	57.9049	0.3994	0.0396	75.1129
8_1^+	0.0090	37.4345	1.19281	28.9525	1.0073	38.6041	$10_1^+ - 8_1^+$	0.4767	0.0566	79.7147	0.6828	0.1162	55.6548	0.4779	0.0569	79.5088
10_1^+	0.4857	39.8573	1.8756	27.8274	1.4852	40.8579	$12_1^+ - 10_1^+$	0.5348	0.0714	86.0135	0.8529	0.1815	53.9367	0.5473	0.0747	84.0521
12_1^+	2.0205	43.0067	2.7284	26.9683	2.0325	43.1511	$14_1^+ - 12_1^+$	0.5768	0.0831	93.6199	1.0261	0.2628	52.6290	0.6092	0.0927	93.2026
14_1^+	2.5973	46.8099	3.7545	26.3145	2.6418	45.4458	$16_1^+ - 14_1^+$	0.6116	0.0934	101.3735	1.2011	0.3603	51.6189	0.6652	0.1105	97.7229
16_1^+	3.2089	50.6867	4.9556	25.8094	3.3070	47.7222	$18_1^+ - 16_1^+$	-	-	-	1.3773	0.4739	50.8241	0.7163	0.1282	102.1813
18_1^+	-	-	6.3329	25.4120	4.0233	49.9697	$20_1^+ - 18_1^+$	-	-	-	1.5542	0.6035	50.1841	0.7634	0.1456	106.5705
20_1^+	-	-	7.8872	25.0924	4.7866	52.1837	$22_1^+ - 20_1^+$	-	-	-	1.7317	0.7493	49.6619	0.8069	0.1627	110.8882
22_1^+	-	-	9.6189	24.8309	5.5936	54.3617	$24_1^+ - 22_1^+$	-	-	-	1.9094	0.9111	49.2278	0.8477	0.1795	115.1344
24_1^+	-	-	11.5284	24.6139	6.4413	56.5038	-	-	-	-	-	-	-	-	-	-

جدول -2: (2/4)

Nucleus			Band		N_π	N_ν	N	Dynamical symmetry									
$^{174}_{72}Hf_{102}$			βI		5	10	15	SU(3)									
	Experimental		IBM-1 (pw)		VMI(pw)				Experimental			IBM-1 (pw)			VMI(pw)		
L^+	Energy (MeV) [18,19]	$\vartheta/\hbar^2$ (MeV) [20]	Energy (MeV) [18,19]	$\vartheta/\hbar^2$ (MeV) [20]	Energy (MeV) [18,19]	$\vartheta/\hbar^2$ (MeV) [20]	$L_i^+ - L_f^+$	E_γ (MeV) [18,19]	$(\hbar\omega)^2$ $(MeV)^2$ (pw)	$2\vartheta/\hbar^2$ $(MeV)^{-1}$ (pw)	E_γ (MeV) [18,19]	$(\hbar\omega)^2$ $(MeV)^2$ (pw)	$2\vartheta/\hbar^2$ $(MeV)^{-1}$ (pw)	E_γ (MeV) [18,19]	$(\hbar\omega)^2$ $(MeV)^2$ (pw)	$2\vartheta/\hbar^2$ $(MeV)^{-1}$ (pw)
0_2^+	0.8274	-	0.8227	24.6790	0.8274	41.0000	$2_2^+ - 0_2^+$	0.0730	0.0008	82.1918	0.0437	0.0003	137.2998	0.0726	0.0008	82.6699
2_2^+	0.9004	41.0959	0.8664	68.6499	0.8999	41.6647	$4_2^+ - 2_2^+$	0.1621	0.064	86.3664	0.2462	0.0148	56.8759	0.1652	0.0066	84.7597
4_2^+	1.0625	43.1832	1.1126	28.4379	1.0652	43.0731	$6_2^+ - 4_2^+$	0.2449	0.0148	89.8326	0.4039	0.0404	54.4662	0.2497	0.0154	88.100
6_2^+	1.307	44.9163	1.5165	27.2331	1.3149	44.9903	$8_2^+ - 6_2^+$	0.3231	0.0259	92.8505	0.5695	0.0807	52.6768	0.3252	0.0263	92.2461
8_2^+	0.6305	46.4253	2.0860	26.3384	1.6401	47.2119	$10_2^+ - 8_2^+$	0.3958	0.0391	96.0081	0.7405	0.1367	51.3132	0.3923	0.0383	96.8559
10_2^+	2.0263	48.0041	2.8266	25.6566	2.0324	49.5989	$12_2^+ - 10_2^+$	0.4626	0.0534	99.4379	0.9145	0.2086	50.3007	0.4523	0.0510	101.7085
12_2^+	2.4889	49.7189	3.7407	25.1504	2.4847	52.0664	$14_2^+ - 12_2^+$	0.5036	0.0633	107.2279	1.0901	0.2966	49.5376	0.5062	0.0639	106.6708
14_2^+	2.9925	53.6139	4.8312	24.7688	2.9909	54.5643	$16_2^+ - 14_2^+$	0.5079	0.0644	122.0713	1.2666	0.4006	48.9476	0.5552	0.0769	111.6645
16_2^+	3.5004	61.03565	6.0978	24.4738	3.5462	57.0637	$18_2^+ - 16_2^+$	-	-	-	1.4438	0.5207	48.488	0.6001	0.0899	116.6447
18_2^+	-	-	7.5417	24.2404	4.1463	59.5478	$20_2^+ - 18_2^+$	-	-	-	1.6215	0.6569	48.1027	0.6415	0.1028	121.5849
20_2^+	-	-	9.1632	24.0514	4.7878	62.0070	$22_2^+ - 20_2^+$	-	-	-	1.7994	0.8090	47.7916	0.6800	0.1155	126.4706
22_2^+	-	-	10.9627	23.8958	5.4678	64.4362	$24_2^+ - 22_2^+$	-	-	-	1.9776	0.9773	47.5317	0.7159	0.1281	131.2939
24_2^+	-	-	12.9403	23.7659	6.187	66.8326	-	-	-	-	-	-	-	-	-	-

جدول -2: (3/4).

Nucleus			Band		N_π	N_ν	N	Dynamical symmetry								
$^{174}_{72}Hf_{102}$			β_2		5	10	15	SU(3)								
	Experimental		IBM-1 (pw)		VMI(pw)			Experimental			IBM-1 (pw)			VMI(pw)		
L^+	Energy (MeV) [18,19]	$\vartheta/\hbar^2$ (MeV) [20]	Energy (MeV) [18,19]	$\vartheta/\hbar^2$ (MeV) [20]	Energy (MeV) [18,19]	$\vartheta/\hbar^2$ (MeV) [20]	$L_i^+ - L_f^+$	E_γ (MeV) [18,19]	$(\hbar\omega)^3$ $(MeV)^3$ (pw)	$2\vartheta/\hbar^2$ $(MeV)^{-1}$ (pw)	E_γ (MeV) [18,19]	$(\hbar\omega)^3$ $(MeV)^3$ (pw)	$2\vartheta/\hbar^2$ $(MeV)^{-1}$ (pw)	E_γ (MeV) [18,19]	$(\hbar\omega)^3$ $(MeV)^3$ (pw)	$2\vartheta/\hbar^2$ $(MeV)^{-1}$ (pw)
0_3^+	1.2390	-	1.3403	28.5742	1.2390	37.0000	$2_4^+ - 0_4^+$	0.0800	0.0011	74.9999	0.0624	0.0006	96.1230	0.0808	0.0011	74.2411
2_4^+	1.3190	37.4999	1.4027	48.0615	1.3198	37.2404	$4_4^+ - 2_4^+$	0.1844	0.0083	75.9219	0.2686	0.0176	52.1221	0.1866	0.0085	75.0225
4_4^+	1.5034	37.9609	16713	26.0611	1.5064	37.7785	$6_4^+ - 4_4^+$	-	-	-	0.5047	0.0631	43.5893	0.2881	0.0205	76.3548
6_4^+	-	-	2.1761	21.7947	1.7945	38.5685	$8_4^+ - 6_4^+$	-	-	-	0.6636	0.1096	45.2053	0.3839	0.0366	78.1363
8_4^+	-	-	2.8397	22.60269	2.1785	39.5563	$10_4^+ - 8_4^+$	-	-	-	0.8356	0.1740	45.4752	0.4734	0.0558	80.2611
10_4^+	-	-	3.6753	22.7376	2.6519	40.6908	$12_4^+ - 10_4^+$	-	-	-	1.0132	0.2561	45.4007	0.5566	0.0773	82.6358
12_4^+	-	-	4.6885	22.7004	3.2086	41.9295	$14_4^+ - 12_4^+$	-	-	-	1.1970	0.3577	45.1112	0.6339	0.1003	85.1854
14_4^+	-	-	5.8856	22.5556	3.8425	43.2398	$16_4^+ - 14_4^+$	-	-	-	1.3893	0.4820	44.6264	0.7057	0.1243	87.8534
16_4^+	-	-	7.2749	22.3132	4.5482	44.5975	$18_4^+ - 16_4^+$	-	-	-	1.5875	0.6295	44.0925	0.7726	0.1491	90.5982
18_4^+	-	-	8.8624	22.0463	5.3208	45.9850	$20_4^+ - 18_4^+$	-	-	-	1.7836	0.7948	43.7305	0.8352	0.1742	93.3898
20_4^+	-	-	10.6461	21.8653	6.1561	47.3897	$22_4^+ - 20_4^+$	-	-	-	1.9733	0.9730	43.5798	0.8939	0.1996	96.2068
22_4^+	-	-	12.6195	21.7899	7.0500	48.8028	$24_4^+ - 22_4^+$	-	-	-	2.1584	01.1642	43.5486	0.9491	0.2251	99.0342
24_4^+	-	-	14.7779	21.7743	7.9991	50.2179	-	-	-	-	-	-	-	-	-	-

جدول (2): (4/4).

Nucleus			Band		N_π	N_ν	N	Dynamical symmetry									
$^{174}_{72}Hf_{102}$			7		5	10	15	SU(3)									
	Experimental		IBM-1 (pw)		VMI(pw)			Experimental				IBM-1 (pw)			VMI(pw)		
L^+	Energy (MeV) [18,19]	$\vartheta/\hbar^2$ (MeV) [20]	Energy (MeV) [18,19]	$\vartheta/\hbar^2$ (MeV) [20]	Energy (MeV) [18,19]	$\vartheta/\hbar^2$ (MeV) [20]	$L_i^+ - L_f^+$	E_γ (MeV) [18,19]	$(\hbar\omega)^2$ $(MeV)^2$ (pw)	$_2\vartheta/\hbar^2$ $(MeV)^4$ (pw)	E_γ (MeV) [18,19]	$(\hbar\omega)^2$ $(MeV)^2$ (pw)	$_2\vartheta/\hbar^2$ $(MeV)^4$ (pw)	E_γ (MeV) [18,19]	$(\hbar\omega)^2$ $(MeV)^2$ (pw)	$_2\vartheta/\hbar^2$ $(MeV)^4$ (pw)
2_3^+	1.2268	-	0.9250	24.7647	1.2333	40.9983	$3_1^+ - 2_3^+$	0.0766	0.0057	78.3289	0.0441	0.0019	136.0545	0.0730	0.0052	82.1915
3_1^+	1.3034	39.1644	0.9691	68.0273	1.3063	41.1928	$4_3^+ - 3_1^+$	0.1455	0.0208	54.9828	0.2543	0.0636	31.4577	0.0968	0.0092	82.6404
4_3^+	1.4489	27.4914	0.2234	15.7289	1.4031	41.4468	$5_1^+ - 4_3^+$	0.2096	0.0434	47.7099	0.0868	0.0075	115.1941	0.1201	0.0143	83.2038
5_1^+	1.6585	23.8549	1.3102	57.5971	1.5233	41.7559	$6_3^+ - 5_1^+$	-	-	-	0.4184	0.1738	28.6786	0.1431	0.0203	83.8728
6_3^+	-	-	1.7287	14.3393	1.6664	42.1155	$7_1^+ - 6_3^+$	-	-	-	0.0972	0.0969	143.9737	0.1654	0.0272	84.6389
7_1^+	-	-	1.8259	71.9869	1.8318	42.5207	$8_3^+ - 7_1^+$	-	-	-	0.6040	0.3634	26.4901	0.1871	0.0348	85.4895
8_3^+	-	-	2.4299	13.2451	2.0189	42.9066	$9_1^+ - 8_3^+$	-	-	-	0.0882	0.0078	204.1046	0.2083	0.0432	86.4177
9_1^+	-	-	2.5181	102.0523	2.2272	43.4486	$10_3^+ - 9_1^+$	-	-	-	0.8000	0.6384	24.9993	0.2288	0.0522	87.4132
10_3^+	-	-	3.3181	12.4997	2.4560	43.9620	$11_1^+ - 10_3^+$	-	-	-	0.0696	0.0048	315.8653	0.2486	0.0617	88.4676
11_1^+	-	-	3.3879	157.9327	2.7047	44.5027	$12_3^+ - 11_1^+$	-	-	-	0.9987	0.9956	24.0291	0.2679	0.0716	89.5729
12_3^+	-	-	4.3866	12.01459	2.9726	45.0671	$13_1^+ - 12_3^+$	-	-	-	0.0488	0.0024	531.9138	0.2866	0.0820	90.7218
13_1^+	-	-	4.4354	26.5957	3.2592	45.6516	$14_3^+ - 13_1^+$	-	-	-	1.1927	1.4207	23.4744	0.3046	0.0926	91.9082
14_3^+	-	-	5.6282	11.7372	3.5639	46.2533	-	-	-	-	0.0331	0.0011	904.1656	0.3221	0.1036	93.1261

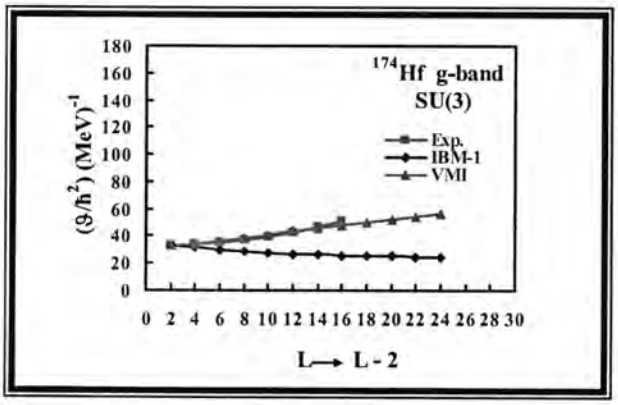

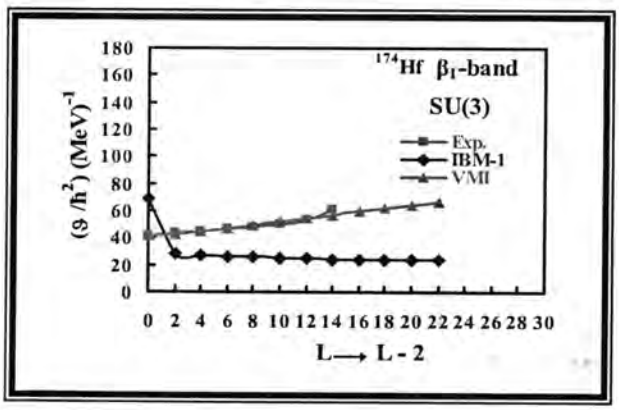

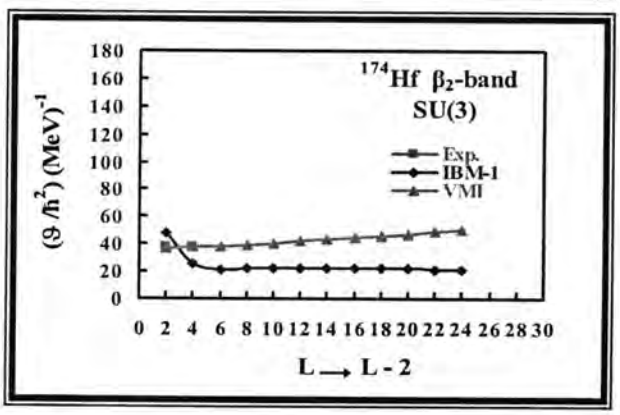

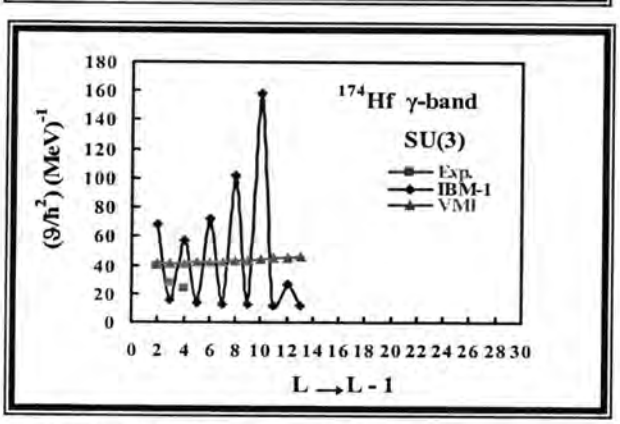

شكل -2 : عزم القصور الذاتي كدالة لتغير الزخم الزاوي للحزم(g,β,γ) لنواة(A=170) Er.

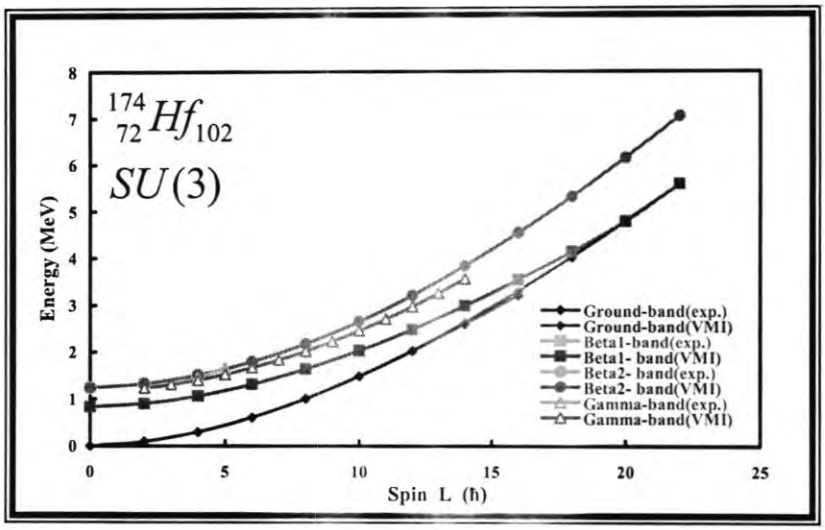

شكل -3 : تقاطع الطاقة كدالة للزخم الزاوي لنواة Hf(A=174) باستخدام نموذج (VMI).

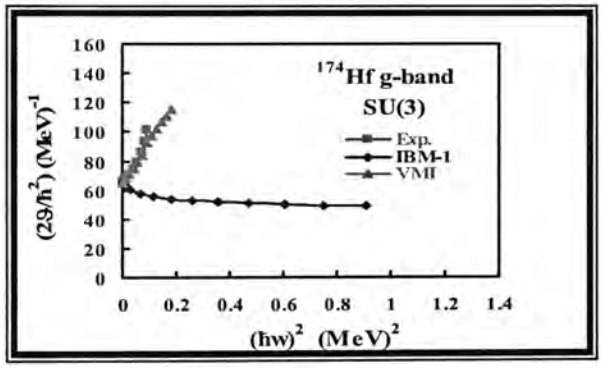

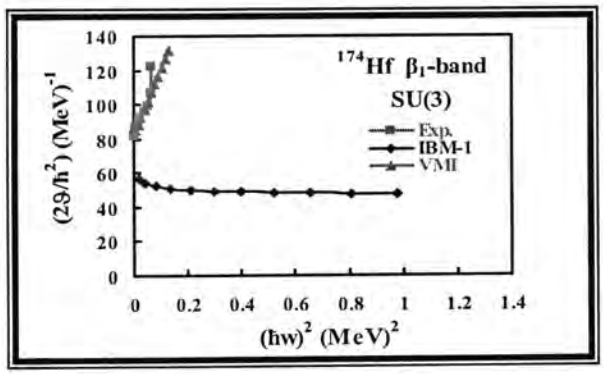

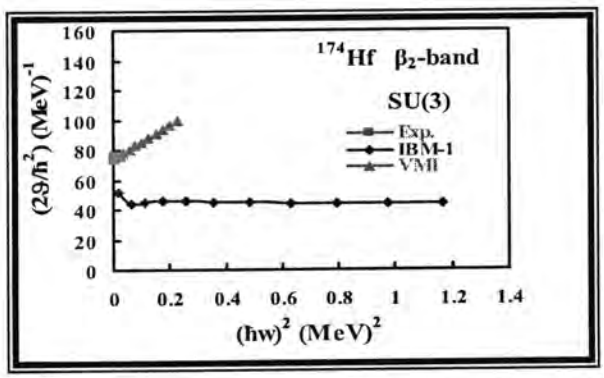

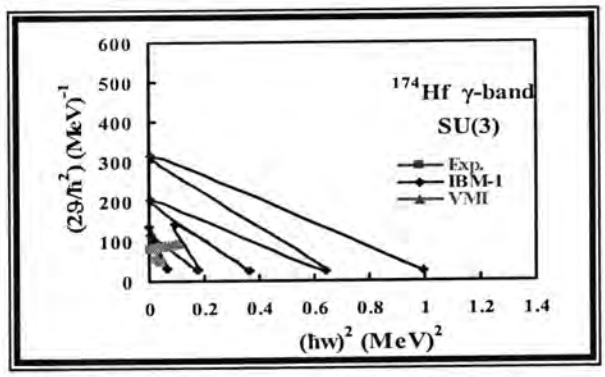

شكل -4 : عزم القصور الذاتي كدالة لمربع الطاقة الدورانية لنواة Hf(A=174) ولكافة الحزم.

المصادر

1. Arima A. and Iachello F., " The Interacting Boson Model", The Syndicate Press of the University of Cambridge,England,PP.3-127(1987).
2. Bonatsos D. " Interacting Boson Model of Nuclear Structure" Oxford University Press, New York,PP.1- 271 (1988).
3. Casten R.F and Warner D.D., "The Interacting Boson Approximation",Rev.Mod.Phys.,Vol.60,P. 389 (1988).
4. Mariscotti M.A.J., Seharff-Goldhaber G. and Branin B., "Study of Variable Moment of Intertia Model (VMI) for Rotation Nuclei",Phys. Rev., Vol.178,P. 1864 (1969).
5. Nyako B.M.,Cresswell J.R.,Forsyth P.D.,Howe D.,Nolan P.N.,Riley M.A. and Twin P.J., "Observation of Super Deformation in ^{152}Dy",Phys.Rev.Lett., Vol.52,P. 507(1984).
6. Ward D., Graham R.L.,Geijer J.S. and Androws H.R., "Experimental Evidence of Band Crossing Spins for Even-Even Nuclei",Phys.Lett. B,Vol.44, P.39(1973).
7. Bohr A., and Mottelson B.R, "Symmetry and Shape of Nuclear Equilibrium Deformation", Mat. Fys. Medd. Dan.Vid. Selsk, Vol.27, P.16(1953).
8. Turkan N. and Maras I., "Microscopic Interacting Boson Model Calculation for Even- Even $^{128-138}$Ce Nuclei ",Pramana Journal of Physics, Vol. 68,P.769 (2007).
9. Sönmezoğlu S.,Okuducu S. and Eser E., "Investigation of Symmetry Properties in Deformed Light Even-Even Nuclei", International Journal and Engineering Sciences. Vol.2, P.1 (2008).
10. Talmi I . , "Simple Models of Complex Nuclei ,The Shell Model and Interacting Boson Model ",Harwood Academic Publishers, PP.187-198(1993).
11. Nojarov R. and Nodjakov E., "Band Coupling and Crossing in Nuclei", Nucl. Phys.A, Vol.397,P.29(1983).
12. Lian A.W. and Toki H., "Evidence on $\Delta I=4$ Bifurcation in Ground Bands of Even- Even and the Theoretical Explanation with the Interacting Boson Model",Phys.Rev.C, Vol.56, P.1821(1997).
13. Banatsos D.,Daskaloyannis C.,Drenska S.B. and Karoussos N., "$\Delta I=2$ Staggering in Rotational Bands of Diatomic Molecules as a

Manifestation of Interband Interactions", Phys. Rev. A, Vol.60, P.253 (1999).

14. Mariscatti M.A.J., "Description of Variable Moment of Inertia Model for Heavy Even-Even Nuclei", Phys.Rev., Vol.172, P.1742 (1970).
15. Xu F.X.,Wu C.S., and Zeng J.Y., "Relations for the Coefficients in the L(L+1) Expansion for Rotational Spectra", Phys.Rev.C, Vol.40, P.2337(1989).
16. Stephons J., "Schoum'16. Murray R., Spiegel T.and Stephons J. Outlines Statistics", Mc Graw-Hill, PP.100-105(1999).
17. Arima A. and Iachello F., "In advance in Nuclear Physics ", Plenum, New York, PP.139-145(1984).
18. Sakai M., "Quasi-Band in Even- Even Nuclei " ,Atomic Data and Nuclear Data Tables,Vol.31, P399 (1984).
19. 19.Lederer C. M. and Shirley V. S., "Table of Isotopes 7^{th} Edition", John Wiley and Sons, New York, PP.1078-1148 (1978).
20. Venkova T. and Andrejtscheff W., "Transition Strengths B(E2) in the Yrast Band of Doubly Even Nuclei ", Atomic Data and Nuclear Data Tables,Vol.26, P.93 (1981).

اختزال الضوضاء الجمعية من الاشارة الكلامية باستخدام مرشح المعدل المحسن

احلام مجيد كاظم وعلي عبد داود الزكي
الجامعة المستنصرية / كلية العلوم/ قسم الفيزياء

تاريخ تقديم البحث 2009/4/19 - تاريخ قبول البحث 209/10/5

ABSTRACT

Audio signal processing is one of the most significant branches of processing digital signals. It has wide applications in many fields, especially in communication and mobile phones systems, but the audio signals are often accompanied by distorted the noise causes weakness of the analysis and discrimination audio signals so for the purpose of improving the efficiency of audio signals must study and analysis of audio signals before, we make simulation to additive Gaussian noise by makes noise with many value of standard deviation and then we add this noise to the signal by additive form we are study effective filtering process by using mean filter to reduce noise, statistics significant features .Therefore mean filter was enhanced by adding some conditions to improve performing and conservation to maintain the significant feature of audio signals that results from using mean filter has been studied also.we notice that mean filter in adaptive form give good result in enhancement signals that mix with noise.

الخلاصة

تعد معالجة الإشارة الصوتية احد الفروع المهمة لمعالجة الإشارات الرقمية وهي واسعة التطبيق في مجالات عدة وخاصة أنظمة الاتصالات والهواتف النقالة إلا إن الإشارات الصوتية غالبا ما يرافقها تشوه وضوضاء والتي تسبب ضعف عملية تحليل وتمييز الإشارات, لذا توجهنا لدراسة الإشارات الصوتية ودراسة الضوضاء كما درسنا الاشارة الصوتية وتاثير الضوضاء الجمعية عليها ولقد قمنا بعملنا هنا بمحاكاة الضوضاء الكاوسية الجمعية وذلك بتوليد الضوضاء بقيم انحراف معياري مختلفة ثم اضافتها الى الاشارة بشكل جمعي ثم دراسة تاثير عملية الترشيح باستخدام مرشح المعدل لاختزال هذة وتم دراسة الخصائص الإحصائية للإشارات الناتجة من المعالجة لتحديد جودة الإشارة بعد المعالجة وتحديد كفاءة المرشح ولوحظ إن عملية المعالجة تؤدي إلى فقدان بعض السمات المهمة للإشارة الصوتية ، لذا تم تحسين المرشح باضافة بعض الشروط الاضافية على العنصر الذي تتم معلجته وذلك للمحافظة على السمات المهمة وتمت معالجة الإشارة المشوبة باستخدام المرشح المحسن ثم دراسة الخصائص الإحصائية للإشارة الناتجة من المعالجة وأعطى مرشح المعدل بصيغته المحسنة نتائج جيدة في تحسين الإشارة المشوبة بالضوضاء .

المقدمة

تعد الضوضاء بيانات غير مرغوب فيها تظهر نتيجة التقلبات التي تحدث على إشارة الصوت أو الإشارات التي تتداخل مع إشارة الصوت فتسبب تشوهها وعدم وضوحها فالميكرفون يعمل على تسجيل الصوت المطلوب ويسجل معه الإشارات الصوتية التي تأتي من مصادر صوتية أخرى بالقرب من مصدر الصوت المطلوب ومنها الضوضاء التي تسببها مراوح الكومبيوتر أو نقرات لوحة المفاتيح أو صوت محرك السيارة أو صوت الريح أو صوت المطر وغيرها والتي تعتبر خلفية ضوضائية وهي تضيف قيم عشوائية إلى كل عنصر من عناصر الإشارة الصوتية وهذه تعتبر أول مؤثر لظهور الضوضاء لذلك فان الإشارة الناتجة من التسجيل الصوتي لا يمكن إن تخلو من الضوضاء، وعملية اختزال الضوضاء هي مسالة مهمة في تطبيقات متعددة مثل اتصالات الهاتف النقال وتمييز الكلام ، ومعالجة الإشارات الطبية والراديو والسونار والعديد من التطبيقات [3-1] لذا توجهنا الى دراسة المرشحات المثلى لغرض ازالة الضوضاء ومن ثم دراسة كفاءة اختزال الضوضاء بمعايير كمية كفوءة.

- عام 2001 درس طارق احمد حسن العامري كامل الاختبار الكمي (الشيئي) objective measures لاختبار الإشارة الكلامية ،حيث إن تقييم الكلام مهم جدا لعمل أنظمة الاتصالات وذلك لأنه يحدد مقدار الضغط في الإشارات الصوتية[4] .
- عام 2004 قدم احمد حمود فليح دراسة لأنظمة تعريف المتكلم وتحديد هوية أصوات المكائن وتمييز الكلمات المنفصلة لنص ثابت وضمن مجموعة مغلقة بدءا من قاعدة البيانات المرجعية المتمثلة بالطبقات المرجعية للأصوات [5].

a. قدم احمد كامل حسن عام 2005 دراسة لإزالة الضوضاء من الصوت باستخدام تحويل المويجة واستخدام طرق مختلفة لإزالة الضوضاء الطبيعية واستند على طريقة فصل المقاطع الصوتية عن المقاطع غير الصوتية[6] .

التمثيل الرقمي للصوت والضوضاء

يعرف الصوت بأنه اضطراب تضاغطي ينتقل خلال المادة فالاهتزازات التي تحدثها الأصوات تعمل على إزاحة جزيئات الهواء وتضطرها على الاقتراب من بعضها البعض والتجمع وبذلك تنتج منطقة ضغط عالٍ تؤدي بها إلى الاندفاع نحو الجزيئات المحيطة بها لينتقل الاضطراب إليها ثم إلى سلسلة الجزيئات التي تليها وهكذا تتولد مناطق ضغط عالٍ (تضاغطات) ومناطق ضغط منخفض (تخلخلات) حيث ان سلسلة التتابعات السريعة للتضاغطات والتخلخلات في الهواء تصل الى الأذن البشرية التي تكون عادة في حالة تلامس مع الهواء مما يسبب حركة طبلة الأذن والإحساس بالسمع والكلام هو نتيجة عمليات معقدة ، تحول (الرسالة الكلامية) التي تصاغ في الدماغ بطريقة ما إلى إشارة عصبية تنقل عبر الأعصاب إلى الجهاز الصوتي الذي يكون مسئولا عن توليد الصوت الذي ينطلق من الفم مولدا موجة كلامية وتحتوي إشارة الكلام معلومات مختلفة حول المتكلم حيث يمكن من خلالها فهم مستوى عال من الخواص حول المتكلم مثل اللهجة والسياق وأسلوب المتكلم والحالة العاطفية للمتكلم وصفات أخرى والموجة الكلامية عبارة عن سلسلة من التغيرات في ضغط الهواء يمكن للأذن البشرية التقاطها كصوت إن التمثيل الرقمي للكلام (المعلومات المحتواة في الإشارة الكلامية) عادة يتطلب عددا كبيرا من الثنائيات (البت bits) ، كما إن العديد من تطبيقات نقل الكلام في مجال الاتصالات تتطلب ضغط الكلام بنسب جيدة بحيث يمكن الحفاظ على مستوى جيد من جودة الكلام , في الأنظمة الصوتية تظهر فيها الضوضاء كإشارات صوتية عشوائية أو أصوات غير مرغوب فيها عند معالجة الإشارة أو تحليلها تعتبر الضوضاء بيانات ليست ذات معنى فهي ناتج عرضي ينتج بتأثير المؤثرات الأخرى وليس بتأثير الإشارة الفعلية وهي بيانات تدخل مع بيانات الاشارة تؤدي الى تحريف أو خرق او تغيير محتوى الرسالة المحمولة في الاشارة الرقمية وخلال عملية نقل الإشارة من جهاز الإرسال الى جهاز الاستلام تحدث تأثيرات غير مرغوبة فيها تضعف الاشارة ومن ابرز هذه التاثيرات هي الضوضاء Noise والتي هي إشارة عشوائية وتأتي نتيجة إشارات كهربائية عشوائية تتولد نتيجة أسباب طبيعية تظهر داخل النظام أو خارجة وهذه التغيرات العشوائية تضيف إلى الإشارة معلومات يمكن إن تخفيها جزئيا أو كليا ، وتعد التغيرات التي تطرأ على الإشارة نتيجة

عمليات الترقيم والتحويل من التماثلي إلى الرقمي من مسببات الضوضاء أيضا وتعالج باستخدام مرشحات تنعيم الإشارة وإزالة الضوضاء [9-7].

وعادة ما تمتزج الكثير من انواع الاشارات الرقمية بالضوضاء الكاوسية او الضوضاء التي لها توزيع كاوسي والتي قد تكون ناتجة عن ضوضاء حرارية في منظومة نقل الاشارة او تسجيلها ، وتمثل هذه الضوضاء عادة بالتوزيع الطبيعي، والذي يتخذ شكل الجرس ويدعى بالتوزيع الكاوسي. ويوصف التوزيع باقتران دالة كثافة الاحتمالية (Probability Density Function) بالمعادلة التالية[11-10] :

$$f(N) = \frac{1}{\sqrt{2\pi}\sigma_N} \exp - \frac{(N-\mu_N)^2}{2\sigma_N^2} \quad 1 \quad \text{.....}$$

إذ أن N يمثل المتغير العشوائي الذي يتوزع توزيعاً طبيعياً .

μ_N يمثل المتوسط الحسابي للمتغيرات العشوائيه (المعدل)

a. σ_N يمثل الانحراف المعياري للمتغيرات العشوائيه حول المعدل μ_N .

مرشحات التنعيم الرقمية Digital Smoothing Filters

تستعمل مرشحات التنعيم الرقمية أساسا لإزالة الآثار الزائفة التي يمكن إن تكون موجودة في الإشارة ، كالضوضاء الناتجة عن عملية ترميز الإشارة ، أو الأخطاء المصاحبة لعملية التسجيل والإرسال والاستلام وتعد المرشحات التقليدية من ابسط التقنيات المستخدمة في تنعيم الاشاره والتي يمكن تطبيقها مباشرة على الإشارة المشوبة ، دون الحاجة إلى معرفة مسبقة بالخصائص الإحصائية التي تتحكم بتوزيع الشدة في مناطق الإشارة ومن ابرز هذه المرشحات ، مرشح المعدل Mean Filter [12-13] ، تبرز كفاءة هذه المرشحات في إخماد تأثير الضوضاء في المناطق المتجانسة من الإشارة .

مرشح المعدل Mean Filter : يعمل هذا المرشح باستخدام نافذة صغيرة متحركة على طول الإشارة ، ويتم الحصول على الإشارة المنعمة Smoothing signal بأخذ معدل قيم ا لعناصر الإشارة المحتواة في النافذة المنزلقة ، واستبدالها بقيمة المعدل ، وبتعبير آخر يتم الحصول على الإشارة المحسنة باستخدام نافذة بتطبيق العلاقة الآتي [12]:

$$R(t) = \frac{1}{N} \sum_{i=-\frac{N-1}{2}}^{\frac{N-1}{2}} I(t+i) \quad 2 \quad \text{.....}$$

حيث أن

R (t) يمثل قيمة المعدل للعناصر

I (t + i) تمثل قيمة عنصر الإشارة في النافذة .

أهم الخصائص الإحصائية التي تحدد جودة للإشارة الصوتية

تستند معالجة الإشارة الصوتية الرقمية بشكل أساسي إلى المعلومات المحتواة في الإشارة وأسلوب توزيعها ، وهذه المعلومات التي تم تحسسها وفقاً للمبدأ الفيزيائي تخضع إلى مبدأ النمذجة الرياضية والتوزيعات الإحصائية لذا فأن إحصائيات الإشارة تكون مهمة جداً في عملية تحليل ومعالجة الإشارة الرقمية وكما إن هذه الإحصائيات تعطي سمات وصفات لطبيعة الإشارات وكيفية توزيع المعلومات فيها[13-15].

a.المعدل(μ) mean : معدل الشدة للإشارة يعرف بالرمز μ وهي مفردة إحصائية تعني متوسط القيمة للإشارة وتأتي من جمع كافة عينات الإشارة الصوتية ثم القسمة على العدد الكلي للعينات N ويحسب المعدل μ من العلاقة آلاتية[13-15]:

$$\mu = \frac{1}{N} \sum_{t=0}^{N} I(t) \quad (3) \quad \text{.....}$$

حيث $I(t)$:رمز عام للاشارة الصوتية

N :عدد عناصر الاشارة الكلي

b.الانحراف المعياري (σ) Standard Deviation : يعرف بأنة مقدار انحراف قيم الإشارة عن المعدل ويحسب الانحراف المعياري σ من العلاقة التالية[13-15]:

$$\sigma_S = \sqrt{\frac{1}{N} \sum (I(t) - \mu)^2} \quad \text{.....(3)}$$

جدول -2: نتائج استقطاع مناطق متجانسة من الاشارة الثانية

σ gus	window	Type	μr	σr	SNRr	σ gus	window	type	μ	σ	SNRr
R2		SIGNAL	130	2.29	56.91	R1		SIGNAL	130	2.13	60.98
2		NOISY	130	2.49	52.32	2		NOISY	130	2.34	55.55
2	3	M	130	2.35	55.40	2	3	M	130	2.21	59.03
2	3	A M	130	2.35	55.40	2	3	A M	130	2.21	59.03
2	5	M	130	2.26	57.61	2	5	M	130	2.15	60.44
2	5	A M	130	2.26	57.61	2	5	A M	130	2.15	60.44
2	7	M	130	2.20	59.28	2	7	M	130	2.12	61.45
2	7	A M	130	2.20	59.28	2	7	A M	130	2.12	61.45
2	9	M	130	2.14	60.85	2	9	M	130	2.08	62.46
2	9	A M	130	2.14	60.85	2	9	A M	130	2.08	62.46
6		NOISY	130	3.91	33.28	6		NOISY	130	3.56	36.57
6	3	M	130	2.99	43.53	6	3	M	130	2.72	47.82
6	3	A M	130	3.10	42.03	6	3	A M	130	2.73	47.75
6	5	M	130	2.71	47.96	6	5	M	130	2.49	52.20
6	5	A M	130	2.84	45.79	6	5	A M	130	2.50	52.09
6	7	M	130	2.55	51.00	6	7	M	130	2.37	54.97
6	7	A M	130	2.69	48.34	6	7	A M	130	2.37	54.84
6	9	M	130	2.44	53.46	6	9	M	130	2.28	56.96
6	9	A M	130	2.58	50.40	6	9	A M	130	2.29	56.82
10		NOISY	130	5.49	23.69	10		NOISY	130	5.47	23.80
10	3	M	130	3.76	34.60	10	3	M	130	3.76	34.61
10	3	A M	130	4.50	28.96	10	3	A M	130	4.50	28.96
10	5	M	130	3.26	39.89	10	5	M	130	3.27	39.77
10	5	A M	130	4.19	31.07	10	5	A M	130	4.19	31.07
10	7	M	130	2.99	43.50	10	7	M	130	3.02	43.18
10	7	A M	130	4.01	32.45	10	7	A M	130	4.04	32.30
10	9	M	130	2.81	46.33	10	9	M	130	2.85	45.77
10	9	A M	130	3.90	33.38	10	9	A M	130	3.94	33.09

المصـــــــــادر

1. Fontaine Jean-Marc . "Sound recording Evolution through its history some stages " University Paris 6-CNRS - MCC -Laboratory' Acoustique jmfontai@ccr.jussieu.frMusicale E-mail : (2002)
2. Kintzel, T." A programmers Guide Sound " Addison Wesly , England(1998) ,
3. Plataniotis K.N.D. Androutsos, A.N.Venet Saopoulos, "Multi channel filter for color image" , signal processing , image communication , 11-pp.171-177, (1998) .

4. Tariq Ahmed Al-Amree " Speaker Identification Using Wavelet Transform And Probabilistic Neural Network" M.Sc. thesis , Computers Department , collage of sience , Al- Mustansiriyah University , (2005)
5. Ahmed Hmood Flesh Al-Saidia" voice and speech recognition systems". M.Sc. thesis, Physics Department , collage of science , Al-Mustansiriyah University ,(2004) .
6. Plataniotis K.N.D. Androutsos, A.N.Venet Saopoulos, "Multi channel filter for color image" , signal processing , image communication , 11-pp.171-177, (1998) .
7. Ahmed Kamil Hassan " Speech Denoising Using Wavelet Transform" M.Sc. thesis , Electrical Engineering Department , College of Engineering , Mustansiriya University ,(2005)
8. Alan Hedge www.© "Sound Nature and Measurement" , Report , Cornell University, January , (2008)
9. بوش \ "أساسيات الفيزياء" الطبعة السابعة الدار الدولية للنشر والطباعة ، 1998
10. Nabeel Mubarak Meerza Al-Dalawy "A study of TV images quality for channels Broadcast Television Terrestrial" M.Sc. thesis , Physics Department , College of Science , AL-Mustansiriyah University , (2008).
11. عبد الله حمود محمد الجبوري، "دراسة الضوضاء المرافقة لصور البث التلفزيوني الأرضي وطرق تقليل تأثيرها"، أطروحة دكتوراه \ قسم الفيزياء \ كلية العلوم \ الجامعة المستنصرية \ 2006 .
12. Gonzalez , R.C. and Wintz, P, "Digital image processing" , Addison-wistey, (1987) .
13. Niblack, .W "An Introduction to digital image processing" , prenticeHall International (UK) LTD , (1986) .

14. Mukul v.shiraikar," An optimal measure of camera focus & Exposure ", electrical engineering Department ,university of Texas ,(2004).

15. CH 2 Steven W. Smith "Statistics, Probability and Noise" Ph.D. Thesis , scientist and Engineers Guide to Digital Signal Processing ,(2006) .